The Dissertation Committee for Leonard Yujya Chang Certifies that this is the approved version of the following dissertation:

PREDICTION OF MICROEMULSION PHASE BEHAVIOR FROM SURFACTANT AND CO-SOLVENT STRUCTURES

Committee:

Gary A. Pope, Supervisor

Upali P. Weerasooriya

Kishore K. Mohanty

David A. DiCarlo

Keith P. Johnston

Prediction of Microemulsion Phase Behavior from Surfactant and Co-solvent Structures

by

Leonard Yujya Chang

Dissertation

Presented to the Faculty of the Graduate School of

The University of Texas at Austin

in Partial Fulfillment

of the Requirements

for the Degree of

Doctor of Philosophy

The University of Texas at Austin

December 2018

Dedication

To my family and friends.

Acknowledgements

I would like to express my deepest gratitude to my advisor, Dr. Gary Pope, for his continuous guidance and support. I have greatly benefitted from his knowledge and experience. I also appreciate the valuable comments and feedback of my committee members, Dr. Upali Weerasooriya, Dr. Kishore Mohanty, Dr. David Dicarlo, and Dr. Keith Johnston. Special thanks goes to Sung Hyun Jang, Mohsen Tagavifar, Arnob Bhuyan, Jonathan Driver, Nadeeka Upamali, and Jith Liyanage for their contributions to my research. I am thankful to the industrial affiliates of the Chemical EOR industrial affiliates program in the Center of Petroleum and Geosystems Engineering for funding the research.

I am also thankful to my friends and colleagues, Lauren Churchwell, Pengpeng Qi, Enakshi Wikramanayake, Zach Quintanilla, Pinaki Ghosh, Bi Nguyen, Erin Shook, Erandi Kulawardana, Gayani Pinnawala-Arachchilage, Gayani Kennedy, Dharmika Lansakara-P, Jiajia Cai, Sophie Dufour, Maryam Shafiekhani, Do Hoon Kim, Chris Britton, Robert Fortenberry, Vincent Lee, Nabi Nizamidin, Himanshu Sharma, Heesong Koh, Jun Lu, Mike Unomah, Sean Li, Denning Wang, Jose Parra, Mathieu Maubert, Julien Deligny, Patrick Lim and Austin Lim, who I have learned from one way or another. As well as Esther Barrientes, Joanna Castillo, Barbara Messmore, and Amy Douglas for their administrative support.

Finally, many thanks go to my family for their love and support.

Prediction of Microemulsion Phase Behavior from Surfactant and Co-solvent Structures

Leonard Yujya Chang, Ph.D.

The University of Texas at Austin, 2018

Supervisor: Gary A. Pope

Structure-property models were developed to predict the optimum salinity, optimum solubilization ratio, and the aqueous stability limit from the molecular structures of surfactants and co-solvents used for enhanced oil recovery. The models are sufficiently accurate to provide a useful guide to experimental testing programs for the development of chemical formulations for enhanced oil recovery and other similar applications requiring low interfacial tension. This is the first time a structure-property model has been developed to predict the optimum solubilization ratio. The solubilization ratio can be used in the Huh equation to predict the interfacial tension, which is the most important property in enhanced oil recovery applications.

The UTCEOR Database was constructed and used to develop the models. The database is a collection of highest-quality experimental chemical EOR data conducted at The University of Texas at Austin from 2005 to 2018. It contains several thousand phase behavior experiments using 34 unique crude oils, 294 unique surfactants, and 70 unique co-solvents. The structures of the surfactants and co-solvents were characterized and include variations in the type of hydrophobe (carbon number, degree of branching, polydispersity, and aromaticity), number of alkoxylate groups (propylene oxide and

ethylene oxide), and the type of head group. The model focuses on blends of anionic surfactants and nonionic co-solvents.

Both the optimum salinity and the optimum solubilization ratio were modeled as a function of monovalent and divalent cations in the brines. The oils were characterized using their equivalent alkane carbon number. The models include the effect of soaps generated from the neutralization of acidic crude oils. Previous models for optimum salinity have not included the effects of divalent cations, soap, and co-solvents among other limitations. Most importantly, the new model can be used to predict interfacial tension as well as optimum salinity whereas previous models were used to predict only optimum salinity.

In this research, the structure-concentration and structure-property effect of co-solvents were modeled separately, whereas previous models convoluted both effects and were not predictive. New measurements were made and combined with literature data to develop improved correlations for the oil-water partition coefficient and the interface-water partition coefficient of co-solvents. These correlations were used with pseudophase theory to more accurately model the structure-concentration effect.

A structure-property model was developed for the aqueous stability that predicts the coacervation of chemical formulations. The interactions between surfactant hydrophobes and the PO groups were modeled because they influence the stability of micelles. The effects of co-solvent, polymer, and divalent cations were included for the first time.

The structure-property models can be used to predict formulations for a given oil, brine and temperature that are likely to achieve ultra-low IFT with aqueous stability at optimum salinity and thus greatly accelerate the process of finding the best formulations to test for chemical EOR.

Table of Contents

List of Tables

List of Figures

CHAPTER 1: INTRODUCTION

1.1 Motivation

Enhanced oil recovery is the recovery of oil by injection of fluids not normally present in the reservoir. The three primary EOR techniques are thermal, gas, and chemical EOR. Thermal EOR methods involve heating the reservoir typically by injecting steam to increase the temperature and reduce the viscosity of the oil. This method is typically limited to heavy oils in shallow reservoirs.

Gas EOR methods involve the injection of gases (e.g. CO_2, N_2, hydrocarbons). Gas injection is most effective when the pressure exceeds the minimum miscibility pressure (MMP). The MMP depends on the gas composition, the oil composition, and temperature, but in general can only be achieved in deep reservoirs. Carbon dioxide is the most commonly used miscible gas. Unfortunately, it is in limited supply near most oil fields. Miscible gas flooding is inherently inefficient because of low gas viscosity (unfavorable mobility ratio) and gravity override unless foam or some other method is used to improve the mobility control.

Chemical EOR methods involve injection of chemicals such as surfactants, polymers, alkalis, and solvents in water. Chemical EOR methods have the advantage of being more flexible in that the properties of the chemicals can be tailored to reservoir conditions whereas the properties of water, steam, CO2, N2, and other gases are fixed. However, chemical EOR is relatively complex, it must be specifically tailored to the reservoir conditions such as temperature and oil properties, and it is generally not easy to apply in low permeability reservoirs among other limitations. Chemical methods such as low-tension gas flooding are aimed at low permeability reservoirs.

Research in chemical EOR flourished in the 1970's and 1980's with the increase in the price of oil. The fundamental principles of chemical EOR were established. There were numerous chemical EOR field pilots. Commercial polymer floods were done on a relatively small scale. Starting in the 1990s, large commercial polymer floods were implemented in the Daqing oil field and more recently worldwide. Recent advances in polymer flooding are not reviewed here because the focus of this research was on chemical EOR methods using surfactants.

The surfactants used in the 1970s and 1980s were primarily petroleum sulfonates. Surfactant methods were called micellar flooding, micellar-polymer flooding, and chemical flooding among other names. Surfactant concentrations ranged from 2-12 wt%. In the 21st century, new surfactants and polymers were developed that have better performance and can be used at harsher conditions (high temperature, high salinity, high hardness, low permeability). Surfactant concentrations have been reduced by an order of magnitude. The surfactant structures can be tailored or custom-made to the match the reservoir conditions. In the late 2000's and early 2010's when oil prices were again high, the interest in chemical EOR increased tremendously and several field projects were initiated.

The focus of current Chemical EOR research is to find new solutions, reduce costs, and improve understanding. Formulation development and optimization is time-consuming and costly. A model that represents the effect of variables on the microemulsion phase behavior based on knowledge from previous studies could be used to make better decisions.

Previous correlations have been developed for the optimum salinity such as the hydrophilic-lipophilic deviation (HLD) model and the model developed by Solairaj et al. (2012). Various extensions to the HLD model have been introduced, but there is still no general equation. For example, there is no general predictive term in the HLD equation for

the effect of co-solvent on the microemulsion. HLD theory is predicated on research from the 1970s and 1980s. The surfactants and co-solvents have changed. New models are required. The HLD model is an empirical equation for the optimum salinity of the microemulsion. The greatest need is for a model to predict interfacial tension (IFT) either directly or indirectly from the microemulsion phase behavior (by using the solubilization ratios in the Huh equation for predicting IFT).

1.2 Objective

The objective of this research was to develop models that can be used to predict the microemulsion and aqueous phase behavior of chemical formulations for a given oil based on the molecular structure of the surfactants and co-solvents with enough accuracy that the results can provide a useful guide to the experimental testing program. These models are quantitative structure-property relationships. The models are structure relationships for the molecular structure of the surfactants and co-solvents, and property relationships for the optimum salinity, optimum solubilization ratio, and the aqueous stability limit. The structure-property models can be used to predict formulations for a given oil, brine and temperature that are likely to achieve ultra-low IFT with aqueous stability at optimum salinity (i.e. the minimum requirements for chemical EOR formulations).

Both experimental and modeling work was performed to better understand the interactions of surfactant and co-solvent structures, oil and brine properties, and the interfacial tension. The models were developed using experimental data in the UTCEOR Database, a collection of highest-quality experimental data conducted at The University of Texas at Austin from 2005 to 2018. The database contains over 2000 microemulsion phase behavior experiments and over 1000 aqueous stability tests using 34 unique crude oils, 294 unique surfactants, and 70 unique co-solvents.

This research focuses on anionic surfactants because they are the most commonly used surfactants for EOR and on co-solvents that are commonly used with surfactants to improve microemulsion properties. There are thousands of combinations of surfactants and co-solvents that could be tested for each oil, so even approximate predictions are very useful in terms of reducing the time and effort required for testing and for prioritizing the chemical combinations to test that are most likely to yield ultra-low IFT and have aqueous stability at reservoir conditions.

1.3 Description of Chapters

The dissertation is organized in seven chapters. Chapter 2 provides background on microemulsions and their properties. Particular attention is given to the descriptions of surfactant and co-solvent structures and to other structure-property models for microemulsion phase behavior.

Chapter 3 is dedicated to the UTCEOR database. Therein described are the purposes for building the database, a description of how the database is structured, and a general description of the data.

Particular attention was paid to improve how co-solvents were modeled. The effect of co-solvent structure on microemulsion phase behavior is a combination of how the structure influences partitioning to the interface (structure-concentration effect) and how the structures at the interface influences the phase behavior (structure-property effect). Previously the effect of co-solvent structure was modeled as a convolution of both effects because it was difficult to do otherwise, but those models were not predictive. In this research, the two effects were modeled separately. In chapter 4, correlations were developed for the oil-water partition coefficient (K_{OW}) and the interface-water partition coefficient (K_{PW}) of co-solvents in order to be used with pseudophase theory to more

accurately model the structure-concentration effect. New measurements of K_{OW} and K_{PW} were made. These new data were combined with the models by Solheim (1990), Dwarakanath and Pope (1998), and Chang et al. (2016) to develop a more complete and accurate K_{OW} model and a rough correlation for K_{PW}. By modeling the structure-concentration effect, the structure-property effect could be more accurately quantified in the following chapters.

Chapter 5 is dedicated to the structure-property models for the optimum salinity and the optimum solubilization ratio. The models capture the effects of surfactant hydrophobe structure (carbon number, branching, polydispersity, and aromaticity), the number propylene oxide (PO) groups, the number of ethylene oxide (EO) groups, and the type of anionic head group (sulfonate, benzene sulfonate, sulfate, carboxylate). The correlations developed in chapter 4 were used to model the structure-concentration effect of co-solvent. The models capture the structure-property effects of co-solvent hydrophobe (aliphatic, phenol), the number of PO groups, number of EO groups, and the hydroxyl group. The models include the effects of soaps generated from the neutralization of acidic crude oils. The oils were characterized using their equivalent alkane carbon number. The optimum salinity was modeled as a function of both monovalent and divalent cations in the brines. The association of divalent cations with anionic surfactants are modeled. The models were the used to estimate the effects of solution gas and pressure on the microemulsion phase behavior of live crude oils. Several methods and diagrams are shown to illustrate how the models can be applied to design formulations for desired microemulsion properties.

Chapter 6 covers the the structure-property model for the aqueous stability limit that predicts the coacervation of chemical formulations. The interactions between surfactant hydrophobes and the PO groups were modeled because they influence the

stability of micelles. The effects of co-solvent, polymer, and divalent cations were included for the first time. Several methods and diagrams are shown to illustrate how the model can be used to shift the aqueous stability limit. Finally, the effects of surfactant, co-solvent, oil, brine, and temperature on the optimum salinity, optimum solubilization ratio, and the aqueous stability limit are discussed.

Chapter 7 gives a summary and critique of the findings and identifies areas for further research.

CHAPTER 2: BACKGROUND

2.1 General Principles of Chemical EOR

Chemical EOR involves injecting chemicals such as aqueous solutions of surfactants and polymers to increase the production from oil reservoirs. The purpose of surfactants is to reduce the interfacial tension (IFT) between oil-water in order to mobilize the (residual) oil trapped by capillary forces in the reservoir rock. A three to four orders of magnitude reduction in the IFT from 10 mN/m to ultra-low values of 0.001 *m*N/m is required to reduce residual oil saturation to low values approaching zero. The purpose of polymers is to increase the viscosity of the injectant in order to create a stable displacement and increase sweep efficiency.

Figure 2.1 shows a capillary desaturation curve for a Berea sandstone. The capillary desaturation curve shows the change of residual saturations of the wetting and non-wetting phases versus the capillary number (N_C), which is a dimensionless ratio of viscous to capillary forces, defined by Equation **2.1**.

$$N_C = \frac{|k\nabla\Phi|}{\gamma} \qquad \textbf{(2.1)}$$

where, k is the absolute permeability, and $\nabla\Phi$ is the flow potential gradient, and γ ais the interfacial tension between oil and brine. In **Figure 2.1**, oil is the non-wetting phase. For typical sandstones, the residual oil saturation decreases from approximately 30% for $N_C < 10^{-6}$ to nearly zero at $N_C > 10^{-3}$. The magnitude of the flow potential gradient is constrained by the well spacing and wellhead pressures and the reservoir permeability is fixed, so the only practical way to increase the capillary number by three to four orders of magnitude is to decrease the IFT.

The capillary number for a water flood in a reservoir with a permeability of 100 mD, a pressure gradient of 1 psi/ft, and IFT between crude oil and water of 30 *m*N/m is 7×10^{-8}. Using the capillary desaturation data for Berea sandstone shown in **Figure 2.1**, a reduction of the IFT by four orders of magnitude to 0.003 mN/m increases the capillary number to 7×10^{-4} and decreases the residual oil saturation to nearly 0%.

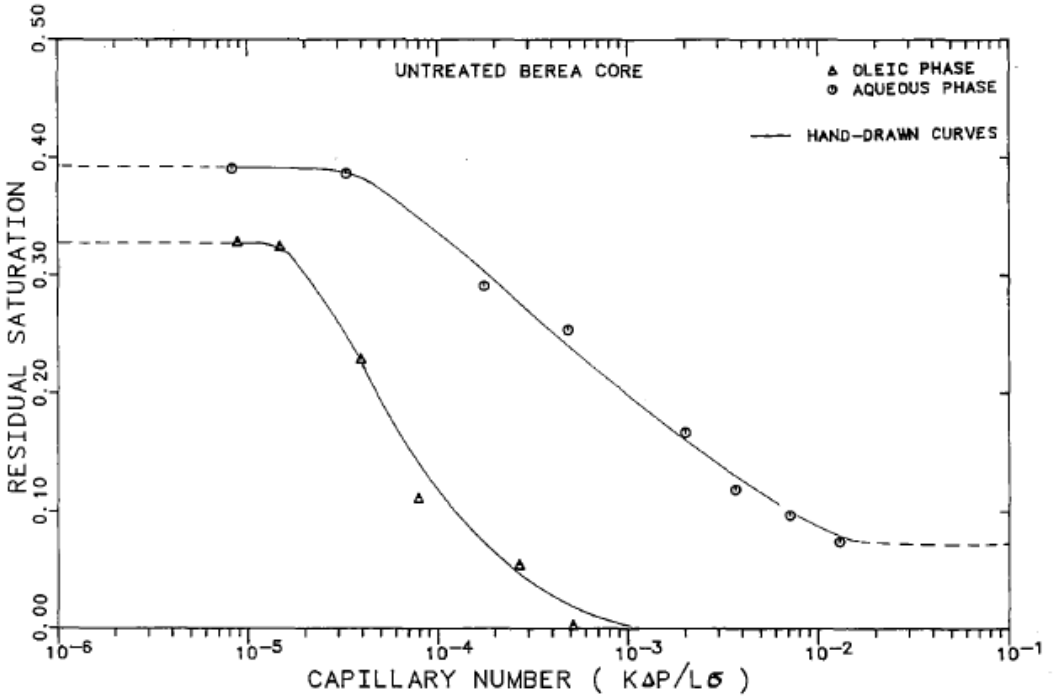

Figure 2.1: Capillary desaturation curve of the wetting (aqueous) and non-wetting (oleic) phases in Berea sandstone (Delshad et al., 1986).

Polymers are used to increase the viscosity of the water in order to reduce the mobility of the water. To have a stable displacement, the mobility of the displacing fluid (ASP slug and polymer drive) must be lower than the mobility of the displaced fluid (oil and water).

A chemical EOR project typically goes through multiple phases of development – reservoir selection, experimental testing, numerical modeling, field tests, field implementation. Each phase is separated by decision points. The focus of this dissertation is on experimental testing, specifically the development of chemical EOR formulations that achieve ultra-low IFT and have aqueous stability.

2.1.1 Surfactant phase behavior screening

Surfactants are screened for ultra-low IFT using microemulsion phase behavior tests. Some mixtures of surfactant, oil, and water form a thermodynamically stable phase called a microemulsion. The microemulsion phase behavior and the interfacial tension are related by the Huh equation.

$$\gamma = \frac{C}{\sigma^2} \tag{2.2}$$

where, C is a constant (typically assumed as 0.3 *m*N/m) and σ is the solubilization ratio. The solubilization ratio is the volume ratio of the oil (or water) to surfactant in the microemulsion phase. When the oil (water) solubilization ratio is 10, the oil-microemulsion (water-microemulsion) IFT is 0.003 *m*N/m.

The goal is to find a surfactant or a combination of surfactants that will attain ultra-low IFT under the specific reservoir conditions (i.e. oil composition, brine composition, temperature and pressure) and meet other requirements necessary for high oil recovery (stable aqueous solution compatible with polymers, low adsorption/retention on rock, microemulsion with low and shear rate-independent viscosity) and scalability (long-term thermal/hydrolytic stability)

The best chemical formulations almost always consist of a mixture of surfactants and in many cases also co-solvent. Since there are multiple types of surfactants and co-

solvents with hundreds of different molecule structures, there are thousands of combinations of surfactants and co-solvents that could be tested for each oil. The choice of surfactants to test for chemical EOR formulations is based in part on an understanding of the general principles governing interfacial phenomena (Winsor, 1954), the behavior of microemulsions (Bourrel & Schechter, 1988), molecular dynamics (Buijse et al., 2012), correlations (Acosta et al., 2003; Bourrel et al., 1980; Ghosh & Johns, 2016a; Salager et al., 1979; Solairaj et al., 2012), analog data and experience (Barnes et al., 2012; Do et al., 2009; Flaaten et al., 2009; Green & Willhite, 1998; Hirasaki et al., 2011; Puerto & Reed, 1983; Reed & Healy, 1977; Salager et al., 2013; Upamali et al., 2016; Zhang et al., 2015).

2.1.2 Core flood testing

The surfactants are usually injected with polymers as a dilute solution in brine, called a surfactant slug. The surfactant slug is typically a small fraction of the total pore volume, and it is followed by a polymer solution called a polymer drive of equal or greater viscosity.

The purpose of core flooding is to evaluate the performance of the formulation dynamically. The experiments are conducted at reservoir temperature with a reservoir core or an outcrop (analogue) core. The oil can be dead crude oil, surrogate crude oil, or live crude oil. The core is initially saturated with brine, and then crude oil is injected under a large pressure gradient to simulate primary drainage and reach the residual water saturation (condition of the reservoir before production). Then, the water is injected until residual oil saturation. This mimics the water flood (secondary recovery). The permeability, the endpoint relative permeability, and the residual saturations are measured during these steps.

Surfactants and polymers are used together. The mobility (kr_W/μ_W) of surfactant slug must be reduced below the mobility of the oil bank to have a stable displacement of the oil bank.

The surfactant slug and polymer drives are typically injected at an interstitial velocity of 1 ft/day since this is the same order of magnitude as the average velocity of a chemical flood of a reservoir. This velocity gives a residence time of about 1 day. The pressure difference between multiple subsections along the core are measured continuously. The produced fluids are collected in graduate test tubes with volumes that are about 5% of the pore volume. The volume of each phase in the test tubes is read and recorded after centrifuging or other means needed to separate the phases. The salinity is measured by refractometer or conductivity meter. The ion composition are measured using ion chromatography. The pH is measured using pH meter. The viscosity is measured using a viscometer. The concentrations of surfactants are measured using high performance liquid chromatography (HPLC) or hyamine titration. The concentrations of co-solvents are measured using HPLC.

A good formulation and well-designed flood are able to (1) reduce the residual oil saturation to nearly 0%, (2) produce the majority of the oil as clean oil in the oil bank as opposed to as microemulsions or macroemulsions, (3) maintain low pressure gradients throughout the flood, (4) have low surfactant retention, (5) no chromatographic separation of the surfactants.

The coreflood performance is based on (1) the reduction of the residual oil saturation (2) the number of pore volumes required to recover the oil and what fraction of the oil is recovered before surfactant breakthrough (3) the pressure gradients and stability of the displacements, (4) surfactant and polymer retention and the separation of surfactants when more than one surfactant is used in the formulation, (5) the produced viscosity and

thermal stability of the polymer and (6) other factors depending on the specific objectives of the experiment.

The reduction in residual oil saturation is controlled by capillary number and the capillary desaturation curve of the rock. Most of the oil can be recovered in the oil bank (not mixed with surfactant) if the experiment is a stable displacement. If the pressure gradients are excessively high, the process may not work or may take too long in the field as pressure gradients are constrained. This can be caused by polymer propagation issues or unfavorable microemulsion viscosity.

Surfactant retention is the mass of surfactant retained per mass of rock. The chemical cost to recover an incremental barrel of oil is directly proportional to the surfactant retention. Lower retentions mean that the surfactant is utilized more efficiently. Factors that influence retention include (1) salinity gradient, (2) microemulsion viscosity, (3) surfactant types, (4) mobility ratio, (5) pH.

2.2 Microemulsion Phase Behavior

Microemulsions are thermodynamically stable mixtures of oil, water, and amphiphilic compounds. Stability denotes a time-invariant state. The properties are also independent of the approach to equilibrium. Microemulsions are uniform phases that form spontaneously. Amphiphilic compounds include surfactants and co-solvents. Amphiphilic compounds possess both hydrophilic and lipophilic parts.

2.2.1 Hydrophilic-Lipophilic Balance (HLB)

Griffin (Griffin, 1949) defined the hydrophilic-lipophilic balance (HLB) value to empirically correlate the relative emulsifying and solubilizing properties of surfactants. The HLB values range from 0 to 20. Lower HLB values are more oil soluble and high

values are more water soluble. Surfactants with lower (respectively, higher) HLB values are more soluble in oil (respectively, water) and tend to form water-in-oil (respectively, oil-in-water) emulsions. Davies (Davies, 1957) developed a method for calculating the contributions of different hydrophilic and lipophilic structures to the HLB value. The HLB values can be used to select a surfactant or a mixture of surfactants that form the desired type of emulsion. Each oil is characterized by a required HLB, corresponding to the HLB of the surfactant resulting in the highest solubilization.

The HLB method does not consider the solubilization capacity of the surfactant and the stability of the emulsion. Furthermore, HLD method does not account for the effects of salinity and temperature.

2.2.2 Winsor R Ratio

Winsor (Winsor, 1954) defined the R ratio as the ratio of the net interaction energies between surfactant and oil (E_{CO}) and between surfactant and water (E_{CW}). Later the definition of the R ratio was extended to include the cohesive energies between oil molecules (E_{OO}), water molecules (E_{WW}), surfactant lipophiles (E_{LL}), and surfactant hydrophiles (E_{HH}) (Bourrel et al., 1987).

$$R = \frac{E_{CO} - E_{OO} - E_{LL}}{E_{CW} - E_{WW} - E_{HH}} \quad \textbf{(2.3)}$$

The lipophilic interactions on the oil side and hydrophilic interactions on the water side of the interface determine the curvature of the interface. $R < 1$, $R = 1$, and $R > 1$ correspond to type I, type III, and type II microemulsions, respectively.

Winsor type I microemulsions exhibit two-phase behavior with oil-in-water microemulsion phase in equilibrium with excess oil phase. Winsor type II microemulsions exhibit two-phase behavior with water-in-oil microemulsion phase in equilibrium with

excess water phase. Winsor type III microemulsions exhibit three-phase behavior with a bicontinuous in oil and water microemulsion in equilibrium with excess water and excess oil phases. An increase of the numerator of the R ratio, for example by increasing the surfactant lipophile length, requires a compensating increase of the denominator, for example a decrease of the salinity, to maintain optimum. These changes tend to increase the solubilization ratio and decrease the IFT. The concept was not sufficient to determine how to reach the optimum from the selection of the surfactant, oil, brine, and temperature.

2.2.3 Optimum Salinity Correlations

Salager (1977) proposed an equation for the optimum salinity of ionic surfactants

$$\ln S^* - K \times EACN + C_C - f(A) - a_T \Delta T = 0 \quad \textbf{(2.4)}$$

Bourrel et al. (1980) proposed a similar equation for the optimum salinity of nonionic surfactants

$$bS^* - K \times EACN + \beta - \phi(A) + c_T \Delta T = 0 \quad \textbf{(2.5)}$$

where, S* is the optimum salinity in wt%, EACN is the equivalent alkane carbon number of the oil, C_C (sometimes represented as σ) and β are the characteristic curvatures of the surfactant, f(A) and ϕ(A) are functions that account for the effect of alcohol co-solvents, ΔT is the temperature difference from a reference temperature of 25 °C. K, a_T, and c_T are constants that depend on the type of surfactant. b is a positive constant that depends on the type of salt.

Equations **(2.4** and **(2.5** are linear equations of independent terms. The characteristics of the oil phase were modeled using EACN. The liquid n-alkanes seemed to mimic the microemulsion phase behavior properties of crude oils. The characteristics of the aqueous phase were represented by the concentration of NaCl. For the surfactant, the

parameter usually used was the HLB, which was quite inaccurate, particularly for anionic surfactants. For alkyl anionic surfactants, the adjustable parameters were the head group type and the hydrophobe length. For nonionic (alcohol ethoxylate) surfactants, the adjustable parameters were the number of ethylene oxide groups and the alcohol type. The characteristic curvatures of the surfactant were defined as functions of the adjustable parameters.

The correlations were developed from systematic studies of the effects of the different variables on the optimum salinity. For example, by using different n-alkanes and fixing the surfactant, co-solvent, and temperature, they were able to determine K. By applying these equations, they were able to determine the constants and assign values to various surfactants and co-solvents. For example, at the reference temperature ($\Delta T=0$) without co-solvent ($f(A)=0$), C_C is $K \times EACN - \ln S^*$. Furthermore, for two surfactants at the same conditions (co-solvent, temperature, oil), $C_{C2} = C_{C1} + \ln(S_1^*/S_2^*)$.

2.2.3.1 Characteristic Curvature

For linear alkyl anionic surfactants, the C_C is a function of the carbon number of the hydrophobe (NC) and the type of anionic head group.

$$C_C = 2.5\, N_C + C \tag{2.6}$$

where, C is a constant that depends on the type of head group. For alcohol ethoxylate surfactants, β is a function of the alcohol type and the number of ethylene oxide groups (N_{EO}).

$$\beta = \alpha - N_{EO} \tag{2.7}$$

Where α is a constant that depends on the alcohol.

Hammond & Acosta (2012) developed a correlation for the characteristic curvature of branched C_{12} to C_{13} propoxy sulfate surfactants that included the contribution of adding a methyl branch at the terminal position (C_L), at the beta-carbon position (C_β), and the positions in between (C_{MB}), as well as the contribution of propoxy groups (N_{PO}) and the anionic head group,

$$C_C = 0.1C_L + 0.071C_{MB} + 0.69C_\beta + 0.158N_{PO} + 3.813 \quad \textbf{(2.8)}$$

2.2.3.2 EACN

The value of K is 0.16 for alkyl sulfonates and alkyl carboxylates, 0.1 for alkyl sulfates and alkoxy sulfates, and 0.15 for alcohol ethoxylates. EACN is positively correlated with the optimum salinity. K can be thought of as the derivative of lnS* with respect to the EACN.

2.2.3.3 Alcohol Co-solvent

In general, surfactant goes to the micellar interface, whereas the co-solvent partitions between the oil, brine, and interface. Only the co-solvent at the interface are likely to influence the phase behavior of the microemulsion. The effect of alcohol is a convolution of the interfacial concentration and the structure-effect of the co-solvent. Hence, values of f(A) are generally not transferrable between disparate microemulsion systems because the interfacial concentration of co-solvent changes as a function of the properties and concentrations of the oil, brine, and surfactant as well as temperature (Salager et al., 2013).

2.2.3.4 Temperature

a_T is 0.01 for alkyl anionic surfactants and c_T is 0.06 for alcohol ethoxylate surfactants. The signs for the temperature effect in equations 4 and 5 are opposite, meaning increasing temperature has opposite effects. The optimum salinity increases with temperature for alkyl anionic surfactants and decreases for alcohol ethoxylate surfactants. Nonionic surfactants interact with water predominantly through hydrogen bonding, whereas AA surfactants interact predominantly through ion-dipole interaction. The strength of hydrogen bonds decreases with temperature, whereas the strength of ion-dipole interaction increases with temperature. This opposite trend allows for mixtures of both types of surfactants to produce intermediate behavior insensitive to temperature (Anton, Graciaa, Lachaise, & Salager, 1992). Alcohol alkoxy sulfate surfactants have both types of interactions, so their behavior is a function of the number of alkoxy groups.

2.2.4 Solairaj 2012 Correlation

Solairaj et al. (2012) developed a correlation for the optimum salinity as a function of EACN, temperature, carbon number of the surfactant hydrophobe, and the number of PO and EO units in the surfactant. The correlation rearranged in terms of the natural logarithm of salinity, units of salinity in wt%, and reference temperature of 25 °C:

$$\ln S^* = 0.083\,\mathrm{EACN} + 0.0690\,\Delta T - 0.221\,N_C - 0.285\,N_{PO} - 0.142\,N_{EO} + 5.314 \qquad \textbf{(2.9)}$$

where, N_C is the mole average carbon number of the surfactant, N_{PO} is the mole average number of propyene oxide groups, and N_{EO} is the mole average number of ethylene oxide groups. The coefficients were determined by regression on 33 optimized phase behavior experiments developed at UT Austin. The formulations were mixtures of various

IOS, ABS, alcohol alkoxy sulfate, alcohol alkoxy carboxylate, and alcohol ethoxylate surfactants.

There were several limitations of the correlation for optimum salinity. The total dissolved solids was used for the salinity without taking into account the effect of divalent cations such as calcium in the brines. By lumping the hydrophobe carbons of different branching structures into a single term, the correlation loses the ability to predict the effects of branching. The effect of co-solvent was neglected.

Most importantly, Solairaj et al. (2012) did not develop an equation for the optimum solubilization ratio even though the greatest need is for a model that can be used to predict what formulations will meet the requirements for ultralow IFT.

2.2.5 Hydrophilic-Lipophilic Difference (HLD)

Salager defined the surfactant affinity difference (SAD) as the difference between the standard chemical potential of the surfactant in the water and oil phase. At the optimum salinity, SAD is zero.

$$\mathrm{SAD} = \mu_W - \mu_O = \mathrm{RT} \ln \frac{C_O}{C_W} \tag{2.10}$$

The chemical potential of water increases with salinity, whereas the chemical potential for oil remains constant. At the optimum salinity, SAD is zero. The dimensionless SAD (divided by RT) is defined as the hydrophilic-lipophilic difference (HLD).

$$\mathrm{HLD} = \frac{\mathrm{SAD}}{\mathrm{RT}} = \ln S - K \times \mathrm{EACN} + C_C - f(A) - a_T \Delta T \tag{2.11}$$

$$\mathrm{HLD} = \frac{\mathrm{SAD}}{\mathrm{RT}} = bS - K \times \mathrm{EACN} + \beta - \phi(A) + c_T \Delta T \tag{2.12}$$

Equations **(2.4** and **(2.5** are obtained at the optimum when HLD is zero. The HLD can be used for EOR applications. However, expressing HLD as a linear equation of

independent terms is an oversimplification because mixtures can be non-ideal and terms are interdependent.

2.2.6 Net-Average Curvature

Acosta et al., 2003 introduced the concept of net average curvature (NAC) that assumes the solubilized water and oil in the microemulsion form hypothetical spherical micelles with interfacial area A_S. The HLD-NAC model scales the net curvature of hypothetical spherical micelles to the HLD using the proportionality constant -1/L, where L is the surfactant length parameter empirically found to be related to the length of the surfactant hydrophobe. Several equations have been proposed to calculate L (Acosta, 2008; Acosta et al., 2003). The characteristic length (ξ) limits the maximum average curvature of the hypothetical spheres, indicating the maximum solubilization capacity of the microemulsion. The interfacial area is the summation of the area contributed by the molecules of surfactant and co-solvent at the interface (Basilio et al., 2017). Typically, the characteristic length is calculated from measured solubilization ratios at the optimum salinity of the microemulsion.

The HLD-NAC equations have been expressed in a more useful and practical dimensionless form for applications to EOR modeling (Ghosh & Johns, 2016b). For type III microemulsions, the oil solubilization ratios (σ_O) and water solubilization ratios (σ_W) are given by equations **(2.13** and **(2.14**, respectively:

$$\frac{1}{\sigma_O} = -\frac{3}{2} I \ln \frac{S}{S^*} + \frac{1}{\sigma^*} \quad \textbf{(2.13)}$$

$$\frac{1}{\sigma_W} = \frac{3}{2} I \ln \frac{S}{S^*} + \frac{1}{\sigma^*} \quad \textbf{(2.14)}$$

where, σ^* is the optimum solubilization ratio and the interfacial volume ratio (I) is defined as follows:

$$I = \frac{V_S}{LA_S} \tag{2.15}$$

where, V_S is the volume of surfactants and A_S is the interfacial area of the surfactants. For type I microemulsions, the oil solubilization ratios are given by:

$$\frac{1}{\sigma_O} = -3I \ln \frac{S}{S^*} + \frac{1}{\sigma_W^0} \tag{2.16}$$

where, σ_W^0 is the volume ratio of water to surfactant. For type II microemulsions, the water solubilization ratios are given by:

$$\frac{1}{\sigma_W} = 3I \ln \frac{S}{S^*} + \frac{1}{\sigma_O^0} \tag{2.17}$$

where, σ_O^0 is the volume of oil divided by the volume of surfactant.

The dimensionless form of the HLD-NAC equations uses I as a tuning parameter to fit oil-water solubilization ratio data as a function of salinity, and S^* and σ^* are inputs. In other words, these equations cannot be used to predict which surfactants to use or the optimum condition for a particular formulation. Figure 2.2(a) shows an example of the solubilization ratios for a surfactant mixture of C_{13}-13PO-SO_4 and C_{20-24} internal olefin sulfonate (IOS) with secondary butyl alcohol (SBA) co-solvent at 55°C for a light crude oil. The measured optimum salinity is 2.4 wt%, and the optimum solubilization ratio is 18 cc/cc. HLD-NAC curves were fit using interfacial areas of C_{13}-13PO-SO_4, C_{20-24} IOS, and SBA of 60, 51, 30 A^2 per molecule (Jin et al., 2015; Rosen, 2004).

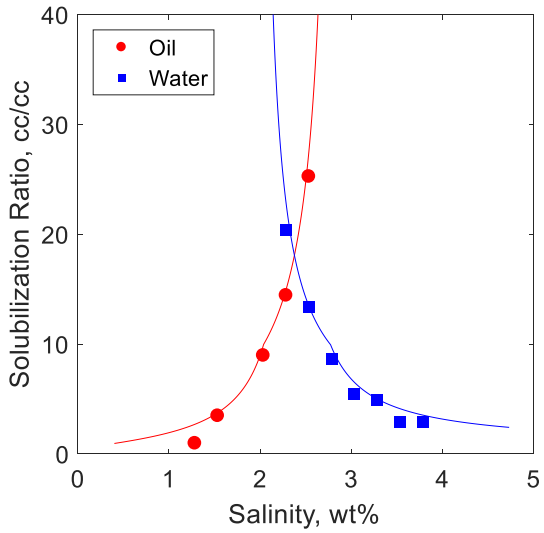

Figure 2.2: HLD-NAC fits the solubilization ratios of 0.5% C_{13}-13PO-SO_4, 0.5% C_{20-24} IOS, 2% SBA, 5000 ppm Na_2CO_3, variable NaCl, 55°C, 50 vol% crude oil K.

2.2.7 Empirical S* and σ* Relationship

The following equation has been proposed (Ghosh & Johns, 2016a) to calculate the optimum solubilization ratio from the optimum salinity:

$$\frac{1}{\sigma^*} = a \ln S^* + b \qquad \textbf{(2.18)}$$

where a and b are constants that depend on the surfactant and, for mixtures, are the molar average of the pure component values (Magzymov et al., 2016). Equation **(2.18** can be used to correlate experimental data. However, there is no advantage to using Equation **(2.18** for chemical formulation development since the same microemulsion phase behavior experiments needed to measure the optimum salinity can also be used to measure the optimum solubilization ratio at the same time. Unlike the approach described in this paper, this correlation does not provide any insight into how to blend the surfactants and co-solvents in the first place to optimize the formulation for EOR or other applications and

how these fundamental variables depend on temperature or the hardness of the brine, or on the effect of soap when the crude oil reacts with alkali. Furthermore, the parameters a and b are known for only a few surfactants. The values for most of the newer surfactants currently used for EOR are not known. The limitation of this approach is analogous to using the characteristic curvature in the HLD model. The biggest challenge is how to decide which surfactants to test in the first place and even more challenging is how to decide what mixtures to test to yield formulations with high performance characteristics for any given reservoir condition. It is also important to validate any model with a very large dataset such as the one used in this study.

2.3 Chemical Structures

Formulations for chemical EOR can include surfactants, co-solvents, alkalis, and polymers. Surfactants are amphiphilic compounds that lower the interfacial tension between two immiscible fluids. The hydrophilic portion of the surfactant molecule is called the hydrophile or hydrophilic head, and the lipophilic portion is called the hydrophobe or lipophilic tail. The salts of fatty acids (R-COONa) are simple surfactants, where the alkyl chain (R) is the tail, the carboxylate group (COO-) is the head, and counterion (Na+) dissociates in aqueous solutions.

A variety of surfactants are used as detergents, wetting agents, emulsifiers, foaming agents, and dispersants. Surfactants are broadly classified by the type of head group: anionic, nonionic, cationic, and amphoteric. Anionic surfactants are by far the most commonly used surfactants in chemical EOR.

This dissertation focuses on anionic surfactants. Anionic surfactants possess a negatively charged head group. The three most common anionic head groups are sulfonates (SO3-), sulfates (SO4-), and carboxylates (COO-).

2.3.1 Sulfonates

Sulfonates are an important class of surfactant for chemical EOR. They are chemically stable at elevated temperatures and the range of pH of interest to EOR.

2.3.1.1 Petroleum Sulfonate

Petroleum sulfonates were the earliest surfactants to be used for chemical EOR and were extensively used and studied in the 1970's and 1980's. These surfactants were produced by sulfonation of crude oil or crude oil distillates. They differ significantly from synthetic sulfonate surfactants because the starting material are more complex mixtures of components (Sandvik et al., 1977).

2.3.1.2 Alkyl Aryl Sulfonate

Alkyl aryl sulfonates are produced by sulfonation of alkyl aromatic hydrocarbons. The alkyl aromatic hydrocarbons are synthesized from normal paraffins (linear alkanes) with mono-unsaturation and benzene, toluene, or xylene. The subsequent surfactants are alkylbenzene sulfonates (ABS), alkyl-toluene sulfonates, and alkyl-xylene sulfonates. Various carbon number cuts are used as the alkyl chains (e.g. C_{12-13}, C_{15-17}).

For ABS surfactants, the benzene is randomly positioned along the linear alkyl chain and the sulfonate is attached to the para position of the benzene ring. ABS surfactants are distributions of both carbon number and positional isomers. ABS surfactants have a twin-tailed structure.

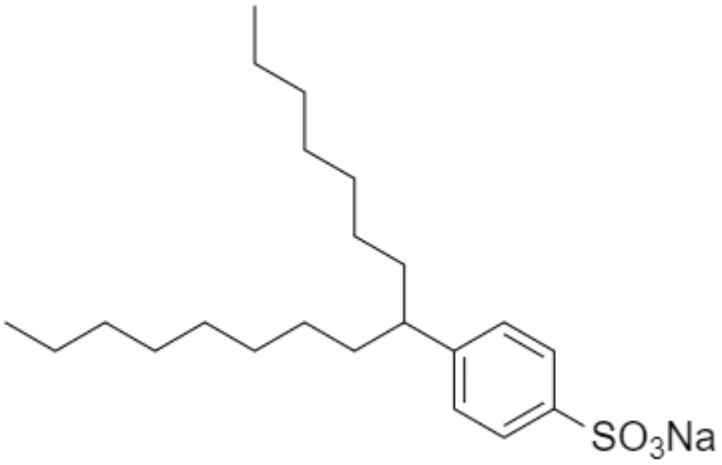

Figure 2.3: Structure of a C16 alkylbenzene sulfonate

2.3.1.3 Olefin Sulfonate

Olefin sulfonate surfactants are produced by sulfonation of olefins (alkenes). The reaction generates a mixture of hydroxyalkane sulfonates, alkene sulfonates, and disulfonates. Alpha olefin sulfonates (AOS) are produced by the sulfonation of terminal alkenes. Internal olefin sulfonates (IOS) are produced by the sulfonation of alkenes where the double bond is randomly positioned along the molecule. The carbon number distribution and the degree of branching of the olefins can vary. The degree of sulfonation (ratio of disulfonate and monosulfonate species) can also vary but are kept very low as the disulfonate is very hydrophilic.

IOS surfactants are mixtures of chemical species with distributions of positional isomers and carbon numbers. Like ABS, IOS surfactants have a *twin-tailed* structure. The alkyl chain of IOS surfactants are typically branched whereas the alkyl chain of ABS surfactants is nearly always linear. Both ABS and IOS are complex surfactant mixtures that tend to minimize the formulation of ordered structures such as liquid crystals and gels.

AOS surfactants have a single tailed structure that tend to pack more closely and have higher viscosity. Consequently, AOS surfactants are not commonly used for SP or ASP but rather for foam flooding and viscous microemulsion flooding.

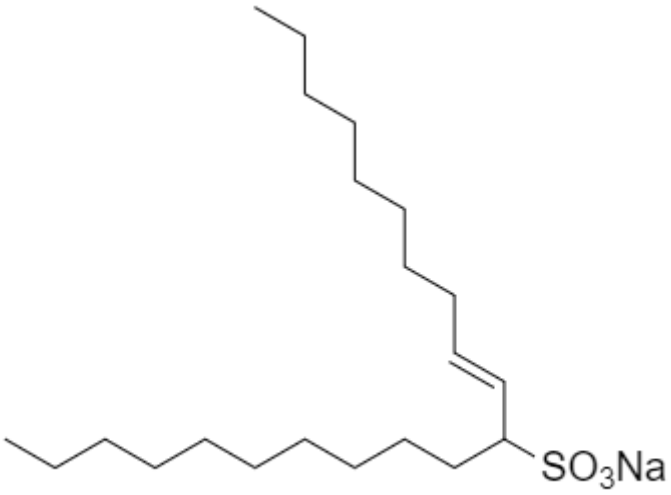

Figure 2.4: Structure of a C16 internal olefin sulfonate

2.3.2 Sulfates and Carboxylates

Modern sulfate and carboxylate surfactants used for EOR are alcohol alkoxy sulfate and alcohol alkoxy carboxylate surfactants. Typically, a block of propylene oxide (PO) groups, followed by a block of ethylene oxide (EO) groups, separate the alcohol from the head group. The PO and EO groups extend the lipophilic and hydrophilic portions of the surfactant and create a more gradual lipophilic to hydrophilic transition. The groups, PO to some extent and EO more so, enhance the tolerance to divalent cations, which complex readily with the anionic groups.

The alcohol alkoxy sulfate are produced by sulfation reaction of the alcohol alkoxylate with sulfur trioxide, chlorosulfonic acid, or sulfamic acid, followed by

neutralization. The hydrolytic stability of the ethoxy-sulfate bond depends on the temperature and pH (Adkins et al., 2010; Talley, 1988). Generally, alcohol alkoxy sulfate surfactants are not recommended for chemical EOR at reservoir temperatures above 65 °C unless the pH can be maintained at approximately 10 such as with sodium carbonate. The alcohol alkoxy carboxylate are produced by carboxymethylation reaction of the alcohol alkoxylate with chloroacetate. The carboxylate surfactants are highly thermally and chemically stable.

There are many hydrophobe structures used for alcohol alkoxy sulfate and carboxylate surfactants. The hydrophobes can be generally categorized into four types: near-midpoint branched, slightly branched, bent, and aromatic hydrophobes.

The (near) midpoint branched hydrophobes are the Guerbet alcohols and epoxide alcohols. These are considered to be large and approximate midpoint branched hydrophobes. The Guerbet alcohols are synthesized in the Guerbet reaction in which two primary aliphatic alcohols are dimerized forming a β-branched dimer alcohol. The epoxide alcohols are formed by the condensation of an alcohol with a 1,2 linear alkyl epoxide molecule. Guerbet alkoxy sulfate and carboxylate surfactants have high performance and low costs and work exceptionally well with high EACN oils, which require large hydrophobes and branched structures (Adkins et al., 2010, 2012; Lu et al., 2014). The hydrophobes range from 16 to 32 carbons.

The slightly branched hydrophobes include C_{13} tridecyl alcohol (TDA), $C_{16\text{-}17}$ (Neodol 67), and $C_{12\text{-}13}$ (Neodol 23) hydrophobes. The synthesis of these hydrophobes vary by manufacturer, but the hydrophobes are all slightly branched, possessing varying degrees of methyl branches. The hydrophobe is typically combined with propoxy sulfates.

A bent hydrophobe, specifically the oleyl alcohol, is a C_{18} alcohol with a cis double bond at the 9-10 carbon position, which creates a bend in the molecule that imparts a

branching effect. Consequently, they exhibit surfactant behavior reminiscent of a large hydrophobe surfactant.

Aromatic hydrophobes, specifically tristyrylphenol, has been demonstrated to be highly effective with waxy and high acid number crude oils to exhibit ultra-low IFT and low microemulsion viscosities with surrogate and live oils (Liyanage et al., 2012). They show special affinity towards oils containing high levels of resins and asphaltenes.

2.3.3 Alkali

Many alkalis have been tested for chemical EOR processes such as sodium hydroxide, sodium carbonate, ammonia, sodium metaborate, sodium silicate, sodium tetraborate, and organic alkalis. The main purposes of alkali are to (1) increase the pH and (2) react with acids in crude oils to generate soap. Increasing the pH can decrease the surfactant retention by switching the surface change of minerals from positive to negative. The soaps generated from the neutralization of acids can reduce the need for synthetic surfactants. In order to use alkali, the divalent cations in the brine are typically removed or chelated.

2.3.4 Soaps

Alkalis can react with acids in crude oils to generate soaps. The soaps can behave as additional surfactant and affect the phase behavior (Nelson et al., 1984). The total acid number (TAN) is defined as the milligrams of potassium hydroxide needed to neutralize one gram of crude oil. The soaps that are generated from an oil depend on the pH. With increasing pH, higher pKa components are neutralized, and their amphiphilic products may behave synergistically or antagonistically. Thus, the soaps generated using different alkali (e.g. sodium carbonate versus sodium hydroxide) can behave differently.

2.3.5 Co-solvents

Co-solvents used in chemical EOR are typically short chain aliphatic alcohols such as sec-butyl alcohol (SBA) and iso-butyl alcohol (IBA). Alcohol ethoxylates and alcohol propoxy ethoxylates are newer co-solvents that have are effective at lower concentrations (Sahni et al., 2010; Upamali et al., 2016).

Co-solvents serve many purposes in chemical EOR formulations. Co-solvent help prevent or break macroemulsions which reduces the time required for microemulsions to coalesce or equilibrate (Bourrel & Schechter, 1988). This is especially beneficial for EOR when the macroemulsions, gels, or liquid crystals have a high viscosity. Co-solvents also reduce the microemulsion viscosity and prevent or minimize non-Newtonian rheology (Fortenberry et al., 2015a; Jang et al., 2016; Tagavifar et al., 2016; Walker et al., 2012). Co-solvents also alter phase behavior, often increasing the solubility of the surfactant in brine (Sahni et al., 2010). Co-solvents are often needed for aqueous stability, especially when as usual polymer is also in the aqueous solution. However, co-solvents increase the IFT and consequently decrease solubilization ratios. For alkaline polymer flooding, co-solvents widen the type III window and reduce the bulk emulsion viscosity and the interfacial viscosity (Fortenberry et al., 2015a).

In general, surfactant goes to the micellar interface, whereas the co-solvent partitions between the oil, brine, and interface. Only the co-solvent at the interface are likely to influence the phase behavior of the microemulsion.

Ternary diagrams are used to represent the phase behavior surfactant, oil, and water. With a partitioning co-solvent, tetrahedric diagrams are needed to represent the phase behavior. The use of pseudocomponents, in which the co-solvent is distributed among the other three components, is a convenient method to reduce dimensionality (Hirasaki, 1982;

Prouvost et al., 1984; Prouvost et al., 1985). The distribution is such that, for any overall composition in the plane formed by the three pseudocomponents, any phase separation must result in phase compositions that lie in the same plane. The plane is a pseudoternary diagram that is a slice through the tetrahedric diagram. The microemulsion phase is a mixture of the aqueous (water + co-solvent), oleic (oil + co-solvent), and interfacial (surfactant + co-solvent) pseudocomponents. The concentrations of co-solvent in the three pseudocomponents are determined by two partition coefficients.

The distinction between surfactant and co-solvent is not always clear cut. Intermediate molecules such as certain nonionic surfactants and lipophilic linkers vary in the degree of partitioning and their effect on solubilization.

CHAPTER 3: UT CHEMICAL EOR DATABASE

The UTCEOR Database is a collection of highest-quality experimental data conducted at The University of Texas at Austin from 2005 to 2018. The database includes the data published in theses and dissertations (Chang, 2014; Dean, 2011; Flaaten, 2007; Fortenberry, 2013; Li, 2016; Lu, 2014; Sahni, 2009; Solairaj, 2011; Unomah, 2013; Walker, 2011; Wang, 2018; Winters, 2012; Yang, 2010) and data published in conference and journal papers (Adkins et al., 2010, 2012; Chang et al., 2019; Flaaten et al., 2009; Jang et al., 2014, 2016; Levitt et al., 2009; Li et al., 2017; Liyanage et al., 2012, 2015; Maubert et al., 2018; Rajapaksha et al., 2014; V. Sahni et al., 2010; Sharma et al., 2016(a), 2016(b); Solairaj et al., 2012(a), 2012(b); Tagavifar et al., 2016; Upamali et al., 2016; Walker et al., 2012; Wang et al., 2018; Yang et al., 2010; Zhao et al., 2008). The database contains over 2000 microemulsion phase behavior experiments, over 1000 aqueous stability tests, over 300 coreflood experiments, over 400 polymer rheology measurements (Kim et al., 2010; Koh, 2015; Kulawardana et al., 2012), and over 100 microemulsion rheology measurements. These experiments used 36 unique crude oils, 294 unique surfactants, and 70 unique co-solvents. The purpose of a database is to store and retrieve data in a way that is accurate and effective. With custom-made tools the database served as a convenient platform to compile, check, manipulate, visualize, and analyze the data.

The data was used to develop the structure-property models, so the database facilitated the main research objective. The data was pooled from the thousands of experiments involved in the research, development, and optimization of formulations for chemical EOR under a wide variety of reservoir conditions. Collectively, the data has more value.

Not all experiments in the database were used to develop the model, because the focus was the phase behavior of blends of anionic surfactants and nonionic co-solvents. The database serves as a powerful tool for gathering and analyzing data. As such, there is useful information that has yet to be discovered in the database which should be considered for future work.

3.1 Methodology

3.1.1 Incorporating Laboratory Experiments

Microemulsion phase transitions are brought about by changing the electrolyte composition or concentration (salinity, hardness), temperature, pressure, surfactant composition (e.g. the ratio of two surfactants is changed), co-solvent concentration, and oil composition. The salinity changes are most often used in what are called salinity scans. In the salinity scans, all other variables - surfactants, co-solvents, oil, and temperature – are fixed and only the salinity is varied. The salinity can be changed by adding salts such as NaCl or $CaCl_2$, by adding an alkali such as Na_2CO_3, or by blending oilfield brines or more commonly synthetic approximations of actual oilfield brines, or by any combination of these options.

Salinity scans are the most practical and convenient method of observing microemulsion phase transitions. Consequently, nearly all microemulsion phase behavior experiments were salinity scans. Therefore, salinity scans and microemulsion phase behavior experiments are used synonymously in this dissertation.

The salinity scans are conducted in sealed graduated glass pipettes. Typically, the scanned salinity window spans 50,000 ppm with increments of 5000 ppm. Salinity scans done without crude oil are called aqueous stability tests or aqueous phase behavior tests.

The main objective of the aqueous stability test is to determine the salinity in which phase separation occurs. Aqueous stability tests are conducted in capped vials or sealed glass ampules depending on the reservoir temperature.

For each project, different combinations of surfactants and co-solvents with the reservoir crude oil and reservoir brines were used in microemulsion phase behavior and aqueous phase behavior tests. This was done iteratively until a formulation was found that exhibited ultra-low IFT and aqueous stability at or above the optimum salinity. The optimum salinity and interfacial tension can be qualitatively determined within hours or days of initial mixing using the emulsion test, depending on the oil properties, temperature, and how often the samples are mixed. With some viscous and active crude oils, it takes several days to generate the soap. Typically, the aqueous stability limit can be determined in less time.

For practical reasons, experiments exhibiting low IFT were kept and monitored more closely than those that did not exhibit low IFT. The fluid interfaces were recorded to calculate the phase volumes and solubilization ratios. The interfaces were recorded over time to determine the change in the phase behavior with time. The best formulations were often repeated multiple times.

Oftentimes, a formulation does not exhibit low interfacial tension within the measured salinity window. This can be due to the optimum being lower or higher than the minimum or maximum scanned salinity, the low IFT region being very narrow, or the formulation is not suitable for the particular oil, temperature and other experimental conditions. These experiments are often monitored significantly less than the better candidates. Interfaces may not be read and only qualitative observations recorded.

Thus, the experimental data are biased toward low IFT formulations. From a modeling perspective, it would be desirable to have more complete data even for

formulations with high IFT. In other cases, undesirable viscous macroemulsions, birefringent phases, gels, and multiple phases with unknown properties form and can persist for extended periods of time. Formulations with such phase behavior do not pass the initial screening test and thus are eliminated with the exception that macroemulsions that do not persist and are not too viscous may be acceptable.

Not all experiments are monitored at the same intervals or for the same duration. Information related to the coalescence rate of emulsions after mixing the fluids is not generally quantitative. Qualitative information is not always recorded. In some cases, the observations are not continued over sufficiently long time periods for the phases to reach equilibrium either because the phases appear to be at equilibrium but are not actually at equilibrium, or because of project deadlines or other similar non-scientific reasons.

The most important criteria for inclusion of the experimental data in the database was that they were at or near equilibrium. Those experiments with more frequent measurements have lower uncertainty. The solubilization ratios asymptotically approach the equilibrium solubilization ratios over time.

The models developed in this dissertation do not attempt to cover all chemical structures but instead focuses on blends of of anionic surfactants and nonionic co-solvents. As such, it was important for wide varieties of surfactant and co-solvent mixtures and reservoir conditions to be used to train the models. However, there were some combinations that were either rarely tested or rarely successful and introduce a form of bias.

For example, carboxylate surfactants are typically only used at temperatures above 70 °C. Sulfates can only be used at temperatures above 70 °C if the pH is buffered between 9 and 11 (e.g. with Na_2CO_3 or $NaBO_2$) because of autocatalytic hydrolysis of the sulfate head group in acidic and extremely basic conditions. For certain conditions, only

carboxylate and sulfonate surfactants can be used. At temperatures below 70 °C, both sulfate and carboxylate surfactants can be used, but the sulfate head group is more hydrophilic than carboxylate head group, so sulfate surfactants generally perform better, especially in terms of aqueous stability. The carboxylate surfactants predominantly used C_{24} to C_{32} Guerbet alcohol or oleyl alcohol as hydrophobes, which is likely due to some bias for crude oils at high temperature.

3.1.2 HLD-NAC Curve Fitting

As shown in the literature review, HLD-NAC can be used to fit relatively symmetric solubilization ratios as shown in **Figure 2.2**. However, with asymmetric phase behavior data such as those shown in **Figure 3.1**, the fit to the data is less satisfactory. In **Figure 3.1**, the HLD-NAC model with $I = 0.13$ fits the oil solubilization ratios but overestimates the water solubilization ratios. Using $I = 0.28$ gives a better fit of the water solubilization ratios but underestimates the oil solubilization ratios. Therefore, two interfacial volume parameters – one for oil and one for water – were used to fit asymmetric phase behavior data such as show in **Figure 3.1**.

All of the solubilization ratio data were fit using the dimensionless HLD-NAC equations. The optimum salinity and optimum solubilization ratio were estimated from the best fit to the experimental data.

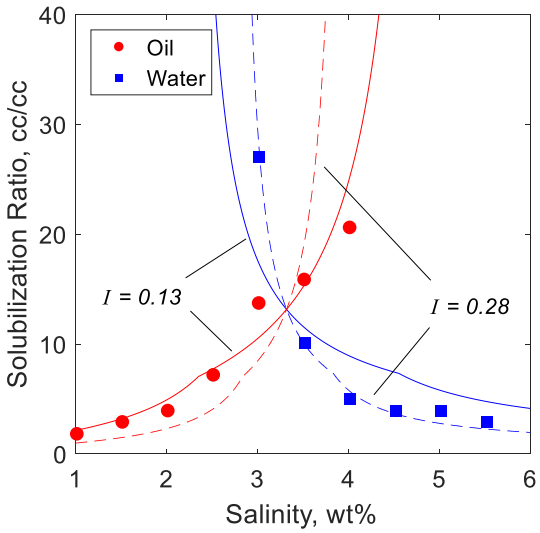

Figure 3.1: HLD-NAC fails to fit asymmetric solubilization ratio data of 0.4% C_{18}-45PO-30EO-COO, 0.6% C_{19-28} IOS, 0.5% Phenol-2EO, variable $NaBO_2$, 40 vol% crude oil E with 28 wt% hexadecane.

3.2 Organization of the Database

The method of storing the experimental data went through multiple iterations, starting as an MS Excel spreadsheet, then transitioning to MS Access database, and currently settling as a MATLAB data structure. A conventional relational database structure was not used because to accommodate the multitude of ways phase behavior experiments and coreflood experiments were conducted required the data to be split into 4-7 hierarchal levels with tables running in series and parallel. In this form, the data was too disjointed and required intimate knowledge of the relationships and the querying language to retrieve the data. In other words, it was incredibly not user-friendly. The current MATLAB iteration of the UTCEOR Database retains some of the functionality of a conventional relational database but is a custom-made structure array that is much easier to navigate. The data was retrieved not by a querying language but by a bit of coding.

The exact structure of the database is not critically important. The data can be easily transferred to a true relational database as referential integrity was strictly enforced. The main takeaways are what information about each experiment was stored and how the data were logically connected.

The database file is a custom MATLAB class called *clsExpts* with defined properties and methods that operate on the data. The first level of the database is described in Table 3.1. The first level contains (1) the list of experiments (*expt*), (2) the list of surfactants and co-solvents (*chemicals*), (3) the list of field brines (*brines*), (4) list of salts (*electrolytes*), (5) list of additives (*additives*), and (6) the list of the properties of the dead crude oils and pure hydrocarbons (*oilProperties*). The *chemicals*, *brines*, *electrolytes*, *additives*, and *oilProperties* arrays will be referred to as data tables. The data tables describe all of the components used in all of the phase behavior experiments. The components used in each phase behavior experiment are logically connected to the data in the data tables.

Table 3.1. Description of tables in the UTCEOR Database

Field Name	Class	Description
expt	structure	List of experiments
chemicals	structure	List of surfactants and co-solvents
brines	structure	List of brines
electrolytes	structure	List of salts
additives	structure	List of additives
oilProperties	structure	List of dead crude oils and pure hydrocarbons

3.2.1 Chemicals Data Table

The *chemicals* data table is a structure array containing the information of all of the surfactants and co-solvents. **Table 3.2** shows the names, class types, and descriptions of the fields of the *chemicals* structure array. Each element (row) corresponds to a surfactant or co-solvent. The *name* field is the molecular structure (e.g. 'C28-45PO-30EO-COO-', 'C15-18 IOS', 'C12 ABS', 'C18-35PO-20EO-SO4-') and is a unique identifier of the chemical. The *type* field has values of either 'Surfactant' or 'Co-solvent'.

The *NC*, *rings*, *doubleBonds*, and *hydrophobe* fields describe the hydrophobe structure, where *NC* is the average number of carbon atoms (e.g. 30 for tristyrylphenol, 18 for oleyl alcohol, 16.5 for C15-18 IOS, etc.), *rings* is the number of rings (e.g. 4 for tristyrylphenol, 1 for phenol), *doubleBonds* is the number of double bonds (e.g. 1 for oleyl alcohol, 3 for phenol, etc.), and *hydrophobe* indicates the branching type. The values for *hydrophobe* include 'IOS' for internal olefin sulfonate surfactants, 'ABS' for alkylbenzene sulfonate surfactants, 'US' for the ultra-short 2-ethyl-hexanol hydrophobe, 'S' for short-chain-branching hydrophobes, 'L' for large-chain-branching or approximate midpoint-branching hydrophobes, 'B' for the oleyl alcohol hydrophobe, and 'A' for the tristyrylphenol hydrophobe, 'aliphatic' for aliphatic alcohol-based co-solvents (e.g. iso-butanol, iso-butanol ethoxylate) , and 'aromatic' for phenol-based co-solvents (phenol ethoxylate). The *NBO*, *NPO*, and *NEO* fields are the average number of butylene oxide (BO), propylene oxide (PO), and ethylene oxide (EO) groups, respectively, in the surfactant or co-solvent molecule. The *HG* field indicates the type of polar head group with values including 'IOS' for sulfonate head group of internal olefin sulfonate surfactants, 'ABS' for the benzene sulfonate head group of alkylbenzene sulfonate surfactants, 'SO4' for the sulfate head group, 'COO' for the carboxylate head group, and 'nonionic' for

nonionic surfactants and co-solvents. The *MW* field is the molecular weight of the molecule in grams per mole, which is calculated from the previous structure properties assuming anionic surfactants are sodium salts.

Table 3.2. Description of the chemicals data table

Field Name	Class	Description
name	char	Chemical structure
type	char	'surfactant' or 'co-solvent'
NC	double	Number of carbon atoms in the hydrophobe
rings	double	Number of rings in the hydrophobe
doubleBonds	double	Number of double bonds in the hydrophobe
NBO	double	Number of butylene oxide groups in molecule
NPO	double	Number of propylene oxide groups in molecule
NEO	double	Number of ethylene oxide groups in molecule
HG	char	'IOS', 'ABS', 'SO4', 'COO', or 'Nonionic'
hydrophobe	Char	'ABS', 'IOS', 'US', 'S', 'L', 'B', 'A', 'aliphatic', 'aromatic'

3.2.2 Brines Data Table

The *brines* data table is a structure array containing the compositions of the field brines. **Table 3.3** shows the field names of the *brines* structure array. Each element corresponds to a brine. The *name* field is the abbreviated name of the brine. The *ions* field is a vector of the concentrations of ions in ppm. The *TDS* field is the sum of the concentrations of all the ions. The *map* field is a cell array containing the names of the ions in the corresponding positions of the *ions* vector. The *name* field is used as the unique identifier of brines.

Table 3.3. Description of brines data tables

Field Name	Class	Description
name	char	Brine name
ions	vector	Vector of ion concentrations (ppm)
TDS	double	Sum of ions (ppm)
map	cell	Name of ions in ions vector

3.2.3 Electrolytes Data Table

The *electrolytes* data table is a structure array containing information on each salt. **Table 3.4** shows field names of the *electrolytes* structure array. Each element corresponds to a salt. The *name* field is the molecular formula of the salt (e.g. Na_2CO_3, NaCl, $NaBO_2$) and *ions* field is the vector of the concentrations of ions in ppm with positions corresponding to those in the *map* field. The *name* field is used as the unique identifier for salts.

Table 3.4. Description of electrolytes data table

Field Name	Class	Description
name	char	Salt name
ions	vector	Vector of ion concentrations (mass fraction)
map	cell	Name of ions in ions vector

3.2.4 Additives Data Table

The *additives* data table is a structure array containing the information of each additive. Additives include polymers, reducing agents, sacrificial agents, and chelating agents. Thiourea and IPA are examples of sacrificial agents that were added together to fluids to react with free radicals that would degrade the polymer. Thus it was called the polymer protection package. **Table 3.5** show the field names of the *additives* structure array. The *name* field is the name of the additive (e.g. FP 3330S, sodium isoascorbate) and serves as the unique identifier.

Table 3.5. Description of additives data table

Field Name	Class	Description
name	char	Additive name
ions	vector	Vector of ion concentrations (mass fraction)
map	cell	Name of ions in ions vector

3.2.5 Oil Properties Data Table

The *oilProperties* data table is a structure array containing the information of all the dead crude oils and pure hydrocarbons. **Table 3.6** show the field names of the *oilProperties* structure array. The *name* field is the name of the oil. The *MW*, *EACN*, *Vm*, *density*, *TAN*, and *SARA* fields are the molecular weight in g/mol, equivalent alkane carbon number, molar volume in cc/mol, density in g/cc, and total acid number in mg KOH/g oil, and the content of saturates (SAT), aromatics (ARO), resins (NSO), and asphaltenes (ASP) in mass fraction. Each of these fields can contain multiple measurements of the property but at most one can be set as default. The default values are used for logically connecting

data. The active field indicates by true or false whether the oil is considered to be an active crude oil (i.e. forms soap in the presence of alkali that has a measurable shift on phase behavior).

Table 3.6. Description of oil properties data table

Field Name	Class	Description
name	char	Name of the oil
MW	double	Molecular weight (g/mol)
EACN	double	Equivalent alkane carbon number
active	Boolean	True or false
Vm	double	Oil molar volume (ml/mol)
density	double	Oil density (g/ml)
TAN	double	Total acid number (mg KOH/g oil)

3.2.6 Experiment List

The *expt* structure array contains the microemulsion phase behavior and aqueous stability experimental data. Each element corresponds to a grouping of experiments that share the same formulation. **Table 3.7** shows the field names of the *expt* structure array.

The *company*, *project*, *abbreviation*, and *name* fields are the name of the company that provided the crude oil, the project (field) name, the project abbreviation, and the name of the experiment, respectively. The *name* field is the unique identifier of experiments. The *experimentalist* field is the name of the experimentalist responsible for the experiment. The *formulation* field is a structure array containing the chemical and ion compositions that may be fixed and scanned in the experiments. The *aqs* field is a structure array containing

the aqueous stability test data. The *pb* field is a structure array containing the microemulsion phase behavior data.

Table 3.7. Description of experiments data table

Field Name	Class	Description
company	char	Name of the company
project	char	Name of the project
abbreviation	char	Project abbreviation
name	char	Name of the experiment
experimentalist	char	Name of experimentalists
formulation	structure	List of surfactants, co-solvents, electrolytes, and additives
aqs	structure	Aqueous stability test data
pb	structure	Microemulsion phase behavior (salinity scan) data

3.2.6.1 Formulation Structure Array

The *formulation* structure array contains the *chemicals*, *electrolytes*, and *additives* structure arrays. **Table 3.8** shows the field names of the *formulation* structure array and the nested structure arrays. Each element of the *chemicals* structure array corresponds to a surfactant or a co-solvent. The *chemicals* structure array contains the *structure*, *name*, *lotnum*, and *conc* fields, which correspond respectively to the chemical structure, commercial name, batch identification number, and concentration in aqueous mass fraction of that chemical.

The *electrolytes* structure array contains the *scanning*, *fixed*, and *brines* fields. The *scanning* field is the molecular formula of the scanning electrolyte (e.g. Na2CO3 scan in brine). The *scanning* field is empty if no scanning electrolyte was used (e.g. salinity scan

varying the ratio of two brines). Each element of the *fixed* structure array corresponds to an electrolyte that was kept at a constant concentration in the experiment. The *fixed* structure array contains the *name* and *conc* fields, which are the molecular formula and concentration in ppm, respectively, of the fixed electrolytes. Each element of the *brines* structure array corresponds to a brine with name specified by the *name* field. The formulations can have either one scanning electrolyte and one brine or no scanning electrolyte and 2 brines. The concentrations of brine are not specified because, in the former, the activity of the brine is assumed to be 100% and, in the later, the sum of the activities is assumed to be 100%.

Each element of the *additives* structure array corresponds to an additive that was kept at a constant concentration in the experiment. The *additives* structure array contains the *name* and *conc* fields, which are the molecular formula and concentration in ppm of the additive.

The *chemicals.structure*, the *electrolyte.scanning*, the *electrolytes.fixed.name*, the *electrolytes.brines.name*, and the *additives.name* were unique identifiers that connect the data to the chemicals, electrolytes, brines, and additives data tables.

Table 3.8. Description of formulation structure array

Field Name	Class	Description
chemicals	structure	List of surfactants and co-solvents
chemicals.structure	char	Chemical structure
chemicals.name	char	Commercial name
chemicals.lotnum	char	Lot Number
chemicals.conc	double	Concentration in mass fraction of aqueous phase
electrolytes	structure	List of salts and brines
electrolytes.scanning	char	Name of scanning electrolyte
electrolytes.fixed	structure	List of fixed electrolytes
electrolytes.fixed.name	char	Name of fixed electrolyte
electrolytes.fixed.conc	double	Concentration of fixed electrolyte (ppm)
electrolytes.brines	structure	List of brines
electrolytes.brines.name	char	Name brine
additives	structure	List of additives
additives.name	char	Name of additive
additives.conc	double	Concentration of additive (ppm)

3.2.6.2 Aqueous Stability Test Structure Array

The *aqs* structure array contains the *polymer* and *data* structure arrays. **Table 3.9** shows the field names of *aqs* structure array and the nested structure arrays. The *polymer* structure array contains the *name* and *conc* fields, which are the name and concentration in ppm of the polymer used in the aqueous stability experiments. The *data* structure array contains the *temp* and *aq_limit* fields, which are the experimental temperature and the

aqueous stability limit in ppm TDS, respectively. The *aq.polymer.name* is a unique identifier for the polymer.

Table 3.9. Description of the aqueous stability test structure array

Field Name	Class	Description
polymer	structure	Polymer properties
polymer.name	char	Polymer name
polymer.conc	double	Polymer concentration (ppm)
data	structure	List of aqueous stability data
data.temp	double	Temperature (°C)
data.aq_limit	double	Aqueous stability limit (ppm TDS)

Microemulsion Phase Behavior Structure Array

The *pb* structure array contains the *oil* and the *scan* structure arrays. **Table 3.10** shows the field names of the *pb* structure array and the nested structure arrays. The *oil* structure array contains the *name* field and *composition* structure array, which are the name and composition of the oil phase used in the microemulsion phase behavior experiment. An example of oil.name is 'Crude E + 7% Toluene'. Each element of the *composition* structure array corresponds to an oil component. The names and mass fractions are specified by the *name* and *massFraction* fields.

Each element of the *scan* structure array corresponds to the interface measurements of the microemulsions in a salinity scan. The *temperature*, *C2, datemade*, *dateread*, and *age* fields are the experimental temperature in Celsius, the oil phase volume fraction, the dates the salinity scan was made, the date the salinity scan was read, and the corresponding

time difference in days. The data, optimum, HLDNAC, and asymHLDNAC fields are structure arrays.

Each element of the *data* structure array corresponds to a sample of the salinity scan. The fields TDS, aq_level, top_int, bot_int, SRO, and SRW are the salinity in ppm TDS, the level of the aqueous phase initially, the level of the lower interface of the microemulsion, the level of the upper interface of the microemulsion, the oil solubilization ratio, and the water solubilization ratio. The interface levels and solubilization ratios have units of ml and cc/cc.

The *optimum* structure array contains the *salinity* and *solubilizationRatio* fields, which are the optimum salinity in ppm TDS and the optimum solubilization ratio in cc/cc, respectively. The *HLDNAC* field and the *asymHLDNAC* field are structure arrays containing parameters and statistics related to the fits of HLD-NAC and asymmetric HLD-NAC equations to the solubilization ratios.

Table 3.10. Description of the microemulsion phase behavior structure array

Field Name	Class	Description
oil	structure	Properties of the oil phase
oil.name	char	Name of the oil phase
oil.composition	char	List of components in the oil phase
oil.composition.name	char	Name of component
oil.composition.massFraction	double	Mass fraction of component
scan	structure	List of salinity scans
scan.temperature	double	Temperature (°C)
scan.C2	double	Volume fraction of oil
scan.datemade	Date	Date made
scan.dateread	Date	Date read
scan.age	double	Age at reading (days)
scan.data	structure	List of data for each pipette in salinity scan
scan.data.TDS	double	Salinity (ppm TDS)
scan.data.aq_level	double	Initial aqueous level (ml)
scan.data.top_int	double	Top of microemulsion level (ml)
scan.data.bot_int	double	Bottom of microemulsion level (ml)
scan.data.SRO	double	Solubilization ratio of oil (vol/vol)
scan.data.SRW	double	Solubilization ratio of water (vol/vol)
scan.optimum	structure	Position of the optimum from crossover
scan.optimum.salinity	double	Optimum salinity (may also be from emulsion test)
scan.optimum.solubilizationRatio	double	Optimum solubilization
scan.HLDNAC	structure	See Table 3.11
scan.asymHLDNAC	structure	See Table 3.11

Table 3.11 shows the fields names of the *HLDNAC* and the *asymHLDNAC* structure arrays. The *includedOil* and *includedWater* fields are vectors of true or false corresponding to the sample of the salinity scan. True values indicate that the corresponding oil or water solubilization ratio was used in the curve fit. The *S*, *SR*, *aOil*, and *aWater* fields are the optimum salinity in ppm TDS, optimum solubilization ratio, $\frac{3}{2}I$ used to fit the oil solubilization ratios, and $\frac{3}{2}I$ used to fit the water solubilization ratios, where I is the interfacial volume parameter (Ghosh & Johns, 2016b). The *SQERR*, *numdata*, and *stdev* fields are the square error, total number of data points, and the standard error of the curve fit.

Table 3.11. Description of the HLD-NAC structure array

Field Name	Class	Description
includedOil	vector	Vector of true/false for each oil solubilization ratio
includedWater	vector	Vector of true/false for each water solubilization ratio
S	double	Optimum salinity (ppm TDS)
SR	double	Optimum solubilization ratio (cc/cc)
aOil	double	3/2*I used to fit oil solubilization ratio
aWater	double	3/2*I used to fit water solubilization ratio
SQERR	double	Sum of the square error
numdata	double	Sample size
stdev	double	Standard error

3.3 Discussion

The data for thousands of high-quality microemulsion phase behavior, aqueous stability, polymer rheology, microemulsion rheology, and coreflood tests were compiled

in the UTCEOR Database. The data was thoroughly checked, stored, and logically connected. Several tools were developed that supported the data-driven approach. The tool functions included (1) sorting and organizing thousands of experiments that have never been compiled (2) appending and manipulating new data, (3) querying the database, and (4) visualizing the data. Querying and visualization of data is convenient and can be used as a form of quality control.

The database contains the data for thousands of experiments. All of the data uses consistent surfactant, co-solvent, salt, brine, additive, and oil names such that the database has referential integrity. Therefore, the contents of the database can be transferred with relative ease to a more convenient format, such as a conventional relational database which can be queried or an excel spreadsheet. Doing so may make the database more user-friendly and effective.

Nearly all surfactants and co-solvents are distributions of molecules. IOS and ABS surfactants are distributions of carbon numbers, isomers, degrees of ramifications, numbers and types of head groups, etc. The numbers of PO and EO groups in surfactant and co-solvent molecules inherently follow distributions related to reaction kinetics. The properties of the surfactants and co-solvents that are captured in the *chemicals* data table are the average molecular structures reported by the manufacturers which may not be representative of the molecular structure (e.g. if the distribution is especially skewed or there is large variation in degree of ramification). The batch numbers of the surfactants, co-solvents, polymers, and crude oils were tracked for most experiment, so it may be possible to account for batch-to-batch variation and improve the subsequent models.

CHAPTER 4: CO-SOLVENT PARTITIONING MODEL

This chapter is devoted to the development of correlations for estimating the partition coefficients of co-solvents in microemulsions. The partition coefficients can be used to estimate the fraction of co-solvent that partitions to the micellar interface and influences the phase behavior.

Microemulsion phase behavior with co-solvent is modeled as a tetrahedric diagram at fixed temperature, pressure, and salinity. Four pseudocomponents are the surfactant, co-solvent, water (brine), and oil. The use of pseudophases, in which the co-solvent is distributed among the other three components, is a convenient method to reduce dimensionality (Hirasaki, 1982; Prouvost et al., 1984; Prouvost et al., 1985) as shown in **Figure 4.1**. The distribution is such that, for any overall composition in the plane formed by the three pseudophases, any phase separation must result in phase compositions that lie in the same plane. The plane is a pseudoternary diagram that is a slice through the tetrahedric diagram. The microemulsion phase is a mixture of the aqueous (water + co-solvent), oleic (oil + co-solvent), and interfacial (surfactant + co-solvent) pseudophases. The concentrations of co-solvent in the three pseudophases are determined by two partition coefficients, the oil-water partition coefficient (K_{OW}) and the interface-water partition coefficient (K_{PW}). K_{OW} was modeled as a function of structure of the co-solvent, temperature, properties of the aqueous phase, and properties of the oleic phase. K_{PW} was modeled as a function of K_{OW}.

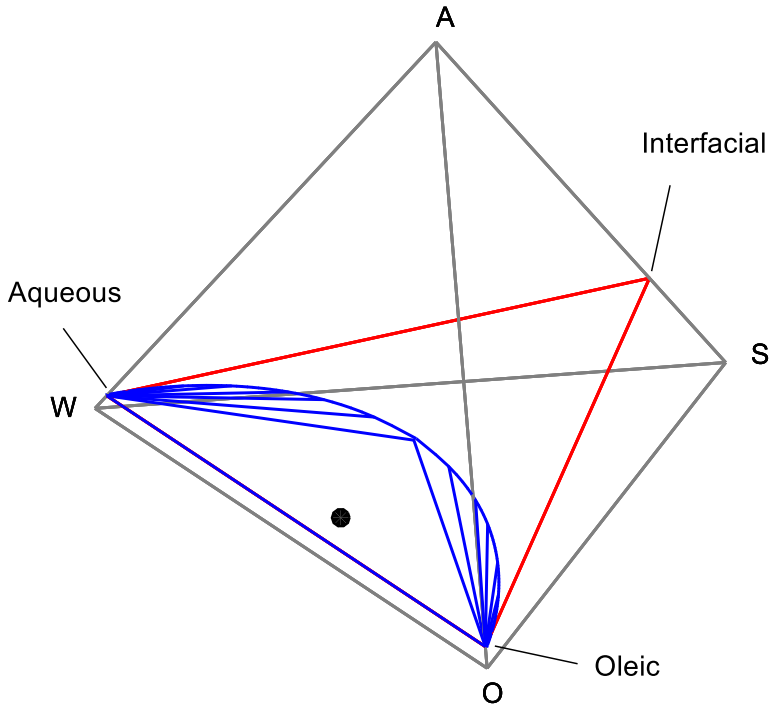

Figure 4.1. Simplification of the four-component tetrahedric diagram using the pseudophases. Vertices of the tetrahedron are the four components – brine (W), oil (O), surfactant (S), and co-solvent (A). Vertices of the pseudoternary triangle are the aqueous, oleic, and interfacial pseudophases. The pseudoternary plane intersects the overall composition (black circle) of 40% brine, 50% oil, 5% surfactant, and 5% co-solvent. The oil-water partition coefficient is 1 and the interface-water partition coefficient is 10. The temperature and pressure are fixed. Salinity is equal to the optimum salinity and the optimum solubilization ratio is 1 cc/cc. On the pseudoternary plane, the three-phase triangle, the 2 two-phase envelopes, and tie-lines are shown in blue.

Chemical floods during the 1970's and 1980's often used surfactant concentrations between 2-12%, and co-solvent concentrations of greater than 2%. The co-solvents were various aliphatic alcohols (e.g. propanol to hexanol). At these high co-solvent concentrations, the co-solvent in the oil self-associates in small aggregates, so the oil-water partition coefficient depends on the overall concentration. Now, the concentrations of surfactant and co-solvent are significantly lower (0.25-1%). Newer co-solvents contain

moles of ethylene oxide (EO) and propylene oxide (PO). They are more effective at lower concentrations compared to the aliphatic alcohols.

The partitioning behavior of the aliphatic alcohols depends on salinity, temperature, oil, and overall composition (Solheim, 1990; Dwarakanath and Pope, 1998). The self-association of alcohol in the oil phase was often modeled in order to capture the concentration dependence of the partition coefficient observed at higher co-solvent concentrations. The previous systematic studies used single component alkanes as analogues of crude oils. However, methods to apply the correlations to real crude oils were lacking.

More recently Chang et al., (2016) conducted a systematic study to determine the relationship of the K_{OW} of alcohol alkoxylate co-solvents with the structure of the co-solvent, temperature, properties of the aqueous phase, and properties of the oleic phase. They proposed a method to apply the correlations developed for analogue crude oils to real crude oils based on commonly measured crude oil properties.

As part of the current research, alcohol alkoxylate co-solvent and aliphatic alcohol data were used to develop an expression to estimate the oil-water partition coefficient as a function of the molecular structures, temperature, salinity, and the properties of the oil phase (applicable for crude oils and analogue oils).

The interface-water partition coefficients of the co-solvents are typically not measured. There is very little experimental data for the interface-water partition coefficients of aliphatic alcohol co-solvents and even less data for alcohol alkoxylate co-solvents. Thus, new measurements of the interface-water partition coefficients of alcohol alkoxylate co-solvents were made. The interface-water partition coefficient was modeled as a function of the oil-water partition coefficient.

4.1 Analytical Method for Alcohol Alkoxylate Co-solvents

The mass or volume fractions of the co-solvents in P-1 of the phases were measured using reversed phase liquid chromatography. The concentration of co-solvent in phase P was calculated from volume balance. Volumes were assumed to be additive, and the densities of all components were assumed to be equal to 1 g/ml.

In liquid chromatography, the compounds in solution are separated based on their affinities to the stationary phase and to the mobile phase. In reversed-phase liquid chromatography, the stationary phase is hydrophobic and the mobile phase is polar. Hydrophobic molecules tend to adsorb to the stationary phase, and hydrophilic molecules tend to remain in the mobile phase and elute first. The polarity of the mobile phase can be adjusted (typically decreased) in order to more efficiently elute the more hydrophobic molecules.

A C18 alkyl (Acclaim Surfactant HILIC) stationary phase and acetonitrile/water mobile phase were used to separate surfactants, but they were unable to retain alcohol-alkoxylate co-solvents. An alkyl diol (Acclaim Mixed-Mode HILIC) column stationary phase and acetonitrile/water mobile phase were used to separate the components of alcohol-alkoxylate co-solvents. The mixed polarity of the stationary phase complicated the elution order of the analyte.

4.1.1 Materials

The co-solvents used in these experiments were isobutyl-alcohol-alkoxylate (IBA-xEO and IBA-wPO-xEO) co-solvents and phenol-alkoxylate (Ph-xEO and Ph-wPO-xEO) co-solvents. The coefficient w, the average number of propylene oxide (PO) groups, ranged from 0 to 1, and the coefficient x, the average number of ethylene oxide (EO) groups,

ranged from 1 to 20. The co-solvents were obtained as neat material from Harcros Chemicals.

Six crude oils and six pure hydrocarbons were used in these experiments. **Table 5.4** shows the properties of the pure hydrocarbons, and **Table 5.5** shows the properties of the dead crude oils. The molecular weights (MW) of the crude oils were obtained from PVT reports or were measured by freezing point depression. The density of the crude oils were measured at 25°C and 1 atm. The fractions of saturates (SAT), aromatics (ARO), resins (NSO), and asphaltenes (ASP) in the crude oils were obtained from PVT reports or were measured by Weatherford Geochemical Services. The aqueous phase brines were mixtures of sodium chloride, sodium carbonate, and sodium metaborate in deionized water. The hydrocarbons were obtained from Fischer Scientific

The solvents used for the mobile phase were acetonitrile (HPLC grade) and water with 0.1 M ammonium acetate buffered to pH = 5.5 with glacial acetic acid. The acetonitrile, ammonium acetate, and glacial acetic acid were obtained from Fischer Scientific.

Table 4.1: Properties of the Hydrocarbons

Name	MW (g/mol)	Density (g/ml)	EACN	ARO (g/g)	Sample size
Cyclohexane	84	0.78	4	0	4
Toluene	92	0.87	1	1	15
Decalin	138	0.90	6	0	4
n-Hexane	86	0.65	6	0	4
n-Octane	114	0.70	8	0	7
n-Hexadecane	226	0.77	16	0	9

Table 4.2: Properties of the Dead Crude Oils

Name	MW (g/mol)	Density (g/ml)	EACN	SAT (g/g)	ARO (g/g)	NSO (g/g)	ASP (g/g)	Sample size
A	230	0.81	12.6	0.31	0.25	0.06	0.01	29
E	430	0.87	11.6	0.34	0.30	0.10	0.04	2
H	320	0.93	12.3	0.26	0.37	0.13	0.06	25
L	273	0.87	11.6	0.44	0.21	0.07	0.00	34
S	238	0.86	10.8	0.32	0.23	0.07	0.01	
U	401	0.91	11.0	0.20	0.26	0.10	0.05	

4.1.2 Analytical Method

All HPLC analyses were performed on a Thermo Scientific Dionex Ultimate 3000 LC system with UV-Vis diode array detector (Dionex Ultimate 3000) and evaporative light scattering detector (Agilent Techologies 1260 Infinity). Co-solvents were separated on the Acclaim Mixed-Mode HILIC-1 column (5 µm, 4.6 x 150 mm) using a mobile phase gradient at a flow rate of 1 ml/min. Phenol alkoxylate co-solvents were analyzed using UV-Vis detector at 260 nm wavelength absorbance. All co-solvents were analyzed using the ESLD with nebulizer and evaporator temperatures ranging from 40 to 60 °C and 60 to 80 °C, respectively, and gas flow rate of 1.5 SLM. The mobile phase and detector settings were modified depending on the co-solvent to increase resolution or detector response.

4.1.3 Experimental Procedures

Stock solutions with concentrations ranging from 1 to 2 wt% were made from the neat co-solvent and deionized water. Standard samples ranging from concentrations of

0.025 to 0.2 wt% co-solvent in deionized (DI) water were made from the stock solution. The samples were kept refrigerated to prevent evaporation.

The oil-water partitioning samples were made in glass vials by mixing 2 ml of oil and 2 ml of 0.5 to 1 wt% co-solvent in brine. The samples were mixed and aged for 3-4 days at constant temperature. The aqueous phases of the samples were extracted via glass Pasteur pipettes and diluted with deionized water to concentrations within the calibration concentration range. The samples were filtered through 0.45 μm filters before HPLC analysis.

The microemulsion samples were made by mixing the oil and aqueous surfactant solution, co-solvent, and brine. The total volume of the sample was designed to have at least 1 ml of microemulsion for the co-solvent analysis and often more for microemulsion viscosity measurements. The samples were mixed and aged at constant temperature until the solubilization ratios remained constant within the uncertainty of the observations, which indicated the phase behavior was at or close to equilibrium. The type I microemulsion, type III microemulsion, and excess water phases were extracted via syringe with thin stainless-steel needle. The mixing zone between phases was discarded to extract uncontaminated phases. The excess water phases were diluted with deionized water and the microemulsion phases were diluted with a solution of 10 wt% IPA and deionized water to concentrations within the calibration range. The diluted microemulsion phase was centrifuged at 2000 rpm for 10 minutes. The aqueous phase was separated from any excess oil, which could not be injected in the HPLC. The diluted excess water phase and the diluted and separated microemulsion phase samples were filtered through 0.45 μm filters before HPLC analysis.

The standard samples were analyzed at the beginning of each sequence of samples of unknown concentrations. The concentrations of the unknown samples were determined

from the calibration curve of the standard samples. The concentrations of co-solvent in the excess oil phases were calculated from mass balance.

4.1.4 Procedure used for distribution of homologues

The co-solvents are a distribution of homologues, differing in the number of alkoxylate groups. **Figure 4.2** shows overlaid chromatograms of phenol-2EO, phenol-4EO, phenol-8EO, phenol-1PO-5EO co-solvents with phenol as a reference. Phenol (retention time of 6 minutes) was not found in any significant quantities in the phenol alkoxylate co-solvents. The homologues eluted in order of increasing number of EO groups. For the phenol-1PO-5EO co-solvent, peak identification and resolution is complicated by the distributions of both PO and EO groups, so the constitutive components of co-solvents containing PO groups were not analyzed.

The constitutive components of the co-solvents could be identified and the partition coefficients could be determined in the cases where there was sufficient baseline-separation of the signals (peaks) of the individual components. Gaussian functions were fit to the components that were moderately overlapping in order to deconvolute the signals. This form of mathematical deconvolution was not always possible especially for complex distributions and high EO content.

The mean partition coefficients are based on the total signal (i.e. no discrimination between individual component response factors). The mean partition coefficients of the phenol-alkoxylate co-solvents are approximately the molar average of the partition coefficients of the constitutive components because the UV-Vis absorbance varies linearly with the moles of the chromophore (phenol). The mean partition coefficients of the IBA-alkoxylate co-solvents is dependent on the separation and the ELSD detector response

factor. The response factor of the ELSD is quadratic with concentration and dependent on the mass and volatility of the analyte.

The partition coefficients of the individual components of many of the co-solvents were measured. The values were not affected by the detector response factor but were affected by the chromatographic resolution. The resolution (peak separation) decreased with increasing numbers of EO groups. Even with mathematical deconvolution, the signals of components with more than approximately 10 EO groups were highly uncertain. The components of co-solvents with PO groups were difficult to resolve and identify, so the partition coefficients of individual component of these co-solvents were not measured. The partition coefficients of the individual components are more accurate than the mean partition coefficients.

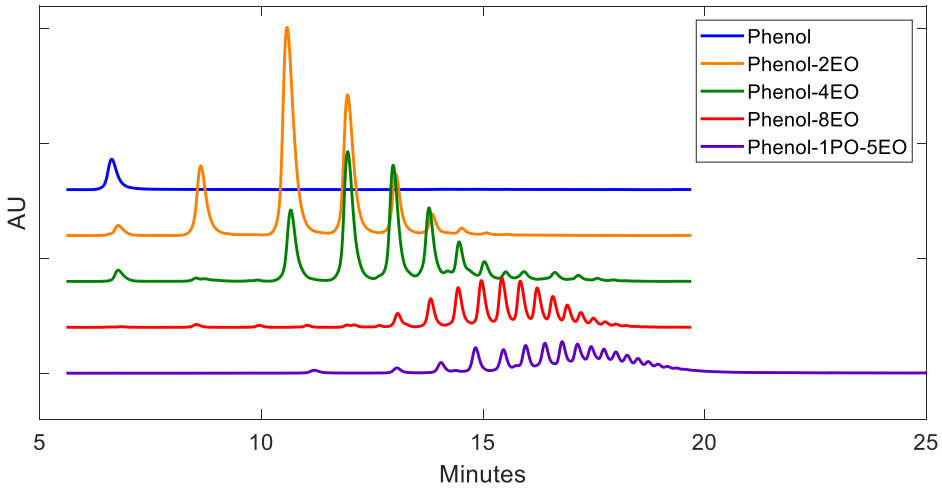

Figure 4.2: Overlay chromatogram of phenol, phenol-2EO, phenol-4EO, phenol-8EO, and phenol-1PO-5EO co-solvents.

4.1.5 Calculation of Oil-Water Partition Coefficients

The co-solvent concentration in the aqueous phases was measured, whereas the co-solvent concentration in the oleic phase was calculated from volume balance. The volumetric balance of the co-solvent is

$$V_W C_{AW} + V_O C_{AO} = V_A \quad \textbf{(4.1)}$$

where, V_W, V_O, and V_A are the volume fractions of water, oil, and co-solvent, respectively. C_{AW} is the concentration of co-solvent in the aqueous phase with units of volume/volume water and C_{AO} is the concentration of co-solvent in the oleic phase with units of volume/volume oil. C_{AW} is calculated from the mass (or volume) fraction of co-solvent in the aqueous phases (f_A^W) using equation **(4.2**.

$$C_{AW} = \frac{f_A^W}{1 - f_A^W} \quad \textbf{(4.2)}$$

The oil-water partition coefficient (K_{OW}) is

$$K_{OW} = \frac{C_{AO}}{C_{AW}} = \left(\frac{V_A - V_W C_{AW}}{V_O C_{AW}}\right) \quad \textbf{(4.3)}$$

Since $f_A^W << 1$ is this study, $C_{AW} \approx f_A^W$. Since all experiments had water oil ratio equal to 1, $V_W \approx V_O$. Equation **(4.3** simplifies to:

$$K_{OW} = \frac{f_{A,i}^W}{f_A^W} - 1 \quad \textbf{(4.4)}$$

where, $f_{A,i}^W$ is the volume fraction of co-solvent in the aqueous phase before mixing. In equation **(4.4**, the partition coefficient is a function of only the ratio of the initial mass fraction and equilibrium mass fraction. Equation **(4.4** is used to calculate the mean K_{OW} of the co-solvent and K_{OW} of the components of the co-solvent. K_{OW} beyond roughly 1 to 2 orders of magnitude from 1 (greater than 100 or less than 0.01) were highly uncertain due to large relative error and were omitted.

The oil-water partition coefficients (K_{OW}) were found to be independent of composition and concentration for initial aqueous concentrations of co-solvent ranging from 0.05 to 2 wt%. So, for example, the same phenol-ethoxymers of the phenol-2EO co-solvent, the phenol-4EO co-solvent, and the phenol-8EO co-solvent have nearly the same partition coefficients. Therefore, the simpler Hirasaki model (Hirasaki, 1982) was used as opposed to the more complex Prouvost model (Prouvost et al., 1985), which models the self-association of co-solvent in the oleic phase.

4.1.6 Calculation of Interface-Water Partition Coefficients

The co-solvent concentrations in type I microemulsion, type III microemulsion, and excess water phases were measured, and the concentration in the type II microemulsion and excess oil phases were estimated from volume balance. The volumetric balance of the co-solvent is

$$V_W C_{AW} + V_O C_{AO} + V_S C_{AS} = V_A \tag{4.5}$$

where, V_S is the volume fraction of surfactant, and C_{AS} is the concentration of co-solvent in the interfacial pseudophase with units of volume/volume surfactant. For a type III microemulsion, another volume balance of the co-solvent is

$$V_{EW} f_A^W + V_{EO} f_A^O + V_M f_A^M = V_A \tag{4.6}$$

where, V_{EW}, V_{EO}, and V_M are the volume fractions of the excess water, excess oil, and microemulsion phases. f_A^M is the volume fraction of co-solvent in the microemulsion phase. For a type III microemulsion, the f_A^W and f_A^M are measured, and f_A^O is calculated using equation **(4.6**. The C_{AW} and C_{AO} are calculated using equations **(4.7** and **(4.8**, respectively.

$$C_{AW} = \frac{f_A^W}{1 - f_A^W} \tag{4.7}$$

$$C_{AO} = \frac{f_A^O}{1 - f_A^O} \tag{4.8}$$

The concentration of co-solvent in the surfactant (C_{AS}) is calculated from equation **(4.5**. C_{AS} cannot be calculated for type I and type II microemulsions because C_{AW} and C_{AO}, respectively, cannot be directly measured. The oil-water partition coefficient (K_{OW}) is defined by equation **(4.9**. The interface-water partition coefficient (K_{PW}) is defined by equation **(4.10**.

$$K_{OW} = \frac{C_{AO}}{C_{AW}} \tag{4.9}$$

$$K_{PW} = \frac{C_{AS}}{C_{AW}} \tag{4.10}$$

Co-solvents and surfactants are both amphiphilic compounds. The distinction is blurred as the hydrophilicity (number of EO groups) and lipophilicity (alcohol carbon number and number of PO groups) of the co-solvent increases. An oil-water partition coefficient (K_{OW}) on the order of 1 can be achieved by increasing the alcohol carbon number, the number of PO groups, and the number of EO groups such that the increase in hydrophilicity is balanced equally by an increase in lipophilicity. As the hydrophilicity and lipophilicity are simultaneously increased, the co-solvent behavior becomes similar to a surfactant.

4.2 Systematic Study of the Oil-Water Partition Coefficient of Alcohol Alkoxylate Co-solvents

The oil-water partition coefficient (K_{OW}) of alcohol alkoxylate co-solvents is a function of the structure of the co-solvent, temperature, properties of the aqueous phase, and properties of the oleic phase. The structures of the co-solvents that were investigated

are the alcohol type, the number of PO groups, and the number of EO groups. The alcohol types that were studied are isobutyl alcohol (IBA) and phenol. Increasing the carbon number and decreasing the branching increases the lipophilicity of the co-solvent and increases the oil-water partition coefficient. Increasing the number of PO (EO) groups increases the lipophilicity (hydrophilicity) of the co-solvent and increases (decreases) K_{OW}. Increasing the salinity of the aqueous phase and increasing the temperature tend to decrease the hydrophilicity and increase K_{OW}.

The composition of the oleic phase influences K_{OW}. Previous correlations of K_{OW} of aliphatic alcohols captured the effect of oil using equivalent alkane carbon numbers (EACN) of oils. The EACN of the oil is the predicted carbon number of the n-alkane in which the value of the property (K_{OW} in this case) are equal. The limitation of using EACN is that the EACN of the oil is not a directly measurable property of the oil. The EACN of an oil depends on the property being measured (i.e. the EACN values of an oil for different properties will not necessarily be the same). Typically, only the liquid n-alkanes (approximately C5 to C16) can be measured. The properties and EACN values outside of this range of liquid n-alkanes are extrapolated. The EACN concept is simpler and more accurate than using solubility-based methods. The EACN reflects the relative hydrophilicity and lipophilicity of the oil. Oleic (non-aqueous) phases such as halocarbons (halogenated hydrocarbons) are relatively more hydrophilic than liquid n-alkanes and have negative EACN. The EACN method is suitable for mixtures of components with known properties. However, crude oils are mixtures of a multitude of different components. The EACN of crude oils cannot be estimated but only measured.

The components of crude oils are broadly categorized as saturates, aromatics, resins, and asphaltenes (SARA). The SARA is a routine measurement of crude oils. The saturates fraction encompass the aliphatic (linear, branched, cyclic) hydrocarbon

components. The aromatics encompass the molecules with cyclic and resonance bonds. Resins and asphaltenes are complex molecules with polar substituents (containing nitrogen, sulfur, and oxygen). Resins are defined as being soluble and asphaltenes are defined as being insoluble in either pentane or heptane solvent. The distinction between these four categories is subjective and depends on the method of analysis. The saturates are the least polar, and the aromatics, resins, and asphaltenes are more polar due to higher electron density from aromaticity and the polar substituents.

4.2.1 Dataset Description

The model for the oil-water partition coefficients (K_{OW}) was developed based on systematic measurements of the partitioning of alcohol alkoxylate co-solvents. The dataset is composed of 93 liquid chromatography measurements with 25 unique oils and 15 unique alcohol-alkoxylate co-solvents. Table 4.3 shows the K_{OW} for IBA-alkoxylate co-solvents. Table 4.4, Table 4.5, and Table 4.6 show the K_{OW} values for phenol-2EO, phenol-4EO, and higher order phenol-alkoxylate co-solvents. There is a total of 419 measurements in the dataset composed of the component K_{OW} data and the mean K_{OW} data when the component K_{OW} data were not measured.

Table 4.3: Oil-Water Partition Coefficients of IBA-1PO-xEO and IBA-xEO

Oil	Co-solvent		S	T	KOW						
	wt%	name	wt%	°C	mean	1	2	3	4	5	6
A	0.5	IBA-1EO	4.6	55	0.120						
A	0.5	IBA-3EO	4.6	55	0.060						
A	0.5	IBA-5EO	4.6	55	0.010						
A	0.5	IBA-7EO	4.6	55	0.030						
H	1	IBA-3EO	4.6	55	0.060						
H	1	IBA-1PO-2EO	4.6	55	0.340						
H	1	IBA-1PO-5EO	4.6	55	0.180						
L	0.5	IBA-5EO	4.6	55	0.053	0.100	0.079	0.051	0.051	0.046	0.035
L	0.5	IBA-5EO	4.6	55	0.078	0.158	0.105	0.081	0.078	0.074	0.066
L	0.5	IBA-5EO	4.6	70	0.122	0.290	0.186	0.134	0.121	0.094	0.085
L	0.5	IBA-5EO	4.6	85	0.138	0.297	0.235	0.168	0.117	0.106	0.088
L	0.5	IBA-5EO	4.6	85	0.148	0.346	0.247	0.174	0.140	0.117	0.099
L+20%Cyc6	0.5	IBA-5EO	4.6	55	0.058	0.085	0.079	0.058	0.052	0.052	0.037
L+40%Cyc6	0.5	IBA-5EO	4.6	55	0.043	0.094	0.065	0.044	0.032	0.027	0.021
L+20%C6	0.5	IBA-5EO	4.6	55	0.030	0.054	0.034	0.023	0.025	0.022	0.019
L+40%C6	0.5	IBA-5EO	4.6	55	0.047	0.097	0.077	0.040	0.036	0.032	0.030
L+12%Tol	0.5	IBA-5EO	4.6	55	0.073	0.169	0.117	0.072	0.065	0.061	0.045
L+40%Tol	0.5	IBA-5EO	4.6	55	0.115	0.272	0.207	0.147	0.105	0.084	0.053
L+20%C8	0.5	IBA-5EO	4.6	55	0.030	0.055	0.036	0.020	0.019	0.021	0.021
L+40%C8	0.5	IBA-5EO	4.6	55	0.032	0.051	0.048	0.032	0.020	0.018	0.014
L+20%Dec	0.5	IBA-5EO	4.6	55	0.011	0.041	0.023	0.001		0.007	0.001
L+40%Dec	0.5	IBA-5EO	4.6	55	0.042	0.089	0.067	0.041	0.026	0.032	0.019
L+20%C16	0.5	IBA-5EO	4.6	55	0.044	0.062	0.050	0.033	0.036	0.043	0.033
L+40%C16	0.5	IBA-5EO	4.6	55	0.036	0.052	0.041	0.029	0.033	0.026	0.022

Table 4.4: Oil-Water Partition Coefficients of Phenol-2EO

Oil	Co-solvent		S	T	KOW						
	wt%	name	wt%	°C	mean	1	2	3	4	5	6
A	0.5	Ph-2EO	4.6	55	0.71	1.43	0.932	0.761	0.559	0.447	0.466
A	0.5	Ph-2EO	4.6	85	1.45	3.16	2.4	2.27	0.684	0.349	
A+20%C16	0.5	Ph-2EO	4.6	55	0.82	2.21	1.73	1.38	0.341		
E	0.5	Ph-2EO	3	55	0.76	1.47	0.94	0.772	0.686	0.355	
E	0.5	Ph-2EO	3	85	1	1.57	1.13	1.01	0.944	0.771	0.758
H	0.5	Ph-2EO	4.6	55	1.15	1.44	1.01				
H	1	Ph-2EO	4.6	55	0.96	1.58	1.12	0.741	0.525	0.373	0.277
H	2	Ph-2EO	4.6	55	0.99	1.61	1.15	0.773	0.552	0.396	0.304
H+12%Tol	0.5	Ph-2EO	4.6	55	1.38	3.11	2.65	2.16	0.648	0.225	
H+12%Tol	0.5	Ph-2EO	4.6	68	1.83	3.7	3.27	2.84	1.01	0.418	0.201
L	0.5	Ph-2EO	4.6	55	0.67	1.2	0.797	0.487	0.31	0.196	0.143
L	0.5	Ph-2EO	4.6	55	0.66	1.18	0.787	0.481	0.307	0.19	
L	0.5	Ph-2EO	4.6	70	0.89	1.48	1.04	0.698	0.474	0.305	
L	0.5	Ph-2EO	4.6	85	1.04	1.64	1.21	0.822	0.589	0.405	0.211
L	0.5	Ph-2EO	4.6	85	1.01	1.59	1.2	0.806	0.551	0.318	
L+20%Cyc6	0.5	Ph-2EO	4.6	55	0.71	1.23	0.84	0.525	0.346	0.221	0.125
L+40%Cyc6	0.5	Ph-2EO	4.6	55	0.73	1.23	0.859	0.545	0.363	0.238	0.128
L+20%C6	0.5	Ph-2EO	4.6	55	0.66	1.16	0.776	0.479	0.311	0.202	0.097
L+40%C6	0.5	Ph-2EO	4.6	55	0.62	1.06	0.723	0.447	0.3	0.209	0.167
L+12%Tol	0.5	Ph-2EO	4.6	55	0.91	1.52	1.07	0.694	0.467	0.309	0.199
L+40%Tol	0.5	Ph-2EO	4.6	55	1.68	2.37	1.95	1.42	1.06	0.766	0.542
L+20%C8	0.5	Ph-2EO	4.6	55	0.64	1.15	0.756	0.458	0.295	0.189	0.109
L+40%C8	0.5	Ph-2EO	4.6	55	0.60	1.02	0.721	0.434	0.276	0.175	0.101
L+20%Dec	0.5	Ph-2EO	4.6	55	0.65	1.17	0.773	0.473	0.304	0.188	0.098
L+40%Dec	0.5	Ph-2EO	4.6	55	0.67	1.17	0.796	0.491	0.325	0.213	0.149
L+20%C16	0.5	Ph-2EO	4.6	55	0.60	1.08	0.704	0.427	0.274	0.173	0.092
L+40%C16	0.5	Ph-2EO	4.6	55	0.53	0.979	0.631	0.371	0.23	0.137	0.067

Table 4.5: Oil-Water Partition Coefficients of Phenol-4EO

Oil	Co-solvent		S	T	KOW							
	wt%	name	wt%	°C	mean	1	2	3	4	5	6	7
Tol	0.5	Ph-4EO	4.6	55	6.06		10.9	8.66	8.74	7.56	7.83	6.5
C8	0.5	Ph-4EO	4.6	55	0.24		0.478	0.273	0.167	0.104	0.038	
C16	0.5	Ph-4EO	4.6	55	0.18		0.393	0.22	0.135	0.090	0.036	
A	0.5	Ph-4EO	0	55	0.34		0.761	0.487	0.389	0.199	0.165	
A	0.5	Ph-4EO	0.1	55	0.36	5.56	1.31	0.875	0.459	0.141		
A	0.5	Ph-4EO	4.6	25	0.36		1.21	0.771	0.422	0.088		
A	0.05	Ph-4EO	4.6	55	0.47		3.11	2.21	1.3	0.75	0.476	0.23
A	0.125	Ph-4EO	4.6	55	0.54		2.22	1.44	0.826	0.44	0.106	
A	0.5	Ph-4EO	4.6	55	0.5	2.92	1.11	0.721	0.496	0.303	0.23	
A	0.5	Ph-4EO	4.6	85	0.81		3.45	2.66	1.74	1.21	0.617	0.455
A	0.5	Ph-4EO	6	55	0.5	4.62	1.22	0.714	0.487	0.219	0.171	
A	0.5	Ph-4EO	6	85	0.98	2.67	1.82	1.29	1.03	0.67	0.577	
A	0.5	Ph-4EO	15	55	1.76		5.45	2.36	2.24	1.4	1.23	0.505
A+20%Tol	0.5	Ph-4EO	4.6	55	1.09		3.01	2.17	1.28	0.73	0.307	
A+20%C8	0.5	Ph-4EO	4.6	55	0.42		0.845	0.524	0.337	0.221	0.114	
A+20%C16	0.5	Ph-4EO	4.6	55	0.51		1.57	1.16	0.682			
H	0.5	Ph-4EO	4.6	55	0.61		1.43	0.844	0.753	0.447	0.415	
H+12%Tol	0.5	Ph-4EO	4.6	55	0.98		2.88	1.97	1.18	0.747	0.093	
H+20%C8	0.5	Ph-4EO	4.6	55	0.5		0.956	0.638	0.431	0.293	0.154	
H+20%C16	0.5	Ph-4EO	4.6	55	0.44		0.869	0.568	0.379	0.256	0.129	

Table 4.6: Oil-Water Partition Coefficients of Phenol-8, 10, 20EO, and 1PO-xEO

Oil	Co-solvent		S	T	KOW								
	wt%	name	wt%	°C	mean	3	4	5	6	7	8	9	10
Tol	0.5	Ph-8EO	4.6	55	2.61					7.34	5.13	3.92	2.91
A	0.5	Ph-8EO	4.6	55	0.046	1.49	0.657	0.322	0.178	0.098	0.066	0.040	
A	0.5	Ph-8EO	4.6	85	0.18	6.76	2	0.935	0.602	0.417	0.3	0.225	0.16
A	0.5	Ph-10EO	4.6	55	0.02								
A	0.5	Ph-20EO	4.6	55	0.03								
A	0.5	Ph-1PO-2EO	4.6	55	1.24								
A	0.5	Ph-1PO-5EO	4.6	55	0.3								
A+20%C16	0.5	Ph-8EO	4.6	55	0.08	4.15	1.6	0.773	0.488	0.314	0.224	0.137	0.105
A+20%Tol	0.5	Ph-8EO	4.6	55	0.07	2.63	1.12	0.541	0.342	0.212	0.155	0.090	0.055
A+20%Tol	0.5	Ph-10EO	4.6	55	-0.03								
H	1	Ph-1PO-2EO	4.6	55	1.93								
H	1	Ph-1PO-5EO	0	55	0.34								
H	1	Ph-1PO-5EO	2.5	55	0.45								
H	1	Ph-1PO-5EO	4.6	25	0.26								
H	1	Ph-1PO-5EO	4.6	55	0.62								
H	1	Ph-1PO-5EO	4.6	85	0.87								
H	1	Ph-1PO-5EO	7.5	55	0.7								
H	1	Ph-1PO-10EO	4.6	55	0.14								
H+12%Tol	0.5	Ph-8EO	4.6	55	0.12	4.34	1.7	0.793	0.511	0.325	0.224	0.148	0.101
H+12%Tol	0.5	Ph-1PO-2EO	4.6	55	3.02								
H+12%Tol	0.5	Ph-1PO-5EO	4.6	55	0.7								

4.2.2 Model Development

The equivalent alkane carbon number (EACN) is often used to characterize crude oils. The EACN is determined by matching the optimum salinity of the crude oil with a pure alkane or other oil with a known EACN. However, measured EACN values did not correlate with the oil-water partition coefficients so they were not used to develop a partition coefficient model. For example, most crude oil EACN values are between 8 and 16, but the oil-water partition coefficient of octane and hexadecane are typically significantly lower than those of crude oils. The partition coefficients for octane and hexadecane were nearly identical. The K_{OW} showed a strong correlation with the concentration of aromatic components. The K_{OW} increased with the concentration of

toluene and decreased with the concentrations n-alkane, decalin, and cyclohexane. While the effect of oil EACN is present, it is overwhelmed by the effect of aromaticity.

The logarithm of K_{OW} could be approximated as a linear function of aromaticity with units of molality of benzene structures. This new method uses the SARA of the crude oils, which is a routine and widely available measurement available in most PVT reports, whereas EACN is not routinely available and is only weakly correlated with K_{OW}. The equation for the oil-water partition coefficient is

$$T_K \ln K_{OW} = a_1 N_I + a_2 N_{Ph} + a_3 N_{PO} + a_4 N_{EO} + a_5 \Delta T + a_6 S + a_7 m_B \qquad \textbf{(4.11)}$$

where, N_I is 1 if the alcohol is isobutyl alcohol (0 otherwise), N_{Ph} is 1 if the alcohol is phenol (0 otherwise), N_{PO} is the number of PO groups, N_{EO} is the number of EO groups, T_K is the absolute temperature in Kelvin, S is the salinity in wt%, m_B is the molality (moles per kilogram) of benzene ring structures in the crude oil defined by equation **(4.12**, and a_1 to a_7 are constants.

$$m_B = 1000 \times \sum_{i}^{O} \frac{\omega_i \, (ARO + NSO + ASP)_i}{MW_i} \qquad \textbf{(4.12)}$$

where, ωi is the mass fraction of oil component i, ARA, NSO, and ASP are the mass fraction of aromatics, resins, and asphaltenes, and O is the number of oil components. The values of ARO, NSO, and ASP of for n-alkanes, cyclohexane, and decalin are assumed to be 0, and the value of ARO for toluene is assumed to be 1. The assumptions are that aromatics, resins, and asphaltenes have molecular weights equal to the crude oil molecular weight, and have 1 benzene ring structure per molecule.

The coefficients a_1 to a_7 in equation **(4.11** were determined by multiple linear regression. The dataset used to develop the model was composed of 419 component K_{OW} and mean K_{OW} measurements. **Figure 4.3** shows the predicted versus measured oil-water

partition coefficients. **Table 4.7** shows the values and standard errors of the coefficients in the model. The coefficient of determination (R^2) is 0.87 and the standard error (standard deviation of the error) is 0.52 for the natural logarithm of the oil-water partition coefficient.

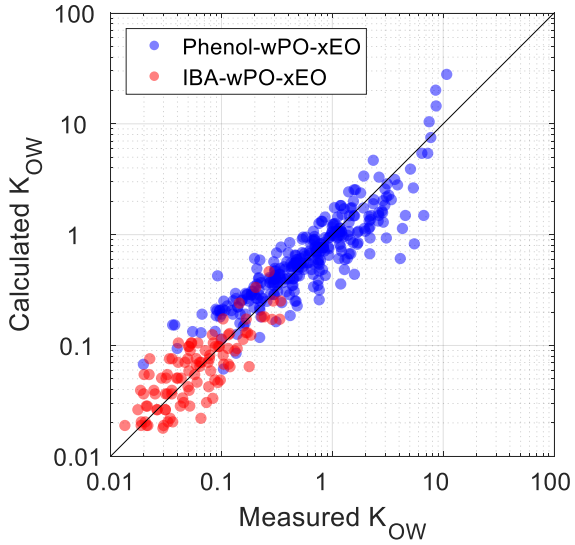

Figure 4.3: Calculated versus measured oil-water partition coefficients of the phenol alkoxylate and the IBA alkoxylate co-solvents.

Table 4.7: Coefficients for K_{OW} Model

Subscript i, Variable	N	a_i	σ_{ai}	$\lvert\sigma_{ai}/a_i\rvert$
1, N_{IBA}	409	-1142	42	4%
2, N_{Phenol}	315	-376	41	11%
3, N_{PO}	104	161	46	29%
4, N_{EO}	14	-109	4	4%
5, ΔT	419	8.49	0.76	9%
6, S	414	32.9	5.5	17%
7, m_B	413	118.3	4.6	4%

The coefficients for the co-solvent structures reflect the hydrophilic and lipophilic natures (K_{OW} shift up or down, respectively) of the structures. The IBA alcohol type is more hydrophilic than the phenol alcohol type. Increasing the number of EO (PO) groups increases (decreases) the hydrophilicity of the co-solvent and decreases (increases) the K_{OW}. Approximately 1.5 EO groups offsets the effect of adding 1 PO group to the co-solvent. Approximately 1 EO group offsets the effect of increasing temperature by 12 °C or increasing the salinity by 3.3 wt% NaCl.

4.2.3 Comparison of Co-solvent Partitioning Model with Experimental Data

The alcohol type, the number of PO groups, and the number of EO groups can be adjusted to achieve a desired oil-water partition coefficient (K_{OW}). Co-solvent with K_{OW} on the order of 1 are ideal for chemical EOR (Sahni et al., 2010). Figure 4.4 shows the K_{OW} versus the number of EO groups for (a) phenol alkoxylate co-solvent and (b) IBA alkoxylate co-solvent with crude oil H and 46,000 ppm NaCl brine at 55 °C. **Figure 4.5** shows the K_{OW} versus the number of EO groups for (a) phenol alkoxylate co-solvent and (b) IBA alkoxylate co-solvent with crude oil A and 46,000 ppm NaCl brine at 55 °C.

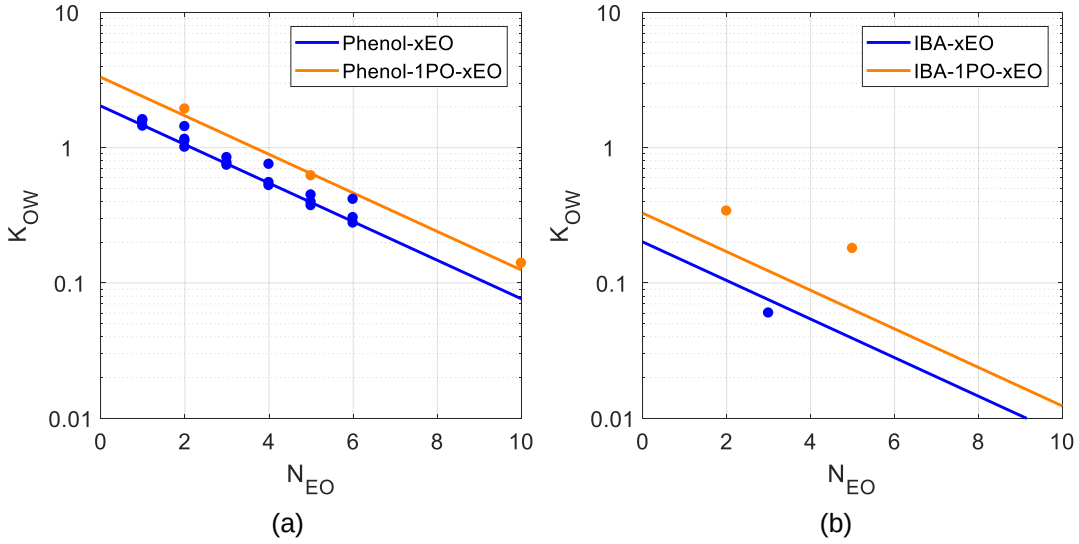

Figure 4.4: Oil-water partition coefficient versus number of EO groups for (a) phenol alkoxylate co-solvent and (b) IBA alkoxylate co solvent with Crude oil H and 4.6 wt% NaCl brine at 55 °C.

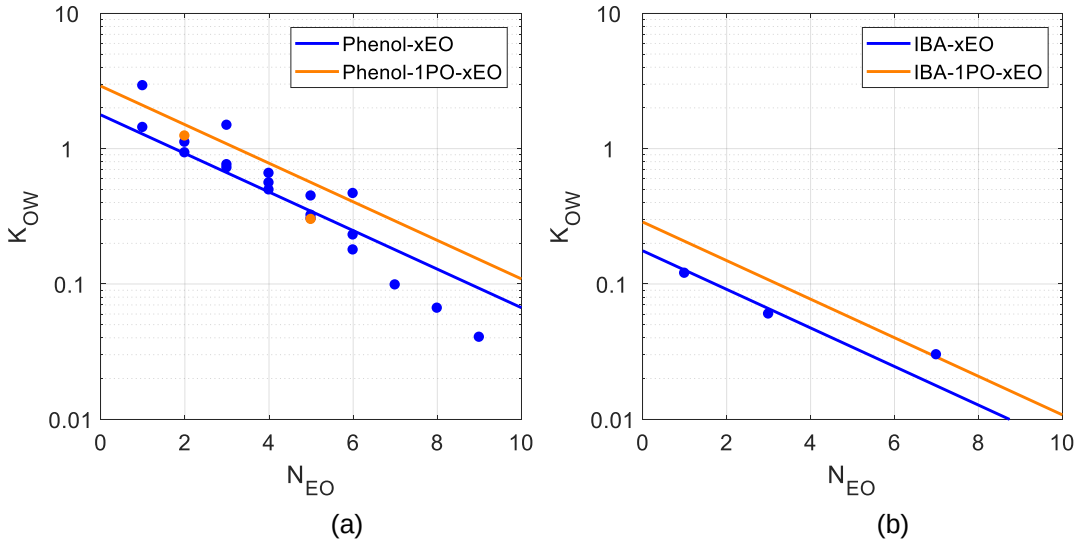

Figure 4.5: Oil-water partition coefficient versus number of EO groups for (a) phenol alkoxylate co-solvent and (b) IBA alkoxylate co-solvent with Crude oil A and 4.6 wt% NaCl brine at 55 °C.

Increasing the temperature and increasing the salinity of the aqueous phase decreases the hydrophilic interactions and increases the K_{OW}. **Figure 4.6** shows the K_{OW} versus the number of EO groups at different temperatures for (a) phenol ethoxylate co-solvent with crude oil A and 4.6% NaCl brine and (b) IBA ethoxylate co-solvent with crude oil L and 4.6% NaCl brine. **Figure 4.7** shows the K_{OW} versus number of EO groups at different brine salinities for (a) phenol-4EO co-solvent with Crude oil H at 55 °C and (b) phenol-1PO-5EO co-solvent with Crude oil A at 55 °C.

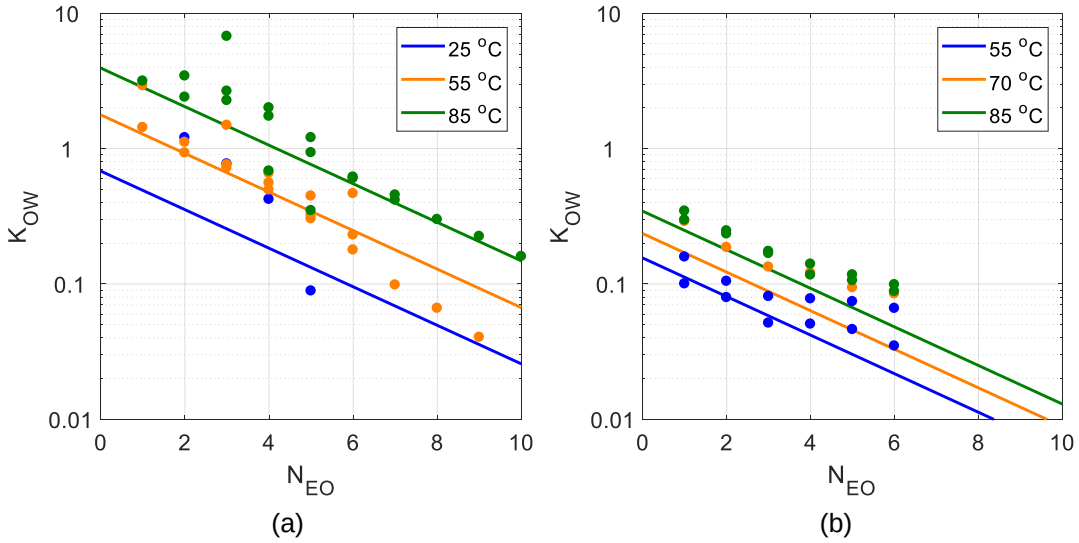

Figure 4.6: Oil-water partition coefficient versus number of EO groups at different temperatures for (a) phenol ethoxylate co-solvents with Crude oil A and 4.6% NaCl brine and (b) IBA ethoxylate solvents with Crude oil L and 4.6 wt% NaCl brine.

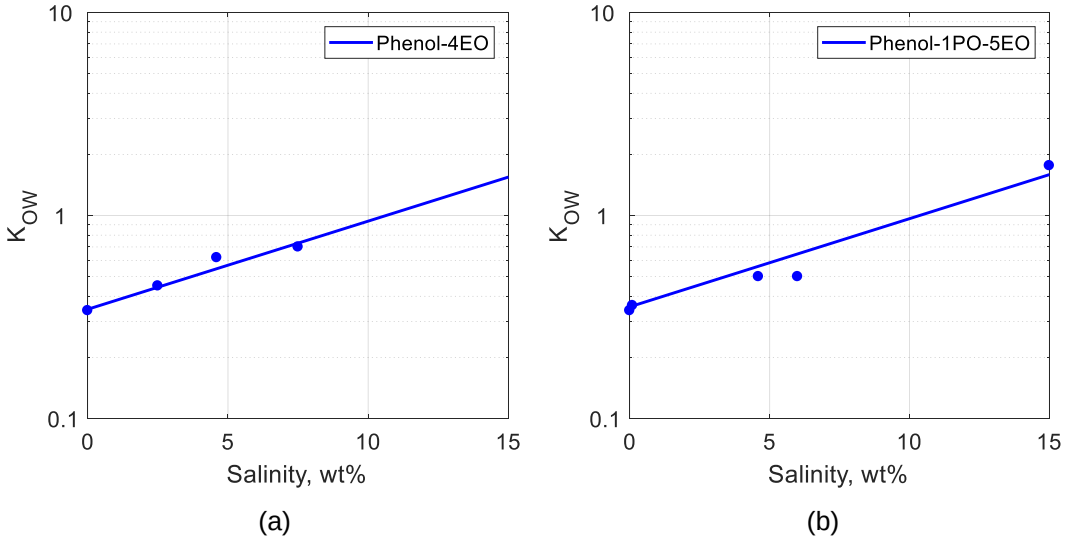

Figure 4.7: Oil-water partition coefficient versus number of EO groups at different brine salinities for (a) phenol-4EO co-solvent with Crude oil H at 55 °C and (b) phenol-1PO-5EO co-solvent with Crude oil A at 55 °C.

The composition of the oil has a significant effect on the K_{OW}. The trends were developed from systematic measurements with mixtures of crude oils, toluene,

cyclohexane, decalin, hexane, octane, and hexadecane. **Figure 4.8** shows the K_{OW} versus the molality of benzene structures (m_B) in moles/kilogram for (a) phenol-ethoxylates and (b) IBA-alkoxylates with various mixtures of crude A, crude H, and crude L with toluene, cyclohexane, decalin, hexane, octane, and hexadecane with 4.6 wt% NaCl brine at 55 °C. Increasing the concentration of n-alkanes, cyclohexane, and decalin in the oil mixtures dilutes the concentration of aromatics from the crude oils and slightly decreases the K_{OW}. Increasing the concentration of toluene in the oil mixtures increases the concentration of aromatics and significantly increases the K_{OW}. The effect on increasing the concentrations of these hydrocarbons on the EACN (based on microemulsion phase behavior) of the oleic phase is not proportional to the effect on the K_{OW}. The molality of benzene structures in the oleic phase correlates better than using EACN for the alcohol alkoxylate co-solvents.

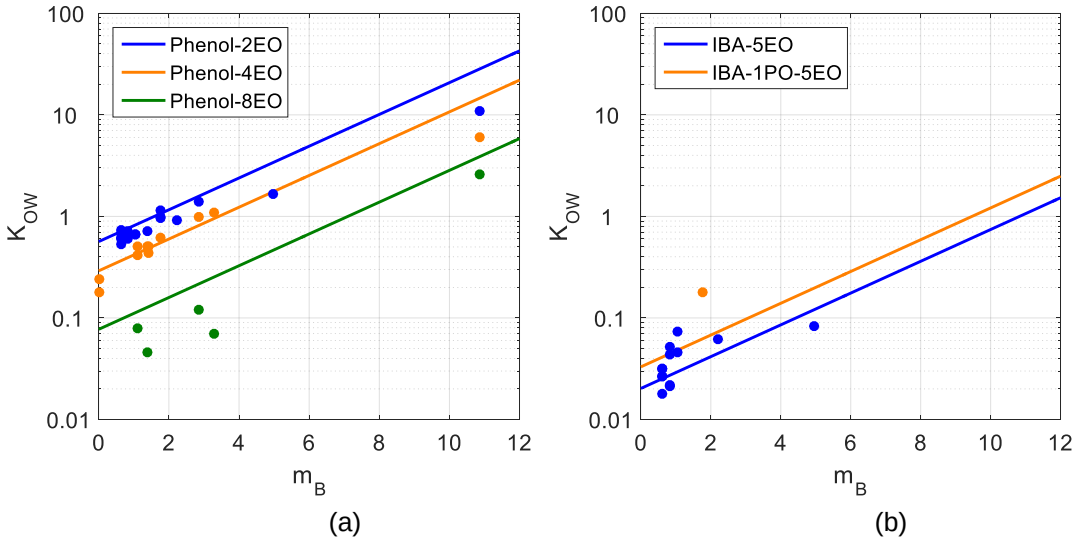

Figure 4.8: Oil-water partition coefficient versus molality of benzene structures (m_B) for (a) phenol-ethoxylates and (b) IBA-alkoxylates with various oil mixtures and 4.6 wt% NaCl brine at 55 °C.

4.3 Combined the Oil-Water Partition Coefficient Model

The oil-water partition coefficient model developed from the systematic study of alcohol alkoxylate co-solvents in Section 4.2 cannot be used to predict the effect of (1) changing the carbon number of the alcohol, (2) changing the isomeric arrangement of the alcohol, and (3) the effect of different n-alkane carbon numbers. The model is also untested for aliphatic alcohols. The data and models in Solheim, 1990 and Dwarakanath et al., 1998 for aliphatic alcohols were used with the model developed in Section 4.2 to develop a combined model for the oil-water partition coefficient that is more complete and accurate.

4.3.1 Solheim, 1990

Solheim (1990) developed a thermodynamic model for the partitioning of isobutyl alcohol and isoamyl alcohol in heptane and brines. In the experiments, the concentration of alcohol, temperature, and salinity were varied. The concentrations of alcohol in the oleic phase were greater than 2 vol%. A self-association model of alcohol in the oleic phase was used to describe the change of the partition coefficient with alcohol concentration. Equation **(4.13** describes the equilibrium reaction between monomeric alcohol and n-meric alcohol in the oil phase.

$$A_n + A_1 \rightarrow A_{n+1} \qquad \textbf{(4.13)}$$

where, A_i is the volume fraction of i-meric alcohol in the oleic phase. The forward reaction has an equilibrium constant of K for all values of n. The volume fraction of monomeric alcohol in the oil $\left(f_{A1}^{O}\right)$ is a function of the volume fraction of total alcohol in the oil $\left(f_{A}^{O}\right)$, defined by equation **(4.14**.

$$f_{A1}^{O} = \frac{f_{A}^{O}}{1 + Kf_{A}^{O}} \qquad \textbf{(4.14)}$$

Equation **(4.15** was proposed to model the partition coefficient, defined as the ratio of the volume fraction of monomeric alcohol in the oil $\left(f_{A1}^{O}\right)$ and the volume fraction of alcohol in the brine $\left(f_{A}^{W}\right)$.

$$T_K \ln\left(\frac{f_{A1}^{O}}{f_{A}^{W}}\right) = a_1 N_C + a_2 \Delta T + a_3 S + a_4 \quad \textbf{(4.15)}$$

where, T_K is the absolute temperature in kelvin, N_C is the carbon number of the alcohol, ΔT is the difference in temperature from a reference temperature of 25 °C, and S is the salinity in wt%. a_1 to a_4 are constants. Equation **(4.16** is the combination of equations **(4.14** and **(4.15**.

$$T_K \ln\frac{f_{A}^{O}}{f_{A}^{W}} = a_1 N_C + a_2 \Delta T + a_3 S + a_4 + T_K \ln\left(1 + K f_{A}^{O}\right) \quad \textbf{(4.16)}$$

The coefficients a_1 to a_4 and K were determined by nonlinear regression and are shown in **Table 4.8**. The equilibrium constant K was assumed to be constant for both isobutyl alcohol and isoamyl alcohol. **Figure 4.9** shows the prediction of the oil-water partition coefficient of monomeric alcohol for the experimental data in Solheim, 1990.

Table 4.8: Coefficients for Solheim, 1990 Kow Model

Coefficient	a_i	σ_{ai}	$\lvert\sigma_{ai}/_{ai}\rvert$
a_1	529	2	0.44%
a_2	25.3	0.2	0.97%
a_3	3.31	0.12	3.50%
a_4	-2661	15	0.55%
K	44.5	2.5	5.69%

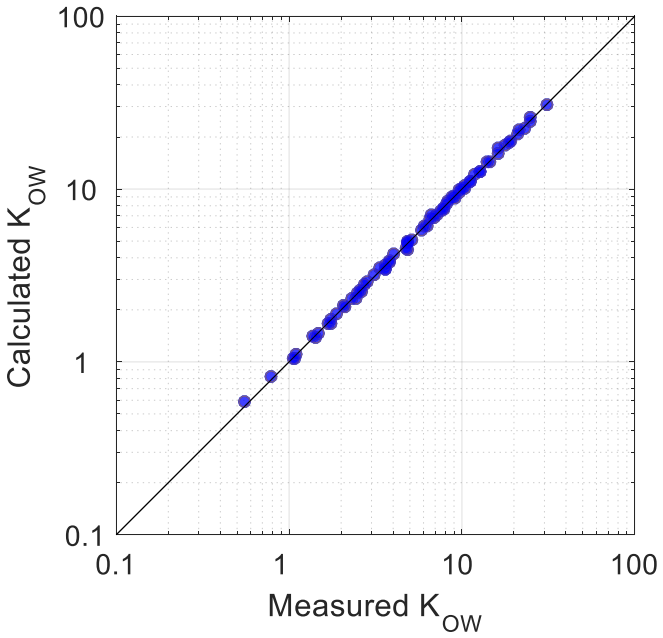

Figure 4.9: Predicted versus measured oil-water partition coefficient of monomeric alcohol for Solheim, 1990.

4.3.2 Dwarakanath and Pope, 1998

Dwarakanath & Pope (1998) developed an empirical relationship for estimating the partition coefficients of aliphatic alcohols with various non-aqueous phase liquids (NAPL). Their approach was based upon defining an equivalent alkane carbon number of the alcohol (N_C) and an equivalent alkane carbon number of the NAPL (EACN). Their model captures the effect of (1) the alcohol carbon number, (2) the alcohol isomeric arrangement, and (3) the oil EACN on the K_{OW}. The concentrations of alcohols used was small, so self-association was ignored. Their equation in units of natural logarithm and assuming the temperature of measurement was 25 °C is:

$$T_K \ln K_{OW} = -2029 + 449.5N_C - 34.67EACN \quad \textbf{(4.17)}$$

In the model, the predicted effect of increasing the oil EACN is relatively small. For example, the oil-water partition coefficient of n-butanol for octane to hexadecane are

0.18 and 0.07, respectively. This was because they were investigating only aliphatic alcohols and halocarbon and alkane oil phases, which all lack aromaticity.

4.3.3 Combined Model Development

Table 4.9 shows a comparison of the coefficients for the model developed in section 4.2 (equation **(4.11**), model fitting the data in Solheim (1990) (equation **(4.16**), and the model in Dwarakanath & Pope (1998) (equation **(4.17**). The dependent variable of the three models are the product of the absolute temperature and the natural logarithm of partition coefficient. The coefficients for salinity in equations **(4.11** and **(4.16** were in agreement. The coefficients for temperature in equations **(4.11** and **(4.16** differ by a factor of 2 to 3. The coefficient for the carbon number of the alcohol (N_C) in equations **(4.16** and **(4.17** were similar but applied for different alcohols. An effective carbon number system is required in order to combine these two equations. The constants in the three equations can be merged.

Table 4.9: Comparison of Oil-Water Partition Coefficient Models

	Alcohol Alkoxylate (Equation **(4.11)**)	Solheim (1990) (Equation **(4.16)**)	Dwarakanath & Pope (1998) (Equation **(4.17)**)
Structure			
○ N_C		529 (iC4 and iC5)	449.5 (isomers of C_5-C_8)
○ N_{PO}	161		
○ N_{EO}	-109		
ΔT	8.49 (25-85 °C)	3.31 (20 and 40 °C)	
Salinity	32.9 (0-15)	25.3 (2-20)	
Oil			
○ m_B	118.3		
○ EACN			-34.67 (C_8-C_{10})
Self-association		$T_K \ln(1 + Kf_A^o)$	
constant		-2661	-2029
○ IBA	-1142		
○ Phenol	-376		

The effective carbon numbers of the different alcohol structures were calculated based on logP, the logarithm (base 10) partition coefficient between octanol and water (Hansch 1995). The effective carbon numbers were calibrated against 1-propanol to 1-hexanol. **Figure 4.10** shows the correlation of logP and effective carbon number.

Table 4.10: Effective Carbon Number (N_C) of Various Alcohols

	logP	N_C
ethanol	-0.31	2
n-propanol	0.25	3
n-butanol	0.88	4
n-pentanol	1.51	5
n-hexanol	2.03	6
iso-propanol (IPA)	0.05	2.63
iso-butanol (IBA)	0.76	3.82
iso-pentanol (IAA)	1.16	4.49
sec-butanol (SBA)	0.61	3.57
tert-butanol (TBA)	0.35	3.13
Phenol	1.46	4.99

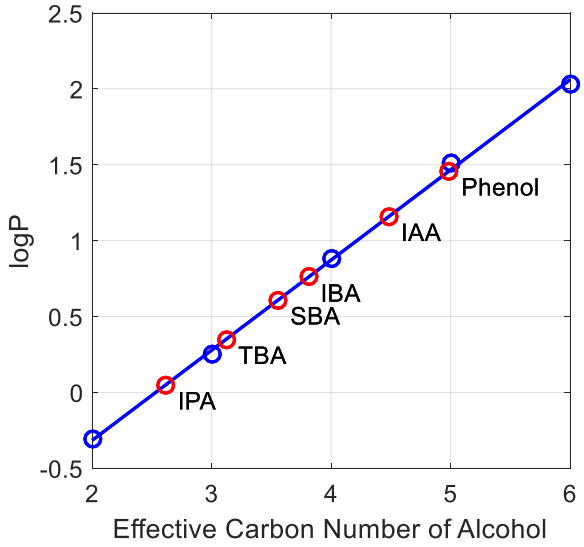

Figure 4.10: logP versus the effective carbon number of the alcohol

The combined model uses the molecular weight and the molality of benzene structures of the oil instead EACN. The molecular weight captures the effect of increasing the carbon number of the oil, and the molality of benzene structures captures the effect of aromaticity. The EACN method is a convolution of the two effects and therefore must be measured for all oils except the liquid n-alkanes. This combination of molecular weight and the molality of benzene structures captures the data well but requires experimental validation. Equation **(4.18** combines the functionalities of equations **(4.11**, **(4.16**, and **(4.17**.

$$T_K\left(\ln K_{OW} - \ln\left(1 + Kf_A^O\right)\right) = a_1 N_C + a_2 \Delta T + a_3 S + a_4 N_{PO} + a_5 N_{EO} + a_6 m_B + a_7 MW + a_8 C_{EO} + a_9 \quad \textbf{(4.18)}$$

where, K_{OW} is the ratio of f_A^O and f_A^W, MW is the molecular weight of the oil, and C_{EO} is 1 if the co-solvent contains 1 or more EO groups and 0 otherwise. K is the self-association constant equal to 44.5. The $\ln\left(1 + Kf_A^O\right)$ term on the left-hand side of the equation was

only used for the data in Solheim, 1990. a_1 to a_9 are coefficients that were determined by linear regression. **Table 4.11** shows the coefficients of the combined model. **Figure 4.11** shows the prediction of the oil-water partition coefficients.

Table 4.11: Coefficients of the Combined Model

Coefficient, Variable	a_i	σ_{ai}	$\lvert\sigma_{ai}/_{ai}\rvert$
a_1, N_C	657	15	2%
a_2, ΔT	7.22	0.66	9%
a_3, S	26.8	3.0	11%
a_4, N_{PO}	122	44	36%
a_5, N_{EO}	-115	4	3%
a_6, m_B	127.6	4.5	4%
a_7, MW	0.560	0.143	26%
a_8, C_{EO}	-598	37	6%
a_9, intercept	-3104	72	2%

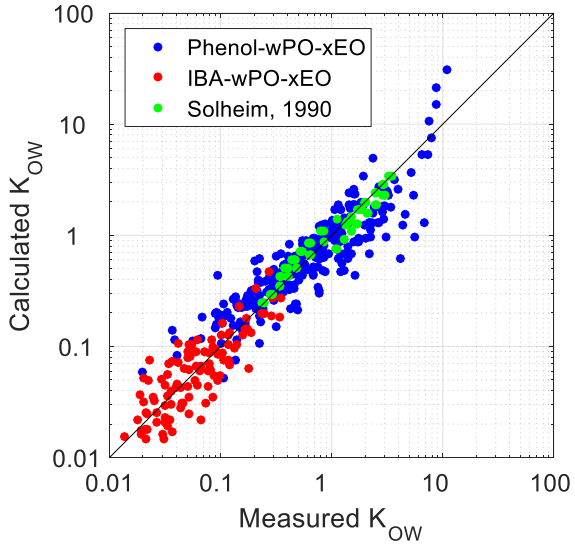

Figure 4.11: Predicted versus measured oil-water partition coefficients of the combined model

4.4 Interface-Water Partition Coefficients of Co-solvents

The phase behavior of water, oil, surfactant, and a partitioning co-solvent is represented by a three-dimensional tetrahydric diagram. The pseudophase model reduces the dimensionality from 3D (tetrahydric) to 2D (pseudo-ternary). The pseudo-ternary diagram is a slice through the tetrahydric diagram such that any phase separation which occurs yields phase compositions lying in the same plane as the overall composition. The vertices of the pseudo-ternary diagram are the aqueous (water and co-solvent), oleic (oil and co-solvent), and interfacial (surfactant and co-solvent) pseudophases. The excess water is the aqueous pseudophase, and the excess oil is the oleic pseudophase. The microemulsion phase is a mixture of the three pseudophases. The oil-water partition coefficient is the ratio of the concentrations of co-solvent in the oleic and aqueous pseudophases. The interface-water partition coefficient (K_{PW}) is the ratio of the concentrations of co-solvent in the interfacial and aqueous pseudophases.

The interfacial pseudophase is a conceptual phase that defines the pseudo-ternary plane. The interfacial pseudophase has volume equal to the volume of surfactant and the associated co-solvent (i.e. ideal mixing). The interface is a surfactant monolayer separating oil and water domains. The interface is affected by oil-surfactant, water-surfactant, and surfactant-surfactant interactions. Therefore, the affinity of the co-solvent for the interface is a function of the surfactant and is also likely affected by the oil and water

There are few experimental measurements of the K_{PW}. Individual measurements are highly uncertain. The K_{PW} and K_{OW} data for multiple measurements at different overall compositions are more accurate. The uncertainty increases as the volumes of surfactant and co-solvent decrease.

4.4.1 Dataset Description

Table 4.12 shows the partition coefficients of phenol ethoxylate co-solvents in different microemulsions. Those with crude A and crude E are repetitions, and those with crude S and crude U are type III microemulsions at different salinities. **Figure 4.12** shows K_{OW} and K_{PW} versus the number of EO groups. **Figure 4.13** shows K_{PW} versus K_{OW} of the components of the co-solvents and the mean of the co-solvents in **Table 4.12**. Lines were included to guide the eye.

The logarithm of K_{OW} decreases linearly with increasing number of EO groups. The K_{PW} is approximately an order of magnitude greater than K_{OW} and in many measurements exhibited a local maximum for the components with K_{OW} equal to 1. The microemulsions with crude S were at the lowest temperature and had the largest maximum K_{PW}. The hydrophilic interaction from hydrogen bonding is greater at low temperature. Both hydrophilic and lipophilic interactions are strong at low temperature.

Table 4.12: Type III Microemulsion Information

Sample	Oil	Chemicals	Electrolytes	T (°C)	σ_O	σ_W	K_{OW}	K_{PW}
A1	50 vol% A	0.66% C_{28}(O)-25PO-25EO-COO 0.3% C_{15-18} IOS 0.4% C_{19-23} IOS **0.6% Phenol-4EO**	6% NaCl	85	1.8	7.4	0.778	8.98
A2				85	6.4	3.7	0.762	9.97
A3				85	3.7	5.5	0.763	7.95
E1	50 vol% E	0.4% C+-45PO-30EO-COO 0.6% C_{19-28} IOS **0.5% Phenol-2EO**	3% $NaBO_2$	85	12.5	7.5	0.953	16.6
E2				85	12.5	10	0.877	16.7
E3				85	15	7.5	1.093	12.4
S1	30 vol% S	0.55% C_{13}-13PO-SO_4 0.20% C_{20-24} IOS **0.75% Phenol-2EO**	3.7% Na_2CO_3	25	16.2	40.0	0.575	28.9
S2			3.85% Na_2CO_3	25	12.0	29.4	0.813	27.9
U1	30 vol% U+20%C6	0.5% C_{28}-35PO-40EO-COO 0.5% C_{15-18} IOS 0.5% C_{19-28} IOS **0.5% Phenol-5EO**	6.2% Soft Brine	78	18.3	12.5	0.769	12.7
U2			6.7% Soft Brine	78	12.4	52.8	0.973	7.98

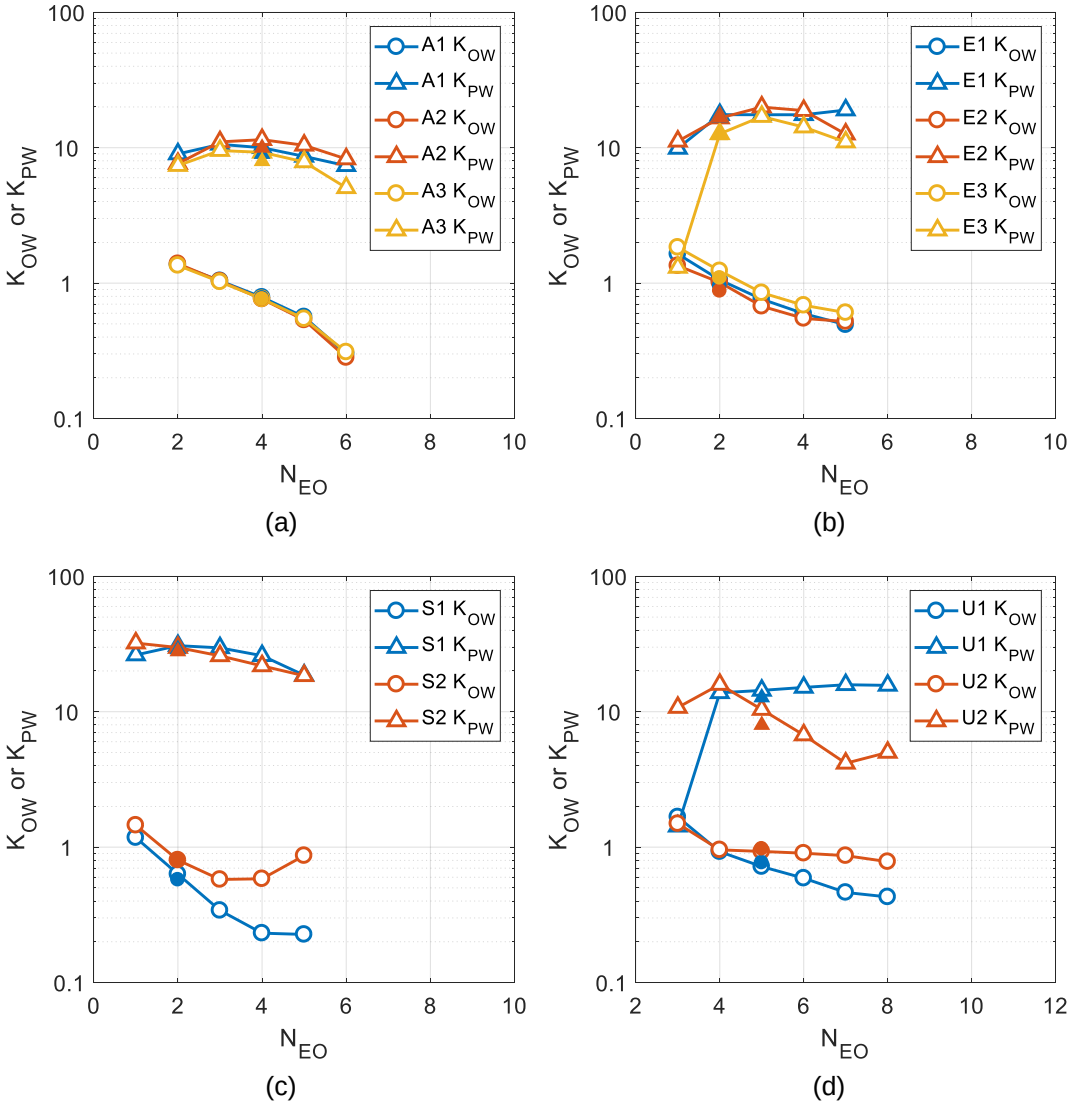

Figure 4.12: Oil-water partition coefficients and surfactant-water partition coefficients versus the number of EO groups for (a) crude A, (b) crude E, (c) crude S, and (d) crude U. Lines are included to guide the eye.

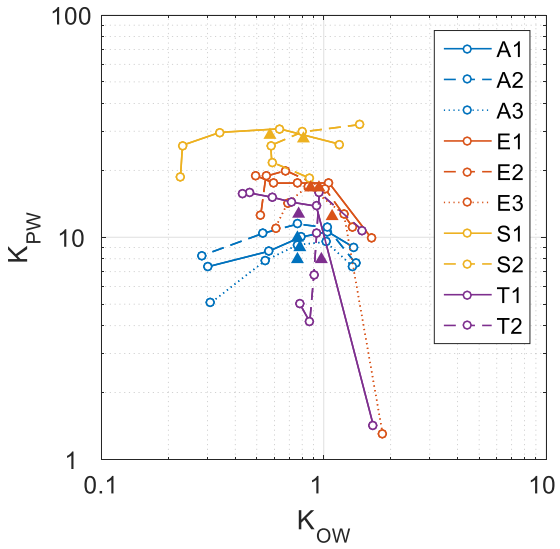

Figure 4.13: The interface-water partition coefficients versus the oil-water partition coefficients of the co-solvent components (open circles) and the mean (solid triangles) of the co-solvents in Table 4.12. Lines are included to guide the eye.

Table 4.13 shows the partition coefficient data for microemulsions reported by Prouvost et al. (1984 and 1985). f_A^W, f_A^O, and f_A^S are the volume percentages of alcohol in the aqueous, oleic, and interfacial pseudophases. Prouvost et al. (1984) proposed equation **(4.19** to calculate the self-association constant, K, of n-alcohols in alkane oils as a function of the carbon number of the alcohol, N_C. f_{A1}^O is the volume percentage of monomeric alcohol in the oleic phase, calculated using K and equation **(4.14**. The oil-water partition coefficient (K_{OW}) is calculated using the concentrations of monomeric alcohol with units of volume/volume solvent.

$$\log_{10} K = 2.693 - 0.233 N_C \qquad \textbf{(4.19)}$$

Table 4.13: Co-solvent Partitioning Data from Literature

Reference	Surfactant/ Oil	CS	T (°C)	S (%)	f_A^W	f_A^O	f_A^S	f_{A1}^O	K	K_{OW}	K_{PW}
Prouvost et al., 1984, Table 4	TRS 10-410 / Decane	i-C_4	30	0.6	1.12	0.26	3.92	0.23	58	0.201	4.19
		i-C_5	30	0.6	0.45	0.57	13.8	0.48	34	1.072	37.02
Prouvost et al., 1985, Table 3		i-C_4	30	1.1	2.31	0.60	6.56	0.45	58	0.189	2.97
Prouvost et al., 1985, Table 5 (From Blevins et al., 1981)	TRS 10-80 / Nonane	i-C_3	25	2.7	5.90	0.11	5.16	0.10	99	0.016	0.87
		i-C_3	25	2.7	6.76	0.13	6.08	0.12	99	0.016	0.89
		i-C_3	25	2.7	9.46	0.22	9.39	0.18	99	0.017	0.99
		i-C_3	25	2.7	11.9	0.32	13.0	0.24	99	0.018	1.11
		i-C_3	25	2.7	12.8	0.37	14.5	0.27	99	0.019	1.16
		i-C_3	25	2.7	13.6	0.42	16.0	0.30	99	0.019	1.21
		i-C_3	25	2.7	15.2	0.54	19.2	0.35	99	0.020	1.33
		i-C_3	25	2.7	16.2	0.63	21.4	0.39	99	0.020	1.42
		i-C_3	25	2.7	17.3	0.76	24.4	0.43	99	0.021	1.54
		i-C_3	25	2.7	19.6	1.17	31.4	0.54	99	0.022	1.88
		i-C_3	25	2.7	20.0	1.27	32.8	0.56	99	0.023	1.96
		i-C_3	25	2.7	20.3	1.38	34.2	0.58	99	0.023	2.03

4.4.2 Model Development

For simplicity, K_{PW} was modeled as a function of K_{OW} defined by equation **(4.20**. **Figure 4.14** is a plot of K_{PW} versus K_{OW} with a trend line calculated from Equation **(4.20**.

$$K_{PW} = 13.34\, K_{OW}^{0.53} \qquad \textbf{(4.20)}$$

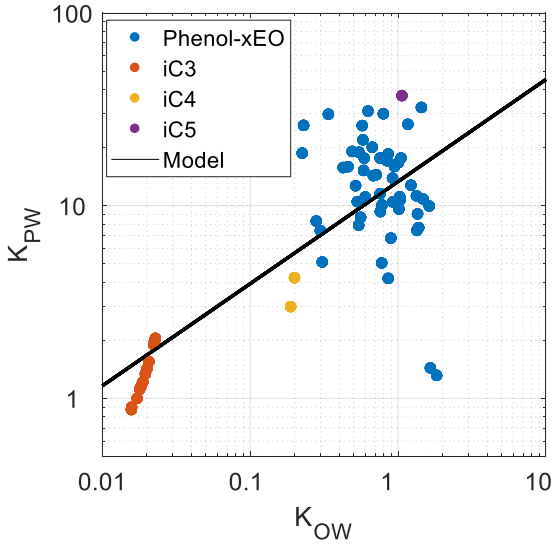

Figure 4.14: Interface-water partition coefficient versus oil-water partition coefficient of various co-solvents in microemulsions.

An oil-water partition coefficient (K_{OW}) of 1 can be achieved by increasing the alcohol carbon number, the number of PO groups, and the number of EO groups such that the increase in hydrophilicity is balanced equally by an increase in lipophilicity. As the hydrophilicity and lipophilicity are simultaneously increased, the molecules become more surfactant-like (e.g. greater K_{PW}). The model does not capture this effect, and therefore will not make accurate predictions of K_{PW}.

4.5 Summary of Co-solvent Partitioning Model

Correlations for estimating the oil-water partition coefficient (K_{OW}) and the interface-water partition coefficient (K_{PW}) of co-solvents were developed. The data used to develop the correlations were measured using liquid chromatography and also obtained from Solheim, 1990, Dwarakanath et al., 1998, Prouvost, et al 1984, and Prouvost, et al 1985.

The oil-water partition coefficient was modeled as a function of the co-solvent structure (alcohol type, number of PO groups, and number of EO groups, and number of hydroxy groups), temperature, salinity, oil molecular weight, and the molality of benzene structures. The effects of pressure, solution gas, and pH were not included in the model. The self-association of the co-solvents in the crude oils was not included in the model, but since the co-solvent concentrations were low (less than or equal to 2 wt% in the aqueous phase before mixing), the effect of self-association is not significant.

The partition coefficients are used to calculate the amount of co-solvent that partitions to the interface in microemulsions using the pseudophase model. Since co-solvent self-association was not modeled, the equations are identical to the Hirasaki model used in the UTCHEM simulator. The volume of co-solvent per volume of surfactant (C_{AS}) is

$$C_{AS} = \frac{V_A K_{PW}}{V_W + V_O K_{OW} + V_S K_{PW}} \tag{4.21}$$

where, V_W, V_O, and V_S are the volume fractions of water, oil, and surfactant, respectively. V_O typically ranges from 0.1 to 0.5 in the microemulsion phase behavior experiments. V_S is typically 0.5-2% of V_W. K_{PW} is an order of magnitude larger than K_{OW}.

Figure 4.15 shows the effects of the partition coefficients on the concentrations of co-solvent associated with water (W), surfactant (S), and oil (O) for a formulation of 1% surfactant and 1% co-solvent with (a) 10 vol% oil, (b) 30 vol% oil, and (c) 50 vol% oil. The concentrations of co-solvent associated with the water, surfactant, and oil are the intercepts of the pseudo-ternary diagram (the pseudophase) with the quaternary diagram. Thus, **Figure 4.15** shows the evolution of the pseudophases with the partition coefficients and the overall composition.

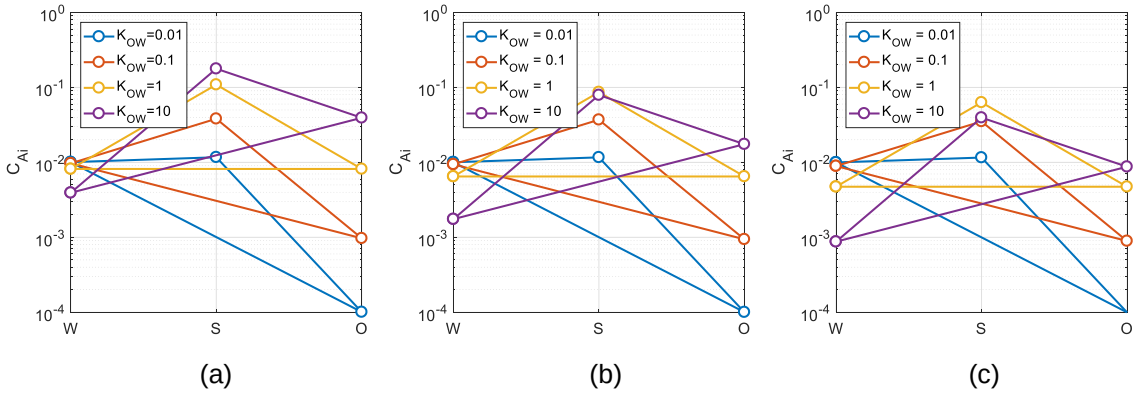

Figure 4.15: The effect of the oil-water partition coefficient on the co-solvent concentrations associated with water, surfactant, and oil for an aqueous solution of 1% surfactant and 1% co-solvent with (a) 10 vol% oil, (b) 30 vol% oil, and (c) 50 vol% oil. Lines are included to guide the eye.

The co-solvent is desired at the interface (i.e. associated with the surfactant), but the co-solvent partitions among the oil, water, and surfactant. As K_{OW} increases, the concentrations of co-solvent associated with the oil and the surfactant increase. When K_{OW} is on the order of 1, the concentration of co-solvent associated with the surfactant is maximized for oil concentrations between 10 and 50 vol%. Therefore, in general, it is desired for the co-solvent to have K_{OW} is on the order of 1.

Nomenclature

a	=	Regression coefficient
A	=	monomeric alcohol in the oil phase
A_n	=	n-meric alcohol in the oil phase
C_{Ai}	=	Concentration of co-solvent associated with component i
C_{EO}	=	Constant equal to 1 for alcohol alkoxylates
f_{A1}^{i}	=	Volume fraction of monomeric alcohol in the oil
f_{A}^{i}	=	Volume fraction of co-solvent in (pseudo)phase i
K	=	Equilibrium constant for self-association of alcohol in oil
K_{OW}	=	Oil-water partition coefficient
K_{PW}	=	Interface-water partition coefficient
m_B	=	Molality of benzene (moles/kg)
MW	=	Molecular weight (g/mol)
N	=	Sample size
N_C	=	(Effective) carbon number of the alcohol
N_{EO}	=	Number of ethylene oxide groups
N_{Ph}	=	Number of phenol groups
N_{PO}	=	Number of propylene oxide groups
R^2	=	Coefficient of determination
S	=	Salinity (wt%)
ΔT	=	Temperature difference from 25 °C
T	=	Temperature (°C)
T_K	=	Temperature (Kelvin)
V_i	=	Volume fraction of component i
σ_O	=	Solubilization ratio of oil
σ_W	=	Solubilization ratio of water
σ_{ai}	=	Standard error or coefficient a_i

Superscripts

0	=	Initial
EW	=	Excess water
EO	=	Excess oil
M	=	Microemulsion phase
O	=	Oleic pseudophase
P	=	Interfacial pseudophase
W	=	Aqueous pseudophase

Subscripts

A	=	Co-solvent
A1	=	Monomeric co-solvent
O	=	Oil
S	=	Surfactant
W	=	Water

Acronyms

ARO	=	Mass fraction of aromatics
ASP	=	Mass fraction of asphaltenes
C16	=	n-hexadecane
C6	=	n-hexane
C8	=	n-octane
Cyc6	=	Cyclohexane
Dec	=	Decalin
EACN	=	Equivalent alkane carbon number of the oil
NSO	=	Mass fraction of resins
SAT	=	Mass fraction of saturates
Tol	=	Toluene

CHAPTER 5: STRUCTURE-PROPERTY MODELS FOR OPTIMUM SALINITY AND OPTIMUM SOLUBILIZATION RATIO

There are thousands of combinations of surfactants and co-solvents that could be tested for each oil, so even approximate predictions are very useful in terms of reducing the time and effort required for testing and for prioritizing the chemical combinations to test that are most likely to yield ultra-low IFT at reservoir conditions. Thus, a predictive model was developed that captures quantitative structure-property relationships between the molecular structures of surfactants and co-solvents and microemulsion phase behavior. Both the optimum salinity and the optimum solubilization ratio (and thus the interfacial tension) are modeled. A dataset consisting of 687 microemulsion phase behavior experiments with 24 unique crude oils, 85 surfactants (internal olefin sulfonates, alkylbenzene sulfonates, alcohol alkoxy sulfates and alcohol alkoxy carboxylates) and 18 co-solvents (alcohols and alcohol alkoxylates) was used for the model development and validation. Variations in the type of hydrophobe (carbon number, degree of branching, polydispersity, and aromaticity), number of propylene oxide groups, number of ethylene oxide groups, and the type of head group (sulfonate, benzene sulfonate, sulfate, carboxylate, hydroxyl) were studied. The oils were characterized using their equivalent alkane carbon number. The model includes the effect of soaps generated from the neutralization of acidic crude oils. The interfacial concentration of co-solvent is calculated using the pseudophase model, the oil-water partition coefficients, and the interface-water partition coefficients. The oil-water partition coefficients and the interface-water partition coefficients were calculated using the models developed in chapter 4.

The model captures many structure-property relationships including the effects of hydrophobe branching, anionic head group type, co-solvent structure and partitioning,

water-oil ratio, and divalent cations. The model is more complete and more general than the hydrophilic-lipophilic deviation model.

The models presented in this chapter are linear functions of the physical parameters. Despite this simplification, the models are sufficiently accurate to provide a useful guide to experimental testing programs for the development of chemical formulations for enhanced oil recovery and other similar applications requiring low interfacial tension.

5.1 Model development

The model developed here for optimum salinity can be considered a generalization of the model developed by Solairaj et al. (2012), which in term was built on the original correlation developed by Salager et al. (1979). The model for the optimum solubilization ratio is based on the model for the optimum salinity.

In general, the properties of the micellar interface (or interfacial pseudophase) control the phase behavior of the microemulsion. It is generally assumed that all the surfactant goes to the interface, whereas only a fraction of the co-solvent goes to the interface due to partitioning. The former is a reasonable assumption because the surfactant concentrations used are typically orders of magnitude greater than the CMC. The partitioning behavior of co-solvents were discussed in Chapter 4.

A wide spectrum of amphiphilic compounds is used in microemulsions. Surfactants form micelles whereas co-solvents tend to dissolve them. Various intermediate-sized molecules such as some alcohol alkoxylates and lipophilic linkers differ in both respects and thus in some sense contradict the binary surfactant/co-solvent categorization. We desire a model that can accommodate all amphiphilic species without needing to discriminate between surfactant/co-solvent.

The concept of the interfacial pseudophase is used to develop the model. The species that go to the micellar interface comprise the interfacial pseudophase and determine the phase behavior of the microemulsion. We model only the amphiphilic species at the interface. We assume molar mixing.

The equation for the optimum salinity:

$$\ln S^* = K\sum_{i}^{O} x_i E_i + a_T \Delta T + \sum_{j}^{M} x_j C_j + a_{17} f_6^S \qquad \textbf{(5.1)}$$

and the optimum solubilization ratio:

$$\sigma^* = L\sum_{i}^{O} x_i E_i + b_T \Delta T + \sum_{j}^{M} x_j D_j \qquad \textbf{(5.2)}$$

where S^* is the optimum salinity in wt% NaCl equivalence, σ^* is the optimum solubilization ratio, x_i is the mole fraction of component i, E_i is the EACN of oil component i, O is the number of components in the oil phase. a_T and b_T are the temperature coefficients, ΔT is the difference in temperature from 25 °C, x_j is the mole fraction of component j, C_j and D_j are the structure characteristic of component j, M is the number of components in the interface. f_6^S is the fraction of surfactant associated with divalent cations. K, L, and b_T are constants.

A linear molar mixing rule was used for multicomponent oil phases. Dead crude oils were treated as single pseudo-components. The EACN of the dead crude oils, toluene, cyclohexane, and decalin were unknown constants that were determined by regression. A linear molar mixing rule was used for the components of the interface, described by the interfacial model. The ion model describes the effect of ions on the optimum salinity.

5.1.1 Interfacial Model

We assume that only the surfactant, soap, and co-solvent structures at the interface influences the microemulsion phase behavior. We assume volumes are additive and the densities of brine, surfactant, and co-solvent are 1 g/ml. The interfacial term is a linear mole fraction average of the structure characteristics of the interfacial components.

All of the synthetic surfactant is assumed to go to the interface. The moles/ml of surfactant j is

$$n_j = \frac{V_j}{V_1 + V_3 + V_7} \frac{\rho_j}{M_j} \tag{5.3}$$

where, V is the volume fraction, ρ is the density in g/ml, M is the molecular weight in g/mol, subscripts 1, 2, 3, 7, S, and j denote brine, oil, surfactant, and co-solvent, soap, and component j. The moles/ml of soap (n_S) and the volume fraction of soap (V_S) are

$$n_s = \frac{V_2 \rho_2 m_D TAN}{56098} \tag{5.4}$$

$$V_s = \frac{n_S M_S}{\rho_S} \tag{5.5}$$

where, m_D is the mass fraction of dead oil in the oil phase, and TAN is the total acid number in mg KOH per gram (dead) oil. Equation **(5.4** assumes the conversion of all acids to soap and the partitioning of all soap to the interface. The molecular weight (M_S) and density (ρ_S) of the soap are assumed to be 400 g/mol and 1 g/ml, respectively. The interfacial concentration of co-solvent k as overall volume fraction (V_j^S) is calculated from Equation **(5.6** and in terms of moles/ml (n_k) it is calculated from Equation **(5.7**.

$$V_j^S = \frac{V_k (V_3 + V_S) K_{PW,k}}{V_1 + V_2 K_{OW,k} + (V_3 + V_S) K_{PW,k}} \tag{5.6}$$

$$n_j = V_j^S \frac{\rho_j}{M_j} \tag{5.7}$$

where, $K_{OW,k}$ is the oil-water partition coefficient of co-solvent k and $K_{PW,k}$ is the interface-water partition coefficient of co-solvent k. $K_{OW,k}$ and $K_{PW,k}$ depend on the properties of all the components and the temperature.

The structure characteristics, C and D, are functions of the molecular structure. Four surfactant types being modeled are internal olefin sulfonate, alkylbenzene sulfonate, alcohol alkoxy sulfate, and alcohol alkoxy carboxylate. The structure of the surfactant is divided by the hydrophobe, the block of PO groups, the block of EO groups, and the head group. The hydrophobe can vary in terms of length, degree of branching, aromaticity, and polydispersity. The blocks of PO and EO groups can vary by the numbers of monomers. The head group can be sulfonate, benzene sulfonate, sulfate, or carboxylate. C_j and D_j are defined as:

$$C_j = \begin{bmatrix} a_1 N_{C,IOS} + a_2 N_{IOS} + a_3 N_{C,ABS} + a_4 N_{ABS} + a_5 N_{C,L} + a_6 N_{C,S} \\ + a_7 N_{C,B} + a_8 N_{C,A} + a_9 N_{PO} + a_{10} N_{EO} + a_{11} N_{SO4} + a_{12} N_{COO} \end{bmatrix}_j \quad \textbf{(5.8)}$$

$$D_j = \begin{bmatrix} b_1 N_{C,IOS} + b_2 N_{IOS} + b_3 N_{C,ABS} + b_4 N_{ABS} + b_5 N_{C,L} + b_6 N_{C,S} \\ + b_7 N_{C,B} + b_8 N_{C,A} + b_9 N_{PO} + b_{10} N_{EO} + b_{11} N_{SO4} + b_{12} N_{COO} \end{bmatrix}_j \quad \textbf{(5.9)}$$

where, $N_{C,IOS}$ and N_{IOS} are the average number of hydrophobe carbon atoms and the average number of sulfonate head groups in the internal olefin sulfonate (IOS) surfactant molecule, $N_{C,ABS}$ and N_{ABS} are the average number of hydrophobe carbon atoms (excluding the benzene carbons) and the average number of benzene sulfonate head groups in the alkylbenzene sulfonate (ABS) surfactant molecule, $N_{C,L}$, $N_{C,S}$, $N_{C,B}$, and $N_{C,A}$ are the number of carbon atoms in the L, S, B, and A type hydrophobes, respectively, defined in **Table 5.1**, N_{PO} is the number of propylene oxide (PO) groups and N_{EO} is the number of ethylene oxide (EO) groups in the surfactant. N_{SO4} is the number of sulfate head groups and N_{COO} is the number of carboxylate head groups per surfactant molecule. The coefficients a_1 to a_{12} and b_1 to b_{12} are constants determined by regression. IOS surfactants

are a mixture of hydroxyalkane sulfonates, alkene sulfonates, and disulfonate species. For simplicity, all IOS surfactants were assumed to be alkene sulfonates. For any particular anionic surfactant, one of the four head group terms in the structure characteristic term is equal to one and the other three are zero. The mole fraction average C_j and D_j for surfactant mixtures is less sparse, so, for example, for a mixture of C_{13}-13PO-SO_4 and an IOS surfactant, the first, second, sixth, ninth, and eleventh terms will be nonzero.

Table 5.1 describes the different types of surfactant hydrophobes. The IOS and ABS type hydrophobes are both distributions of carbon numbers and positional isomers. ABS surfactant molecules have an additional benzene ring, which were not counted as a part of the hydrophobe but part of the benzene sulfonate head group. The carbon number range and degree of branching on the IOS and ABS hydrophobes can vary significantly. The L type hydrophobes are large (C_{16} to C_{32}) twin-tailed hydrophobes having nearly the same tail lengths. The S type hydrophobes are small (C_8 to C_{17}) hydrophobes with varying carbon number ranges and degrees of branching. The B type hydrophobe is for oleyl alcohol (C_{18}), which has a mid-point bent configuration. The A type hydrophobe is for tristyrylphenol (C_{30}), which has aromaticity. The carbon number of the IOS, ABS, L, and S type hydrophobes are variable. The B and A type hydrophobes correspond to only the oleyl alcohol and tristyrylphenol hydrophobes, respectively.

Table 5.1. Description of Hydrophobe Categories

Type	Structural Configuration	Surfactant(s)
IOS	Distribution of carbon number and positional isomers	C_{15}-C_{28} IOS
ABS	Distribution of carbon number and positional isomers	C_{12}-C_{30} ABS
L	Twin-tailed of approximate equal length	Guerbet (C_{16}-C_{32}), dimerized epoxide (C_{16}(O)-C_{32}(O)) alkoxy sulfate or carboxylate
S	Small hydrophobe with slight branching	2-ethyl-hexanol (C_8), approximate C_{13} alcohol (C_{13}, $C_{12\text{-}13}$, $C_{12\text{-}15}$), or approximate C_{16} alcohol ($C_{16\text{-}17}$) alkoxy sulfate or carboxylate
B	Mid-point bent	Oleyl alcohol (C_{18}) alkoxy sulfate or carboxylate
A	Aromatic	Tristyrylphenol (C_{30}) alkoxy sulfate or carboxylate

Formulations with alkali and active oils generate soaps. Each crude oil generates a unique soap. The soaps are treated as a surfactant with unknown hydrophobe structure and carboxylate head group. The structure characteristics for soap S, C_S and D_S, are defined as:

$$C_S = a_S + a_{12}N_{COO} \quad \textbf{(5.10)}$$

$$D_S = b_S + b_{12}N_{COO} \quad \textbf{(5.11)}$$

where, a_S and b_S are constants representing the effect of the unknown hydrophobe structure and are different for different active crude oils. The soaps that are generated from an oil depends on the pH. With increasing pH, higher pKa components are neutralized, and their amphiphilic products may behave synergistically or antagonistically. Thus, the soaps generated using different alkali (e.g. sodium carbonate versus sodium hydroxide) can behave differently. However, for simplicity it was assumed that the properties of the soap were not pH dependent.

The structure of the co-solvents is divided by the hydrophobe (alcohol), the block of PO groups, the block of EO groups, and the hydroxyl group. The hydrophobe can vary in terms of the number of carbon atoms, degree of branching, and aromaticity. The blocks of PO and EO groups can vary in terms of the numbers of monomers. The structure characteristics for co-solvent k, C_k and Dk, are defined as:

$$C_{\mathrm{k}} = \left[a_{13}N_{\mathrm{OH}} + a_{14}N_{\mathrm{C,CS}} + a_{15}N_{\mathrm{PO,CS}} + a_{16}N_{\mathrm{EO,CS}}\right]_{\mathrm{k}} \quad \textbf{(5.12)}$$

$$D_{\mathrm{k}} = \left[b_{13}N_{\mathrm{OH}} + b_{14}N_{\mathrm{C,CS}} + b_{15}N_{\mathrm{PO,CS}} + b_{16}N_{\mathrm{EO,CS}}\right]_{\mathrm{k}} \quad \textbf{(5.13)}$$

where, N_{OH} is the number of hydroxyl groups, $N_{C,CS}$ is the number of alcohol carbon atoms, $N_{PO,CS}$ is the number of PO groups, and $N_{EO,CS}$ is the number of EO groups in the co-solvent molecule. N_{OH} for alcohols and alcohol alkoxylates is equal to one.

5.1.2 Ion Model

Formation brines are composed of various ions (see **Table 5.2**) and the ion composition can change as the injected fluids propagate through the reservoir due to cation exchange (Pope et al., 1978). Divalent cations have an especially significant effect on the phase behavior of anionic surfactants. The optimum salinity decreases with increasing concentration of divalent cations whereas the optimum solubilization ratio remains nearly constant (Aoudia et al., 1995; Healy et al., 1976).

The complexity of real brines is simplified by grouping the ions as monovalent cations, divalent cations, or anions. These pseudo-ions were used to determine cation exchange between the interface and the brine using the mass action law (Hirasaki, 1982). The geochemical interactions (e.g. chelation and precipitation) among these ions were

ignored. **Table 5.2** shows the molecular weight, the conversion factors from wt% to meq/ml, and number of occurrences of the ions in the dataset. f_6^S is defined as:

$$f_6^S = \frac{C_6^S}{C_3} \tag{5.14}$$

where, C is the concentration in meq/ml; subscripts 3, 5, and 6 represent anionic surfactant, pseudo-anion, and pseudo-divalent cation; superscript S denotes adsorbed cation on micelles. The surfactants are at the interface, and the pseudo-anions are free ions in the brine. No superscript denotes overall concentration (sum of the concentrations in the micelle and brine). Only the anionic surfactants associate with cations, so co-solvents are assumed to have no influence. The mass action equation for the exchange of monovalent and divalent cations between the micelle and brine is

$$\frac{\left(C_3 - C_6^S\right)^2}{C_6^S} = \beta_S C_3 \frac{\left(C_5 - C_6 + C_6^S\right)^2}{C_6 - C_6^S} \tag{5.15}$$

where, β_S is the ion exchange constant for the surfactant. The calculations were done using a value of β_S equal to 0.4 (Wang, 1979). C_6^S was determined using non-linear minimization bounded between 0 and the minimum of C_6 and C_3 for the brine composition at the optimum salinity.

Table 5.2: Ion Properties

Ion	MW (g/mol)	Conversion (meq/ml/wt%)	N
Na^+	22.99	0.435	685
K^+	39.10	0.256	259
Mg^{2+}	24.31	0.823	169
Ca^{2+}	40.08	0.499	164
Sr^{2+}	87.62	0.228	11
Cl^-	35.45	0.282	579
$HCO3^-$	61.02	0.164	247
$BO2^-$	42.81	0.234	103
OH^-	17.01	0.588	1
$C_2H_3O_2^-$	59.04	0.169	4
$CO3^{2-}$	60.01	0.333	429
$SO4^{2-}$	96.06	0.208	449
$B4O7^{2-}$	155.23	0.129	25
$SiO3^{2-}$	76.08	0.263	25
$EDTA^{4-}$	288.21	0.139	97

C_5 is the meq/ml of anions at optimum salinity. For consistency with the HLD equation, the optimum salinity is defined as wt% equivalent NaCl as follows:

$$S^* = 5.844\, C_5 \tag{5.16}$$

where 5.844 is the product of the molecular weight of NaCl (58.44 g/mol) and the conversion factor from mg/ml to wt%. **Figure 5.1** shows the optimum salinity in wt% NaCl equivalent versus the optimum salinity in wt%. The difference is relatively small because the most abundant salts are NaCl or have similar equivalent weights.

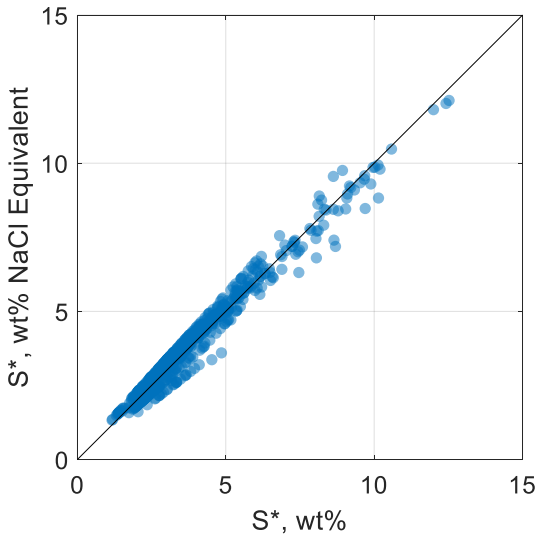

Figure 5.1. Optimum salinity in wt% NaCl equivalent versus optimum salinity in wt%

Figure 5.2 shows the variation of the optimum with the f_6^S for three datasets. For experiments with crude oil R, C_6 varied from 683 to 2182 ppm for a formulation of 0.25% C_{28}-35PO-50EO-COO, 0.25% C_{12} ABS, 0.25% C_{13}-13PO-SO_4, and 0.5% n-butanol-3EO with 30 vol% oil at 44 °C. For experiments with crude oil V, C_6 varied from 67 to 1582 ppm for a formulation of 1.5% $C_{16\text{-}17}$-7PO-SO_4, 0.5% $C_{15\text{-}18}$ IOS, and 2% IBA with 50 vol% oil at 25 °C. For experiments with crude oil S, C_6 varied from 0 to 1323 ppm for a formulation of 0.1% $C_{12\text{-}13}$-13PO-SO_4, 0.2% $C_{20\text{-}24}$ IOS, 0.2% C_{13}-45PO-10EO-SO_4, and 0.25% C_8-7PO-SO_4 with 30 vol% oil at 25 °C. **Figure 5.2**(b) shows the optimum solubilization ratio versus f_6^S. The solubilization ratio slightly increases f_6^S but this is likely caused by slower rate of separation of microemulsions. The effect of divalent cations on the optimum solubilization ratio is a second order effect, but can be misinterpreted using data as first order effect if the microemulsions are not fully equilibrated.

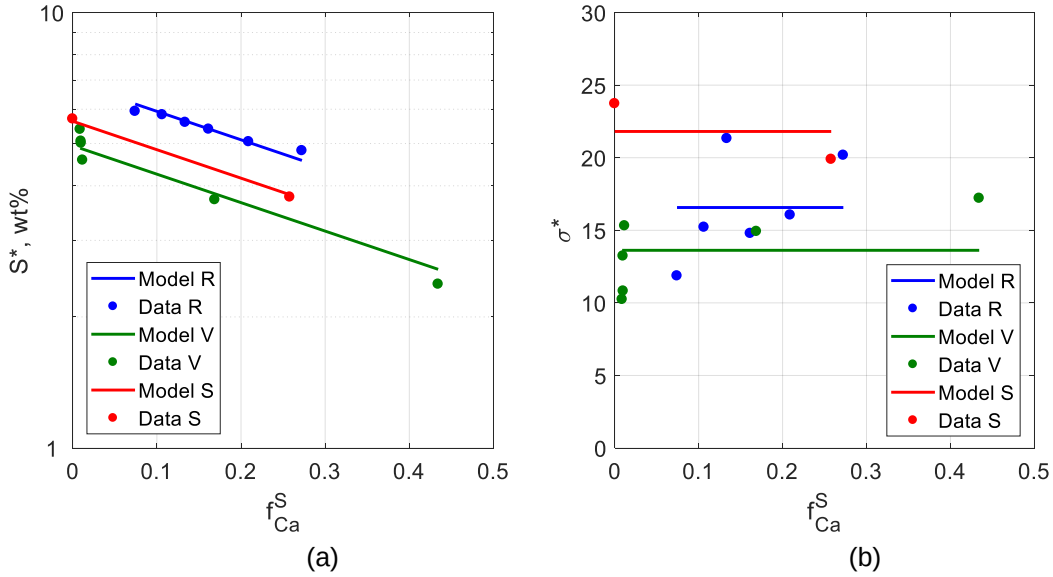

Figure 5.2: Comparison of experimental data with calculated (a) optimum salinity and (b) optimum solubilization ratio versus the fraction of divalent cations adsorbed to surfactant (f_{Ca}^{S}) for (1) 30 vol% Crude R using formulation 0.25% C_{28}-35PO-50EO-COO, 0.25% C_{12} ABS, 0.25% C_{13}-13PO-SO_4, and 0.5% TEGBE at 44 °C, (2) 50 vol% Crude V using formulation 1.5% C_{16-17}-7PO-SO_4, 0.5% C_{15-18} IOS, and 2% IBA at 25 °C, (3) 30 vol% Crude S using formulation 0.1% C_{12-13}-13PO-SO_4, 0.2% C_{20-24} IOS, 0.2% C_{13}-45PO-10EO-SO_4, and 0.25% C_8-7PO-SO_4 at 25 °C.

5.1.3 Solubilization Ratio Model

The typical units of solubilization ratio are volume of oil or water per volume of surfactant, but this neglects the contributions of the soap and co-solvent at the interface. In fact, using this definition, the solubilization ratios of ACP formulations would be undefined (divide by zero). It is therefore better to divide by the interfacial volume. Thus, the solubilization ratio is defined in this work as:

$$\sigma^* = \frac{V_O^M}{V_3 + V_S + V_7^S} = \frac{V_W^M}{V_3 + V_S + V_7^S} \qquad \textbf{(5.17)}$$

where V_O^M is the volume fraction of solubilized oil pseudocomponent, V_W^M is the volume fraction of solubilized water pseudocomponent, and V_7^S is volume fraction of the interfacial

co-solvents (sum of all V_j^S). For simplicity, the co-solvent volume in the water and oil pseudocomponents are assumed to be negligible compared to the volumes of oil and brine, respectively.

Figure 5.3 shows the true optimum solubilization ratio versus the apparent optimum solubilization ratio. The apparent optimum solubilization ratios neglect the volumes of soap and interfacial co-solvent, so they are greater than or equal to the true values.

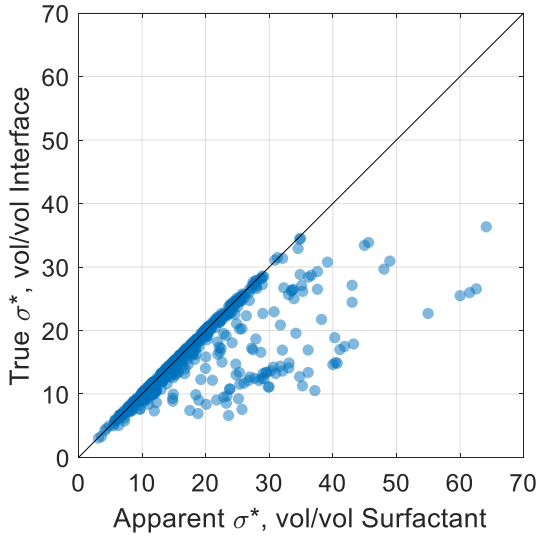

Figure 5.3. Optimum salinity in wt% NaCl equivalent versus optimum salinity in wt% and (b) the true optimum solubilization ratio versus the apparent optimum solubilization ratio.

Figure 5.4 shows the variation of the (a) optimum salinity and (b) optimum solubilization ratio with the mole fraction of soap for various oil volume fractions of mixtures of crude oil J and n-alkanes with 0.5% $C_{12\text{-}13}$-13PO-SO_4, 0.5% $C_{19\text{-}23}$ IOS, and 0.5% phenol-6EO at 55 °C. Crude oil J is an active crude oil with a TAN of 1.18 mg KOH/g oil, and the alkali was Na_2CO_3. The oil volume percentages ranged from 10 to 40 vol% and were controlled such that only the oil EACN varied for three different mole fractions of

soap. The oil volume fraction also affects the interfacial concentration of co-solvent. The oil-water and interface-water partition coefficients were assumed to be 1 and 10, respectively. The optimum salinity and optimum solubilization ratio vary linearly with the mole fraction of soap and is relatively independent of the EACN.

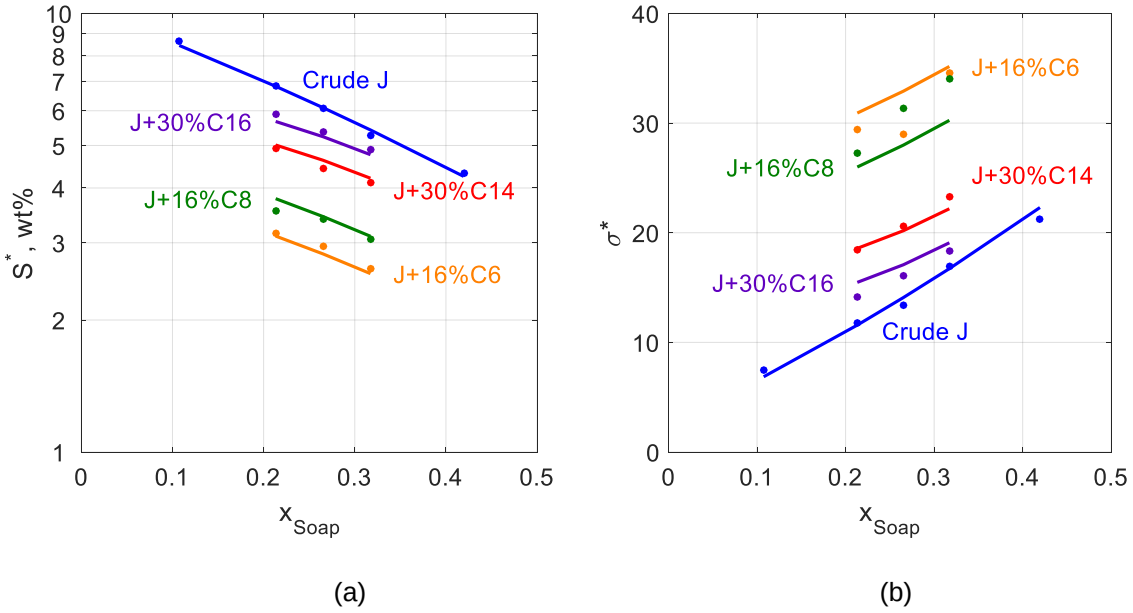

Figure 5.4: Comparison of experimental data with calculated (a) optimum salinity and (b) optimum solubilization ratio versus the mole fraction of soap for mixtures of crude oil J and n-alkanes using formulation 0.5% $C_{12\text{-}13}$-13PO-SO_4, 0.5% $C_{19\text{-}23}$ IOS, and 0.5% phenol-6EO at 55 °C.

5.1.4 Temperature Model

Temperature can increase or decrease the optimum salinity depending on the surfactant type. The $a_T\Delta T$ term in HLD model can be thought of as a first order approximation of a nonlinear temperature effect, where a_T is equal to the derivative of the lnS* with respect to temperature $\left(\frac{d \ln S^*}{dT}\right)$. The true temperature effect would be the integral of the derivative of logarithm optimum salinity with respect to temperature $\left(\frac{d \ln S^*}{dT}\right)$ from

the experimental temperature (T) to the reference temperature of 25 °C. The objective is to capture the effect of temperature for single surfactant systems with respect to variables such as the structure and temperature and for surfactant mixtures (i.e. develop mixing rules).

a_T is 0.01 for most alkyl anionic (AA) surfactants (Acosta & Bhakta, 2009; Salager, 1977) and is negative for nonionic surfactants (Bourrel et al., 1980; Bourrel & Schechter, 1988). Nonionic surfactants interact with water predominantly through hydrogen bonding, whereas AA surfactants interact predominantly through ion-dipole interaction. The strength of hydrogen bonds decreases with temperature, whereas the strength of ion-dipole interaction increases with temperature. This opposite trend allows for mixtures of both types of surfactants to produce intermediate behavior insensitive to temperature (Anton et al., 1992). Alcohol alkoxy anionic (AAA) surfactants have both types of interactions, so a_T decreases with increasing numbers of PO and EO groups.

Figure 5.5(a) shows a_T versus the number of alkoxylate (PO and EO) groups for alkyl sulfate and sulfonate (Acosta & Bhakta, 2009; Salager, 1977; Velásquez et al., 2010), alcohol alkoxy sulfate (Aoudia et al., 1995; Hammond & Acosta, 2012; Velásquez et al., 2010), and alkoxy glycidyl sulfonate (Puerto et al., 2012). Several of these experiments also contained a co-solvent, but there did not appear to be a strong effect. An upper limit of approximately 0.01 is attained with surfactants without alkoxylate groups. The a_T values were constant for the temperature ranges studied (between 20 to 70 °C). A lower limit of approximately -0.01 is attained with about 7 or more alkoxylate groups. The aT values were consistent across multiple studies for temperatures ranging from 20 to 120 °C.

Some studies (Barnes et al., 2008; Puerto et al., 2012) report that a_T of internal olefin sulfonate surfactants gradually decreases from positive to negative with temperature for temperatures between 80 to 150 °C. There is insufficient data to assume this trend is

general for alkyl anionic surfactants. A constant a_T of 0.01 is adequate for temperatures less than ~80 °C and slightly overestimates at higher temperatures. For simplicity, a_T of alkyl anionic surfactants is assumed to be constant with respect to temperature. The equation used to fit the data is:

$$a_T = \frac{a_{T1} + a_{T2}\left(w(N_{PO} + N_{EO})\right)^3}{1 + \left(w(N_{PO} + N_{EO})\right)^3} \quad \textbf{(5.18)}$$

where a_{T1} is the upper limit equal to 0.01, a_{T2} is the lower limit equal to -0.01, and w is a weighting factor found to be 1/3. The data also suggests that the trends are relatively independent of the type of anionic head group (i.e. whether sulfonate, sulfate, or carboxylate).

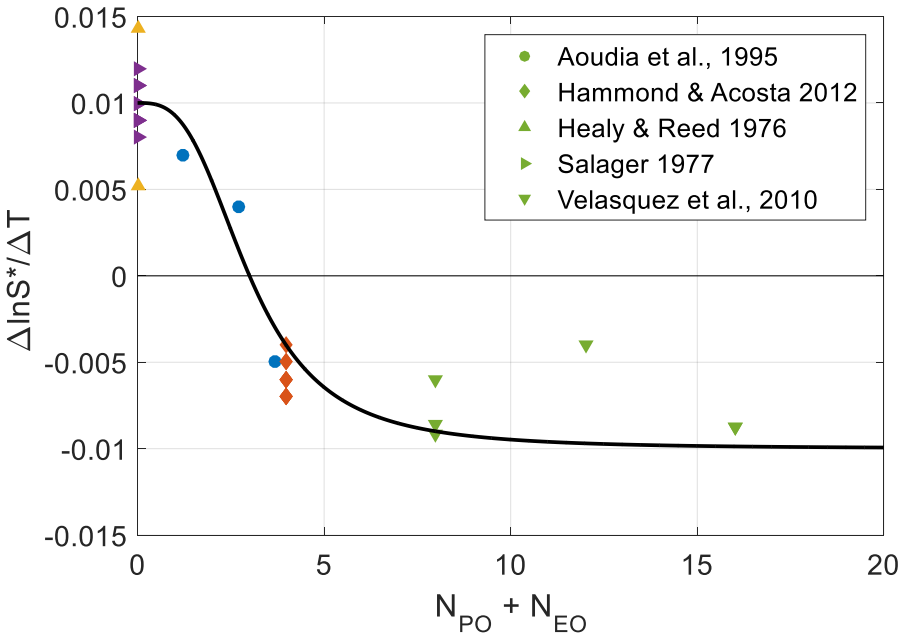

Figure 5.5: Slope of logarithm optimum salinity and temperature versus number of alkoxylate groups for various anionic surfactants.

Mixtures of similar surfactants (e.g. nonionic-nonionic and AA-AA) tend to follow a linear molar mixing rule (Bourrel et al., 1980; Salager et al., 1979). Mixtures of alkyl

anionic and nonionic surfactants form mixed micelles that behave nonlinearly and was modeled using an excess free energy term (Acosta & Bhakta, 2009). Mixtures of alkyl anionic and alcohol alkoxy anionic surfactants have not been well studied. The behavior is likely to be nonlinear. **Table 5.3** shows the microemulsion phase behavior data at different temperatures for various AA and AAA surfactant mixtures from the dataset. x_A is the surfactant mole fraction of AAA surfactant. The AAA surfactants have 13 or more PO + EO groups and would have an expected a_T = -0.01. Crude oils F, I, and J were active oils that generated soap. The experiments with crude F used an alkali-co-solvent-polymer (ACP) formulation (Fortenberry et al., 2015b) that did not have synthetic surfactant. The experiments had slopes of about 0.01, which agreed with those of alkyl anionic surfactants.

Figure 5.6 shows the slope versus the mole fraction of AAA surfactant for the data in **Table 5.3**. Mixtures have a_T of approximately -0.01 (that of AAA surfactants) even though 70-90% of the molecules were AA surfactants. One mechanism for why the AAA surfactants dominate the interfacial interactions is that they extend farther into the bulk phases than the AA surfactants. The equation used to fit the data is:

$$a_T = \frac{a_{T1} + w_2 x_A a_{T2}}{1 + w_2 x_A} \tag{5.19}$$

where, w_2 is a weight factor of about 80. This equation is only applicable for AA-AAA surfactant mixtures where AAA has more than 13 alkoxy groups. The data also suggests that the trends are independent of oil.

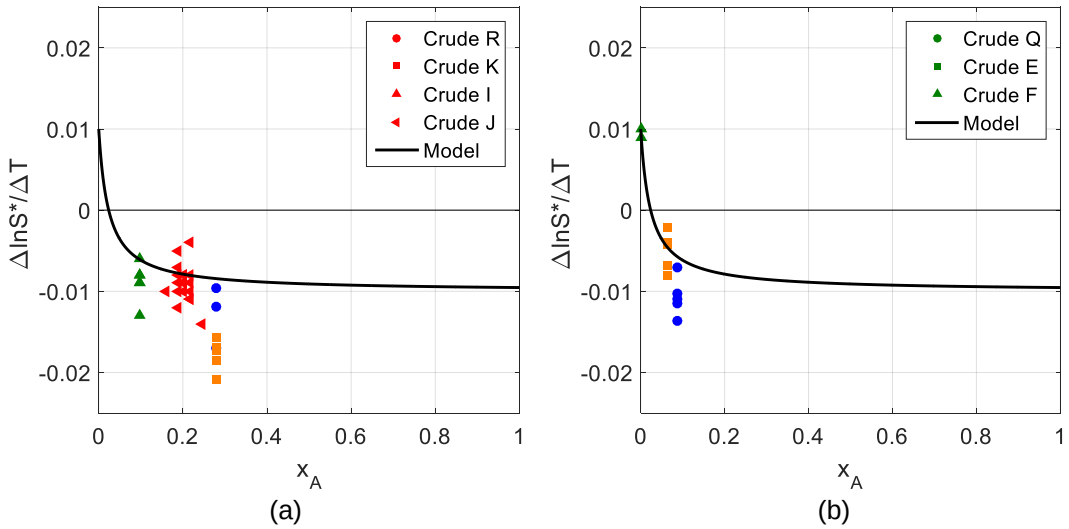

Figure 5.6: Slope of lnS* and temperature versus the mole fraction of alcohol alkoxy anionic surfactant (x_A).

Table 5.3: Temperature data for surfactant mixtures

Formulation	Oil	X_A	Temperature 1			Temperature 2			$\frac{\Delta \ln S^*}{\Delta T}$
			T (°C)	S^* (wt%)	σ^* (v/v)	T (°C)	S^* (wt%)	σ^* (v/v)	
0.4% C_{28}-35PO-10EO-COO 0.6% C_{19-28} IOS 1% TEGBE	Q	0.09	85	3.30	15.9	100	2.78	18.7	-0.011
	Q+15.9%C10	0.09	85	2.54	18.6	100	2.17	22.5	-0.010
	Q+27.4%C16	0.09	85	2.97	20.0	100	2.67	27.0	-0.007
	Q+12.5%C6	0.09	85	2.26	22.9	100	1.84	26.2	-0.014
	Q+5.7%Tol	0.09	85	2.59	19.5	100	2.19	28.1	-0.011
0.4% C_{18}-45PO-30EO-COO 0.6% C_{19-28} IOS 0.5% Phenol-2EO	E	0.06	85	3.17	11.0	100	3.07	13.0	-0.002
	E+27.7%C16	0.06	85	3.52	10.8	100	3.32	13.2	-0.004
	E+12.7%C6	0.06	85	2.29	15.0	100	2.07	25.6	-0.007
	E+13.3%C8	0.06	85	2.72	10.3	100	2.41	21.0	-0.008
	E+4.87%Tol	0.06	85	2.63	11.5	100	2.46	16.7	-0.004
0.5% C_{13}-13PO-SO_4 0.5% C_{20-24} IOS 1% TEGBE	R	0.28	38	5.40	10.2	55	4.05	12.0	-0.017
	R+27%C16	0.28	38	4.77	16.9	55	3.90	16.4	-0.012
	R+12.8%C8	0.28	38	4.26	11.8	55	3.62	9.9	-0.010
0.5% C_{13}-13PO-SO_4 0.5% C_{20-24} IOS 2% IBA	K	0.28	38	2.74	9.5	55	2.06	15.3	-0.017
	K+31.3%C16	0.28	38	3.27	8.5	55	2.51	10.9	-0.016
	K+14.8%C6	0.28	38	1.92	12.3	55	1.40	17.4	-0.019
	K+15.5%C8	0.28	38	2.22	12.3	55	1.55	25.0	-0.021
	K+6.82%Tol	0.28	38	2.10	11.7	55	1.56	26.5	-0.017
0.25% C_{13}-13PO-SO_4 0.25% C_{15-18} IOS 1% TEGBE **Crude I Soap**	I	0.10	38	5.09	25.4	55	4.08	23.9	-0.013
	I+12.5%Dec	0.10	38	4.56	29.7	55	3.97	27.8	-0.008
	I+23.2%C16	0.10	38	5.41	29.1	55	4.67	23.9	-0.009
	I+10.4%C6	0.10	38	4.17	31.8	55	3.62	33.2	-0.008
	I+10.6%C8	0.10	38	4.53	29.6	55	4.08	30.4	-0.006
	I+3.72%Tol	0.10	38	4.66	26.8	55	4.03	26.1	-0.009
0.5% C_{12-13}-13PO-SO_4 0.5% C_{19-23} IOS 0.5% Phenol-6EO **Crude J Soap**	J	0.24	75	6.6	10	55	8.75	8.75	-0.014
	J+15.5%C6	0.22	75	3.15	36	55	3.8	3.8	-0.009
	J+16.3%C8	0.22	75	3.55	34	55	4.45	4.45	-0.011
	J+29.6%C14	0.22	75	4.95	21	55	6.1	6.1	-0.010
	J+29.8%C16	0.22	75	5.95	17	55	6.5	6.5	-0.004
	J+5.6%Tol	0.22	75	3.85	24	55	4.8	4.8	-0.011
	J	0.22	75	5.75	15	55	6.8	6.8	-0.008
	J+15.5%C6	0.20	75	2.95	38	55	3.45	3.45	-0.008
	J+16.3%C8	0.20	75	3.4	38	55	4.1	4.1	-0.009
	J+29.6%C14	0.20	75	4.4	25	55	5.4	5.4	-0.010
	J+29.8%C16	0.20	75	5.35	20	55	6.4	6.4	-0.009
	J+8.6%Tol	0.20	75	3.05	33	55	3.65	3.65	-0.009
	J	0.20	75	5.15	19	55	6	6	-0.008
	J+15.5%C6	0.19	75	2.7	47	55	3.1	3.1	-0.007
	J+16.3%C8	0.19	75	3.05	42	55	3.65	3.65	-0.009
	J+29.6%C14	0.19	75	4.05	32	55	4.9	4.9	-0.010
	J+29.8%C16	0.19	75	4.9	24	55	6.2	6.2	-0.012
	J+7.4%Tol	0.19	75	3	36	55	3.55	3.55	-0.008
	J	0.19	75	4.75	23	55	5.25	5.25	-0.005
	J	0.16	75	3.55	34	55	4.3	4.3	-0.010
1% IBA-5EO **Crude F Soap**	F+9.67%Dec	0.00	100	1.37	31.1	85	1.19	18.8	0.009
	F+10.2%C8	0.00	100	1.41	37.3	85	1.21	17.2	0.010

5.2 Description of Experimental Dataset

The UTCEOR Database is a collection of the experimental surfactant phase behavior measurements conducted at the University of Texas at Austin. The dataset used to develop the structure-property model for the optimum salinity and the optimum solubilization ratio was created by querying the database for the experiments that met the following criteria:

1. The structure (e.g. hydrophobe/alcohol type and carbon number, average numbers of PO and EO groups, type of head group) of the surfactants and co-solvents are known and an average molecular weight can be calculated.
2. The surfactants are sulfonate, sulfate, or carboxylate. The sulfonate surfactants are either internal olefin sulfonate or alkyl benzene sulfonate. The sulfate and carboxylate surfactants are alcohol alkoxy anionic surfactants that have the form of hydrophobe-xPO-yEO-SO4 or hydrophobe-xPO-yEO-COO, where sum of x and y are greater than or equal to 7. The hydrophobe must fall within one of the four types (L, S, B, or A).
3. The co-solvents are aliphatic alcohols, aliphatic alcohol alkoxylated, or phenol alkoxylates. The number of carbon atoms in the alcohol were less than 7, the number of PO groups were less than 2, the number of EO groups are less than or equal to 10.
4. The oil phase was either dead crude oil or surrogate oil.
5. Winsor type I, III, and II microemulsions are observed in the salinity scan. Low IFT is observed at optimum salinity.
6. The most recent solubilization ratio measurements are used.

These criteria exclude experiments that used nonionic, cationic, and zwitterionic surfactants. Some anionic surfactants that did not meet the criteria include alpha olefin sulfonates, dihexyl sulfosuccinate, gemini surfactants (Upamali et al., 2016), and alcohol alkoxy sulfonates.

Most of the formulations were optimized to yield ultra-low IFT at optimum salinity. Co-solvents were used in most formulations to optimize performance for EOR even though they increase the IFT. The dataset has a total of 687 phase behavior experiments using 24 reservoir crude oils, 85 unique surfactants, and 18 unique co-solvents.

5.2.1 Oils

The phase behavior experiments used 114 unique dead and surrogate oils. The surrogate oils are mixtures of the dead crude oil with one of 11 hydrocarbons: n-hexane, cyclohexane, toluene, n-octane, n-decane, decalin, n-dodecane, n-tetradecane, n-pentadecane, n-hexadecane, and n-octadecane. **Table 5.4** shows the properties of the pure hydrocarbons, and **Table 5.5** shows the properties of the dead crude oils. The molecular weights (MW) of the crude oils were obtained from PVT reports, or were measured by freezing point depression, or were estimated from viscosity correlations (Closmann & Seba, 1990). The equivalent alkane carbon number (EACN) of the crude oils, cyclohexane, toluene, and decalin are the values calculated by the regression in the Results section. The crude oil densities (ρ) in g/ml were measured at 25°C and 1 atm. The total acid numbers (TAN) in mg KOH per gram oil of the active crude oils were measured or were obtained from PVT reports. Crude oils with TAN > 0.5 were treated as active in the presence of Na2CO3, except for crude oil R, which, despite its high TAN, was not active. The fractions of saturates (SAT), aromatics (ARO), resins (NSO), and asphaltenes (ASP) in the crude

oils were obtained from PVT reports or were measured by Weatherford Geochemical Services. The number of occurrences (N) of these oil components are also shown.

Figure 5.7(a) shows the distributions of EACN and the proportions of experiments using dead and surrogate oils. 60% of the experiments used dead crude oils and 40% used surrogate oils. **Figure 5.7**(b) shows the distribution of EACN and the proportions of experiments using inactive and active oils. Of the 24 crude oils, 17 are inactive oils and 7 are active oils. 80% of the experiments used inactive crude oils, and 20% used active crude oils. 18% of the experiments used both alkali and an active oil and thus generated soap. The EACN of the oils ranged from 6.8 to 19.0.

Table 5.4: Properties of Pure Hydrocarbons

Name	MW (g/mol)	EACN	σ_{EACN}	ρ (g/ml)	TAN (mg/g)	N
Cyclohexane	84	8.2	1.7 (21%)	0.78	0	42
Toluene	92	4.8	1.5 (31%)	0.87	0	132
Decalin	138	10.4	1.9 (19%)	0.90	0	17
n-Hexane	86	6.0	-	0.65	0	16
n-Octane	114	8.0	-	0.70	0	18
n-Decane	142	10.0	-	0.73	0	4
n-Dodecane	170	12.0	-	0.75	0	1
n-Tetradecane	198	14.0	-	0.76	0	5
n-Pentadecane	212	15.0	-	0.77	0	4
n-Hexadecane	226	16.0	-	0.77	0	22
n-Octadecane	255	18.0	-	0.78	0	4

Table 5.5: Properties of the Dead Crude Oils

Name	MW (g/mol)	EACN	σ_{EACN}	ρ (g/ml)	TAN (mg/g)	Active	SAT (g/g)	ARO (g/g)	NSO (g/g)	ASP (g/g)	N
A	230 [P]	11.8	1.9 (16%)	0.81	-	0	0.31	0.25	0.06	0.01	11
B	310 [P]	16.0	2.2 (14%)	0.88	2.08	1	0.51	0.22	0.24	0.04	13
C	430 [F]	19.0	2.8 (15%)	0.85	0.72	1	0.59	0.19	0.07	0.00	42
D	259 [F]	8.6	2.3 (27%)	0.87	-	0	0.25	0.28	0.11	0.08	3
E	430 [F]	11.2	1.8 (16%)	0.87	0.15	0	0.34	0.30	0.10	0.04	114
F	566 [C]	14.9	5.1 (34%)	0.98	3.5	1	0.08	0.53	0.22	0.10	7
G	245 [P]	9.6	1.7 (18%)	-	-	0	-	-	-	-	15
H	320 [F]	11.4	1.9 (16%)	0.93	0.11	0	0.26	0.37	0.13	0.06	42
I	435 [C]	12.0	3.6 (30%)	0.94	2.05	1	0.33	0.39	0.23	0.05	12
J	307 [F]	16.9	2.4 (14%)	0.90	1.18	1	0.31	0.28	0.11	0.02	38
K	293 [F]	8.5	1.6 (19%)	0.86	0.17	0	0.38	0.24	0.08	0.01	33
L	273 [F]	11.7	1.9 (16%)	0.87	-	0	0.44	0.21	0.07	0.00	18
M	308 [C]	13.3	2.0 (15%)	0.88	-	0	0.28	0.36	0.20	0.08	9
N	272 [C]	9.2	1.8 (19%)	0.87	-	0	-	-	-	-	6
O	432 [P]	11.1	3.0 (27%)	0.86	1	1	0.58	0.25	0.08	0.00	15
P	457 [C]	14.7	2.2 (15%)	0.90	0.77	1	0.28	0.49	0.09	0.00	11
Q	349 [F]	14.3	2.0 (14%)	0.89	0.3	0	0.52	0.19	0.06	0.01	56
R	412 [C]	10.0	1.7 (17%)	0.89	0.8	0	0.23	0.43	0.10	0.02	47
S	238 [F]	10.4	1.8 (17%)	0.86	-	0	0.32	0.23	0.07	0.01	48
T	315 [C]	11.7	1.8 (16%)	0.86	0.08	1	0.31	0.36	0.05	0.00	30
U	401 [F]	14.8	2.2 (15%)	0.91	-	0	0.20	0.26	0.10	0.05	37
V	262 [C]	10.1	1.8 (17%)	-	-	0	0.34	0.21	0.04	0.00	19
W	284 [C]	15.8	2.2 (14%)	0.84	0.2	0	0.28	0.35	0.07	0.02	19
X	230 [P]	10.0	-	0.84	-	0	0.50	0.38	0.10	0.02	45

[P] stated in a PVT report

[F] measured from freezing point depression

[C] estimated from Closmann & Seba (1990) correlation

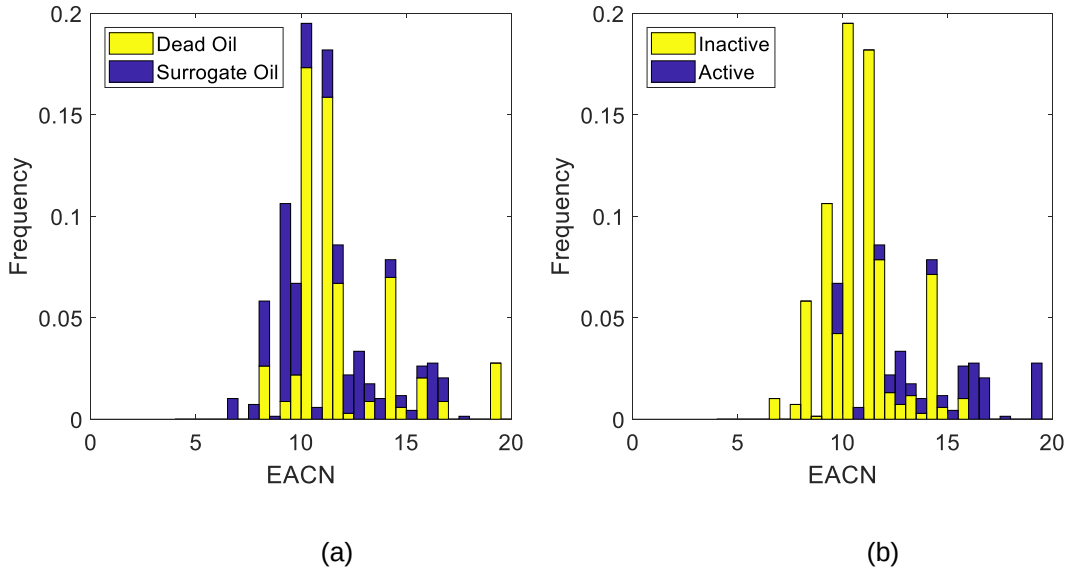

Figure 5.7: (a) Distribution of oil EACN with the proportions of dead and surrogate oil type. (b) Distribution of oil EACN with the proportions of inactive and active oil type.

5.2.2 Brines

The brines were mixtures of sodium chloride, potassium chloride, magnesium chloride, calcium chloride, strontium chloride, sodium bicarbonate, sodium sulfate, sodium carbonate, sodium metaborate, sodium acetate, sodium hydroxide, sodium tetraborate, sodium silicate, and tetrasodium ethylenediaminetetraacetate (EDTA-Na_4) in deionized water. Sodium carbonate, sodium metaborate, sodium acetate, sodium hydroxide, sodium tetraborate, and sodium silicate were alkalis assumed to generate soap with active oils.

38% of the experiments did not have alkali and did not have EDTA, 11% did not have alkali and had EDTA, 25% had alkali and did not have EDTA, and 26% had alkali and EDTA. 25% (169) of the experiments used hard brines. **Figure 5.8**(a) shows the concentration of monovalent cation (C_{11}) versus the concentration of divalent cations (C_6). **Figure 5.8**(a) shows the f_6^S versus C_6. f_6^S increases with increasing C_6 but not linearly. As

C_{11} decreases, f_6^S increases and becomes more sensitive to C_3. Overall, the f_6^S is nearly insensitivity of to C_3. At high salinity, increasing C_6 increases f_6^S approximately linearly. At low salinity, a small increasing of C_6 has a large effect on f_6^S.

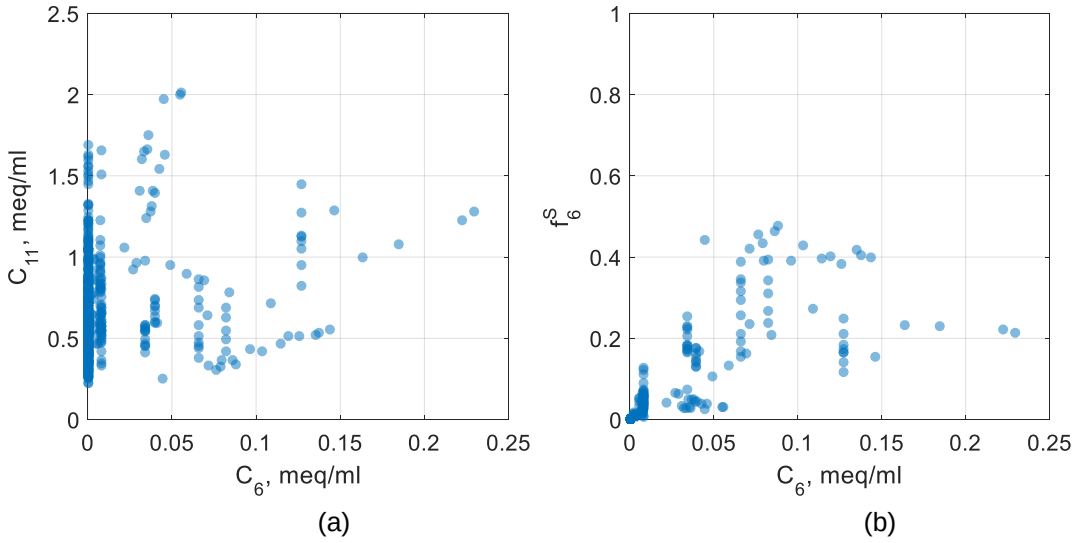

Figure 5.8: (a) The concentrations of monovalent cations (C_{11}) versus divalent cations (C_6) in meq/ml for the experiments in the dataset. (b) The fraction of calcium adsorbed to the surfactant (f_6^S) versus C_6.

5.2.3 Chemicals

The chemical formulations are various combinations of 85 surfactants and 18 co-solvents. Of the surfactants, 5 are internal olefin sulfonates (IOS), 7 are alkylbenzene sulfonates (ABS), 49 are alcohol alkoxy sulfates (SO4), and 24 are alcohol alkoxy carboxylates (COO). The IOS and ABS surfactants have various hydrophobe carbon number distributions ranging from 15 to 28 carbons and 12 to 30 carbons, respectively. The hydrophobes of the SO4 and COO surfactants were C_{16} to C_{32} Guerbet alcohols (Adkins et al., 2010, 2012; Lu et al., 2014), C_{28} epoxide alcohol, C_{18} oleyl alcohol (Upamali et al., 2016), C_{30} tristyrylphenol (Liyanage et al., 2015), ~C_{13} alcohols with various degrees of branching, ~C_{16} alcohols with various degrees of branching, and 2-ethyl-hexanol

(Upamali et al., 2016). Of the co-solvents, two were alcohols (isobutyl alcohol and sec-butyl alcohol) and 16 were alcohol alkoxylates of isobutyl alcohol, normal butanol, or phenol. The number of EO groups in the alcohol alkoxylates ranged from 1 to 10 and a few of them also included one or two PO groups.

Figure 5.9(a) shows the distribution of the temperature and the proportion of experiments using sulfate and carboxylate surfactants. 65% used sulfate surfactants, 29% used carboxylate surfactants and 5% used both sulfate and carboxylate surfactants. **Figure 5.9**(b) shows the distribution of temperature and the proportion of experiments using co-solvent. 80% of the experiments used co-solvents and 20% did not.

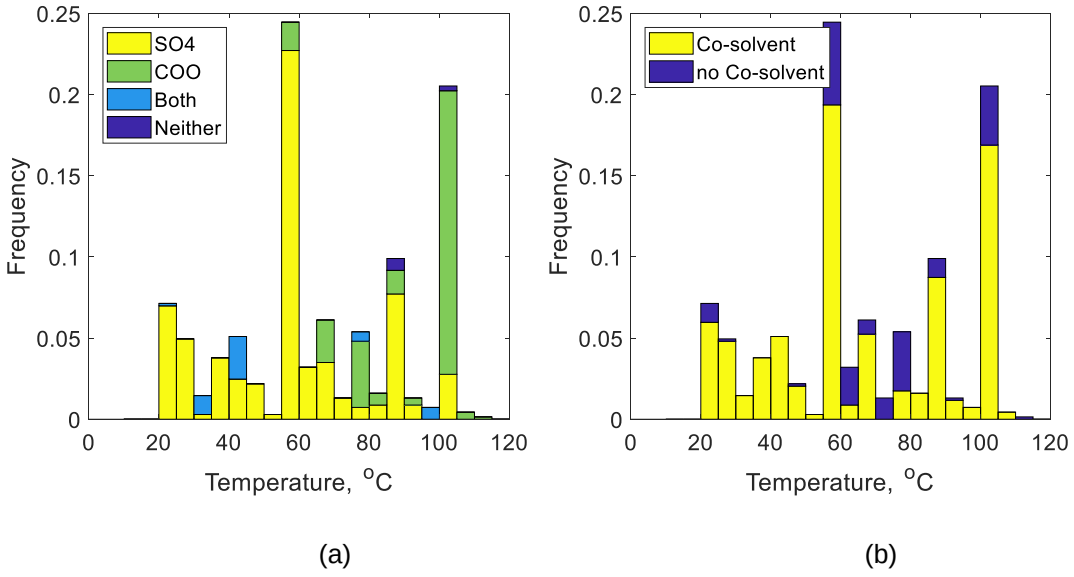

Figure 5.9: (a) Distribution of temperature with the proportion of experiments using sulfate/carboxylate surfactants. (b) Distribution of temperature with the proportion of experiments using co-solvent.

For alcohol alkoxy anionic surfactants, the average numbers of propoxy and ethoxy groups ranged from 0 to 45 and 0 to 80, respectively. **Figure 5.10** shows the distribution of PO and EO groups for (a) alcohol-alkoxy-sulfate and (b) alcohol-alkoxy-carboxylate

surfactants. Of the alcohol alkoxy anionic surfactants, 72% were alcohol-alkoxy-sulfate surfactants and 28% were alcohol-alkoxy-carboxylate surfactants. Most of the sulfate surfactants with less than 15 PO groups had S type hydrophobes without ethoxy groups. There are no S type hydrophobe alkoxy carboxylate surfactants in the dataset. Nearly all carboxylate surfactants contained at least 10 EO groups, with the exception of a C_{30}(TSP)-45PO-COO surfactant.

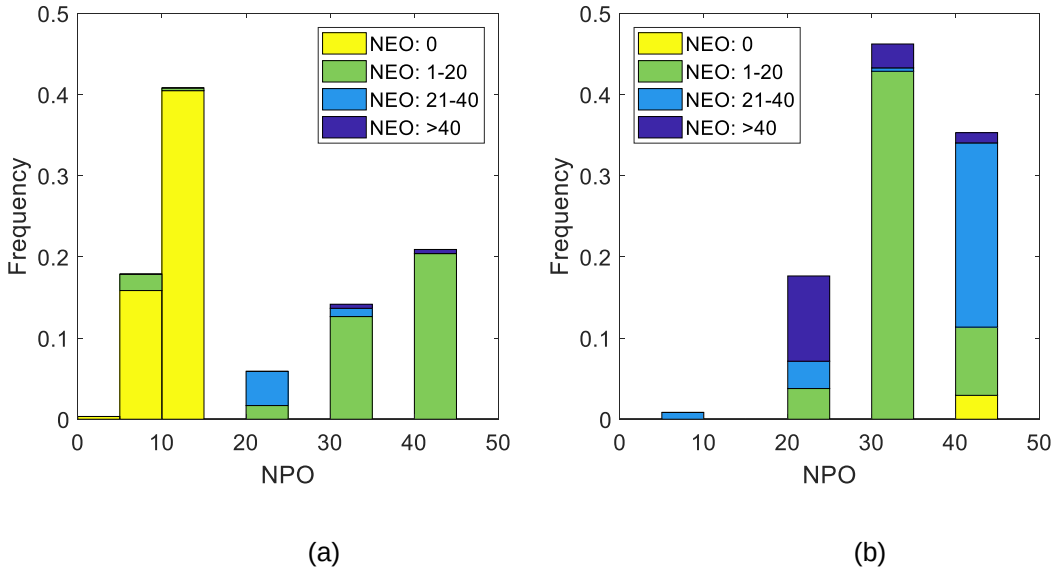

Figure 5.10: Distribution of the numbers of PO groups (NPO) and the number of EO groups (NEO) for (a) alcohol alkoxy sulfate and (b) alcohol alkoxy carboxylate surfactants.

The temperature coefficient a_T is a function of the mole fraction of alcohol-alkoxy-sulfate and –carboxylate surfactant (x_A). **Figure 5.11** shows the distribution of x_A for formulations using (a) IOS and (b) ABS as the co-surfactants and the proportions of the alcohol-alkoxy-anionic surfactant that are sulfate (SO4), carboxylate (COO), and both sulfate and carboxylate. The average, standard deviation (St. Dev.), and number of samples (N) for each of these surfactant mixtures are shown in **Table 5.6**. 78% of the experiments

used IOS co-surfactants, and 19% used ABS co-surfactants. Soaps were considered as alkyl anionic surfactants.

The average mole fraction of alkoxy-carboxylate surfactants was approximately 9 mol% with a narrow distribution (standard deviation of 2 mol%), whereas the average mole fraction of alkoxy-sulfate surfactants was approximately 25 mol% with a much broader distribution (standard deviation of 16 mol%). The carboxylate surfactants were larger molecules (>20 PO and >10 EO groups), whereas sulfate surfactants were a bimodal distribution of lower molecular weight (~13PO and 0 EO groups) and higher molecular weight (>20 PO and >10 EO groups) surfactants as seen in **Figure 5.10**. The broader molecular weight distribution for sulfate surfactants likely contributes to the broader mole fraction distribution.

The narrow mole fraction distribution of carboxylate surfactants of about 9 mol% is peculiar. 9 mol% may be an optimal mole fraction in terms of synergistic interactions (e.g. IFT, interfacial fluidity, or coalescence rate). Further investigation is required.

Table 5.6: Mole Fractions of Alcohol-alkoxy-anionic Surfactant (x_A)

Name	Mole Fraction Sulfate			Mole Fraction Carboxylate			Mole Fraction SO4 and COO		
	Average	St. Dev.	N	Average	St. Dev.	N	Average	St. Dev.	N
IOS	0.26	0.16	390	0.08	0.02	140	0.33	0.07	10
ABS	0.19	0.20	43	0.11	0.02	59	0.31	0.01	26

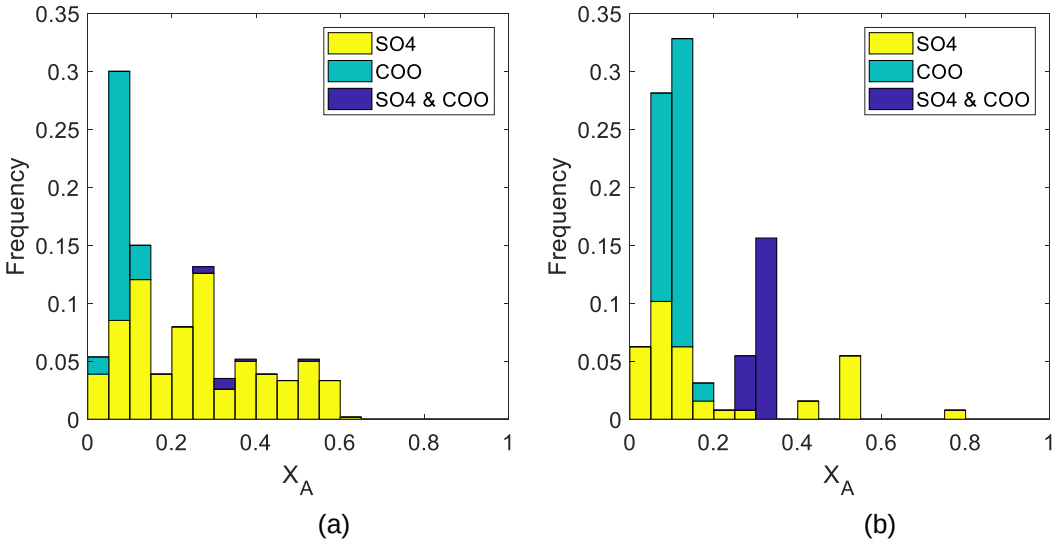

Figure 5.11: Distribution of the mole fraction of alcohol-alkoxylate-sulfate and -carboxylate (x_A) for (a) IOS and (b) ABS surfactants with the proportion of experiments using sulfate, carboxylate, and both sulfate and carboxylate.

Figure 5.12 shows the distribution of (a) the mole fraction of alkyl anionic surfactant and (b) the calculated temperature coefficient (a_T) for the experiments in the dataset. Mole fraction of 0 (1, respectively) corresponds to a_T = 0.01 (a_T = -0.01, respectively). Equation **(5.19** gives tremendous weight to the AAA surfactant.

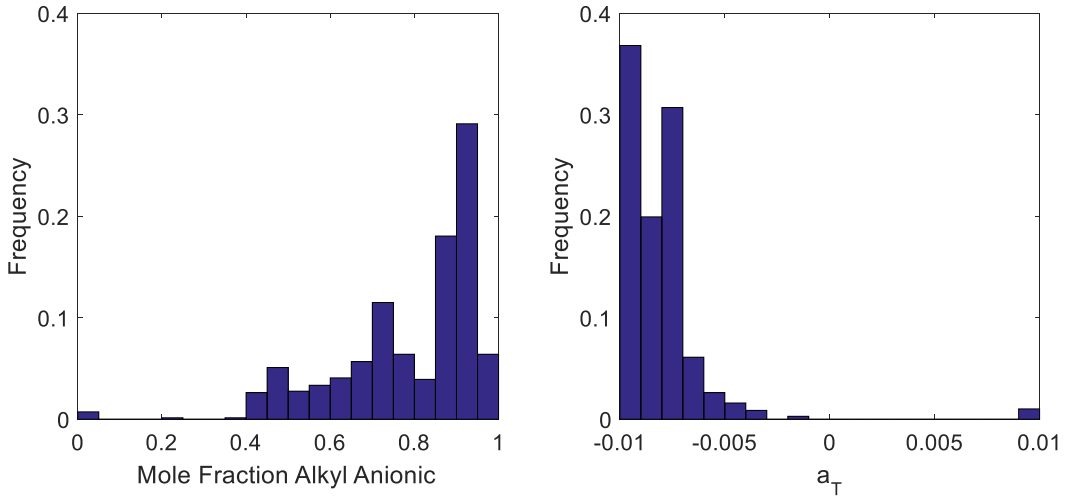

Figure 5.12: Distribution of (a) the mole fraction of alkyl anionic surfactant and (b) the calculated temperature coefficient (a_T) for the dataset.

The interfacial concentration of co-solvent depends on the overall composition of oil, water, surfactant, and co-solvent and the partition coefficients. **Figure 5.13** shows the distribution of the (a) oil-water partition coefficient (K_{OW}) and (b) the interfacial-water partition coefficient (K_{PW}) for the different co-solvent types. 22% were alcohols, 41% were alcohol ethoxylates, 1% were alcohol propoxy ethoxylates, 32% were phenol ethoxylates, and 4% were phenol propoxy ethoxylates. The distributions of K_{PW} and K_{OW} have the same shape but are scaled differently. On average, the K_{OW} is 0.30 and K_{PW} is 7.1.

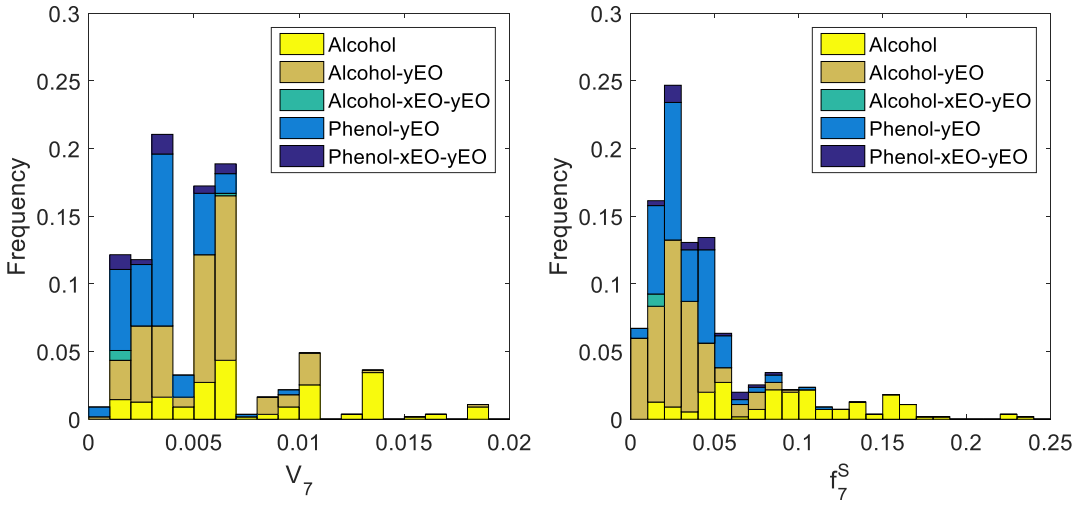

Figure 5.14 shows the distribution of the (a) overall volume fraction of co-solvent and (b) the interfacial volume fraction of co-solvent for the different co-solvent types. Despite partitioning to the water and oil phases, the co-solvent still comprises a significant volume fraction of the interface.

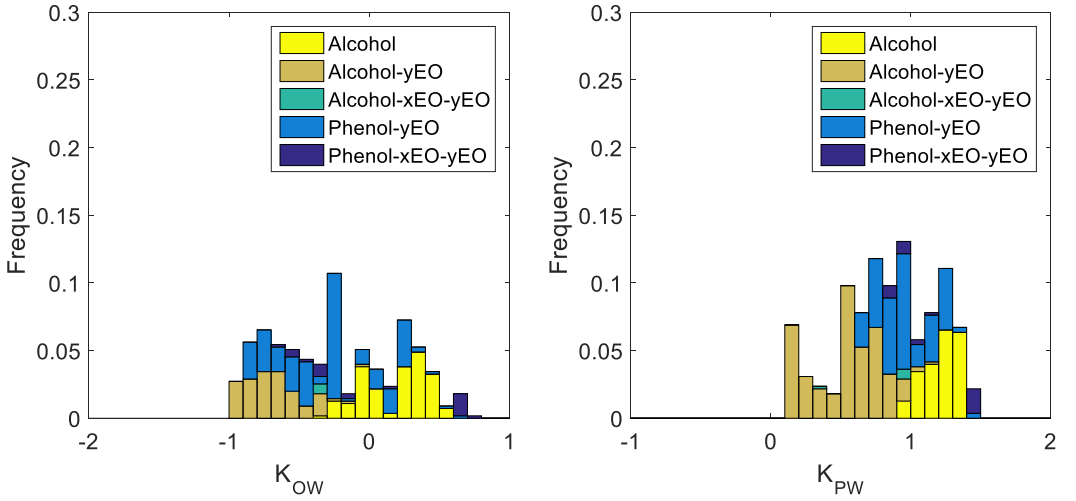

Figure 5.13: Distribution of oil-water partition coefficient (K_{OW}) and the interface-water partition coefficient (K_{PW}) with the proportion that are alcohols, alcohol ethoxylates, alcohol propoxy ethoxylates, phenol ethoxylate, and phenol propoxy ethoxylates.

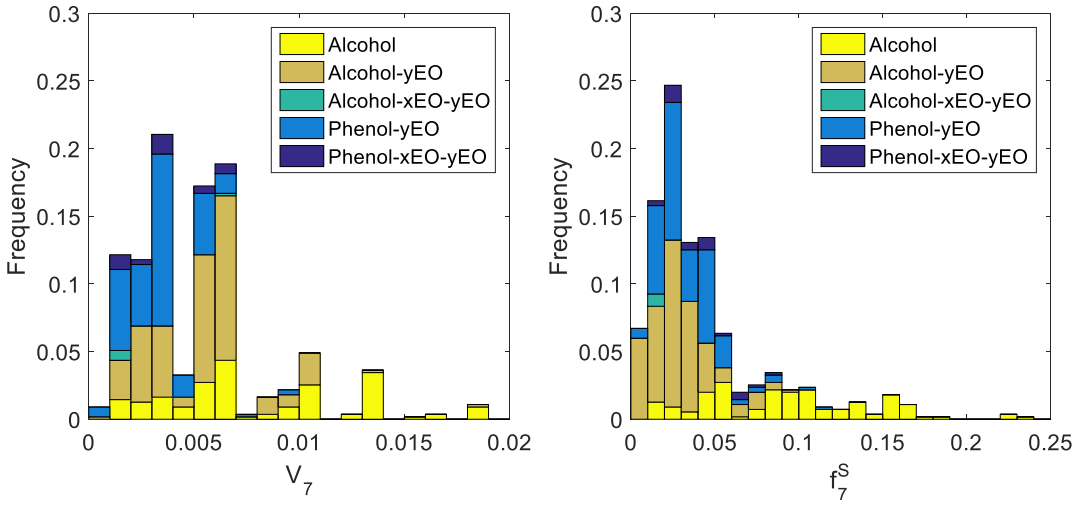

Figure 5.14: Distribution of (a) volume fraction of co-solvent and (b) interfacial volume fraction of co-solvent with the proportion that are alcohols, alcohol ethoxylates, alcohol propoxy ethoxylates, phenol ethoxylate, and phenol propoxy ethoxylates.

5.2.4 Microemulsion Phase Behavior Properties

The microemulsion phase behavior experiments in the dataset were pooled from multiple projects. During the formulation development, the surfactant and co-solvents in the formulations were systematically varied and the phase behavior observed over a range of salinity. Emulsion tests were done to quickly identify promising formulations exhibiting low IFT. The emulsion test is a visual observation of the emulsion appearance and coalescence behavior after mixing. It is a quick and reliable screening method for identifying the best formulations without having to wait long times for the phases to reach equilibrium (Flaaten et al., 2009; Levitt et al., 2009). Qualitative observations include the microemulsion fluidity, the tendency to form undesirable long-range structures (viscous macroemulsions, gels, and birefringent microemulsions), and the coalescence rate. The best formulations based on the emulsion test are then observed for longer times until the fluids equilibrate. The phase volumes are measured and used to calculate solubilization

ratios after the phase volumes stop changing and the phases appear to be at or near equilibrium. Only high-quality data were included in the dataset and used for the correlations.

Figure 5.15 shows the distribution of the optimum salinity and optimum solubilization ratio for different types of formulations. 18% were surfactant-polymer (SP), 64% were alkali-surfactant-polymer without soap (ASP), 17% were ASP with soap (ASP soap), and 1% are alkali-co-solvent-polymer (ACP) formulations. The optimum solubilization ratios were calculated as the volume of oil (or water) in the microemulsion divided by the volume of the interface, which includes the volumes of surfactant, soap, and interfacial co-solvent.

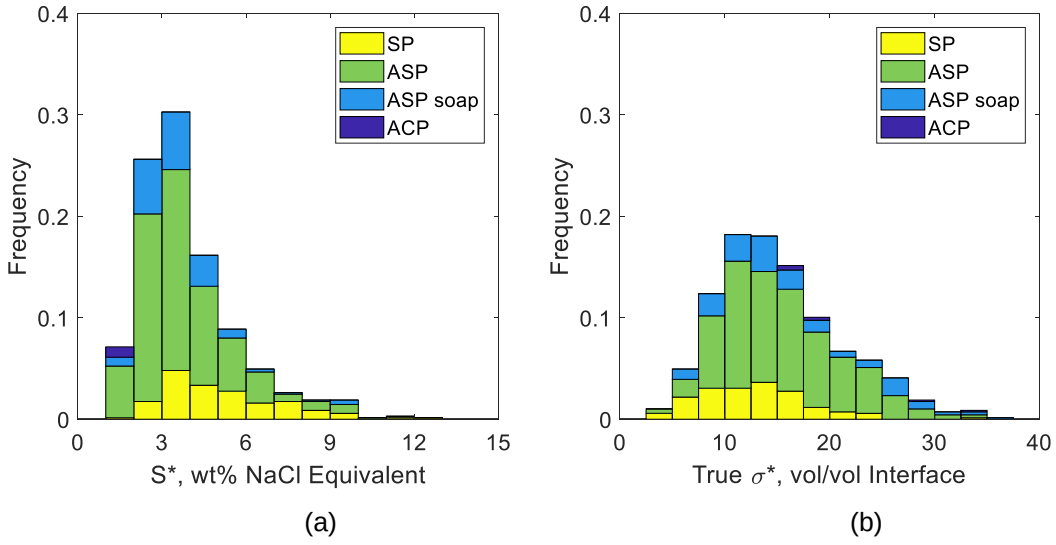

Figure 5.15: Distribution of (a) the optimum salinity and (b) the true optimum solubilization ratio for surfactant polymer (SP), alkali surfactant polymer with soap (ASP soap) and without soap (ASP), and alkali co-solvent polymer (ACP) formulations.

Figure 5.16(a) shows the distribution of the natural logarithm of the interfacial volume parameter (ln *I*) and the proportion of the formulation types. The arithmetic average

is reported when two I values were used. The distribution is approximately Gaussian with a mean of -1.43 (I = 0.24) and standard deviation of 0.53. **Figure 5.16**(b) shows the distribution of the oil volume fraction (V_2) and formulation type. The oil volumes have a significant impact on the experiments containing co-solvent (80%) and soap (18%).

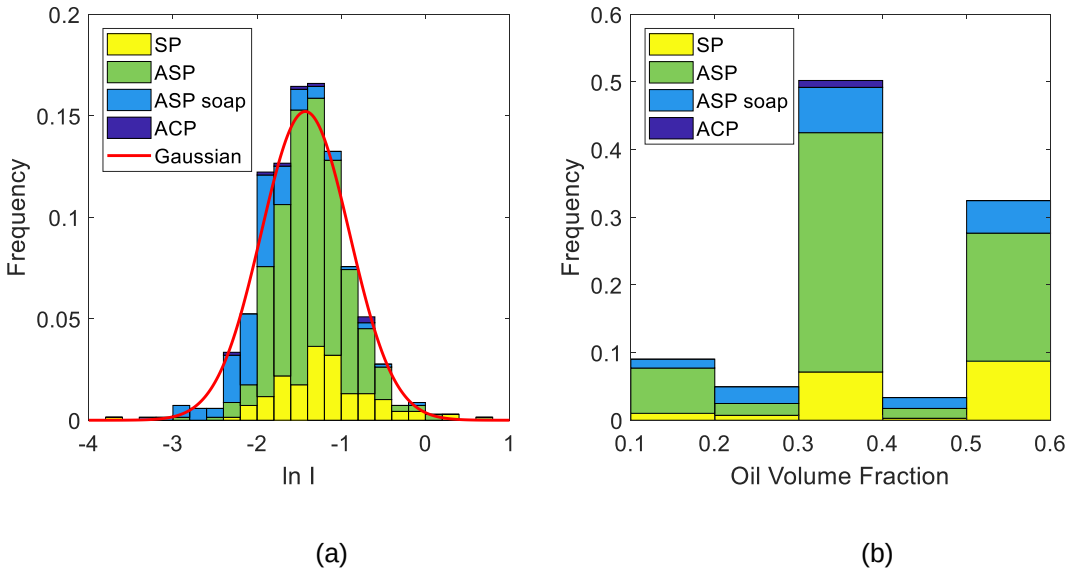

Figure 5.16: (a) Distribution of the natural logarithm of the interfacial volume ratio, I, and (b) the distribution of the volume fraction of oil for different types of formulations.

5.2.5 Experimental Uncertainty

When comparing values calculated from the model with the data, some rough idea of the experimental uncertainty is needed to interpret the results of the model comparisons. Salinity scans for microemulsion phase behavior were typically done at 0.5 wt% salinity intervals. The phase volumes in sealed pipettes were observed over at least several weeks. The volume of oil solubilized in the microemulsion is calculated from the difference between the initial interface and the interface between the oil and microemulsion phases. The volume of water solubilized in the microemulsion is calculated from the difference

between the initial interface and the interface between the water and microemulsion phases. The effect of thermal expansion was neglected. Solubilization ratios were calculated assuming a surfactant density of 1 g/cc.

Monotonically increasing (decreasing) curves versus salinity were fit to the oil (water) solubilization ratios in order to estimate the optimum solubilization ratio from the intersection of the curves. However, the emulsion test is often a more reliable estimate of the optimum salinity than the point where the solubilization ratio curves cross. The solubilization ratios nearly always decrease with time until equilibrium is reached. Typically, 20 interface readings at different times are required for estimating the solubilization ratios. The sealed graduated pipettes used in this study are marked every 0.1 ml and the total fluid volume in the pipette is 4 ml. Phase volumes can be read within an uncertainty of about 0.05 ml. For a typical optimum solubilization ratio of 15, an error in the oil volume of 0.05 ml corresponds to an error in the optimum solubilization ratio of 2.5.

Figure 5.17 shows solubilization ratios of six repetitions of a sodium carbonate scan using the formulation 0.5% C_{28}-35PO-10EO-SO_4-, 0.5% C_{19-28} IOS, 1.0% n-butanol-3EO with 50 vol% crude oil Q at 85 °C. For this example, the uncertainty in the optimum salinity is about 0.4 wt% and the uncertainty in the optimum solubilization ratio is about 6 cc/cc. The experimental uncertainty in these values for the entire dataset is difficult to quantify so the following estimates are very approximate. The optimum salinity varied from 0.5 to 15 wt% with an uncertainty of roughly 0.5 wt%. The optimum solubilization ratio varied from 8 to 40 cc/cc with an uncertainty of roughly 5 cc/cc. This uncertainty of 5 cc/cc in the optimum solubilization ratio is larger than the value of 2.5 cc/cc estimated from the error in reading the phase volumes for several reasons: (1) variations in the batches of surfactants and crude oils, (2) not enough time is allowed for equilibrium, and (3) the

presence of macroemulsions at the interfaces increases the uncertainty in the interface readings.

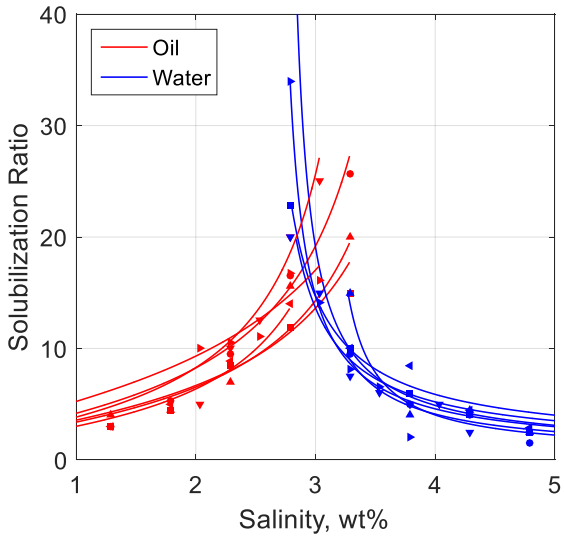

Figure 5.17: Repetitions of 0.5% C_{28}-35PO-10EO-SO_4, 0.5% C_{19-28} IOS, 1.0% n-butanol-3EO, variable Na_2CO_3 with 50 vol% crude oil Q at 85 °C.

The composition of crude oils can vary by well, time, treatment conditions (e.g. handling, separation, filtration), etc. The surfactants and co-solvents can vary by manufacturer, the season, etc. The structures of the surfactants and co-solvents are also uncertain as the purity of reagents and reaction conditions can affect the distribution of homologues, polydispersity, ramification of hydrophobes, extent of reactions, and impurities. Over the last two decades, multiple batches of the same crude oils, surfactants, and co-solvents were used and their properties could have varied. This type of uncertainty can be reduced by following standardized procedures and obtaining the highest quality chemicals.

5.3 Results

The dataset was split into a training set and a test set. The training set was used to develop the model, and the test set was used to cross-validate the model. The training set is composed of the experimental data with crude oils A through W and has a sample size of 647. The test set is composed of the experimental data with crude oil X and has a sample size of 45, which comprises 6.5% of the dataset. Crude oil X is inactive.

Applying equation **(5.1** results in a system of 647 linear equations for the optimum salinities and applying equation **(5.2** results in a system of 647 linear equations for the optimum solubilization ratios in the training set. For the optimum salinity, there were 51 unknowns (1 for K, 23 for the K×EACN of the dead oils, 3 for the K×EACN of cyclohexane, toluene, and decalin, 12 for surfactant structure coefficients, 4 for co-solvent structure coefficients, 7 for the unique soap structure coefficients, and 1 for the coefficient of f_6^S). These 51 unknowns were determined by multiple linear regression. Since a_T was calculated using equation **(5.19**, the $a_T\Delta T$ term is known. The EACN of the oils were calculated by dividing the K×EACN values by K. The EACN of the oils were then used as input for the optimum solubilization ratio equations. For the optimum solubilization ratio, there were 25 unknowns (1 for G, 12 for surfactant structure coefficients, 4 for co-solvent structure coefficients, 7 for the unique soap structure coefficients, and 1 for the temperature coefficient b_T). These 25 unknowns were determined by multiple linear regression. The ratio of equations to unknowns is approximately 12.5 for the optimum salinity and is approximately 25.6 for the optimum solubilization ratio.

5.3.1 Optimum Salinity and Optimum Solubilization Ratio Correlations

Figure 5.18 shows the predicted versus measured optimum salinity (S^*) and optimum solubilization ratio (σ^*). The values and standard errors of EACN for the different diluents and dead crude oils are shown in **Table 5.4** and **Table 5.5**, respectively. **Table 5.7** shows the slopes of the oil EACN (K and L), the temperature coefficient b_T, and the average of a_T. **Table 5.8** shows the coefficients for the surfactant and co-solvent structures and the coefficient for f_6^S. **Table 5.9** shows the coefficients for the soap structures. The number of experiments (N), the standard error (σ_{ai}), and the relative standard error ($|\sigma_{ai}/ai|$) for each coefficient are shown.

The coefficient of determination (R^2) values are 0.83 for the prediction of the natural logarithm of S^* ($\ln S^*$) and 0.84 for the prediction of the S^*. The standard errors (standard deviation of the error) are 0.17 for the $\ln S^*$, 0.66 wt% NaCl equivalent for S^*, and 0.17 for the relative optimum salinity ($\Delta S^*/S^*_{Measured}$). The R^2 of the optimum solubilization ratio is 0.38. The standard errors are 4.7 cc/cc for σ^* and 0.40 for the relative optimum solubilization ratio ($\Delta\sigma^*/\sigma^*$). The standard error in the optimum solubilization ratio is about the same as in the example shown in **Figure 5.17**. As discussed above, the volume measurement itself contributes an uncertainty of about 2.5 cc/cc and the total uncertainty is roughly 5 cc/cc. Although it is possible to reduce this experimental error for specific experiments with ideal phase behavior, it is not practical to do so for the very large dataset presented here and a very large dataset such as this is needed because of the wide variety of chemicals and oils that are used in chemical EOR.

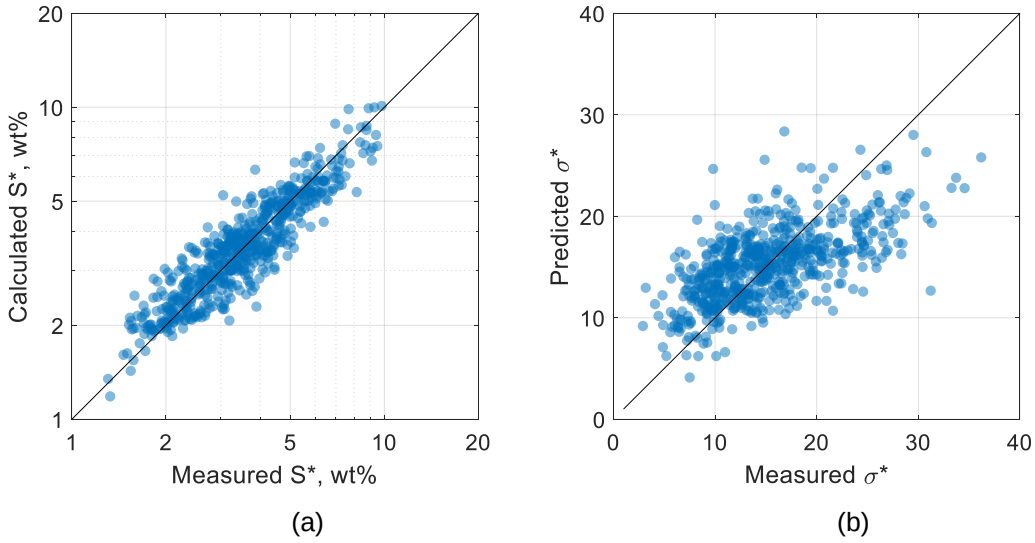

Figure 5.18: Predicted versus measured (a) optimum salinity and (b) optimum solubilization ratio.

Table 5.7: Coefficients for EACN and Temperature

Subscript i, Variable	N	Optimum Salinity			Optimum Solubilization Ratio		
		a_i	σ_{ai}	$\lvert\sigma_{ai}/a_i\rvert$	b_i	σ_{bi}	$\lvert\sigma_{bi}/b_i\rvert$
K (L), EACN	74 (647)	0.115	0.012	10%	-0.86	0.14	16%
a_T (b_T), ΔT	627				0.064	0.015	23%

Table 5.8: Coefficients for Surfactant and Co-Solvent Structures

Subscript i, Variable	N	Optimum Salinity			Optimum Solubilization Ratio		
		a_i	σ_{ai}	$\lvert\sigma_{ai}/a_i\rvert$	b_i	σ_{bi}	$\lvert\sigma_{bi}/b_i\rvert$
1, $N_{C,IOS}$	502	-0.209	0.014	7%	1.44	0.2	14%
2, N_{IOS}	502	5.15	0.36	7%	-13.1	4.1	31%
3, $N_{C,ABS}$	128	-0.195	0.018	9%	1.14	0.35	30%
4, N_{ABS}	128	3.62	0.31	9%	-2.8	5.1	183%
5, $N_{C,L}$	272	-0.111	0.016	14%	0.60	0.32	53%
6, $N_{C,S}$	324	-0.114	0.016	14%	1.23	0.37	30%
7, $N_{C,B}$	70	-0.073	0.034	47%	-0.69	0.75	109%
8, $N_{C,A}$	37	-0.024	0.015	61%	-0.39	0.35	91%
9, N_{PO}	638	-0.115	0.014	12%	1.91	0.29	15%
10, N_{EO}	429	0.103	0.013	13%	0.05	0.29	530%
11, N_{SO4}	438	2.78	0.26	9%	1.9	5.0	269%
12, N_{COO}	355	2.4	0.47	20%	1.7	9.4	564%
13, N_{OH}	509	2.32	0.51	22%	22.0	11.8	54%
14, $N_{C,CS}$	509	-0.574	0.119	21%	-2.2	2.9	132%
15, $N_{PO,CS}$	28	0.91	0.35	38%	8.5	8.8	103%
16, $N_{EO,CS}$	405	0.475	0.079	17%	-6.5	1.9	29%
17, f_6^S	148	-1.41	0.12	8%			

Table 5.9: Coefficients for the Soap Structures

Crude Oil Name	N	Optimum Salinity			Optimum Solubilization Ratio		
		ai	σai	|σai/ai|	bi	σbi	|σbi/bi|
B	6	-1.99	0.47	24%	16.2	10.5	65%
C	42	-3.58	0.52	15%	25.7	10.1	39%
F	7	-4.41	0.61	14%	29.0	10.0	34%
I	12	-2.73	0.67	25%	23.9	10.2	43%
J	38	-4.05	0.51	13%	56.1	10.8	19%
O	15	-2.91	0.52	18%	14.1	9.7	69%
P	6	-3.65	0.51	14%	54.3	11.3	21%

For the optimum salinity correlation, K was based on 74 experiments with crude oils diluted with n-alkanes of known EACN. The value of K determined this way is 0.115 with a standard error of 0.012, which is in good agreement with the values of K reported in the literature for anionic surfactants (K=0.16 for alkyl sulfonates and alkyl carboxylates, K=0.1 for alkyl sulfates and alkyl alkoxy sulfates) (Salager et al., 2013). The value of L, the slope of σ* versus EACN, was determined using 647 experiments. L is -0.86 with a standard error of 0.14.

The temperature coefficient a_T for the optimum salinity was calculated using equation **(5.19**. The average is -0.008 because nearly all of the experiments contained alcohol alkoxy anionic surfactants, which dominate the interfacial interaction. The temperature coefficient b_T for the optimum solubilization ratio determined by regression is 0.064 with a standard error of 0.015.

The coefficients for the surfactant structures (subscripts 1 to 12) in the optimum salinity correlation are a reflection of the hydrophilic and lipophilic natures (optimum salinity shift up or down, respectively) of the structures. The positive coefficients or hydrophilic structures are the surfactant head groups (N_{IOS}, N_{ABS}, N_{SO4}, N_{COO}) and the number of EO groups (N_{EO}). The negative coefficients or lipophilic structures are the surfactant hydrophobes ($N_{C,IOS}$, $N_{C,ABS}$, $N_{C,L}$, $N_{C,S}$, $N_{C,B}$) and the number of PO groups (N_{PO}). The coefficient for the tristyrylphenol hydrophobe ($N_{C,A}$) has high relative uncertainty and contributes very little to the lipophilicity. The magnitudes reflect the hydrophilic or lipophilic strength. For example, the head groups in decreasing order of hydrophilic strength are the sulfonate (N_{IOS} = 5.15), benzene sulfonate (N_{ABS} = 3.62), sulfate (N_{SO4} = 2.78), and carboxylate (N_{COO} = 2.4).

The effect of co-solvent on the optimum is a product of the interfacial concentration and the structure-property effect. The correlations developed in Chapter 4 were used to predict the partition coefficients and estimate interfacial concentrations so that the regression determined the structure-property effect. For the optimum salinity, the coefficients for the hydroxyl group (N_{OH}) and the numbers of PO ($N_{PO,CS}$) and EO ($N_{EO,CS}$) groups are positive and are hydrophilic in nature. The coefficient for the carbon number of the alcohol ($N_{C,CS}$) is negative and is lipophilic in nature. The effect of PO groups is expected to increase lipophilicity, but again could be a convolution of the effects on the interfacial concentration and optimum.

The coefficient for f_6^S, a_{17}, was based on 148 experiments with divalent cations (mostly calcium and magnesium). The concentrations of divalent cations ranged from 0.25 to 1.45 meq/ml (equivalent of 0.5 to 2.9 wt% calcium), the ratio of divalent cations to monovalent cations ranged from 0.003 to 0.26, and f_6^S ranged from 0.008 to 0.478.

The linear optimum solubilization ratio model is used as a simple approximation of the actual complex behavior, but it does capture the experimental data sufficiently well to be useful. Many of the lipophilic structures ($N_{C,IOS}$, $N_{C,ABS}$, $N_{C,L}$, $N_{C,S}$, and N_{PO}) have positive coefficients. This reflects how increasing the size of the lipophile increases the lipophile-oil interaction and increases the optimum solubilization ratio. The hydrophilic structures (N_{ABS}, N_{SO4}, N_{COO}, and N_{EO}) have high uncertainty and do not contribute significantly to the optimum solubilization ratio.

The Winsor R ratio concept can be used to rationalize why the variation of some hydrophilic structures can have little or no effect on the optimum solubilization ratio. In a salinity scan, the surfactant hydrophile-water interaction (denominator of Winsor R equation) decreases with increasing salinity, and the surfactant lipophile-oil interaction (numerator of Winsor R equation) is largely unaffected by salinity except indirectly through the interface, so it remains approximately constant. Thus, by increasing salinity, R transitions from <1 to 1 to >1 by decreasing the denominator of Winsor R. At the optimum, R = 1 and the interaction energy of the lipophile-oil and hydrophile-water are equal, and the bending moments on both sides of the interface are equal and opposite, resulting in zero net curvature. The magnitude of the interaction energy at the optimum is determined by the surfactant lipophile-oil interaction. Winsor theorized that the magnitude of the interaction energy and the interfacial tension were negatively correlated, and thus, positively correlated with the optimum solubilization ratio. A more complex model that captures lipophile-lipophile, oil-lipophile, and oil-oil interaction energies would be expected to more accurately predict the optimum solubilization ratio.

Co-solvents generally decrease the optimum solubilization ratio. The coefficients for the co-solvent structure are generally negative. Increasing with $N_{C,CS}$ and $N_{EO,CS}$ and decreasing with $N_{PO,CS}$ decrease the optimum solubilization ratio. However, the coefficient

for $N_{C,CS}$ is very uncertain because $N_{C,CS}$ varied from only 4 for isomers of butyl alcohol to 6 for phenols, which is more hydrophilic than hexanol due to aromaticity. The true effect of increasing $N_{C,CS}$ is likely opposite, as increasing the chain length increases lipophilicity and can increase the oil solubilization by the lipophilic linker effect (Graciaa et al., 1993).

The coefficients in **Table 5.8** and **Table 5.9** are only suitable for the ranges of structures, mixtures, and conditions tested. Extrapolations of the model to single component mixtures is not recommended as nearly all experiments used mixtures of at least two surfactants and a co-solvent. The structure characteristics (C_i and D_i) of the surfactants and co-solvents calculated using the coefficients in **Table 5.8** and **Table 5.9** are listed in the Appendix A. C_i for surfactants is similar but not the same as $-C_C$ used in HLD equations. D_i is a new characteristic of the surfactant and co-solvent that captures the effect of structure on the optimum solubilization ratio.

5.3.2 Model Predictions

For a given reservoir, the oil composition (EACN), temperature, and the brine used to make up a specific surfactant solution are effectively fixed. The formulation must be matched to these characteristics. A chemical formulation that gives the desired optimum for the desired reservoir conditions is not unique. The model can be used as a guide in the initial development and optimization of formulations for new reservoirs.

The most useful feature of the model for chemical EOR formulation development is prediction of the optimum solubilization ratios resulting from (1) different surfactant structures, (2) different co-solvent structures (3) soap generation and (4) mixtures of different components. IFT on the order of 0.003 mN/m or less is needed for an efficient chemical enhanced oil recovery process. This IFT corresponds to a solubilization ratio of about 10. Thus, the goal is to use the model to predict which formulations might have an

optimum solubilization ratio greater than 10. Because of the uncertainty in both the predictions and the measurements, it makes more sense to test formulations with predicted values greater than 15.

5.3.2.1 Effects of Surfactant

Figure 5.19 shows the effect of increasing the number of PO groups for 10 mol% C_{16} to C_{32} (L type), C_{13} to C_{16} (S type), C_{18} (B type), and C_{30} (A type) hydrophobe-propoxy-10EO-carboyxlate and 90 mol% C_{12} ABS with an oil EACN of 10 at 100 °C. Increasing the hydrophobe carbon number and increasing the number of PO groups are methods of increasing the optimum solubilization ratio. For this surfactant molar ratio, the predicted effect of adding ~30 PO groups to the molecule is an increase in the optimum solubilization ratio of 5 cc/cc, but this also increases the lipophilicity and decreases the optimum salinity. In order to maintain the optimum salinity, the lipophilicity must be balanced out with an increase of the hydrophilicity. Increasing the hydrophobe carbon number makes less difference than increasing the number of PO groups. A larger mole fraction of the carboxylate surfactant results in a more negative (positive) slope of the optimum salinity (solubilization ratio) with N_{PO}.

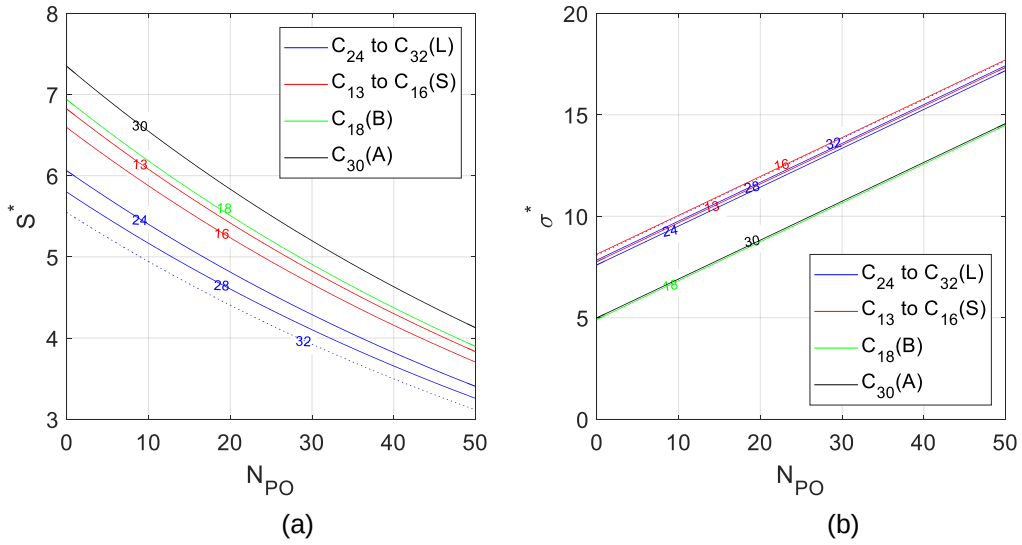

Figure 5.19: Prediction of the effect of the number of PO groups (NPO) on (a) the optimum salinity and (b) the optimum solubilization ratio for 10 mol% C_{16} to C_{32} (L type), C_{13} to C_{16} (S type), C_{18} (B type), and C_{30} (A type) hydrophobe-propoxy-10EO-COO and 90 mol% C12 ABS with oil EACN = 10 at 100 °C.

Figure 5.20 shows the optimum for different oil EACN using 15 mol% C_{28}-25PO-30EO-sulfate/carboxylate and 85 mol% of co-surfactant at 50 °C. In **Figure 5.20**(a), the co-surfactants are C_{15-17} ABS and C_{24} ABS and, in **Figure 5.20**(b), the co-surfactants are C_{15-18} IOS and C_{19-28} IOS. As the oil EACN increases, the optimum salinity increases and the optimum solubilization ratio decreases. Increasing $N_{C,IOS}$ and $N_{C,ABS}$ increases the solubilization ratio and decreases the optimum salinity. Switching from a sulfate to a carboxylate head group in the primary surfactant decreases the salinity and the optimum solubilization ratio slightly. Switching from a C_{15-17} ABS to a C_{15-18} IOS (both approximately 16 carbons) has a larger effect of shifting the optimum salinity up and the solubilization ratios down, which indicates that the sulfonate head group is more hydrophilic than the benzene sulfonate head group. Increasing the ratio of secondary surfactant increases the optimum salinity and the optimum solubilization ratio. One way to

generate a high salinity microemulsion is to reduce the $N_{C,IOS}$ or $N_{C,ABS}$ and increase the concentration of IOS or ABS.

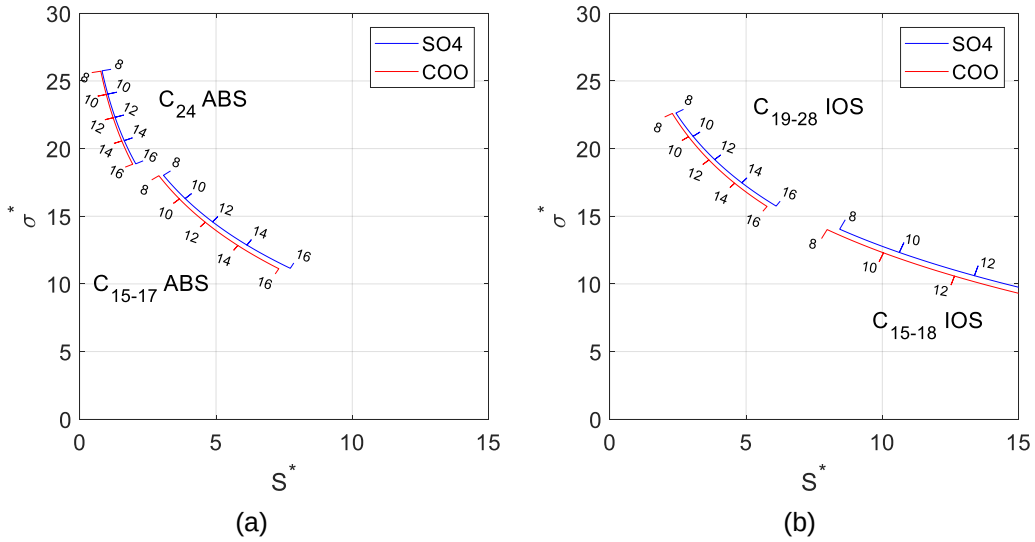

Figure 5.20: Prediction of the of effect EACN and sulfate/carboxylate anionic head group for (a) 15 mol% C28-25PO-30EO-sulfate/carboxylate and 85 mol% ABS surfactant and for (b) 15 mol% C28-25PO-30EO-sulfate/carboxylate and 85 mol% IOS surfactant at 50 °C. The numbers on the lines are the EACN of the oil.

Figure 5.21 shows the predicted optimum shifts resulting from a change in the number of PO groups (N_{PO}) and the number of EO groups (N_{EO}) for blends of 20 mol% C_{13} (S type), or C_{28} (L type), or C_{18} (B type), or C_{30} (A type) hydrophobe-alkoxy-sulfate and 80 mol% C_{20-24} IOS, and oil with an EACN of 12 at 50 °C. Increasing N_{PO} increases the optimum solubilization ratio and decreases the optimum salinity. Increasing N_{EO} increases the optimum solubilization ratio and increases the optimum salinity. To maintain a specific optimum salinity, the ratio of N_{PO} to N_{EO} can be increased (decreased) by approximately 2.5:2.8 and, for these formulations, results in an increase (decrease) of the optimum solubilization ratio by approximately 1 cc/cc. These figures can be used to find what ranges of N_{PO} and N_{EO}, and which hydrophobe type, are most likely to give ultra-low

IFT at a desired optimum salinity. The size of the "net" formed by the lines of constant N_{EO} and constant N_{PO} can be expanded (shrunk) by increasing (decreasing) the mole fraction of the alcohol alkoxy sulfate surfactant. Similar figures can be generated for different surfactant structures, surfactant mole fractions, temperatures, and EACNs.

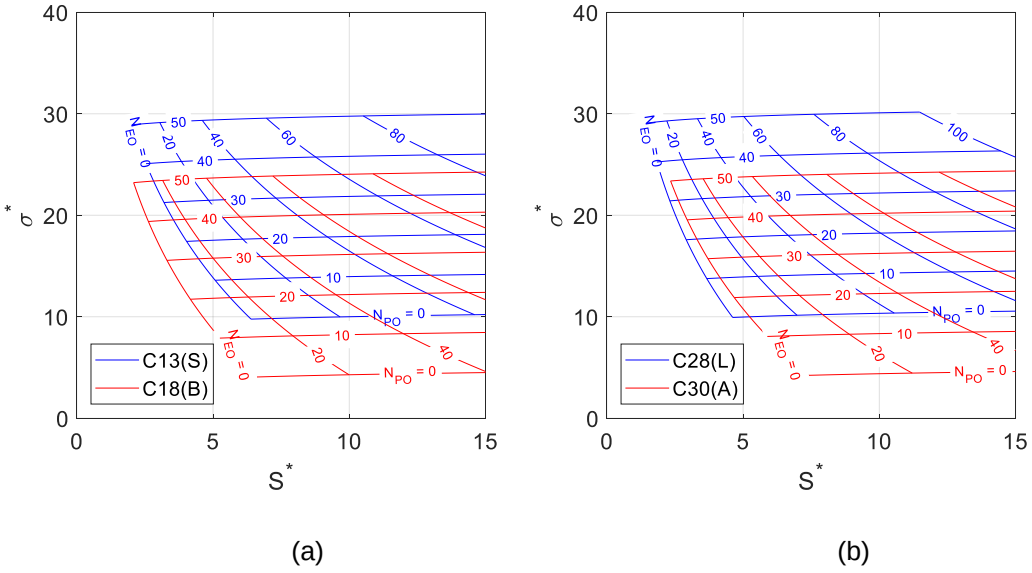

Figure 5.21: Predicted shifts in the optimum resulting from a change in the number of PO groups (NPO) and the number of EO groups (NEO) for 20 mol% C13 (S), or C28 (L), or C18 (B), or C30 (A) hydrophobe–propoxy-ethoxy-sulfate and 80 mol% C_{20-24} IOS, and oil with an EACN = 12 at 50 °C.

5.3.2.2 Effects of Co-solvent

Figure 5.22 and **Figure 5.23** show the effects of increasing the concentration of IBA alkoxylate and phenol-alkoxylate co-solvents, respectively, on the optimum for a formulation of 1 wt% of 20 mol% C_{13}-13PO-SO_4 and 80 mol% C_{20-24} IOS, and 30 vol% crude S (EACN = 10.8 and m_B = 1.3) at 25 °C. The oil-water partition coefficient of the co-solvents were calculated assuming 5 wt% NaCl salinity. **Table 5.10** shows the partition

coefficients as well as the interfacial mole fraction of co-solvent, and the change of the optimum salinity and optimum solubilization ratio for 1% co-solvent.

Co-solvents increase or decrease the optimum salinity depending on their structure, but almost always decrease the optimum solubilization ratio. The optimum solubilization ratio decreases less with increasing number of EO and PO groups in the co-solvent. The effect of co-solvent on the interfacial fluidity and aqueous stability are not captured here. Upamali et al. (2016) showed that the concentration of co-solvent required to achieve the same quality microemulsion phase behavior can be reduced if the number of EO groups is properly selected. The required co-solvent concentration was further reduced when 1 PO group was added to the co-solvent since this resulted in more partitioning to the interface.

Table 5.10: Effect of 1% Co-solvent

Co-solvent	K_{OW}	K_{PW}	F_{7S}	ΔS^*	$\Delta\sigma^*$
IBA	1.18	14.53	0.394	-0.70	-4.11
IBA-1EO	0.04	2.29	0.093	0.05	-1.57
IBA-5EO	0.01	1.02	0.018	0.19	-0.78
IBA-1PO-2EO	0.05	2.75	0.061	0.46	-0.86
IBA-1PO-5EO	0.02	1.49	0.022	0.33	-0.74
Phenol-2EO	0.39	8.14	0.164	-0.55	-4.44
Phenol-4EO	0.18	5.42	0.089	0.12	-3.53
Phenol-6EO	0.08	3.60	0.049	0.31	-2.58
Phenol-1PO-2EO	0.81	11.97	0.157	0.12	-2.80
Phenol-1PO-5EO	0.26	6.50	0.075	0.64	-2.79

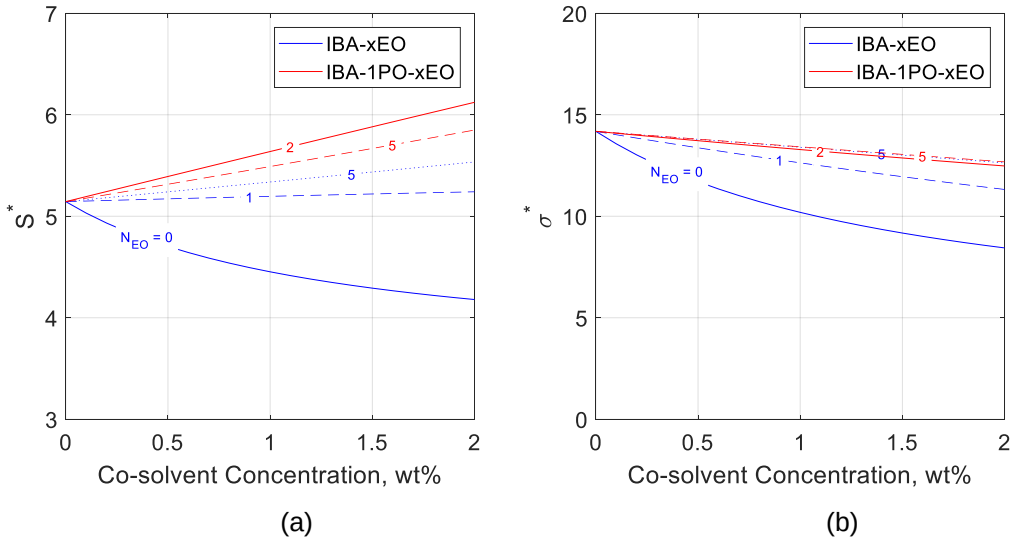

Figure 5.22: Predicted effect of increasing the concentration of IBA alkoxylate co-solvents on the (a) optimum salinity and (b) optimum solubilization ratio for a formulation of 1 wt% of 20 mol% C_{13}-13PO-SO_4 and 80 mol% C_{20-24} IOS, and 30 vol% crude S (EACN = 10.8 and m_B = 0.0013) at 25 °C.

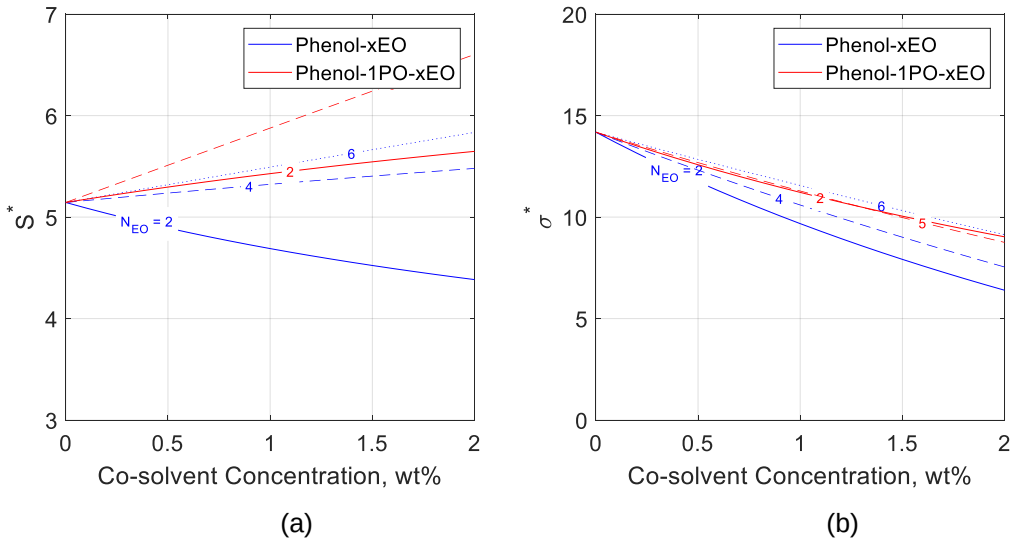

Figure 5.23: Predicted effect of increasing the concentration of phenol alkoxylate co-solvents on the (a) optimum salinity and (b) optimum solubilization ratio for a formulation of 1 wt% of 20 mol% C_{13}-13PO-SO_4 and 80 mol% C_{20-24} IOS, and 30 vol% crude S (EACN = 10.8 and m_B = 0.0013) at 25 °C.

Figure 5.24 shows the effect of (a) 0.5% phenol-2EO and (b) 0.5% IBA-1PO-5EO co-solvent on a formulation with 1 wt% of a blend of 20 mol% C_{13}(S) hydrophobe-alkoxy-sulfate and 80 mol% $C_{20\text{-}24}$ IOS, and 30 vol% crude S (EACN = 10.8 and m_B = 0.0013) at 25 °C. Adding co-solvent decreased the optimum solubilization ratio significantly more than it shifted the optimum salinity, but the relationship is more complex. By constraining the weight percent of the surfactant blend to 1 wt%, the mass of co-solvent at the interface is constant if the weight percent of co-solvent is also kept constant. However, an increase in molecular weight of the alcohol-alkoxy-sulfate by adding PO and EO groups decreases the molar concentration of surfactant, and thus increases the weight on the co-solvent terms. Therefore, in addition to shifting the overall position of the 'net', the co-solvent also stretches the 'net', elongating it horizontally and shrinking it vertically.

The model does not provide any information on the shift of the aqueous solubility limit and the microemulsion viscosity with these changes. Aqueous solubility of the surfactants in the brine at optimum salinity (including polymer in most cases) and low microemulsion viscosity are critical to the success of a chemical flood and must be measured with separate experiments.

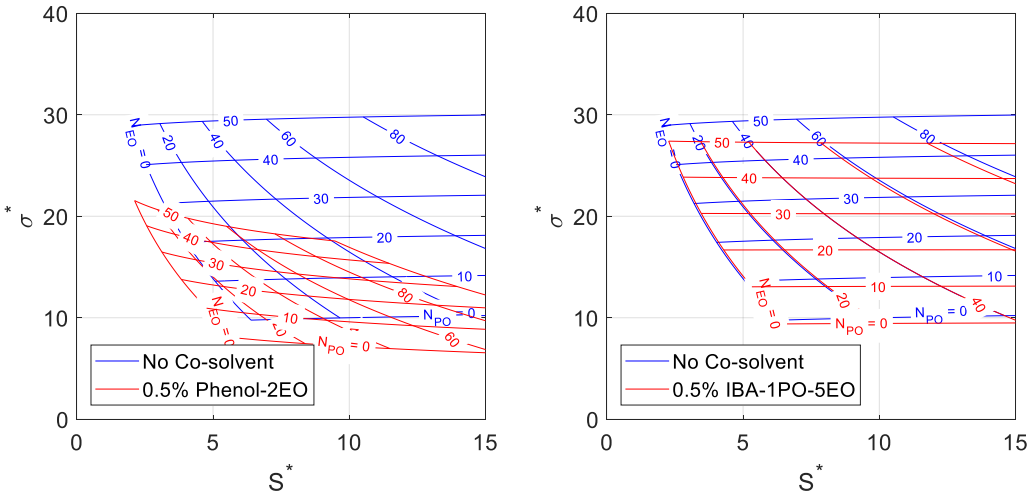

(a) (b)

Figure 5.24: Predicted shift in the optimum resulting from increasing the concentration of (a) Phenol-4EO and (b) IBA-1PO-5EO co-solvent for a formulation with 1 wt% of 20 mol% C13(S) hydrophobe-alkoxy-sulfate and 80 mol% C20-24 IOS, and 50 vol% oil with an EACN of 12 at 50 °C.

5.3.2.3 Effects of Divalent Cations

For the dataset, the optimum salinities were known and the values of f_6^S were directly calculated. Predicting the optimum salinity when there are divalent cations in the brine is more complex because the optimum salinity and f_6^S are coupled and depend on how the ion composition changes with the salinity scan. By combing terms, equation (*5.1* can be rewritten as:

$$\ln S^* = \ln S_0^* + a_{17} f_6^S \qquad \textbf{(5.20)}$$

where, $\ln S_0^*$ is the natural logarithm of the optimum salinity without divalent cations in the brine and f_6^S is the fraction of divalent cation associated with the surfactant at the optimum salinity. Similarly, equation **(5.20** with salinity expressed in meq/ml of anion is:

$$\ln C_5^* = \ln C_{5,0}^* + a_{17} f_6^S \qquad \textbf{(5.21)}$$

Then, $\ln S_0^*$ and $\ln C_{5,0}^*$ are functions of the oil, temperature, surfactant, co-solvent, and soap but are independent of the ion composition of the salinity scan. In salinity scans, the concentration of anions (C_5) increases and f_6^S varies depending on how the ion composition changes with the salinity scan.

Figure 5.25 shows (a) f_6^S and (b) C_5^* versus C_5 for different concentrations of divalent cations (C_6). C_6 of 0.01, 0.05, and 0.1 meq/ml are equal to 200, 1000, and 2000 ppm calcium equivalent, respectively. In this example, C_3 = 0.015 meq/ml and $C_{5,0}^*$ = 1 (5.8

wt% NaCl equivalent). Without divalent cations, f_6^S is zero and C_5^* is equal to $C_{5,0}^*$ for all values of C_5.

In a salinity scan with $C_6 = 0.01$, at low salinities f_6^S is large and $C_5^* << C_{5,0}^*$, and at high salinities f_6^S approaches 1 and C_5^* approaches $C_{5,0}^*$. Graphically, the optimum salinity is attained in **Figure 5.25**(b) when C_5^* equals C_5 (i.e. intercept of C_5^* curve and y=x line). For C_6 = 0.01, 0.05, and 0.1, the optimum salinities are C_5 = 0.964, 0.814, and 0.609 meq/ml, respectively.

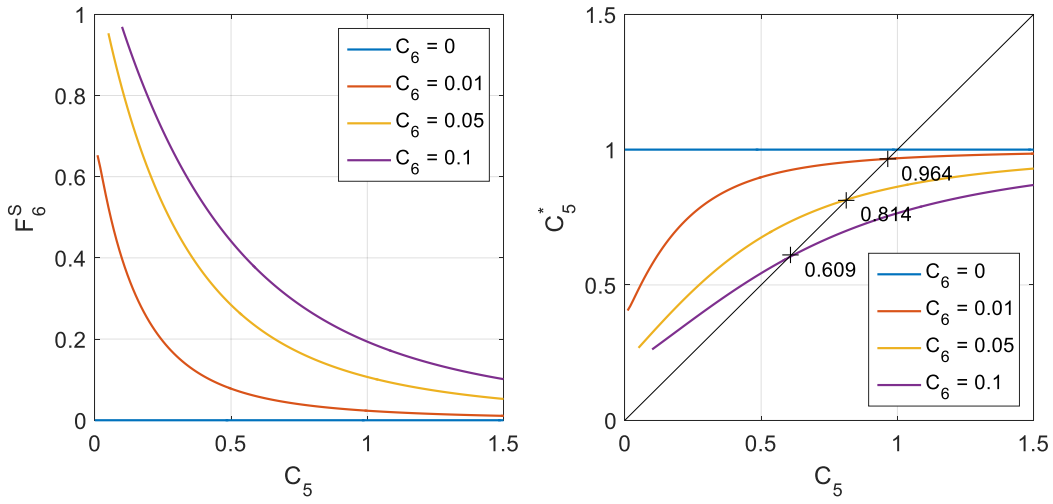

Figure 5.25. (a) f_6^S and (b) C_5^* versus C_5 for different concentrations of divalent cations. C_3=0.015 meq/ml and $C_{5,0}^*$=1.

Figure 5.26 shows (a) f_6^S and (b) C_5^* versus the C_5 for mixtures of seawater (C_5=0.6, C_6=0.21C_5) and fresh water, superimposed on **Figure 5.25**. C_5 varies from 0 to 0.6, and C6 varies from 0 to 0.126. The f_6^S and C_5^* curves intercept those shown in **Figure 5.25**. f_6^S goes through a maximum, and C_5^* goes through a minimum. The optimum salinity in this case is C_5 = 0.544 meq/ml.

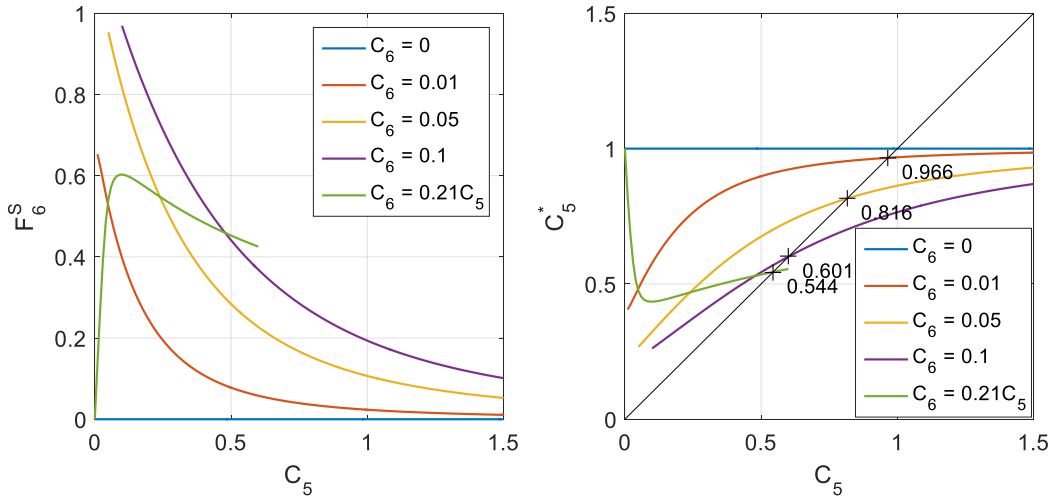

Figure 5.26. (a) f_6^S and (b) C_5^* versus the C_5 for different concentrations of divalent cations. C_3 = 0.015 meq/ml and $C_{5,0}^*$ = 1.

The variation of f_6^S and C_5^* with salinity scan depends on the how the ion composition changes in the salinity scan. A nonlinear root finder based on the secant method was used to find the concentration of surfactant with associated divalent cations at the optimum salinity. The solution is bounded between 0 and min(C_3, C_6). The error tolerance used was 10^{-8} meq/ml.

Figure 5.27 shows the optimum salinity versus (a) C_{Ca}, the concentration of calcium in the brine in wt%, and (b) f_6^S with lines of constant C_{Ca} for formulations of 1 wt% of 10 mol% C_{28}-40PO-xEO-COO and 90 mol% $C_{15\text{-}18}$ IOS with 50 vol% oil with EACN = 12 at 100 °C. The number of EO groups in the carboxylate surfactant varied from 20 to 80. The predicted optimum solubilization ratios for N_{EO} = 20, 40, 60, and 80 were 13.5, 13.9, 14.2, and 14.5, respectively, and were independent of the concentration of calcium. Increasing the number of EO groups seems to reduce the effect of calcium on the optimum salinity. Increasing the number of EO groups increases the optimum salinity and decreases C_3, the concentration of surfactant in meq/ml. C_3 is 0.015 meq/ml for N_{EO}=20

and 0.011 meq/ml for N_{EO}=80, so the effect of N_{EO} on C_3 is not significant. The primary cause is that increasing N_{EO} makes the surfactant more hydrophilic and increases the concentrations of ions required at the optimum salinity. A higher concentration of monovalent cation in the brine increases the competition between monovalent and divalent cation adsorption on the surfactant. The lines terminate when the optimum salinity approaches that corresponding to pure $CaCl_2$.

Figure 5.27(b) shows that the logarithm of the optimum salinity varies linearly with f_6^S. However, f_6^S is not a linear function of C_{Ca}. For a constant C_{Ca}, f_6^S increases with decreasing N_{EO}. For example, increasing the concentration of calcium from 0.1 to 0.3 wt% increases f_{Ca}^S from 0.03 to 0.11 (factor of 3.6) for N_{EO}=80 but increases f_{Ca}^S from 0.10 to 0.44 (factor of 4.4) for N_{EO}=20. Increasing N_{EO} increases the (apparent) tolerance of the surfactant to divalent cations. Diagrams like **Figure 5.27** can be used to design formulations in hard brines.

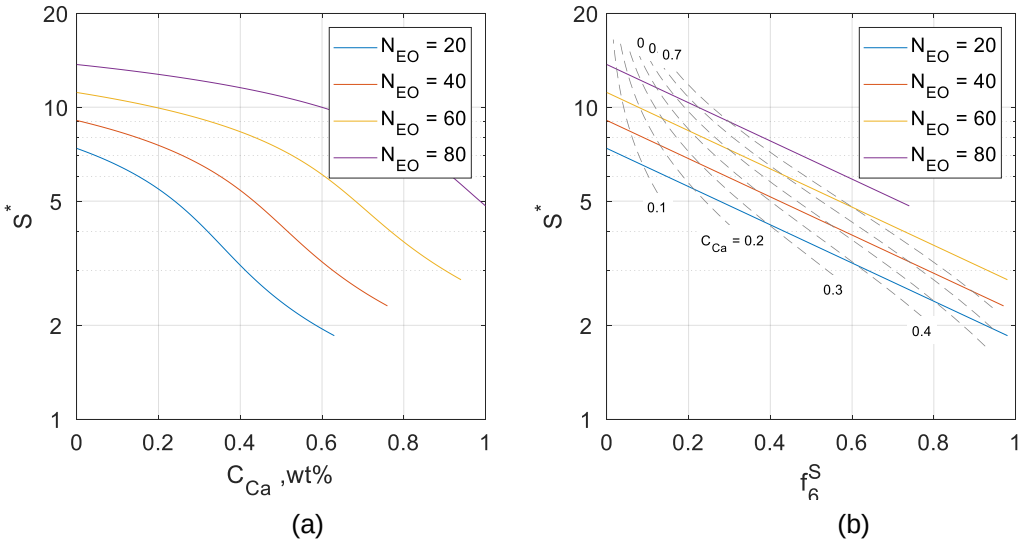

Figure 5.27: The optimum salinity versus (a) C_{Ca}, the concentration of calcium in the brine, and (b) f_{δ}^{S}, the fraction of divalent cations to adsorb on the surfactant, with lines of constant C_{Ca} for formulations of 1 wt% of 10 mol% C_{28}-40PO-xEO-COO and 90 mol% C_{15-18} IOS with 50 vol% oil with EACN = 12 at 100 °C. The number of EO groups (N_{EO}) in the carboxylate surfactant varies from 20 to 80.

Figure 5.28 shows how increasing the concentration of calcium shifts the "net" formed by the lines of constant N_{EO} and constant N_{PO} for a formulation with (a) 1 wt% of 10 mol% C_{28}(L) hydrophobe-alkoxy-carboxylate and 90 mol% C_{15-18} IOS and (b) 1 wt% of 10 mol% C_{18}(B) hydrophobe-alkoxy-carboxylate and 90 mol% C_{15-18} IOS, and 50 vol% oil with an EACN of 12 at 100 °C. The number of PO groups varied from 0 to 50 and the number of EO groups varied from 0 to 100. Adding 0.3 wt% calcium decreases the optimum salinity but does not affect the optimum solubilization ratio. The decrease in optimum salinity is greater for lower N_{EO} and higher N_{PO}.

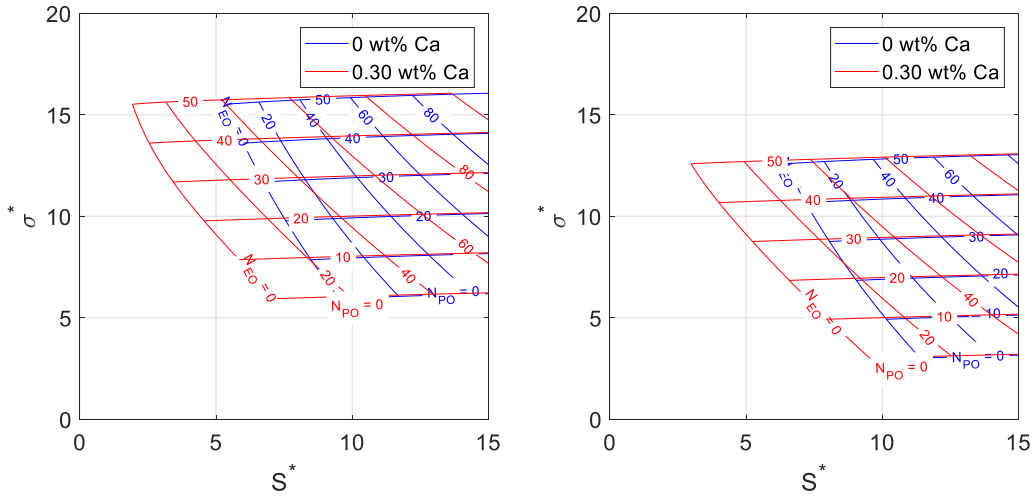

Figure 5.28: Predicted shift in the optimum resulting from increasing the concentration of calcium for a formulation with (a) 1 wt% of 10 mol% C_{28}(L) hydrophobe-alkoxy-carboxylate and 90 mol% $C_{15\text{-}18}$ IOS and (b) 1 wt% of 10 mol% C_{18}(B) hydrophobe-alkoxy-carboxylate and 90 mol% $C1_{5\text{-}18}$ IOS, and 50 vol% oil with an EACN of 12 at 100 °C. The number of PO groups varied from 10 to 50 and the number of EO groups varied from 20 to 100.

5.3.3 Cross-Validation

The dataset was split into a training set and a test set. The training set was used to develop the model, and the test set was used to cross-validate the model. Cross validation is used to assess the accuracy of the predictions of the model and give insight on how the model will generalize to an independent dataset.

The test dataset was composed of 45 experiments (about 7% of the dataset) using an inactive crude oil X with a measured EACN of 10. The formulations contained IOS, ABS, and sulfate surfactants and alcohol and alcohol ethoxylate co-solvents. All six types of surfactants hydrophobes were used. The oil phase was either the dead crude oil or a surrogate crude oils with cyclohexane, decalin, or tetradecane. The temperature was 55 °C. Twenty-four of the experiments contained divalent cations.

Figure 5.29 shows the predicted versus measured optimum salinity and optimum solubilization ratio for the training and test datasets. For the test set, the standard errors are 0.21 for the $\ln S^*$, 1.52 wt% for S^*, 0.20 for the relative optimum salinity ($\Delta S^*/S^*_{Measured}$), 7.3 cc/cc for σ^*, and 0.34 for the relative optimum solubilization ratio ($\Delta\sigma^*/\sigma^*$). As discussed above, the volume measurement itself contributes an uncertainty of about 2.5 cc/cc and the total uncertainty is roughly 5 cc/cc.

Figure 5.30 shows comparisons of experimental data and the predicted solubilization ratios using the HLD-NAC model with $I = 0.25$ for (a) 0.18% $C_{12\text{-}13}$-13PO-SO_4, 0.12% $C_{19\text{-}23}$ IOS, 0.3% IBA with 20 vol% crude X at 55 °C and (b) 0.6% C_{18}(B)-45PO-10EO-SO_4, 0.4% $C_{15\text{-}17}$ ABS, 1% Phenol-4EO with 50 vol% Crude X at 55 °C.

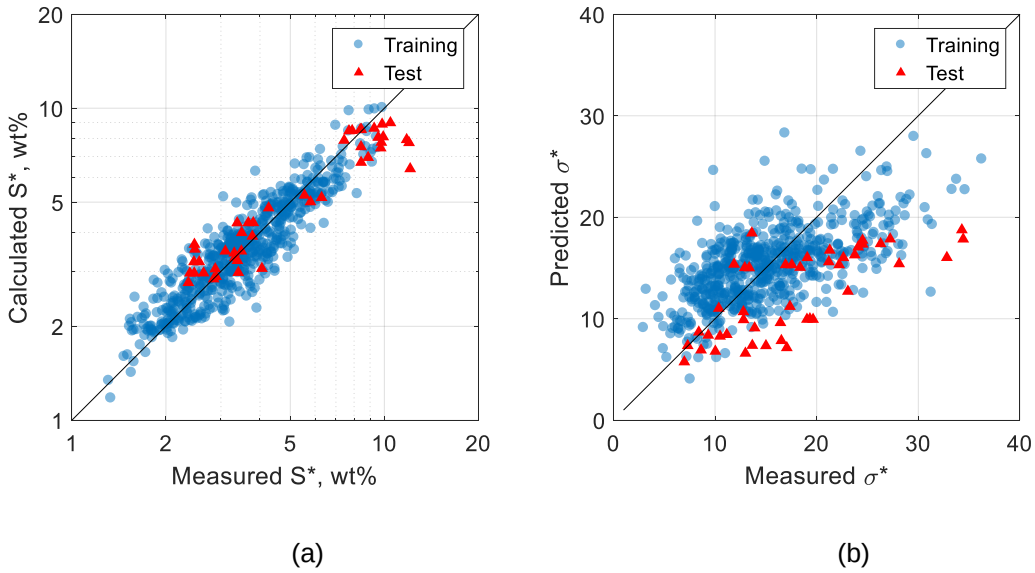

Figure 5.29. Predicted versus measured (a) optimum salinity and (b) optimum solubilization ratio for the training and test datasets.

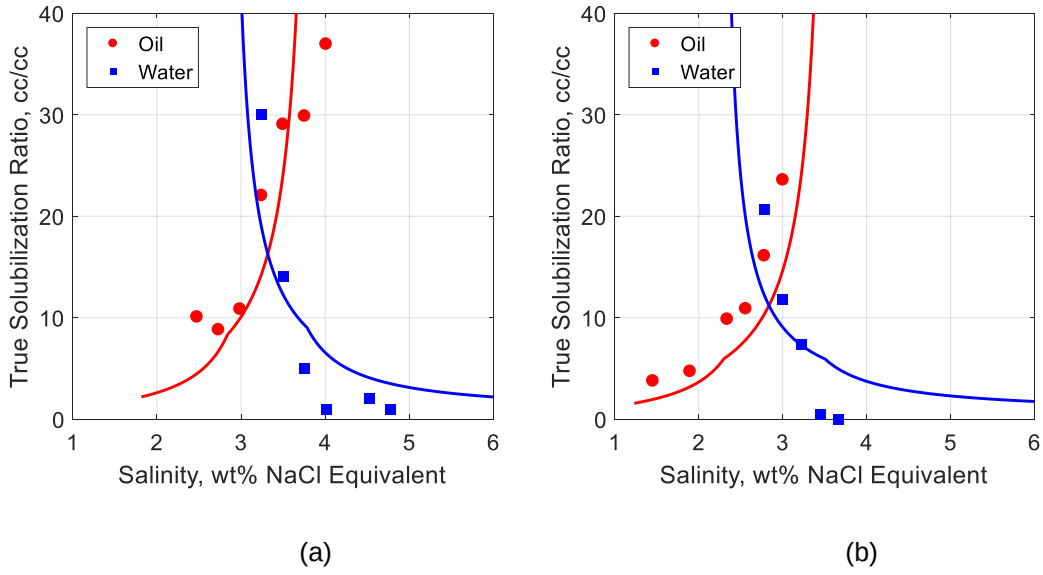

Figure 5.30. Comparisons of experimental data with predicted solubilization ratios for (a) 0.18% C_{12-13}-13PO-SO_4, 0.12% C_{19-23} IOS, 0.3% IBA with 20 vol% crude X at 55 °C and (b) 0.6% C_{18}(B)-45PO-10EO-SO_4, 0.4% C_{15-17} ABS, 1% Phenol-4EO with 50 vol% Crude X at 55 °C.

5.3.4 Oil EACN Relationships

The crude oils used in this study were characterized using EACN based on the optimum salinities. The EACN concept has significant limitations. First, a formulation that generates low IFT microemulsions with the oil is required to accurately measure EACN. Second, the measurements are difficult and uncertain. Third, crude oils are too complex to be modeled with a single parameter such as EACN as reflected in the fact that the apparent EACN is different depending on the formulation and brine used to measure it. Thus, it would be desirable to characterize a crude oil with properties of the crude oil that are directly measurable and more accurately characterize the oil such as the molecular weight, density, molar volume, and SARA rather than only EACN.

5.3.4.1 EACN Based on Optimum Solubilization Ratio

The EACN values used in the σ^* model were those obtained from regression of S^*. However, for comparison, the EACN values were also determined from regression of the σ^* data. **Figure 5.31** shows the predicted versus measured optimum solubilization ratio using (a) EACN based on optimum salinity ($EACN_S$) and (b) EACN based on optimum solubilization ratio ($EACN_\sigma$). **Figure 5.32** shows comparisons of (a) the EACN values and (b) the structure coefficients using $EACN_S$ and $EACN_\sigma$. **Table 5.11** shows the EACN values. **Table 5.12** shows the coefficients for EACN (L) and temperature (bT). **Table 5.13** shows the coefficients for surfactant and co-solvent structures (b_1 to b_{16}). **Table 5.14** shows the coefficients for the soap structures (b_{Si}).

The $EACN_S$ method had 24 unknowns, and the $EACN_\sigma$ method had 51 unknowns (26 additional due to 23 crude oils and 3 surrogate diluents). Several of the coefficients changed, but the correlations were not significantly improved by using $EACN_\sigma$ (R^2 of 0.48 and standard error of σ^* of 4.4 cc/cc) over $EACN_S$ (R^2 of 0.38 and standard error of σ^* of 4.7 cc/cc). **Figure 5.32** shows how $EACN_S$ and $EACN_\sigma$ are correlated.

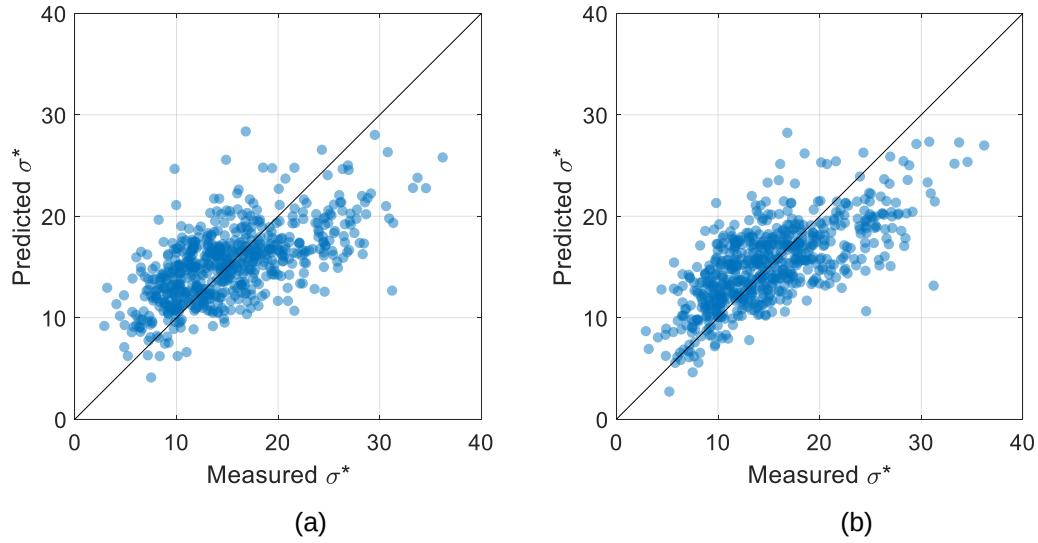

Figure 5.31. Predicted versus measured optimum solubilization ratio using (a) EACN based on optimum salinity correlation and (b) EACN based on optimum solubilization ratio correlation.

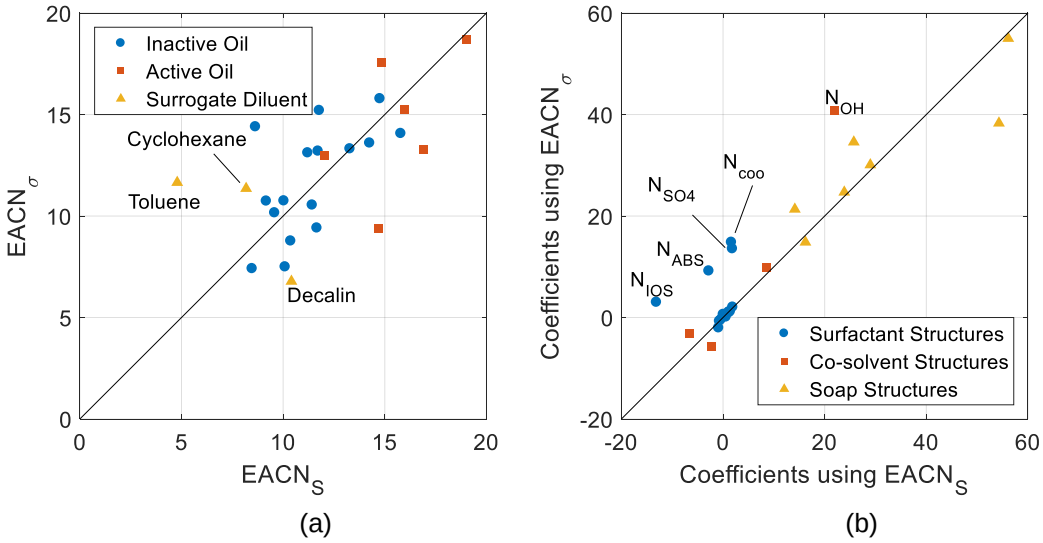

Figure 5.32. Comparison of (a) EACN and (b) structure coefficients for correlations using EACN based on S* and EACN based on σ*.

Table 5.11: Oil EACN Values

Oil	N	EACN Based on S*			EACN Based on σ*		
		b_i	σ_{bi}	$\lvert\sigma_{bi}/b_i\rvert$	b_i	σ_{bi}	$\lvert\sigma_{bi}/b_i\rvert$
Cyclohexane	42	8.2	1.7	21%	11.4	2.8	25%
Toluene	131	4.8	1.5	31%	11.7	2.8	24%
Decalin	17	10.4	1.9	19%	6.8	2.6	38%
A	11	11.8	1.9	16%	15.2	3.2	21%
B	10	16.0	2.2	14%	15.3	3.2	21%
C	42	19.0	2.8	15%	18.7	4.2	22%
D	3	8.6	2.3	27%	14.4	3.9	27%
E	114	11.2	1.8	16%	13.1	2.9	22%
F	7	14.9	5.1	34%	17.6	7.6	43%
G	15	9.6	1.7	18%	10.2	2.7	27%
H	42	11.4	1.9	16%	10.5	2.7	25%
I	12	12.0	3.6	30%	13.0	5.3	41%
J	38	16.9	2.4	14%	13.3	3.2	24%
K	33	8.5	1.6	19%	7.4	2.4	33%
L	18	11.7	1.9	16%	13.2	3.0	22%
M	9	13.3	2.0	15%	13.3	3.1	23%
N	6	9.2	1.8	19%	10.7	2.9	27%
O	15	11.1	3.0	27%	17.3	4.9	28%
P	11	14.7	2.2	15%	9.4	2.9	30%
Q	59	14.3	2.0	14%	13.6	3.0	22%
R	47	10.0	1.7	17%	10.7	2.7	25%
S	48	10.4	1.8	17%	8.8	2.6	29%
T	30	11.7	1.8	16%	9.4	2.5	26%
U	37	14.8	2.2	15%	15.8	3.3	21%
V	19	10.1	1.8	17%	7.5	2.5	33%
W	19	15.8	2.2	14%	15.2	3.2	21%

Table 5.12: Coefficients for EACN and Temperature

Subscript i, Variable	N	EACN Based on S*			EACN Based on σ*		
		a_i	σ_{ai}	$\lvert\sigma_{ai}/a_i\rvert$	b_i	σ_{bi}	$\lvert\sigma_{bi}/b_i\rvert$
L, EACN	72	-0.866	0.135	16%	-2.032	0.313	15%
b_T, ΔT	627	0.064	0.015	23%	0.147	0.040	27%

Table 5.13: Coefficients for Surfactant and Co-Solvent Structures

Subscript i, Variable	N	Using EACN Based on S*			Using EACN Based on σ*		
		b_i	σ_{bi}	$\lvert\sigma_{bi}/b_i\rvert$	b_i	σ_{bi}	$\lvert\sigma_{bi}/b_i\rvert$
1, $N_{C,IOS}$	502	1.44	0.20	14%	1.20	0.37	31%
2, N_{IOS}	502	-13.10	4.12	31%	3.01	9.65	321%
3, $N_{C,ABS}$	128	1.14	0.35	30%	1.07	0.46	43%
4, N_{ABS}	128	-2.78	5.10	183%	9.18	8.71	95%
5, $N_{C,L}$	272	0.60	0.32	53%	0.11	0.42	394%
6, $N_{C,S}$	324	1.23	0.37	30%	0.98	0.41	42%
7, $N_{C,B}$	70	-0.69	0.75	109%	-0.72	0.89	123%
8, $N_{C,A}$	37	-0.39	0.35	91%	-0.44	0.38	86%
9, N_{PO}	638	1.91	0.29	15%	2.05	0.36	18%
10, N_{EO}	429	0.05	0.29	530%	0.61	0.34	56%
11, N_{SO4}	438	1.85	4.99	269%	13.56	7.03	52%
12, N_{COO}	355	1.66	9.36	564%	14.83	12.62	85%
13, N_{OH}	509	22.03	11.83	54%	40.76	13.44	33%
14, $N_{C,CS}$	509	-2.17	2.88	132%	-5.62	3.08	55%
15, $N_{PO,CS}$	28	8.54	8.77	103%	9.83	9.03	92%
16, $N_{EO,CS}$	405	-6.50	1.87	29%	-3.20	2.08	65%

Table 5.14: Coefficients for the Soap Structures

Crude Oil Name	N	Using EACN Based on S*			Using EACN Based on σ*		
		b_i	σ_{bi}	$\lvert\sigma_{bi}/b_i\rvert$	bi	σbi	|σbi/bi|
B	6	16.22	10.47	65%	14.85	12.17	82%
C	42	25.73	10.09	39%	34.58	13.56	39%
F	7	28.98	9.95	34%	30.08	15.66	52%
I	12	23.86	10.20	43%	24.70	17.71	72%
J	38	56.12	10.78	19%	55.00	13.55	25%
O	15	14.13	9.71	69%	21.34	13.58	64%
P	6	54.29	11.31	21%	38.31	13.23	35%

5.3.4.2 Oil Property-EACN Relationships

The crude oil properties in **Table 5.5** were used in an attempt to correlate $EACN_S$ and $EACN_\sigma$. **Figure 5.33** shows $EACN_S$ and $EACN_\sigma$ versus the molecular weight (MW), density (ρ), and molar volume ($V_m = MW/\rho$). The data for n-alkanes and surrogate diluents are shown for reference. **Figure 5.34** shows the $EACN_S$ and $EACN_\sigma$ versus the mass fractions of saturates, aromatics, resins, and asphaltenes (SARA). Molar volume is molecular weight divided by density. SARA is a measure the "topped" fraction of the crude oil. Topping is the process of heating the oil in order to remove volatile components and reach a stable sample mass. The fractions that were removed were as high as 40%. The removed components likely have a significant effect on the EACN, therefore SARA may not be a representative predictor.

$EACN_S$ is proportional to the logarithm of the optimum salinity. Since EACN follows a linear molar mixing rule, mixtures of crude oil and an n-alkane or surrogate diluent follow a line between the two points. Increasing the concentration of a high EACN diluent increases the lnS, and increasing the concentration of a low EACN diluent

decreases the lnS. For n-alkanes, the molecular weight, density, molar volume of the mixture only decreases even though the lnS can increase or decrease.

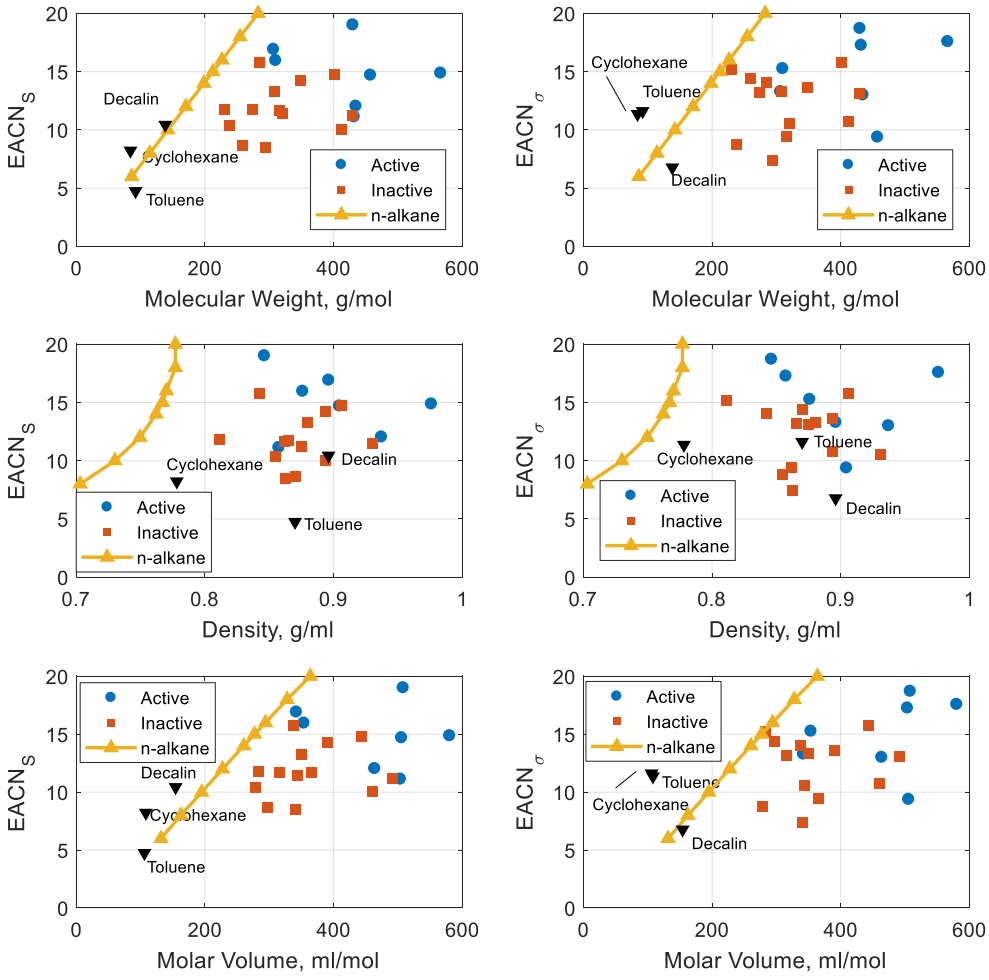

Figure 5.33. EACN$_S$ and EACN$_\sigma$ versus oil molecular weight, density, and molar volume for the active oils, inactive oils, n-alkanes, and surrogate diluents.

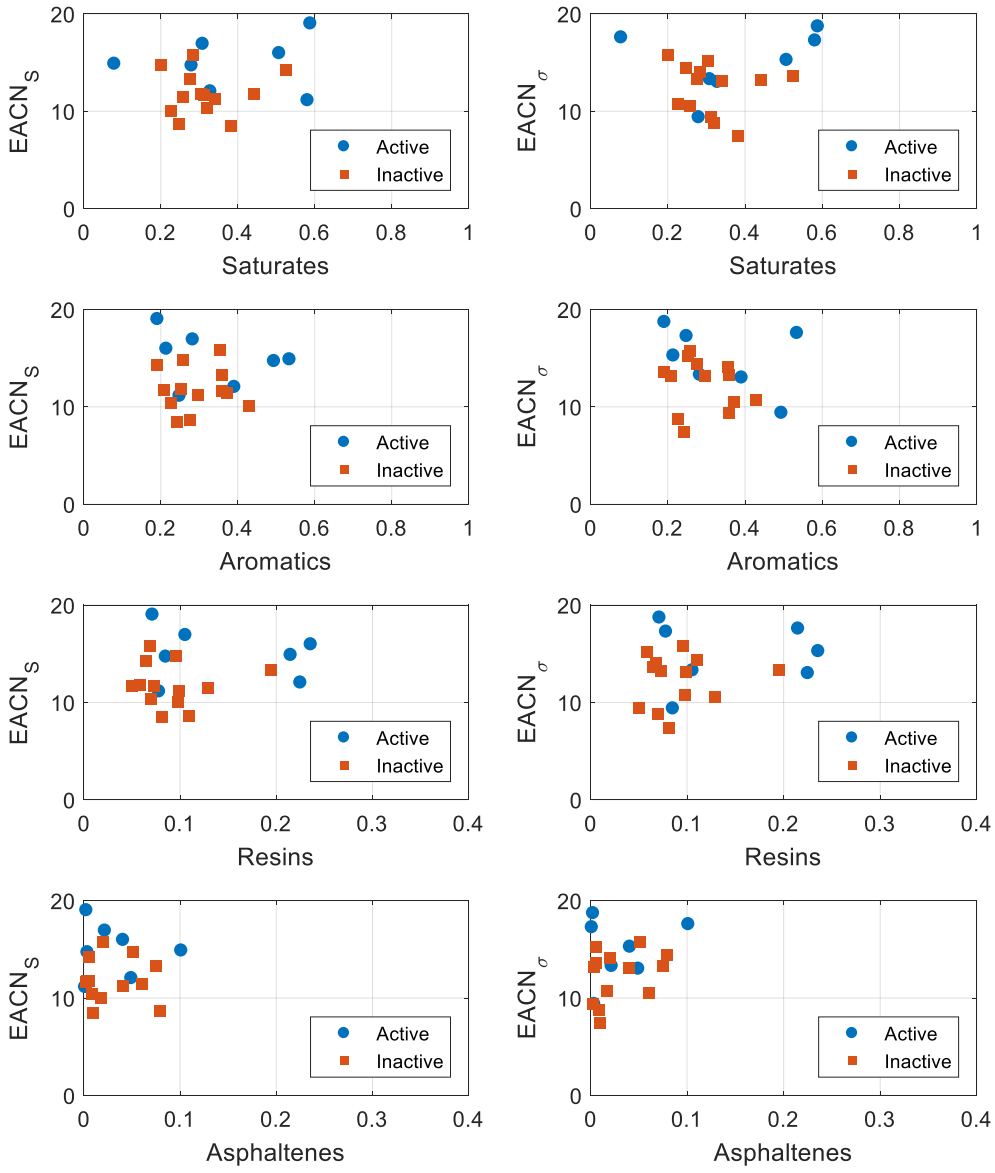

Figure 5.34. $EACN_S$ and $EACN_\sigma$ versus mass fractions of saturates, aromatics, resins, and asphaltenes.

The predictor variables explored were molecular weight, density, molar volume, and the mass fraction of saturates, aromatics, resins, and asphaltenes. Crude oils G, N, and V were not used in the correlation because some of their properties were not known. The highest R^2 values achievable with any combination of the 7 variables and a constant were 0.113 for $EACN_S$ and 0.637 for $EACN_\sigma$. The following correlation for $EACN_\sigma$ using the molar volume (Vm), aromatics (ARO), and asphaltene (ASP) is proposed:

$$EACN_\sigma = 0.0204\, V_m - 20.31\, ARO + 49.87\, ASP + 9.78 \qquad \textbf{(5.22)}$$

Figure 5.35 shows the predicted versus measured $EACN_\sigma$. The R^2 is 0.47. Molar volume is used in place of molecular weight and density. The correlation captures the increase in EACN with increasing molecular size (molar volume) and the decrease with increasing content of aromatics and polar compounds. A correlation for $EACN_S$ with available data was not found.

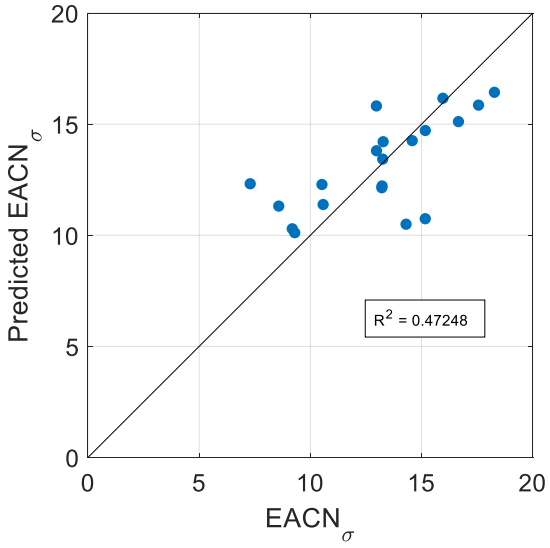

Figure 5.35. Predicted $EACN_\sigma$ versus measured EACNσ.

5.3.4.3 Substituting and Supplementing EACN

Rather than correlating the EACN values obtained from the regression with the measured oil properties, the measured oil properties could replace or supplement the EACN in the model equations. EACN is determined for each crude oil and after all is a fitting parameter. If a strong correlation exists between EACN and the oil properties, the EACN could simply be replaced with the oil property correlation.

For the optimum salinity equation, replacing EACN with a crude oil property reduces the number of unknowns from 51 to 25. Replacing EACN with molecular weight, density, or molar volume decreased R^2 from 0.83 to about 0.64 and increased the standard error of S* from 0.66 wt% to about 1.0 wt%. The relative error of the coefficient for the oil property varied about 30%. Using molecular weight, density, or molar volume in addition to EACN in the optimum salinity equation (52 unknowns) yields no significant improvement of R^2 or standard error of S*.

In the optimum solubilization ratio correlation, replacing $EACN_S$ with molecular weight, density, or molar volume (number of unknowns unaffected) slightly decreases R^2 to about 0.35 and slightly increases the standard error of σ* to about 4.8 cc/cc. Using MW, density, or molar volume in addition to $EACN_S$ yields no significant improvement of R^2 or standard error of σ*.

There was no significant advantage to substituting or supplementing EACN with molecular weight, density, or molar volume for either S* or σ* correlations. Gas chromatography compositional analysis may be more useful than the bulk properties and SARA. Further work is required to find a relationship between the EACN and the oil properties.

5.3.5 Modeling the Effect of Solution Gas and Pressure on Phase Behavior

Differences between live oil and dead oil phase behavior are attributed to the effect of solution gas on the oil composition and the effect of pressure (Austad et al., 1990; Austad & Strand, 1996; Kim et al., 1985; Kim et al., 1988; Skauge & Fotland, 1990). The two effects are difficult to separate and the observations reported in the literature are contradictory to a significant extent.

Jang et al. (2014) investigated the shift of the optimum salinity and optimum solubilization between dead crude oils, surrogate crude oils, and live crude oils. Table 5.15 is a summary of the measured phase behavior data from Jang et al. (2014) supplemented by more recent measurements. All dead crude oils were inactive. The surrogate crude oils were mixtures of dead crude oils and toluene. The dead crude oil and surrogate crude oil experiments were conducted at atmospheric pressure (P ~1 bar). The live crude oils were mixtures of dead crude oil and solution gas, pressurized to reservoir pressure. Solution gases included methane (CH_4), ethane (C_2H_6), propane (C_3H_8), butane (C_4H_{10}), and carbon dioxide (CO_2). The experiments were conducted at reservoir temperatures. All the formulations used an alcohol-alkoxy sulfate or carboxylate with one or more alkylbenzene sulfonates or an internal olefin sulfonate co-surfactants.

The structure-property model was used to quantify the effects of the solution gas components and pressure. The EACN values of several of the crude oils and toluene were determined in section 5.3. The salinity scans in some of the experiments included divalent cations, so the effect of f_6^S was accounted for to isolate the effects due to solution gas and pressure. The effects of surfactant, co-solvent, and temperature were constant within each group of experiments.

A pressure term was added to equation for the optimum salinity:

$$\ln S^* = K \sum_{i}^{O} x_i E_i + a_T \Delta T + \sum_{j}^{M} x_j C_j + a_{17} f_6^S + a_P \Delta P \quad \textbf{5.23}$$

and to the equation for the optimum solubilization ratio:

$$\sigma^* = L \sum_{i}^{O} x_i E_i + b_T \Delta T + \sum_{j}^{M} x_j D_j + b_P \Delta P \quad \textbf{5.24}$$

where, ΔP is the difference between the pressure and 1 bar, and a_P and b_P are constants.

Table 5.15: Microemulsion Phase Behavior Data

Crude	Optimum		Ion Composition at S*, meq/ml			f_6^S	P, bar	Oil Composition, mole fraction						
	S*	σ*	C_5	C_6	C_s^m			CH_1	C_2H_6	C_3H_8	C_4H_{10}	CO_2	Tol	DO
D	2.4	14	0.407	0.059	0.0153	0.389	110	0.129	0.112	0.081	0.048			0.630
	1.88	15	0.318	0.048	0.0153	0.431	1						0.290	0.710
H	6.38	14	1.149	0.008	0.0148	0.014	262	0.394	0.037	0.026	0.03			0.513
	3.25	10	0.558	0.008	0.0148	0.052	1						0.462	0.538
U	8.8	18	1.510	0.127	0.0207	0.124	159	0.296	0.075	0.075	0.057			0.497
	5.5	11	0.945	0.127	0.0207	0.252	1						0.421	0.579
U2	9	10	1.541	0	0.0241	0	172	0.236	0.059	0.055	0.043			0.607
	10	8	1.712	0	0.0241	0	1							1
	6.2	12	1.062	0	0.0241	0	1						0.421	0.579
L	4.25	14	0.754	0	0.0141	0	68	0.145	0.022	0.059	0.075			0.699
	4.3	13	0.763	0	0.0141	0	139	0.145	0.022	0.059	0.075			0.699
	4.85	6.5	0.867	0	0.0141	0	1							1
	2.8	12	0.480	0	0.0141	0	1						0.284	0.716
L2	3.4	23	0.593	0	0.0141	0	172	0.399						0.601
	3.95	22	0.697	0	0.0141	0	1							1
	1.7	30	0.272	0	0.0141	0	1						0.397	0.603
V	1.95	13	0.333	0.004	0.0292	0.049	69	0.173						0.827
	2.3	11	0.393	0.004	0.0292	0.040	1							1
X	3.65	27	0.554	0	0.0174	0	59	0.097	0.038	0.034	0.03	0.111		0.690
	3.35	18	0.509	0	0.0174	0	1							1
Y	2.8	28	0.432	0	0.0170	0	197	0.325	0.097	0.076	0.055			0.447
	4.25	13	0.653	0	0.0170	0	1							1
A	7	16	1.227	0.361	0.0213	0.406	172	0.463						0.537
	6.5	19	1.140	0.335	0.0213	0.418	1							1
Z	6.6	20	1.129	-	-	-	317	0.333	0.082	0.067	0.050	0.008		0.460
	8.6	13	1.472	-	-	-	1							1
AA	7.2	10	1.232	-	-	-	241	0.105	0.052	0.072	0.063	0.013		0.694
	6.3	10	1.078	-	-	-	1							1
AB	1.98	25	0.339	-	-	-	117	0.259	0.013	0.028	0.034	0.028		0.637
	2.1	17	0.359	-	-	-	1							1
U3	9	8	1.540	-	-	-	172	0.192	0.055	0.052	0.029	0.002		0.670
	8.8	7	1.506	-	-	-	1							1

5.3.5.1 EACN of light alkanes are NOT their ACN

Jang et al. (2014) proposed that the EACN values of light alkanes (methane, ethane, propane, and butane) have an apparent EACN higher than their respective alkyl carbon numbers (ACN). This theory is tested by using the model to solve for the EACN values. These results are compared to those calculated assuming that the respective EACN values are the ACN in the next section.

The EACN for the solution gases, crude oils Y through AB, and the pressure coefficients were determined using regression. Applying equation **5.23** results in a system of 32 linear equations for the optimum salinities with 24 unknowns (5 for K×EACN of methane, ethane, propane, butane, and CO2, 4 for K×EACN of crude oils Y through AB, 1 for a_P, and 14 constants for the unique formulations). Applying equation **5.24** results in a similar system of 32 linear equations with 15 unknowns (1 for b_P, and 14 constants for the unique formulations). **Table 5.16** show the coefficients for solution gas and pressure. **Figure 5.36** shows the predicted versus measured optimum salinity and optimum solubilization ratio for the live oil microemulsion phase behavior dataset. The standard errors are 0.19 for $\ln S^*$ and 3.33 cc/cc for σ^*.

Table 5.16: Coefficients for Effects of Pressure and Solution Gas

Coefficient, Variable	N	Optimum Salinity			Optimum Solubilization Ratio		
		x	σ_x	$\lvert\sigma_x/x\rvert$	x	σ_x	$\lvert\sigma_x/x\rvert$
a_P (b_P), ΔP	15	0.0017	0.0023	136%	0.0085	0.0068	79%
EACN CH_4	15	7.7	9.4	122%			
EACN C_2H_6	12	15.2	89.7	591%			
EACN C_3H_8	12	-23.1	-178.0	769%			
EACN C_4H_{10}	12	31.4	121.1	386%			
EACN CO_2	5	13.7	22.7	165%			

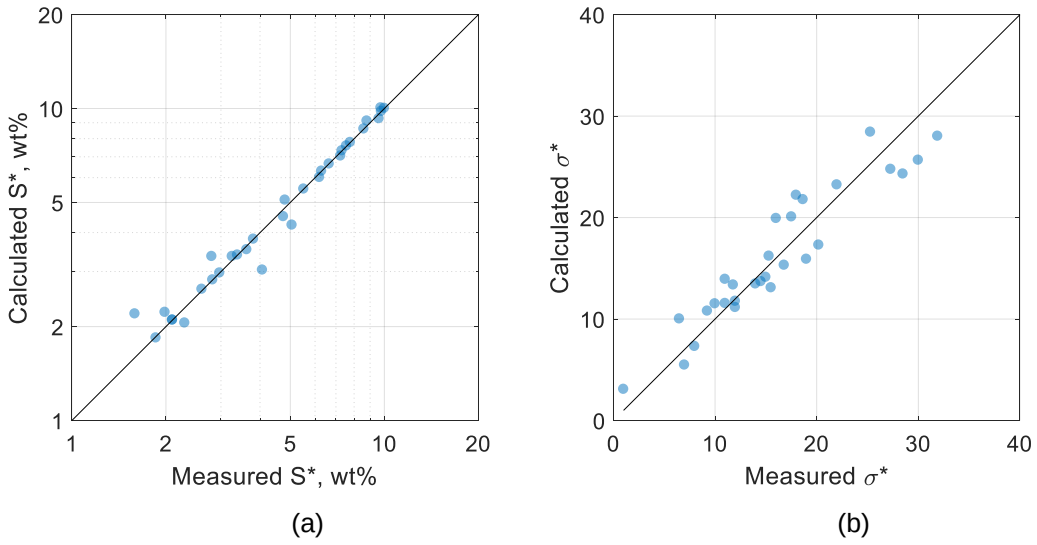

Figure 5.36: Predicted versus measured (a) optimum salinity and (b) optimum solubilization ratio for the live oil phase behavior data assuming EACN of gaseous alkane are not equal to their carbon numbers.

5.3.5.2 EACN values of light alkanes are respective carbon numbers

Applying equation **5.23** results in a system of 32 linear equations for the optimum salinities with 20 unknowns (1 for K×EACN of CO2, 4 for K×EACN of crude oils Y through AB, 1 for a_P, and 14 constants for the unique formulations). Applying equation **5.24** results in a system of 32 linear equations for the optimum salinities with 15 unknowns (1 for b_P and 14 constants for the 14 groups of experiments) when the EACN values from the optimum salinity regression are used. Only the EACN of CO2, a_P, and b_P shown in **Table 5.17** are useful. **Figure 5.37** shows the predicted versus measured optimum salinity and optimum solubilization ratio for the live oil microemulsion phase behavior dataset. The standard errors are 0.16 for $\ln S^*$ and 3.32 cc/cc for σ^*.

Table 5.17: Coefficients for Effects of Pressure and CO2

Coefficient, Variable	N	Optimum Salinity			Optimum Solubilization Ratio		
		x	σ_x	$\lvert\sigma_x/x\rvert$	x	σ_x	$\lvert\sigma_x/x\rvert$
a_P (b_P), ΔP	15	0.0033	0.0004	13%	-0.0033	0.0067	206%
EACN CO_2	5	16.2	18.1	111%			

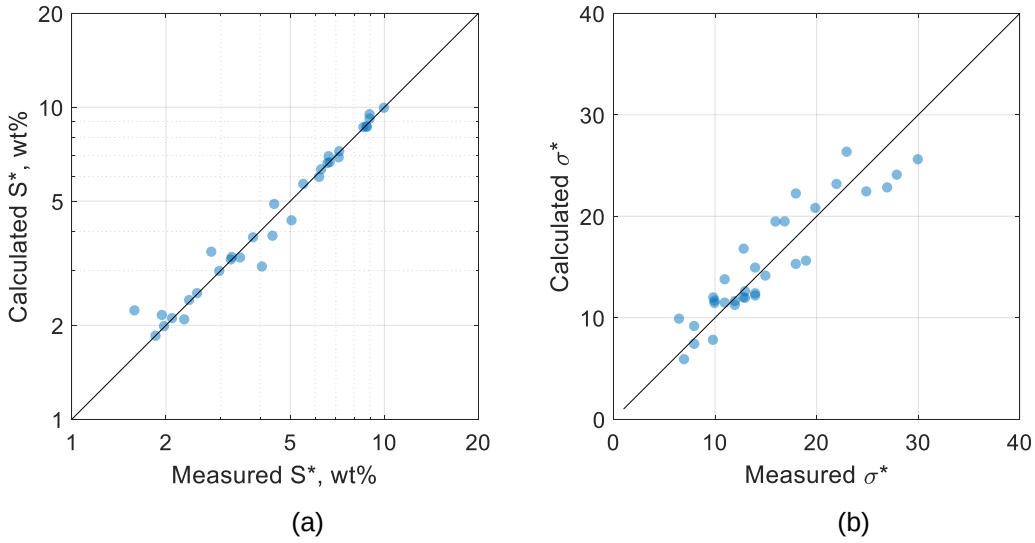

Figure 5.37: Predicted versus measured (a) optimum salinity and (b) optimum solubilization ratio for the live oil phase behavior data assuming EACN n-alkane = carbon number.

5.3.5.3 Discussion

The effects of the surfactant, co-solvent, and temperature for each series of experiments were assumed to be constant and were determined by regression as opposed to being calculated using the structure-property models because the uncertainty in the in the live oil phase behavior measurements were less than that of the model. The EACN values of toluene and crudes A, D, H, L, U, V, and X were those obtained from section 5.3.1. The coefficients for pressure a_P and b_P were based on the 15 measurements, and the EACN of CO2 was based on 5 measurements. The coefficients K=0.115 and L=-0.859 were used.

In section 5.3.5.1, the EACN values of methane to butane were neither monotonically increasing nor concave upwards as proposed in the literature, the EACN of CO2 was determined to be 13.7, and the pressure coefficients were both positive (a_P = 0.0017, b_P = 0.0085). The EACN values of crudes Y, Z, AA, and AB were reasonable,

varying from 14 to 20. In section 5.3.5.2, the EACN values of methane to butane were constrained to their ACN. The EACN of CO2 was determined to be 16.2, the pressure coefficient for S^* was +0.0033 and the pressure coefficient for σ^* was -0.0033. The EACN values of crudes Y, Z, AA, and AB were reasonable but varied from 13 to 23. In both cases, increasing the methane content decreases S^* and increasing pressure increases S^*. In the former case where EACN≠ACN, the EACN of methane is 7.7 and decreases the EACN to a lesser extent than in the latter case where EACN=ACN, the EACN of methane is 1, and, thus, shifts the S* to a lesser extent. However, it is offset by the effects of pressure where a_P when EACN≠ACN is approximately half that when EACN=ACN. The methane decreases the EACN and increases the σ^*. When EACN≠ACN, pressure increases the σ^* and, when EACN=ACN, it is the opposite. The σ^* depends on the density of the oil, which is roughly proportional to the pressure. Therefore EACN=ACN appears to be correct. The EACN of CO2 was based on 5 live oil microemulsion phase behavior measurements and is predicted to be between 13.7 and 16.2 but has high uncertainty.

The standard errors of $\ln S^*$ and σ^* are nearly the same in both cases, however, the EACN=ACN case has fewer parameters and is simpler and is therefore recommended for approximating the effects of solution gas and pressure. It is recommended that further research be undertaken to separate the effects of composition and pressure by conducting more live oil microemulsion phase behavior measurements. The effects of pressure can be isolated by conducting phase behavior experiments at multiple pressures above the bubble point of the crude oil.

5.4 Discussion

5.4.1 Co-solvent

The effect of co-solvent on the optimum is a product of the interfacial concentration (i.e. how much co-solvent goes to the interface) and the structure-property effect (i.e. how the structure of the interfacial co-solvent affects the optimum). The interfacial concentration of co-solvent is a function of the composition and nature of oil, brine, surfactant, and co-solvent as well as temperature. Both the structure-concentration and structure-property effects need to be captured in order to predict the effect of co-solvent. The correlations developed in Chapter 4 were used to predict the partition coefficients and estimate interfacial concentrations so that the regression determined the structure-property effect. These two effects are difficult to decouple because the structure of the co-solvent affects the interfacial concentration, and the interfacial concentration is still quite uncertain. The structure coefficients a_{13}-a_{16} and b_{13}-b_{17} are an improvement to those determined using constant partition coefficient (Chang et al., 2018) but may still convolute both effects. K_{OW}=1 and K_{PW}=10 are good approximate values of most co-solvents (Chang et al., 2016; Sahni et al., 2010). Using these partition coefficients give nearly identical R^2 and standard errors, but the values of the $a_{13\text{-}16}$ and $b_{13\text{-}16}$ adjusted to compensate. Furthermore, having an interface term as opposed to separate surfactant and co-solvent terms is more physically correct and improves robustness. Intermediate molecules (e.g. lipophilic linkers) can be modeled using this equation.

It should be noted that increasing the volume of the interface (e.g. by increasing interfacial co-solvent or soap) decreases the true optimum solubilization ratio (σ^*). Changes that decrease σ^* in general artificially increases R^2 and decreases standard error by shifting σ^* towards the <0,0> origin and reduces scatter. However, doing so diminishes

the predictive value. In fact, if all of the co-solvent were assumed to go the interface, the R^2 value of S* decreases and the R^2 value of σ* *increases*, but the correlation would be meaningless.

5.4.2 Temperature

The temperature coefficient, a_T, is equal to the derivative of the lnS* with respect to temperature. a_T is 0.01 for most alkyl anionic (AA) surfactants and is negative for nonionic surfactants (Bourrel et al., 1980; Bourrel & Schechter, 1988). Nonionic surfactants interact with water predominantly through hydrogen bonding, whereas AA surfactants interact predominantly through ion-dipole interaction. The strength of hydrogen bonds decreases with temperature, whereas the strength of ion-dipole interaction increases with temperature. This opposite trend allows for mixtures of both types of surfactants to produce intermediate behavior insensitive to temperature (Anton et al., 1992). Alcohol alkoxy anionic (AAA) surfactants have both types of interactions. a_T decreases with increasing numbers of PO and EO groups. A lower limit of approximately -0.01 is attained with about 7 or more PO and EO groups (Acosta & Bhakta, 2009; Aoudia et al., 1995; Hammond & Acosta, 2012; Salager et al., 1979; Velásquez et al., 2010). The a_T for mixtures of AA and AAA surfactants has not been well established. All formulations except the ACP formulations (crude F) have both AA and AAA surfactants. Since nearly all of the AAA surfactants in the dataset have more than 7 PO groups, it is reasonable to assume a_T is about -0.01.

If instead of using the temperature model and a_T were determined using regression, a_T=-0.008 with standard error of 0.0015 (19%). In addition, the values of EACN decreased and a_S increased for crude F. In other words, the EACN and soap adjust to numerically compensate the incorrect temperature effect. Because crude F makes up about 1% of the

dataset, it does not significantly affect the overall R^2 or standard error. The regressed a_T of = -0.008 and the temperature model are in agreement for the vast majority of the experiments in the dataset and reflect how the AAA surfactants dominate the interfacial interactions. This is likely because they extend farther into the bulk phases than the AA surfactants.

The temperature model is only applicable for mixtures of AA and AAA surfactants where the AAA surfactant has more than 7 alkoxylate groups. More experiments are required in order to develop a complete temperature model that can accommodate the entire range. Ideally, a_T is expected to approach +0.01 when the mole fraction of AA approaches 1 and when the numbers of PO and EO groups in AAA surfactant approach 0.

5.4.3 Soap

The soap was modeled as a surfactant with unknown structure. The main assumptions were the soap molecular weight (M_S) and 100% conversion of TAN to soap. TAN does not distinguish between acids that generate soap and those that consume alkali without producing soap. The water-soluble active soap number (WSASN) is a measure of the acids that partition between oil and aqueous phases at low and high salinities (i.e. acids that generate soaps that prefer the interface). For a crude oil with TAN = 0.84 mg/g, WSASN was determined to vary from 0.21 to 0.36 mg/g, depending on the temperature and titration method. The logarithm optimum salinity is expected to more closely (linearly) relate with WSASN than with TAN (Ding et al., 2016).

For active crude oils, the effects of dead oil EACN and soap can be numerically convoluted because both are proportional to the concentration of dead oil. This manifests as unrealistic EACN or a_S values. Causes include incorrectly accounting for the amount of

soap generated from the crude oil and not having a variety of different water-oil ratios for each formulation in the dataset.

TAN controls the moles of soap, and M_S controls the mass (and thus volume) each mole of soap. Doubling TAN or M_S, doubles the interfacial volume, which halves the true optimum solubilization ratio. However, doubling TAN, doubles the moles of soap, shifting the mole fraction balance of the synthetic surfactants and the soap, causing the logarithm optimum salinity relationship to become less linear as shown by Ding et al. (2016). Furthermore, the assumptions for M_S is that there is only one carboxylate head group per molecule of soap, but it is possible, given the complexity of asphaltene and resin molecules, that soap molecules may contain more than one anionic head group, which could decrease the effective M_S. For comparison to the assumed MS = 400 g/mol, the molecular weight of oleate ($C_{18}H_{33}O_2$), a commonly used analogue for soaps, is 281 g/mol. Because both TAN and M_S of the active crude oils are uncertain, the sensitivities the optimum salinity and optimum solubilization ratios to TAN and M_S were studied in order to determine if there exists an optimal TAN and M_S.

The experiments with crude oils C, J, and O were with various dead and surrogate oils and used multiple water-oil ratios for each formulation. The TAN was varied by a factor f_{TAN} of 0.1 to 2 and MS by a factor f_{MS} of 0.5 to 1.5. **Figure 5.38** shows the sensitivity of the normalized mean squared errors (MSE) of (a) the optimum salinity and (b) optimum solubilization ratio for the three active crude oils as functions of f_{ASN} and f_{MS}. For S*, increasing f_{ASN} increased the MSE for crudes C and O, whereas the opposite was found for crude J. For σ*, increasing f_{ASN} decreased MSE for all crude oils. f_{MS} had no significant effect on S*, whereas increasing f_{MS} significantly decreased the MSE of σ*. Increasing f_{MS} increases the volume of the interface which (1) decreases the true solubilization ratios and (2) numerically decreases the scatter, but at some point, the true solubilization ratios would

be so small and that the predicted IFT based on the Huh relationship would not match the experimental observations.

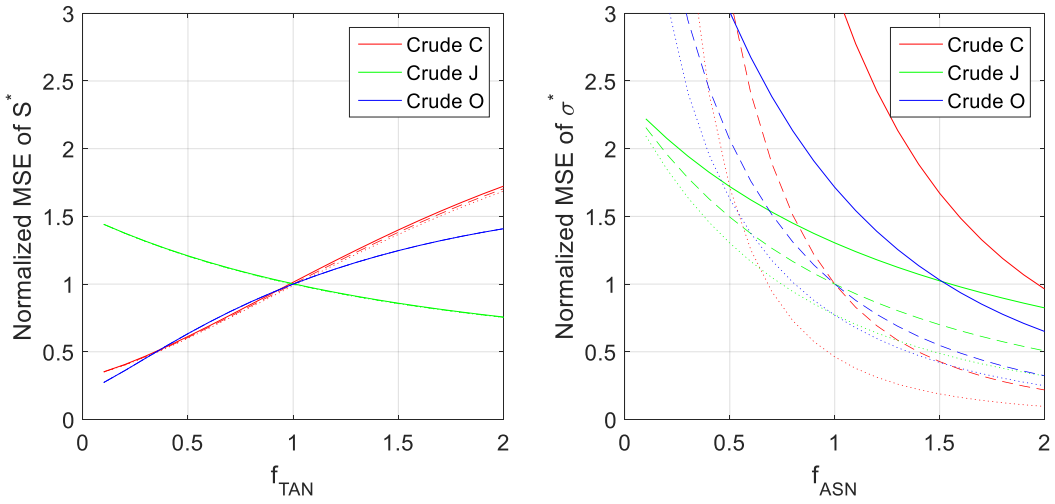

Figure 5.38: Sensitivity of mean squared error (MSE) of (a) optimum salinity and (b) optimum solubilization ratio to the total acid number (TAN) and molecular weight of soap (M_S).

In the TAN and M_S space investigated, no local minimums in MSE of S* and σ* were found. Optimal TAN or M_S could not be identified from the data.

5.4.4 Ion Model

The effect of divalent cations on the optimum salinity were captured using the $a_{17}f_6^S$ term. For comparison, without the $a_{17}f_6^S$ term the R^2 decreases from 0.84 to 0.79 for the prediction of the S^* and the standard error increases from 0.65 to 0.75 wt% NaCl equivalent for S^*. The effect on the optimum solubilization ratio is small by comparison. An alternative method to using f_6^S is to instead assign a weighting factor to the wt% of divalent cations. The optimal weighting factor was found to be approximately 10, which agrees with the empirical rules that divalent cations have an order of magnitude greater effect on the optimum salinity than monovalent cations. However, the weighting factor

method tends to undervalue and overvalue the impact of divalent cations at low and high salinities, respectively, and therefore is not as robust or accurate as the f_6^S method.

5.4.5 EACN

The crude oils used in this study were characterized using equivalent alkane carbon numbers (EACN) based on the optimum salinities. Microemulsion phase behavior using a pure n-alkane with the same EACN as the crude oil is often different than the phase behavior using the crude oil. The EACN values for cyclohexane, toluene and decalin obtained from the regression of the S* data were greater than the values of 4, 1, and 6, respectively, obtained from the empirical rules in Cayias et al. (1976). Puerto & Reed (1983) have pointed out the limitations of using EACN to characterize crude oils and have proposed replacing EACN with an equivalent oil defined as an oil with the same optimum salinity, optimum solubilization ratio and molar volume. More research is needed to develop an accurate method to characterize crude oils using commonly available data.

5.4.6 Improved Model Equation

The Winsor R concept can be used to rationalize the change of solubilization with different variables (Bourrel et al., 1987). He modeled the surfactant lipophile-oil interaction energy (E_{CO}) as proportional to the product of the surfactant lipophile carbon number and the EACN of the oil. They modeled the lipophile-lipophile interaction energy (E_{LL}) as proportional to the products of binary combinations of surfactant lipophiles. They modeled the oil-oil interaction energy (E_{OO}) as proportional to the products of binary combinations the oil molecules. Thus, for N number of oil components and surfactant lipophiles, the number of binary interaction parameters is $(N^2+N)/2$. Quantifying the interactions of these (pseudo) components is likely to improve prediction of the optimum

solubilization ratio. This can be taken a step further by studying the interactions of the alkyl (S and L), unsaturated (B and A), and aromatic (A) hydrophobes with the different SARA (saturate, aromatic, resin, and asphaltene) components of the oils. Since the number of parameters in the σ^* correlation is nearly half that for the optimum salinity, several of the most important interactions can be added to the equation and still maintain a reasonable ratio.

The data was not weighted in the regressions. Several trends are established by only a few key experiments (e.g. the experiments with oil diluted with n-alkanes used to establish the value of K). Some experiments are higher quality than others, or they have been repeated numerous times, or more complete data such as measured partition coefficients are available. Using weighing factors taking these factors into account might improve the models.

Accurately predicting the optimum salinity and the optimum solubilization ratio are of great importance, but if the formulation is not aqueous soluble at the optimum salinity, it should not be injected into a reservoir for chemical EOR. In addition, if the microemulsion is very viscous or extremely shear thinning, the surfactants are more likely to have high retention and not propagate through the reservoir. Therefore, developing models for the solubility of the surfactants and co-solvents in the brine and for the interfacial rigidity (bending and saddle-splay moduli) of the microemulsion would add great value and complement the models for the optimum salinity and optimum solubilization ratio.

The predictions of the models have limitations due to the nature of the data in the dataset. We do not recommend using the model to predict the phase behavior when there is only one surfactant or the oil is a pure hydrocarbon, because the dataset includes very few experimental data of those types, and also because ideal Winsor microemulsions are

not usually observed without using a co-surfactant and/or co-solvent in the formulation. The model's validity is limited to the ranges and types of surfactants, co-solvents, oils, and temperatures presented in the Materials and Methods section.

The EACN of a new oil must be measured to take advantage of the model and this requires using either a preliminary formulation, or the use of a correlation to predict EACN from other measured oil properties. If EACN is measured, then it is best to start by using a good formulation developed for similar oils (molecular weight, density, SARA) at similar reservoir conditions. If such data are unavailable, formulations using a mixture of either a sulfate or carboxylate surfactant, either an IOS or ABS co-surfactant, and a co-solvent are recommended as the starting point. Starting with a co-solvent is very advantageous since co-solvents speed up equilibration and thus provide useful preliminary data in less time. Co-solvents also reduce complications caused by macroemulsions. Once a formulation with low IFT is found, the optimum salinity (by emulsion test) can be used to estimate the oil EACN. Then the model should be used to design experiments with an optimum solubilization ratio of at least 15 cc/cc because the uncertainty in the optimum solubilization ratio is approximately 5 cc/cc. The co-solvent concentration may be reduced or in favorable cases even eliminated as part of an optimization study.

The optimum salinity and optimum solubilization ratio can be adjusted by changing the carbon number of the IOS ($N_{C,IOS}$) or ABS ($N_{C,ABS}$) co-surfactants and/or by changing the carbon numbers, the number of PO (N_{PO}) groups, or the number of EO (N_{EO}) groups of the alcohol-alkoxy sulfate or carboxylate surfactants. For the dataset used in this study, the average mole percentage of carboxylate surfactant was 9 mol% (standard deviation of 3 mol%) and average mole percentage of sulfate surfactant was 27 mol% (standard deviation of 18 mol%).

For practical purposes, dead crude oil or surrogate oils are initially used rather than live crude oil for the ease of experimentation. The optimum salinities of dead crude oils and live crude oils are similar, whereas the optimum solubilization ratios of live crude oil are typically higher than those of the dead crude oil (Jang et al., 2014). Therefore, finding an ultra-low IFT (σ^*>10) formulation for the dead oil is likely to yield a similar optimum salinity and a slightly higher σ^* for the live crude oil. Microemulsion phase behavior is also a weak function of pressure. The effects of solution gas and pressure were modeled, but addition testing and refinement of the models is justified. It is recommended that further research be undertaken to separate the effects of composition and pressure by conducting more live oil microemulsion phase behavior measurements.

Nomenclature

a_i = regression constants
a_P = Slope of lnS* and pressure
a_S = Effect of hydrophobe structure of the soap
a_{T1} = Temperature coefficient for alkyl anionic surfactant
a_{T2} = Temperature coefficient for alcohol alkoxy anionic surfactant
b_i = regression constants
b_P = Slope of σ* and pressure
b_S = Effect of hydrophobe structure of the soap
C_i = Structure characteristic of component i when used in the $\ln S^*$ equation
C_i = Concentration of component i (meq/ml)
$C^*_{5,0}$ = Optimum salinity without divalent cations (meq/ml)
C^*_5 = Optimum salinity (meq/ml)
D_i = Structure characteristic of component i for σ^*

$EACN_S$ = EACN based on optimum salinity

$EACN_\sigma$ = EACN based on optimum solubilization ratio

f_6^S = fraction of surfactant with associated divalent cation

I = Interfacial volume parameter

K = Slope of lnS* and EACN

$K_{OW,i}$ = Oil-water partition coefficient of component i

$K_{PW,i}$ = Interface-water partition coefficient of component i

L = Slope of σ* and EACN

m_D = Mass fraction of dead oil in the oil phase

M_i = Molecular weight of component i (g/mol)

MW = Molecular weight of the oil (g/mol)

N = Sample size

N_{ABS} = Number of benzenesulfonate head groups

$N_{C,A}$ = Carbon number of the A-type hydrophobe

$N_{C,ABS}$ = Carbon number of the ABS hydrophobe

$N_{C,B}$ = Carbon number of the B-type hydrophobe

$N_{C,CS}$ = Carbon number of the co-solvent hydrophobe

$N_{C,IOS}$ = Carbon number of the IOS hydrophobe

$N_{C,L}$ = Carbon number of the L-type hydrophobe

$N_{C,S}$ = Carbon number of the S-type hydrophobe

N_{COO} = Number of carboxylate head groups

N_{EO} = Number of ethylene oxide groups

$N_{EO,CS}$ = Number of ethylene oxide groups in the co-solvent

n_i = Concentration of component i (moles/ml)

N_{IOS} = Number of sulfonate head groups

N_{OH} = Number of hydroxyl groups

N_{PO} = Number of propylene oxide groups

$N_{PO,CS}$ = Number of propylene oxide groups in the co-solvent

N_{SO4} = Number of sulfate head groups

ΔP = Difference between the pressure and 1 bar

S^* = Optimum salinity (wt%)

S_0^* = Optimum salinity without divalent cations (wt%)

ΔT = Temperature difference from 25 °C

TAN = Total acid number (mg KOH/g oil)

V_i = Volume fraction of component i

V_m = Molar volume of oil (ml/mol)

V_O^M = Volume of oil solubilized in microemulsion (volume fraction)

V_W^M = Volume of water solubilized in microemulsion (volume fraction)

V_i^S = Volume fraction of interfacial component i

w = Weighting factor = 1/3

w_2 = Weighting factor = 80

x_A = Surfactant mole fraction of alcohol alkoxy anionic surfactant

x_i = mole fraction of component i

β_S = Ion exchange constant for the surfactant

ρ = Density (g/ml)

ρ_i = Density of component i (g/ml)

σ^* = Optimum solubilization ratio (cc/cc)

σ_{ai} = Standard error of regression coefficient a_i

σ_{EACN} = Standard error of EACN

Superscripts

*	=	Optimum
M	=	Microemulsion
S	=	Surfactant

Subscripts

1	=	Brine
2	=	Oil
3	=	Surfactant
5	=	pseudo-anion
6	=	Pseudo-divalent cation
7	=	Co-solvent
11	=	Pseudo-monovalent cation
S	=	Soap

Acronyms

AA	=	Alkyl anionic surfactant
AAA	=	Alcohol alkoxy anionic surfactant
ARO	=	Mass fraction of aromatics
ASP	=	Mass fraction of asphaltenes
DO	=	Dead Oil
EACN	=	Equivalent alkane carbon number
HLD	=	Hydrophilic-Lipophilic difference
NSO	=	Mass fraction of resins
SAT	=	Mass fraction of saturates
TAN	=	Total acid number (mg KOH/g oil)
Tol	=	Toluene

CHAPTER 6: STRUCTURE-PROPERTY MODEL FOR AQUEOUS STABILITY LIMIT

A homogeneous, stable aqueous chemical solution under reservoir conditions is essential for the successful application of chemical EOR. Separation of chemicals in the reservoir can lead to fractionation, high retention, and loss of performance. Any such problems observed in the laboratory would be magnified in the reservoir. It is also desirable for the aqueous chemical solution to be stable at surface conditions. However, the requirement is not as strict as it is in the reservoir due to lower residence times and other mitigating factors. Therefore, the aqueous stability tests were done at reservoir temperature.

Several variables affect the solubility of surfactants in the brine including salinity, temperature, and molecular structure. The solubility of alkyl anionic surfactants increases with increasing temperature, whereas the solubility nonionic surfactants decreases with increasing temperature. The cloud point of a nonionic surfactant is the temperature at which the aqueous solution starts to phase separate. The cloud point decreases with increasing salinity, pH, and hardness (Bourrel et al., 1980; Shinoda & Takeda, 1970). Alcohol alkoxy anionic surfactants ultimately behave more like nonionic surfactants than alkyl anionic surfactants as their solubility decreases with increasing temperature (Arachchilage et al., 2018). Co-surfactants and co-solvents can be used to increase the solubility of the surfactant (Sahni et al., 2010). Mixtures of surfactants form mixed micelles that can behave nonideally in terms of the reducing the critical micelle concentration, increasing the aqueous stability limit, and decreasing the surfactant adsorption (Scamehorn et al., 1982a, 1982b).

The aqueous stability limit is defined as the salinity when either precipitation or phase separation are observed. Coacervation is liquid-liquid separation due to the inversion of micelles. Precipitation is liquid-solid separation which occurs because of insoluble salt formation. The addition of water-soluble polymers used for mobility control typically lower the aqueous stability limit. Anionic surfactants are typically less soluble in hard brines.

Aqueous stability tests were conducted for each new formulation tested. The procedure is identical to that of the salinity scan for microemulsion phase behavior except performed without oil and typically with 1000 to 3000 ppm of aqueous polymer. The samples were aged at reservoir temperature for up to a year, and their turbidity (i.e. haziness ranging from clear to cloudy) and type of phase separation were recorded periodically.

Precipitations can occur due to certain ions exceeding the solubility product. The precipitation may also occur with or without the surfactant present (e.g. due to incompatible brines). Precipitation may also interfere with coacervation. The purpose herein it so model phase separation due to coacervation and not precipitation, as precipitation has many root causes not related to hydrophilic-lipophilic interactions.

6.1 Model Development

The model developed for the aqueous stability limit uses a similar concept to that of the optimum salinity. At low salinities, the surfactant forms micelles in the brine, and at high salinities, the micelles invert and form a surfactant-rich phase.

Similar to the behavior of microemulsions, as the salinity increases the interface curves toward the water. Instead of transitioning from an oil-in-water emulsion to a water-in-oil emulsion, the micelles invert. The difference is that lipophilic interactions are only between that of surfactant lipophiles. The Winsor R ratio has been incredibly useful for

interpreting the effects of chemical formulation changes on microemulsion phase behavior. For microemulsions, the cohesive energy between lipophile and oil (E_{LO}) is arguably more dominate than the cohesive energy between lipophiles (E_{LL}). Bourrel & Schechter, (1988) theorized that E_{LO} is proportional to the $\sqrt{E_{LL}E_{OO}}$. For micelles, there is no oil, and the only cohesive energy is between lipophiles:

$$R = \frac{E_{LL}}{E_{CW} - E_{WW} - E_{HH}} \quad \textbf{(6.1)}$$

where, $R < 0$ corresponds to formation of micelles, $R > 0$ corresponds to formation of inverted micelles, and $R = 1$ is the stability limit. Increasing salinity for anionic surfactants and increasing temperature for non-ionic surfactants decreases the hydrophile-water (E_{CW}) interaction, which increases R. Thus, increasing salinity can cause anionic surfactant solutions to phase separate and increasing temperature can cause nonionic surfactant solutions to phase separate. Decreasing the cohesive energy between lipophiles (E_{LL}), for example by reducing the size of the lipophiles, increases the stability limit (i.e. decreasing the hydrophobicity of the surfactants increases the aqueous solubility).

For surfactant mixtures that form mixed micelles, E_{LL} becomes a summation of all binary lipophilic interactions. We assume these interactions are between the 6 lipophile types and the PO groups. The hydrophilic interactions (i.e. effects of EO, head groups, and co-solvent) were included in the structure-property model for the optimum salinity described in Chapter 5. Because the hydrophilic interactions (i.e. effects of EO, head groups, and co-solvent) are very similar between micelles and microemulsions, and because the hydrophilic interactions were adequately captured in the optimum salinity equation, a similar equation to that used for the optimum salinity was used for the aqueous stability model:

$$\ln A_Q = c_T \Delta T + \sum_i^M x_i \delta_i + c_{17} f_6^S + c_P \omega_P + \sum_j^L \sum_k^L \kappa_{jk} \sqrt{\sum_i^M x_i N_{j,i}} \sqrt{\sum_i^M x_i N_{k,i}} \quad \textbf{(6.2)}$$

where A_Q is the aqueous stability limit in wt% NaCl equivalence, c_T the temperature coefficient, ΔT is the difference in temperature from 25 °C, x_i is the mole fraction of component i, δ_i is the structure characteristic of component i defined by equation **(6.6**, M is the number of components in the interface, f_6^S is the fraction of surfactant associated with divalent cations, c_P is a constant, and ω_P is the concentration of polymer in wt%, L is the lipophile type I, A, L, S, B, T, and P (correspond to internal olefin sulfonate, alkyl benzene sulfonate, L-type hydrophobe, S-type hydrophobe, oleyl B-type hydrophobe, tristyrylphenol A-type hydrophobe, and propylene oxide), κ_{jk} are binary interaction constants between lipophiles of type j and k, shown in **Table 6.1**, and $N_{j,i}$ is the j-type lipophile structure number of component i.

6.1.1 Interfacial Model

The assumptions are (1) the surfactant and co-solvent structures at the interface influence the microemulsion phase behavior, (2) volumes are additive, and (3) the densities of brine, surfactant, and co-solvent are 1 g/ml. The amount of surfactant at the interface in moles/ml of surfactant j is

$$n_j = \frac{V_j}{V_1 + V_3 + V_7} \frac{\rho_j}{M_j} \quad \textbf{(6.3)}$$

where, V is the volume fraction, ρ is the density in g/ml, M is the molecular weight in g/mol, subscripts 1, 3, 7, and j denote brine, surfactant, co-solvent, and component j.

The amount of co-solvent j at the interface as overall volume fraction (V_j^S) is calculated from Equation **(6.4** and as moles/ml (n_k) it is calculated from Equation **(6.5**.

$$V_j^S = \frac{V_k V_3 K_{PW,k}}{V_1 + V_3 K_{PW,k}} \quad \textbf{(6.4)}$$

$$n_j = V_j^S \frac{\rho_j}{M_j} \quad \textbf{(6.5)}$$

where, $K_{PW,k}$ is the interface-water partition coefficient of co-solvent k, which depends on the structures of the surfactant and co-solvent, temperature, and salinity. For simplicity $K_{PW,k}$ was assumed to be 10.

The surfactant structure characteristics, δ_i (analogous to C_i and D_i in section 5.1.1) are defined as:

$$\delta_j = \begin{bmatrix} c_1 N_{C,IOS} + c_2 N_{IOS} + c_3 N_{C,ABS} + c_4 N_{ABS} + c_5 N_{C,L} + c_6 N_{C,S} \\ +c_7 N_{C,B} + c_8 N_{C,A} + c_9 N_{PO} + c_{10} N_{EO} + c_{11} N_{SO4} + c_{12} N_{COO} \end{bmatrix}_j \quad \textbf{(6.6)}$$

where, $N_{C,IOS}$ and N_{IOS} are the average number of hydrophobe carbon atoms and the average number of sulfonate head groups in the internal olefin sulfonate (IOS) surfactant molecule, $N_{C,ABS}$ and N_{ABS} are the average number of hydrophobe carbon atoms (excluding the benzene carbons) and the average number of benzene sulfonate head groups in the alkylbenzene sulfonate (ABS) surfactant molecule, $N_{C,L}$, $N_{C,S}$, $N_{C,B}$, and $N_{C,A}$ are the number of carbon atoms in the L, S, B, and A type hydrophobes, respectively, defined in **Table 5.1**, N_{PO} is the number of propylene oxide (PO) groups and N_{EO} is the number of ethylene oxide (EO) groups in the surfactant. N_{SO4} is the number of sulfate head groups and N_{COO} is the number of carboxylate head groups per surfactant molecule. The coefficients c_1 to c_{12} are constants determined by regression.

The co-solvent structure characteristics, δ_i, are defined as:

$$\delta_k = \left[c_{13} N_{OH} + c_{14} N_{C,CS} + c_{15} N_{PO,CS} + c_{16} N_{EO,CS}\right]_k \quad \textbf{(6.7)}$$

where, N_{OH} is the number of hydroxyl groups, $N_{C,CS}$ is the number of alcohol carbon atoms, $N_{PO,CS}$ is the number of PO groups, and $N_{EO,CS}$ is the number of EO groups in the co-solvent molecule.

6.1.2 Lipophile-Lipophile Interaction Model

Table 6.1 shows the binary interaction constants between the 7 lipophile types. Numerically, only the constants above the main diagonal are used. The terms where j = k (on the main diagonal) are redundant with terms calculated in the single summation term (e.g. κ_{BB} and c_7 are redundant). The six binary interaction constants between L, S, and B and the binary interaction constant between I and A (in white) were not used because these combinations were not encountered in the dataset.

Table 6.1: Binary Interaction Constants κ_{ij}

	N_{CIOS}	N_{CABS}	N_{CL}	N_{CS}	N_{CB}	N_{CA}	N_{PO}
N_{CIOS}		K_{IA}		K_{IS}	K_{IB}	K_{IT}	K_{IP}
N_{CABS}			K_{AL}	K_{AS}	K_{AB}	K_{AT}	K_{AP}
N_{CL}							K_{LP}
N_{CS}							K_{SP}
N_{CB}							K_{BP}
N_{CA}							K_{TP}
N_{PO}							

6.1.3 Ion Model

The ion model for the aqueous stability is identical to that used for the optimum salinity in Section 5.1.1. The complexity of real brines is simplified by grouping the ions as monovalent cations, divalent cations, or anions. These pseudo-ions were used to determine cation exchange between the interface and the brine using a mass action law (Hirasaki, 1982). The geochemical interactions (e.g. chelation and precipitation) among these ions were ignored. **Table 6.2** shows the molecular weight, the conversion factors from wt% to meq/ml, and number of occurrences of the ions in the dataset. f_6^S is defined as:

$$f_6^S = \frac{C_6^S}{C_3} \tag{6.8}$$

where, C is the concentration in meq/ml; subscripts 3, 5, and 6 represent anionic surfactant, pseudo-anion, and pseudo-divalent cation; superscript S denotes adsorbed cation on micelles. The surfactants are at the interface, and the pseudo-anions are free ions in the brine. No superscript denotes overall concentration (sum of the concentrations in the micelle and brine). Only the anionic surfactants associate with cations, so co-solvents are assumed to have no influence. The mass action equation for the exchange of monovalent and divalent cations between the micelle and brine is

$$\frac{\left(C_3 - C_6^S\right)^2}{C_6^S} = \beta_S C_3 \frac{\left(C_5 - C_6 + C_6^S\right)^2}{C_6 - C_6^S} \tag{6.9}$$

where, β_S is the ion exchange constant for the surfactant. The calculations were done using a value of β_S equal to 0.4 (Wang, 1979). C_6^S was determined using non-linear minimization bounded between 0 and the minimum of C_6 and C_3 for the brine composition at the optimum salinity.

Table 6.2: Ion Properties

Ion	MW	meq/ml/wt%	N
Na^+	22.99	0.435	858
K^+	39.10	0.256	385
Mg^{2+}	24.31	0.823	209
Ca^{2+}	40.08	0.499	207
Sr^{2+}	87.62	0.228	48
Cl^-	35.45	0.282	760
$HCO3^-$	61.02	0.164	428
$BO2^-$	42.81	0.234	81
OH^-	17.01	0.588	31
$C_2H_3O_2^-$	59.04	0.169	1
$CO3^{2-}$	60.01	0.333	628
$SO4^{2-}$	96.06	0.208	533
$B4O7^{2-}$	155.23	0.129	22
$SiO3^{2-}$	76.08	0.263	29
$EDTA^{4-}$	288.21	0.139	172

C_5 is the meq/ml of anions at aqueous stability limit. The aqueous stability limit (A_Q) wt% equivalent NaCl is defined as:

$$A_Q = 5.844\, C_5 \tag{6.10}$$

where 5.844 is the product of the molecular weight of NaCl (58.44 g/mol) and the conversion factor from mg/ml to wt%. **Figure 6.1** shows the aqueous stability limit in wt% NaCl equivalent versus wt% TDS. The difference is relatively small because the most abundant salts are NaCl or have similar equivalent weights.

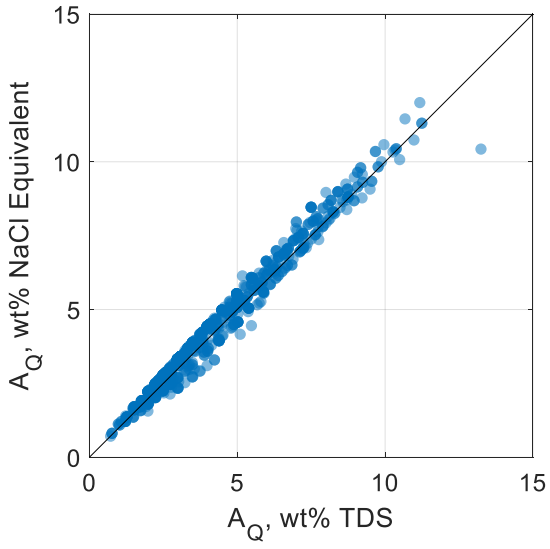

Figure 6.1. Optimum salinity in wt% NaCl equivalent versus optimum salinity in wt%

6.1.4 Example calculations

Equation **(6.2** can be expressed as a linear equation with 33 terms. A formulation with 40 mol% C_{12} ABS (component i=1) and 60 mol% C_{13}-7PO-SO_4 (component i=2) at 60 °C gives the following:

$$\ln \mathrm{A_Q} = c_\mathrm{T}\Delta\mathrm{T} + \left[\mathrm{x_1c_3}N_{CABS,1} + \mathrm{x_1c_3}N_{ABS,1} + \mathrm{x_2c_6}N_{CS,2} + \mathrm{x_2c_9}N_{PO,2} + \mathrm{x_2c_{11}}N_{SO4,2}\right] + c_{17}\mathrm{f_6^S} + \left[\kappa_{IOS-S}\sqrt{\mathrm{x_1}N_{CABS,1}}\sqrt{\mathrm{x_2}N_{CS,2}} + \kappa_{IOS-PO}\sqrt{\mathrm{x_1}N_{CABS,1}}\sqrt{\mathrm{x_2}N_{PO,2}} + \kappa_{S-PO}\sqrt{\mathrm{x_2}N_{CS,2}}\sqrt{\mathrm{x_2}N_{PO,2}}\right] \quad \textbf{(6.11)}$$

$$\ln \mathrm{A_Q} = c_\mathrm{T}(60-25) + [0.4\mathrm{c_3}12 + 0.4c_4 1 + 0.6c_6 13 + 0.6c_9 7 + 0.6c_{11}1] + c_{17}\mathrm{f_6^S} + \left[\kappa_{IOS-S}\sqrt{0.4*12}\sqrt{0.6*13} + \kappa_{IOS-PO}\sqrt{0.4*12}\sqrt{0.6*7} + \kappa_{S-PO}\sqrt{0.6*13}\sqrt{0.6*7}\right] \quad \textbf{(6.12)}$$

6.2 Description of Experimental Dataset

The UTCEOR Database is a collection of the experimental surfactant phase behavior measurements conducted at the University of Texas at Austin. The dataset used for the development of the structure-property model for the aqueous stability was created by querying the database for the experiments that met the following criteria:

1. The structure (e.g. hydrophobe/alcohol type and carbon number, average numbers of PO and EO groups, type of head group) of the surfactants and co-solvents are known and an average molecular weight can be calculated.
2. The surfactants are sulfonate, sulfate, or carboxylate. The sulfonate surfactants are either internal olefin sulfonate or alkyl benzene sulfonate. The sulfate and carboxylate surfactants are alcohol alkoxy anionic surfactants that have the form of hydrophobe-xPO-yEO-SO4 or hydrophobe-xPO-yEO-COO, where x≥0, y≥0, and x+y≥7. The hydrophobe must fall within one of the four types (L, S, B, or T).

3. The co-solvents are aliphatic alcohols, aliphatic alcohol alkoxylated, or phenol alkoxylates. The number of carbon atoms in the alcohol were less than 7, the number of PO groups were less than 2, the number of EO groups are less than or equal to 10.
4. The formulation contains both alcohol alkoxy anionic surfactant(s) and sulfonate co-surfactant(s). The co-surfactants are either all internal olefin sulfonate or all alkylbenzene sulfonate. The lipophile of the alcohol alkoxy anionic surfactants are either all L-type, all S-type, all B-type, or all T-type hydrophobes.
5. The aqueous stability limit is the highest salinity in which the sample is a stable solution i.e. coacervation, cloudiness, or precipitation are observed in the next sample.

These criteria removed experiments that used nonionic, cationic, and zwitterionic surfactants. Some anionic surfactants that did not meet the criteria include alpha olefin sulfonates, dihexyl sulfosuccinate, gemini surfactants (Upamali et al., 2016), and alcohol alkoxy sulfonates. Criteria 4 allows for only 8 types of mixtures (IOS with either L, S, B, or T, and ABS with either L, S, B, or T). IOS only, ABS only, and AAA only mixtures do not form mixed micelles and typically do not behave synergistically. There were insufficient experimental results using IOS and ABS to justify adding κ_{IA} to the model, so experiments using both IOS and ABS were removed.

Tests in which all of the samples showed phase separation or when all of the samples were stable are inconclusive. In the former, the limit is less than or equal to the minimum salinity tested, and in the latter, the limit is greater than or equal to the maximum salinity tested. Inequalities could not be used. The dataset has a total of 858 aqueous stability experiments using 121 unique surfactants and 19 unique co-solvents.

6.2.1 Brines

The brines were mixtures of sodium chloride, potassium chloride, magnesium chloride, calcium chloride, strontium chloride, sodium bicarbonate, sodium sulfate, sodium carbonate, sodium metaborate, sodium acetate, sodium hydroxide, sodium tetraborate, sodium silicate, and tetrasodium ethylenediaminetetraacetate (EDTA-Na_4) in deionized water.

Figure 6.2 shows (a) the concentration of monovalent cation (C_{11}) versus the concentration of divalent cations (C_6) and (b) the fraction of surfactant with adsorbed divalent cation (f_6^S) versus C_6.

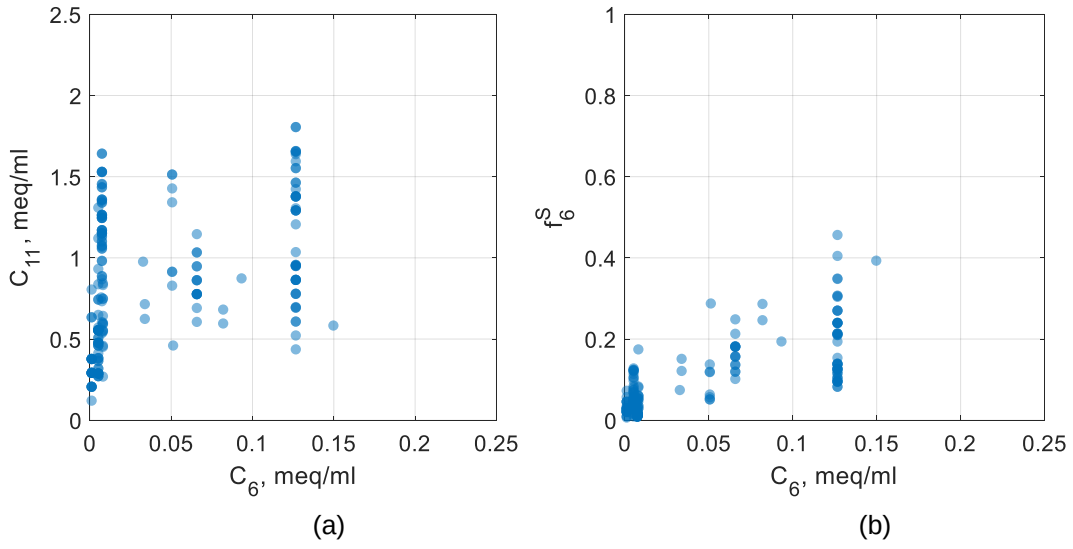

Figure 6.2: (a) The concentrations of monovalent versus divalent cations in meq/ml for the experiments containing divalent cations. (b) The fraction of surfactant with adsorbed divalent cation versus the concentration of divalent cations.

6.2.2 Chemicals

The chemical formulations are various combinations of 114 surfactants and 19 co-solvents. Of the surfactants, 4 are internal olefin sulfonates (IOS), 11 are alkylbenzene

sulfonates (ABS), 69 are alcohol alkoxy sulfates (AAS), and 37 are alcohol alkoxy carboxylates (AAC). The IOS and ABS surfactants have various hydrophobe carbon number distributions ranging from 15 to 28 carbons and 11 to 18 carbons, respectively. The hydrophobes of the AAS and AAC surfactants were C_{16} to C_{32} Guerbet alcohols (Adkins et al., 2010, 2012; Lu et al., 2014), C_{28} epoxide alcohol, C_{18} oleyl alcohol (Upamali et al., 2016), C_{30} tristyrylphenol (Liyanage et al., 2015), ~C_{13} alcohols with various degrees of branching, ~C_{16} alcohols with various degrees of branching, and 2-ethyl-hexanol (Upamali et al., 2016). Of the co-solvents, two were alcohols (isobutyl alcohol and sec-butyl alcohol) and 17 were alcohol alkoxylates of isobutyl alcohol, normal butanol, or phenol. The number of EO groups in the alcohol alkoxylates ranged from 1 to 10 and a few of them also included one or two PO groups.

Figure 6.3(a) shows the distribution of the temperature and the proportion of experiments using sulfate and carboxylate surfactants. 64.2% used sulfate surfactants, 35.7% used carboxylate surfactants and 0.1% used both sulfate and carboxylate surfactants. **Figure 6.3**(b) shows the distribution of temperature and the proportion of experiments using co-solvent. 68% of the experiments used co-solvents and 32% did not.

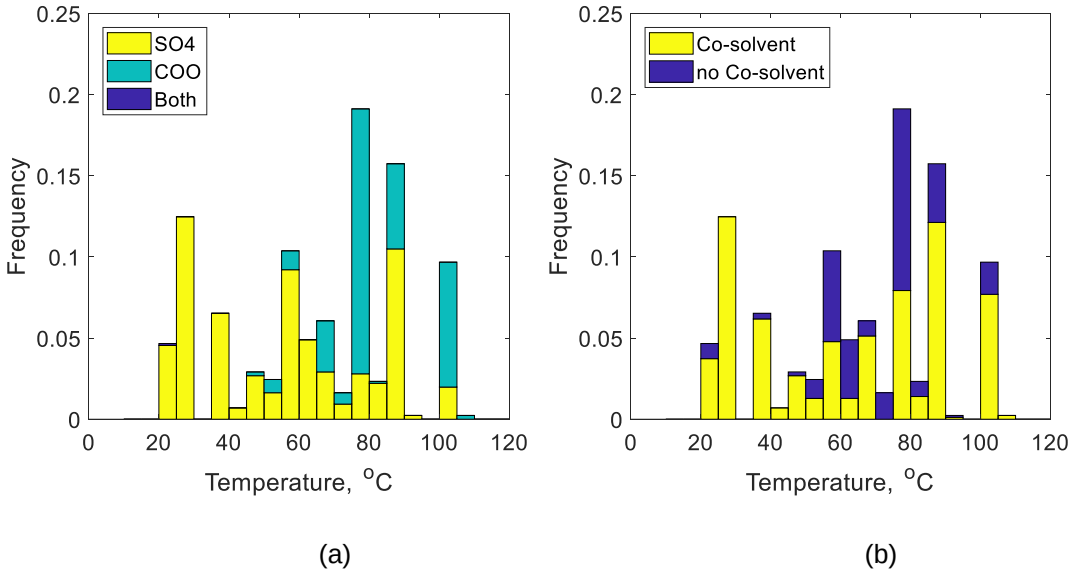

Figure 6.3: (a) Distribution of temperature with the proportion of experiments using sulfate/carboxylate surfactants. (b) Distribution of temperature with the proportion of experiments using co-solvent.

For alcohol alkoxy anionic surfactants, the average numbers of propoxy and ethoxy groups ranged from 0 to 65 and 0 to 100, respectively. **Figure 6.4** shows the distribution of PO and EO groups for (a) alcohol-alkoxy-sulfate and (b) alcohol-alkoxy-carboxylate surfactants. Of the alcohol alkoxy anionic surfactants, 66% were alcohol-alkoxy-sulfate surfactants and 34% were alcohol-alkoxy-carboxylate surfactants. Most of the sulfate surfactants with less than 15 PO groups had S type hydrophobes without ethoxy groups. There was one S type hydrophobe alkoxy carboxylate surfactants (C_{13}-35PO-45EO-COO) in the dataset and it was used once. Nearly all carboxylate surfactants contained at least 10 EO groups, with the exception of C_{30}(TSP)-45PO-COO.

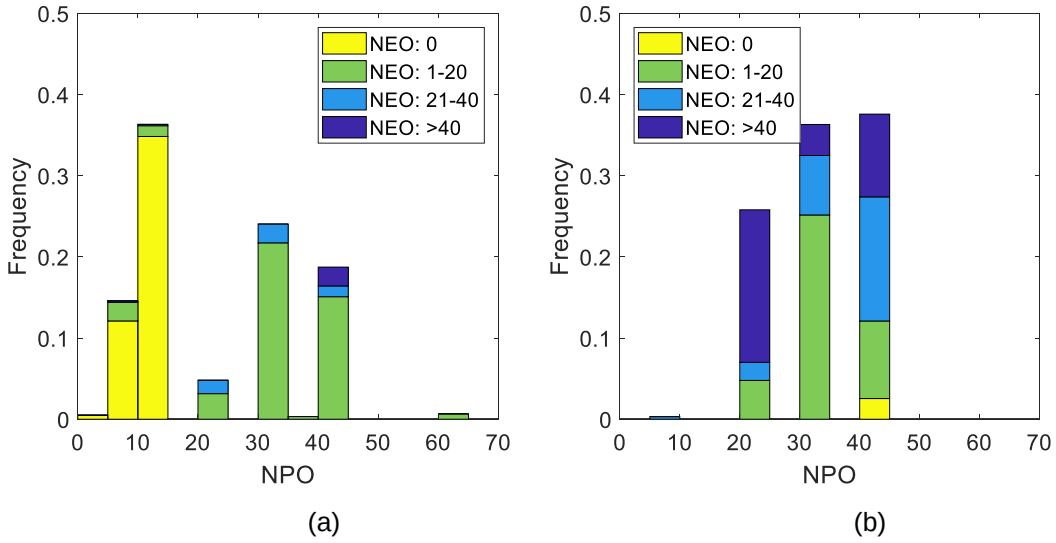

Figure 6.4: Distribution of the numbers of PO groups (NPO) and the number of EO groups (NEO) for (a) alcohol alkoxy sulfate and (b) alcohol alkoxy carboxylate surfactants.

Figure 6.5 shows the distribution of the concentration of surfactant (C_3) in (a) wt% and (b) molarity with the proportions using C number of surfactant and co-solvent components. The average number of components is about 3. 18% of the experiments used 2 components, 63% used 3, and 16% used 4. One formulation used 4 surfactants and 2 co-solvents (C=6) in order to study the effects of high polydispersity.

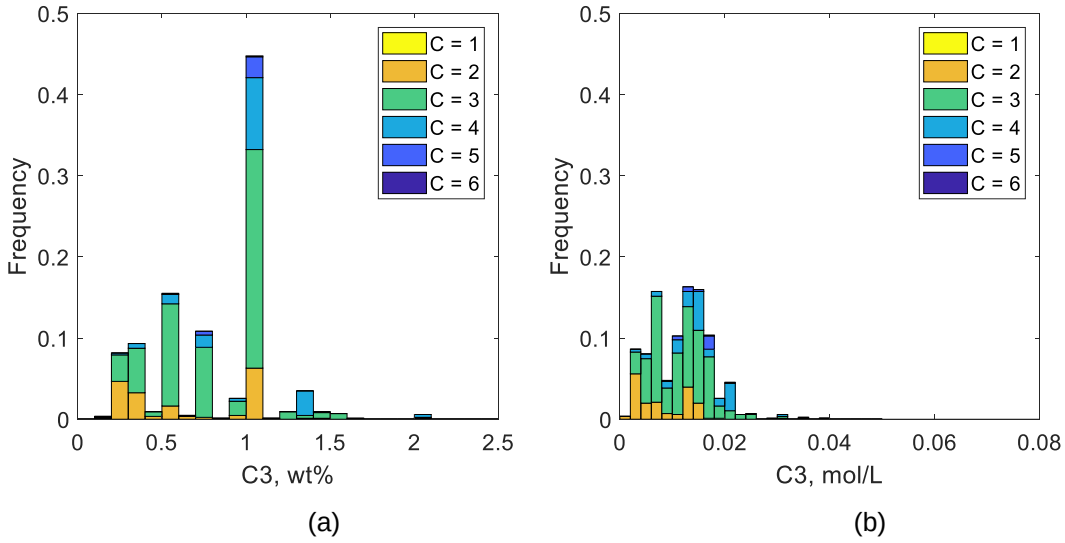

Figure 6.5: Distribution of the concentrations of surfactant in (a) wt% and (b) Molarity with the proportion of experiments using C number of surfactant and co-solvent components.

Figure 6.6 shows the distribution of the mole fraction of AAA (x_A) for formulations using (a) IOS and (b) ABS as the co-surfactants and the proportions of the alcohol-alkoxy-anionic surfactant that are sulfate (SO4), carboxylate (COO), and both sulfate and carboxylate. The average, standard deviation (St. Dev.), and number of samples (N) for each of these surfactant mixtures are shown in **Table 6.3**. 68% of the experiments used IOS co-surfactants, and 32% used ABS co-surfactants.

The average mole fraction of alkoxy-carboxylate surfactants was approximately 9 mol% with a narrow distribution (standard deviation of 3 mol%), whereas the average mole fraction of alkoxy-sulfate surfactants varied significantly more. The carboxylate surfactants were larger molecules (majority had >20 PO and >10 EO groups), whereas sulfate surfactants were a bimodal distribution of lower molecular weight (~13PO and 0 EO groups) and higher molecular weight (>20 PO and >10 EO groups) surfactants as seen in **Figure 6.4**.

Table 6.3: Mole Fractions of Alcohol-alkoxy-anionic Surfactant (X_A)

Name	Mole Fraction Sulfate			Mole Fraction Carboxylate			Mole Fraction SO4 and COO		
	Average	St. Dev.	N	Average	St. Dev.	N	Average	St. Dev.	N
IOS	0.27	0.19	385	0.08	0.03	210	0.42	-	1
ABS	0.33	0.20	166	0.10	0.03	96	-	-	0

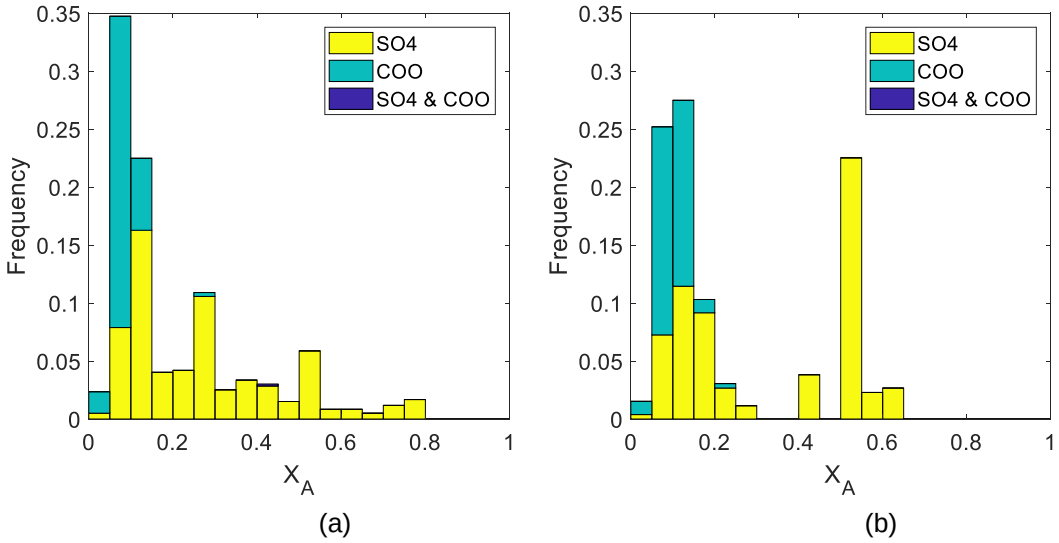

Figure 6.6: Distribution of the mole fraction of alcohol-alkoxylate-sulfate and -carboxylate (X_A) for (a) IOS and (b) ABS surfactants with the proportion of experiments using sulfate, carboxylate, and both sulfate and carboxylate.

Figure 6.7 shows the distribution of the (a) overall volume fraction of co-solvent (V_7) and (b) the interfacial volume fraction of co-solvent (f_7^S) for the different co-solvent types. Despite partitioning to the brine, the co-solvent comprises a significant volume fraction of the interface.

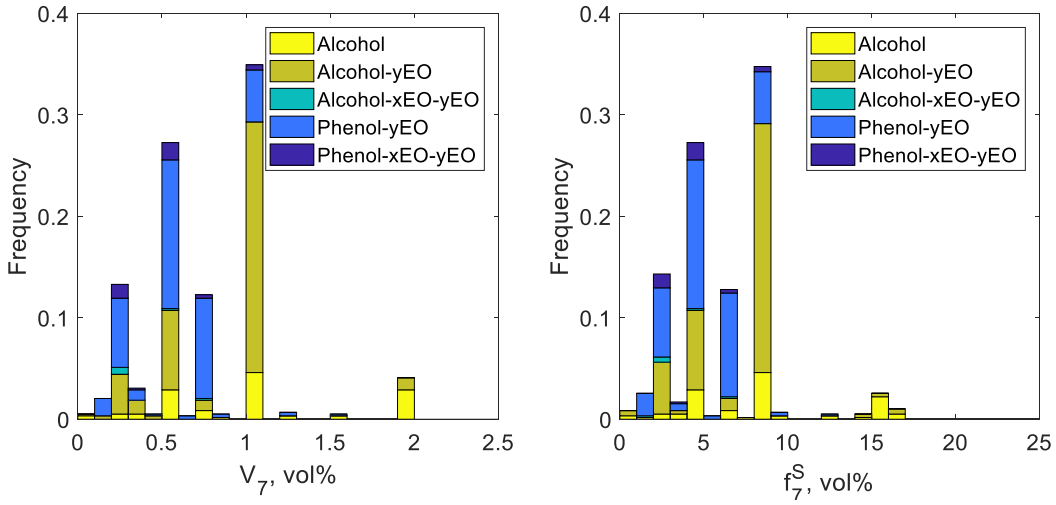

Figure 6.7: Distribution of (a) volume fraction of co-solvent and (b) interfacial volume fraction of co-solvent with the proportion that are alcohols, alcohol ethoxylates, alcohol propoxy ethoxylates, phenol ethoxylate, and phenol propoxy ethoxylates.

In most chemical flooding applications, polymer is added to the aqueous surfactant solution for mobility control. Samples with polymer tend to phase separate more quickly than samples without polymer, which enables more rapid screening. Polymer typically reduces the aqueous stability limit but the shift may not be detectable within the precision of the measurement. Polymers are not typically used in the microemulsion phase behavior screening tests until the chemical formulation is optimized and ready for coreflood testing because the polymer increases the time for equilibration by increasing the viscosity and by other mechanisms.

Three aqueous polymers were used in the aqueous stability tests. They were Flopam 3630S, Flopam 3330S, and Flopam AN-125 from SNF. FP 3630S and FP 3330S are co-polymers of acrylamide and sodium acrylate (partially-hydrolyzed polyacrylamide or HPAM). AN-125 is a tertiary polymer of acrylamide, sodium acrylate, and sodium acrylamido tertiobutyl sulfonate (ATBS sometimes abbreviated as AMPS). The monomer content and molecular weight affect the properties of the polymer such as viscosity,

solubility, thermal stability, and hydrolytic stability. The acrylamide (AM) moieties can be hydrolyzed to acrylate (AA) moieties, which typically increases the polymer viscosity. The rate of hydrolysis is a function of the AM/AA ratio, pH, and temperature (Levitt et al., 2009). The polymer structure likely affects the aqueous stability limit but it was not modeled.

6.2.3 Aqueous Phase Behavior Properties

Figure 6.8 shows the distribution of the aqueous stability limit with the proportions (a) that contained alkali and divalent cations and (b) by the type of polymer. 13% contained alkali and divalent cations (AS(P) in hard brine), 74% contained alkali without divalent cations (AS(P) in soft brine), 11% contained no alkali and divalent cations (S(P) in hard brine), and 1% contained no alkali and no divalent cations (S(P) in soft brine). Experiments with alkali and divalent cations used either (1) chelating agents such as tetrasodium EDTA, sodium sulfosuccinate, or sodium acetate, or (2) a weak alkali such as sodium metaborate with a brine containing low hardness. 7% contained Flopam AN-125, 32% contained Flopam 3630S, 48% contained Flopam 3330S, and 13% contained no polymer.

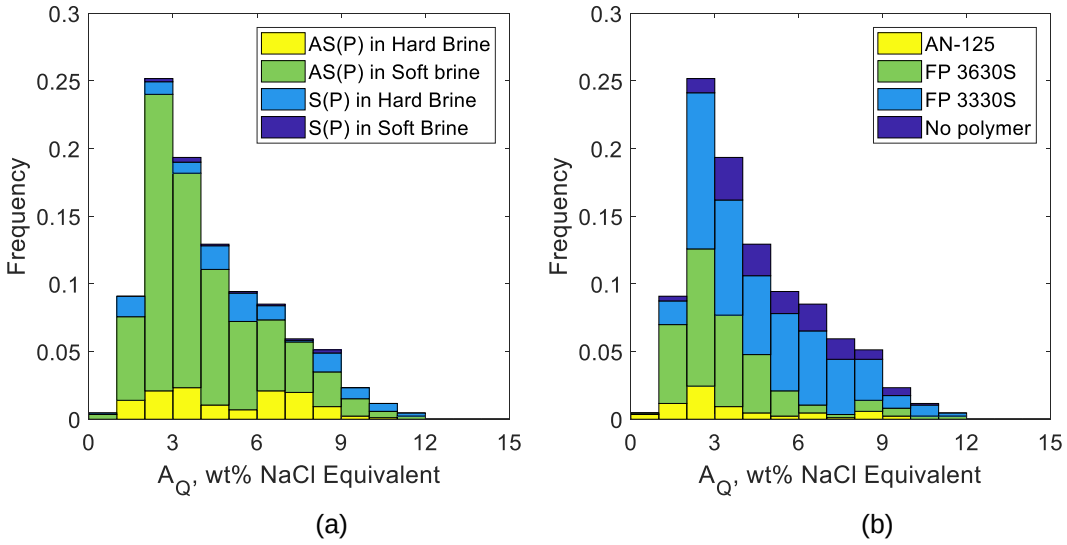

Figure 6.8: Distribution of (a) the apparent optimum solubilization ratio and (b) the true optimum solubilization ratio with the proportions of surfactant polymer (SP), alkali surfactant polymer with soap (ASP soap) and without soap (ASP), and alkali co-solvent polymer (ACP) formulations.

6.2.4 Experimental Uncertainty

When comparing values calculated from the model with the data, some rough idea of the experimental uncertainty is needed to interpret the results of the model comparisons. The salinity scans for aqueous stability and for microemulsion phase behavior were typically done at 0.5 wt% salinity intervals. The measurement of the aqueous stability limit is based on two samples - the highest salinity sample that forms a solution and the lowest salinity that phase separates. The uncertainty is at best 0.5 wt%, the salinity increment. Without polymer there can be multiple samples that show intermediate levels of haziness that may or may not become a solution, and the uncertainty increases due to human subjectivity in how to interpret the visual observations.

Figure 6.9 shows repetitions of aqueous stability tests for 9 different formulations. The mean, standard deviation, relative deviation, and number of repetitions are shown in

Table 6.4. The average deviation from the mean is 0.39 wt% or about 12% relative deviation. The experimental uncertainty in the aqueous stability limit is approximately 0.5 wt%, which is comparable to the precision of the measurement.

Table 6.4: Repetitions of Aqueous Stability Tests

Formulation	Chemicals	T (°C)	Mean (wt%)	St. Dev. (wt%)	Rel. Dev. (wt%)	N
A	0.55% C_{12-13}-13PO-SO4, 0.2% C_{15-16} ABS, 0.75% Phenol-2EO, 0.25% HPAM	27	2.73	0.09	3%	4
B	0.5% C_{13}-13PO-SO4-, 0.5% C_{20-24} IOS, 2% IBA,	38	2.73	0.51	19%	10
C	0.15% C_{12-13}-13PO-SO_4, 0.15% C_{20-24} IOS, 1% IBA-5EO, 0.2% HPAM	55	4.12	1.06	26%	6
D	0.125% C_{30}(TSP)-45PO-COO, 0.125% C_{20-24} IOS, 0.2% HPAM	55	2.69	0.47	18%	4
E	0.125% C_{18}-45PO-20EO-SO_4, 0.125% C_{19-28} IOS, 0.2% HPAM	55	3.96	0.14	3%	6
F	0.12% C_{30}(TSP)-35PO-10EO-SO_4, 0.08% C_{15-18} ABS, 0.15% HPAM	62	2.04	0.28	14%	4
G	0.5% C_{28}-35PO-10EO-SO_4, 0.5% C_{19-28} IOS, 1% TEGBE, 0.125% HPAM	85	3.21	0.56	17%	13
H	0.25% C_{28}-35PO-10EO-SO_4, 0.25% C_{19-28} IOS, 0.5% TEGBE, 0.125% HPAM	65	3.11	0.28	9%	9
I	0.5% C_{18}-45PO-20EO-SO_4, 0.5% C_{12} ABS,	100	8.93	0.35	4%	5

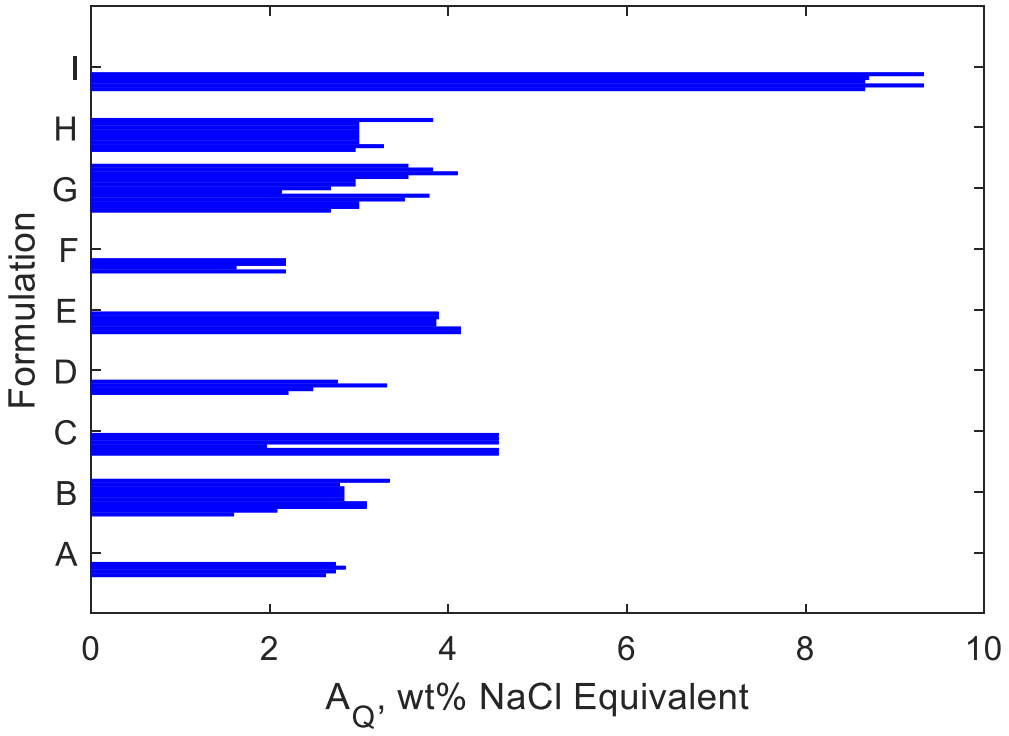

Figure 6.9: Repetitions of aqueous stability tests for formulations A to I.

6.3 Results

The dataset has a sample size of 817. Applying equation **(6.2** results in a system of 858 linear equations with 33 unknowns (1 for the temperature coefficient, 12 for the surfactant structure coefficients, 4 for the co-solvent structure coefficients, 1 for the coefficient of f_6^S, and 14 for the various lipophile-lipophile interactions, 1 for the polymer coefficient). These unknowns were determined by multiple linear regression. The ratio of equations to unknowns is 26.

6.3.1 Aqueous Stability Limit Correlation

Figure 6.10 shows the predicted versus measured aqueous stability limit (A_Q). **Table 6.5** shows the coefficients for temperature, f_6^S, and the surfactant and co-solvent structure characteristics and polymer. **Table 6.6** shows the constants for the lipophile-lipophile interactions. The number of experiments (N), the standard error (σ_{ci}), and the relative standard error ($|\sigma_{ci}/ci|$) for each coefficient are shown.

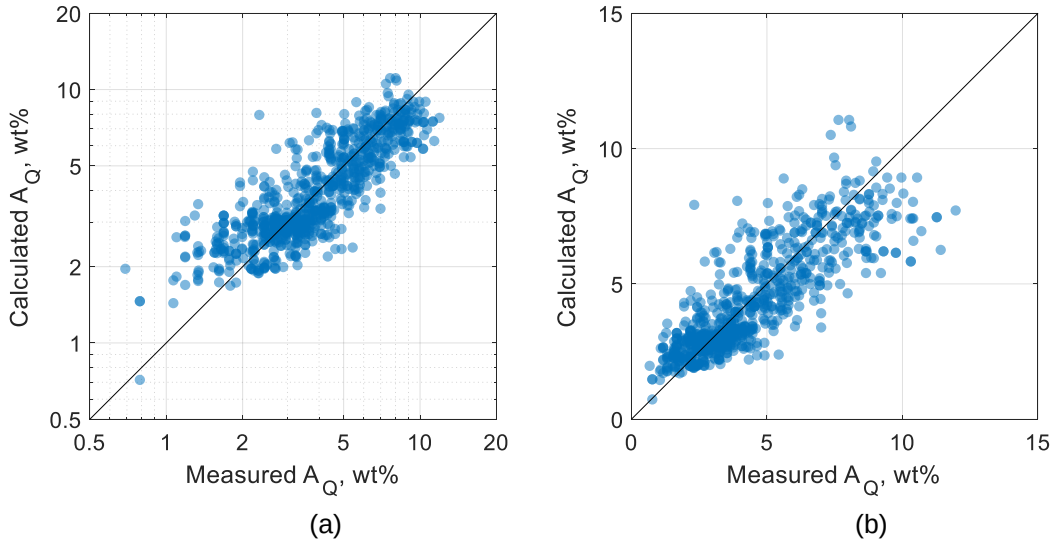

Figure 6.10: Predicted versus measured aqueous stability limit in (a) log and (b) linear scale.

Table 6.5: Coefficients for the aqueous stability model

Coefficient, Variable	N	C_i	σ_{Ci}	$\lvert\sigma_{Ci}/c_i\rvert$
c_T, ΔT	854	-0.0067	0.001	15%
c_1, $N_{C,IOS}$	596	-0.253	0.014	5%
c_2, N_{IOS}	596	7.13	0.23	3%
c_3, $N_{C,ABS}$	262	-0.266	0.025	9%
c_4, N_{ABS}	262	5.28	0.25	5%
c_5, $N_{C,L}$	401	-0.31	0.034	11%
c_6, $N_{C,S}$	326	-0.19	0.039	20%
c_7, $N_{C,B}$	77	-0.254	0.111	44%
c_8, $N_{C,A}$	54	-0.179	0.041	23%
c_9, N_{PO}	840	-0.1106	0.0301	27%
c_{10}, N_{EO}	609	0.10	0.01	10%
c_{11}, N_{SO4}	552	4.42	0.34	8%
c_{12}, N_{COO}	307	3.24	0.47	15%
c_{13}, N_{OH}	581	1.03	0.40	39%
c_{14}, $N_{C,CS}$	581	0.015	0.1006	670%
c_{15}, $N_{PO,CS}$	30	0.042	0.488	1150%
c_{16}, $N_{EO,CS}$	503	0.414	0.043	10%
c_{17}, f_6^S	209	-0.482	0.200	42%
c_P, ω_P	743	-0.318	0.119	38%

Table 6.6: Lipophile-Lipophile Interaction Constants

Coefficient	N	κ_{ij}	$\sigma_{\kappa ij}$	$\lvert\sigma_{\kappa ij}/\kappa_{ij}\rvert$
$\kappa_{I,L}$	280	0.0299	0.0202	68%
$\kappa_{I,S}$	234	-0.0231	0.0222	96%
$\kappa_{I,B}$	64	0.081	0.054	66%
$\kappa_{I,T}$	18	0.0039	0.0284	725%
$\kappa_{I,P}$	578	0.0406	0.0245	60%
$\kappa_{A,L}$	121	0.0430	0.0364	85%
$\kappa_{A,S}$	92	-0.03057	0.03865	126%
$\kappa_{A,B}$	13	0.121	0.078	64%
$\kappa_{A,T}$	36	0.009	0.0371	414%
$\kappa_{A,P}$	262	0.0504	0.0421	84%
$\kappa_{L,P}$	401	0.1308	0.0687	53%
$\kappa_{S,P}$	308	-0.00925	0.05782	625%
$\kappa_{B,P}$	77	-0.065	0.139	214%
$\kappa_{T,P}$	54	0.0615	0.0677	110%

The coefficient of determination (R^2) values are 0.71 for the prediction of the natural logarithm of A_Q ($\ln A_Q$) and 0.70 for the prediction of A_Q. The standard errors

(standard deviation of the error) are 0.29 for the $\ln A_Q$, 1.24 wt% NaCl equivalent for A_Q, and 0.34 for the relative A_Q ($\Delta A_Q/A_{QMeasured}$).

The uncertainty in the measurement is about 0.5%, higher if there were intermediate haziness states and when considering other factors such as variations by batch. Although it is possible to reduce this experimental error for specific experiments, it is not practical to do so for the very large dataset presented here and a very large dataset such as this is needed because of the wide variety of chemicals and oils that are used in chemical EOR.

The temperature coefficient c_T was calculated -0.0067 with relative standard error of 15%. With increasing temperature, surfactant solubility is predicted to decrease. In general, the solubilities of alcohol alkoxy anionic (AAA) decrease and alkyl anionic (AA) surfactants increase with temperature. The dominant surfactant-water interaction for AAA is hydrogen bonding between alkoxy groups and water, which decreases with temperature. All formulations in the dataset were mixture of both AAA and AA surfactants, typically with more AA by mole. The negative temperature coefficient indicates that the AAA surfactants dominate the hydrophilic interactions. This may be due to the larger size of AAA molecules as they can extend further from micelles. Although differing in magnitude, the temperature coefficients for optimum salinity and aqueous stability limit are both negative and show that AAA surfactants dominate the hydrophilic interactions.

Temperature can also affect the solubility products of divalent cation salts, leading to precipitation instead of coacervation. Formulations containing only AA surfactants, which have very high theoretical solubility, sometimes precipitate at low salinities. The aqueous stability limit can typically be increased significantly by the addition of small mole fractions of AAA, which may be due to synergistic interactions between the alkoxy groups and anionic head groups or alkoxy groups and divalent cations.

The coefficients for the surfactant structures (subscripts 1 to 12) reflect the hydrophilic and lipophilic natures of the structures. The coefficients for the hydrophilic structures (N_{EO}, N_{IOS}, N_{ABS}, N_{SO4}, N_{COO}) were positive, and the coefficients for the lipophilic structures ($N_{C,IOS}$, $N_{C,ABS}$, $N_{C,L}$, $N_{C,S}$, $N_{C,B}$, N_{PO}) were negative. These coefficients reflect how increasing the hydrophilicity or deceasing the lipophilicity tends to increase the aqueous solubility. The magnitude of the coefficients for anionic head groups reflect the hydrophilic strength. In order of decreasing hydrophilic strength are the sulfonate (N_{IOS} = 7.13), benzene sulfonate (N_{ABS} = 5.28), sulfate (N_{SO4} = 4.42), and carboxylate (N_{COO} = 3.24).

The coefficients for lipophilic structures ($N_{C,IOS}$, $N_{C,ABS}$, $N_{C,L}$, $N_{C,S}$, $N_{C,B}$, N_{PO}) reflect the interactions between similar lipophiles, and the coefficients $\kappa_{j,k}$ reflect the interactions between dissimilar lipophiles. Therefore coefficients for lipophilic structures ($N_{C,IOS}$, $N_{C,ABS}$, $N_{C,L}$, $N_{C,S}$, $N_{C,B}$, N_{PO}) can be expressed as $\kappa_{j,j}$ where j is the lipophile structure. The values of $\kappa_{j,j}$ were mostly negative, reflecting how increasing lipophilicity, decreases aqueous solubility. However, the values of $\kappa_{j,k}$ were generally positive, indicating that mixing dissimilar lipophiles weakens lipophile-lipophile interaction and increases the aqueous stability. The lipophile pairs with negative $\kappa_{j,k}$ values (I-S, A-S, S-P, and B-P) reflect strong lipophilic interactions that decrease the aqueous solubility.

The effect of co-solvent is a product of the interfacial concentration and the structure-property effect. The interfacial concentration of co-solvent was calculated using interface-water partition coefficient (K_{PW}) of 10. The temperature, salinity, and the structures of the surfactant and co-solvent would influence K_{PW} but were not modeled. Therefore, the coefficients for the co-solvent structure may convolute the structure-concentration and structure-property effects. The co-solvent structure coefficients were positive, but adding co-solvent may decrease the aqueous stability limit if the co-solvent is

more lipophilic than the surfactants. The coefficients for N_C and N_{PO} had high relative error likely because the alcohol and PO groups have a large influence on the partition coefficient. Isobutyl alcohol (IBA) and phenol were the two types of co-solvent hydrophobes used. Phenol has a higher carbon number than IBA but is aromatic, which increases hydrophilicity. The model did not capture the aromaticity, and therefore the regression determined a positive coefficient for $N_{C,CS}$ that matches the data, but is physically incorrect. Increasing carbon number of the alcohol decreases the aqueous solubility. Therefore the co-solvent model should only be used for IBA and phenol based co-solvents.

The coefficient for f_6^S, c_{17}, was based on 209 experiments with divalent cations. The concentrations of divalent cations (C_6) ranged from 0.0014 meq/ml (30 ppm calcium equivalent) to 0.15 meq/ml (3000 ppm calcium equivalent). The ratio of divalent to monovalent cations ranged from 0.0018 to 0.29 by equivalence, and f_6^S ranged from 0.0053 to 0.458. Compared to the optimum salinity (coefficient for f_6^S, a_{17} = -1.36), the aqueous stability limit (coefficient for f_6^S, c_{17} = -0.482) is predicted to be less sensitive to C_6. This may be a result of using datasets with many non-overlapping experiments (233 or 26% overlapping experiments for A_Q and 307 or 45% overlapping experiments for S^*) or may reflect physical differences between the interfaces of a microemulsion and of a micelle.

The coefficient for polymer concentration, c_P, is -0.318. Adding polymer is predicted to decrease the aqueous stability limit. Three types of polymers were used but the differences were not modeled. The ionic strength (and possibly the solubility) of the polymer increases with the acrylate and ATBS content. The acrylate content can increase over time through hydrolysis, and the extent of hydrolysis depends on pH and temperature. The polymer with ATBS were used almost exclusively at higher temperature and higher salinity conditions, where the HPAM polymers may have issues with stability. This may introduce bias in the determination of c_P.

6.3.2 Model Predictions

The aqueous stability limit model can be used as with the optimum salinity model as a guide in the initial development and optimization of formulations. Aqueous stability is used in context to the optimum salinity. A formulation is aqueous stable if the chemicals without oil form a clear aqueous solution at the salinity that achieves the lowest IFT with the crude oil (i.e. $A_Q \geq S^*$). In which case the excess aqueous stability is the difference between A_Q and S^*. An excess aqueous stability on the order of 1 wt% (sum of experimental uncertainties of S* and A_Q) would be desired to allow room for error.

Figure 6.11 shows the effect of number of PO (N_{PO}) groups on A_Q for a formulation containing 10 mol% C_{16} to C_{32} (L type), C_8 to C_{16} (S type), C_{18} (B type), and C_{30} (A type) hydrophobe-propoxy-10EO-COO and 90 mol% C_{12} ABS with 0.2% polymer at 100 °C. The predicted A_Q may be non-monotonic functions of N_{PO} because of the lipophile-N_{PO} interactions. For S, L, and A-type hydrophobes, the A_Q is predicted to initially increase, level off, and then decrease with increasing N_{PO}. The concave downward trend is favorable and is often described as surfactant synergy. For the B-type hydrophobe, the concavity of A_Q is significantly less pronounced and A_Q appears as monotonically decreasing. Typically, formulations are designed not by moles but by mass. **Figure 6.12** shows the effect of N_{PO} on A_Q for a formulation containing the same surfactants but fixed at 1:1 mass ratio. A_Q appears as monotonic functions of N_{PO} that increase or decrease depending on the carbon number and type of hydrophobe.

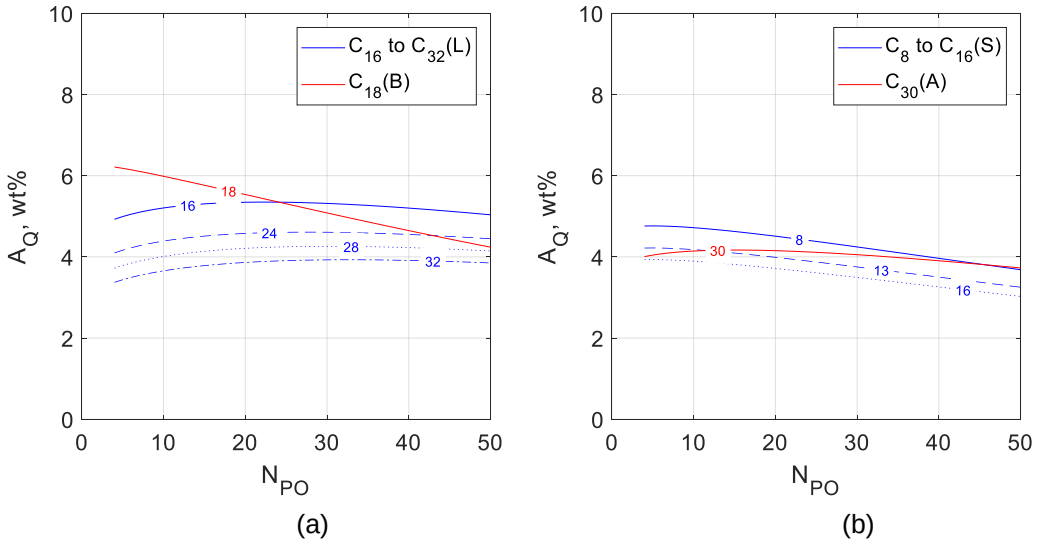

Figure 6.11: Prediction of the effect of the number of PO groups (NPO) on the aqueous stability limit for a formulation of 10 mol% C_{16} to C_{32} (L type), C_8 to C_{16} (S type), C_{18} (B type), and C_{30} (A type) hydrophobe-propoxy-10EO-COO and 90 mol% C12 ABS with 0.2% polymer at 100 °C.

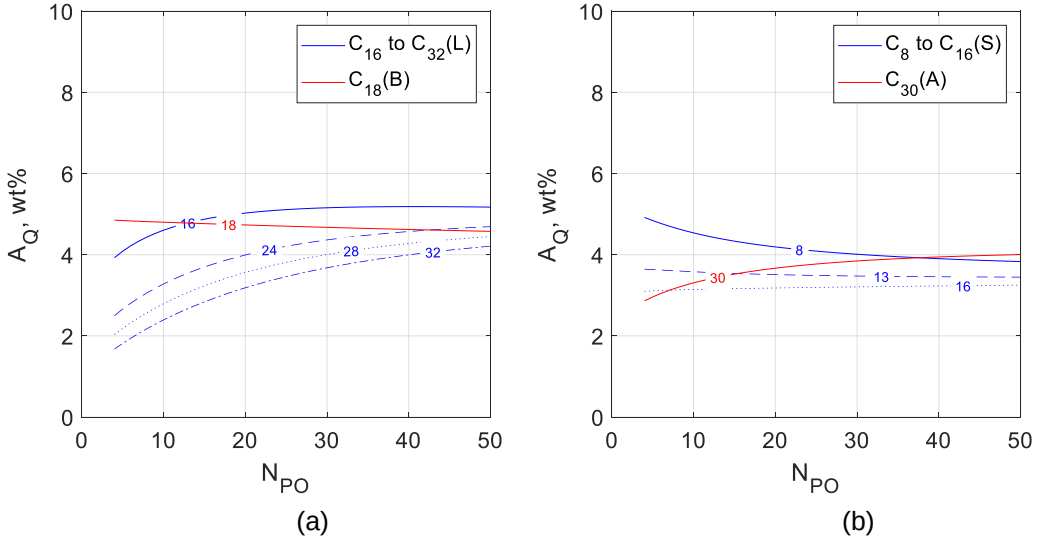

Figure 6.12: Prediction of the effect of the number of PO groups (NPO) on the aqueous stability limit for a formulation of 0.5% C_{16} to C_{32} (L type), C_8 to C_{16} (S type), C_{18} (B type), and C_{30} (A type) hydrophobe-propoxy-10EO-COO and 0.5% C12 ABS with 0.2% polymer at 100 °C.

Figure 6.13 shows the effect of number of EO (N_{EO}) groups on A_Q for a formulation containing 0.5% C_{16} to C_{32} (L type), C_8 to C_{16} (S type), C_{18} (B type), and C_{30} (A type) hydrophobe-35PO-ethoxy-COO and 0.5% C_{12} ABS with 0.2% polymer at 100 °C. A_Q monotonically increases with N_{EO}.

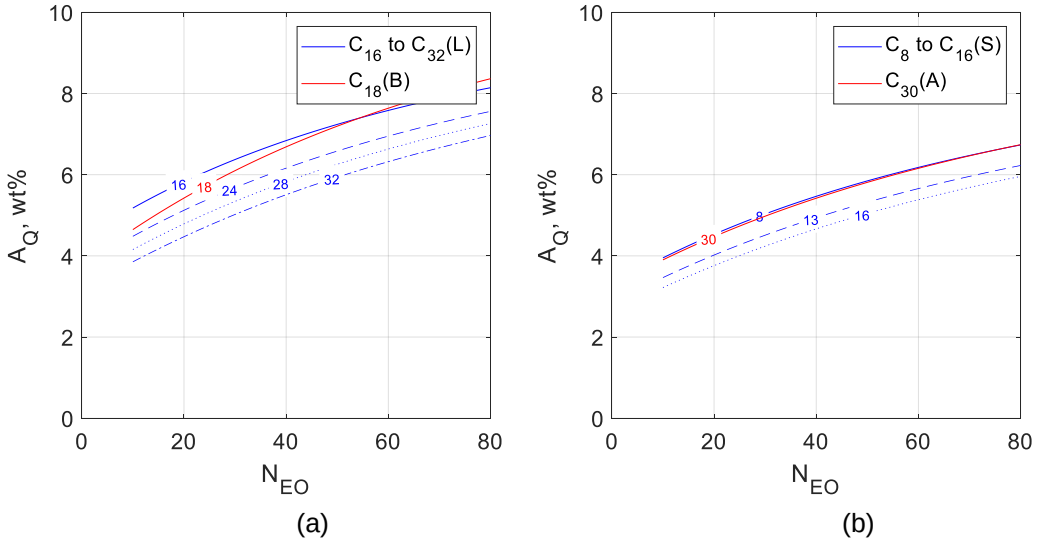

Figure 6.13: Prediction of the effect of the number of EO groups (NEO) on the aqueous stability limit for a formulation of 0.5% C_{16} to C_{32} (L type), C_8 to C_{16} (S type), C_{18} (B type), and C_{30} (A type) hydrophobe-35PO-ethoxy-COO and 0.5% C12 ABS with 0.2% polymer at 100 °C.

Figure 6.14 shows the effect of the mole fraction of co-surfactant on A_Q for a formulation containing C_{28}(L)-35PO-10EO-COO and (a) various ABS surfactants and (b) various IOS surfactants with 0.2% polymer at 100 °C. For mixtures of IOS-L and ABS-L, A_Q is predicted to have a concave downward trend, with the maximum at nearly 90-95 mol% co-surfactant. Despite significant quantities of data at high mole fractions of co-surfactant, there is no data at 100 mol% co-surfactant. Predictions of 100% co-surfactant are likely to be incorrect as the temperature coefficient (c_T =-0.0067) is opposite sign from

the true behavior of alkyl anionic surfactants. The effect of temperature is extremely nonlinear as seen with the optimum salinity.

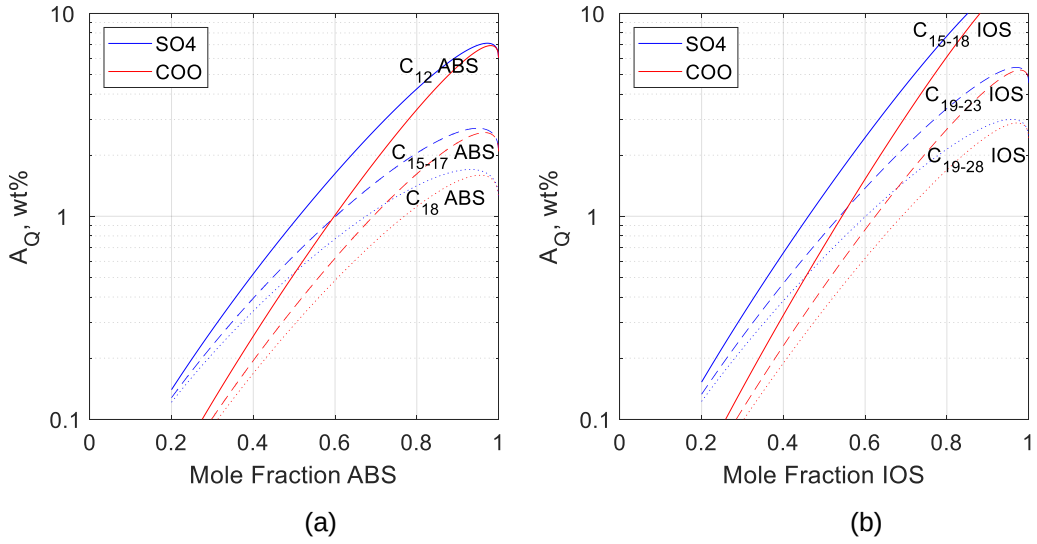

Figure 6.14: Prediction of the effect of the mole fraction of (a) ABS and (b) IOS co-surfactants on the aqueous stability limit for formulation with C_{28} (L type)-35PO-10EO-SO4 or C_{28} (L type)-35PO-10EO-COO with 0.2% polymer at 60 °C.

Figure 6.15 shows the effect of co-solvent concentration (C_7) on A_Q for a formulation containing 0.5% C13-13PO-SO4, 0.5% C20-24 IOS, co-solvent, 0.2% polymer at 25 °C. A_Q is predicted to increase or decrease depending on the structure of the co-solvent. Increasing the number of EO (less so PO) increases the hydrophilicity and is predicted to increase A_Q.

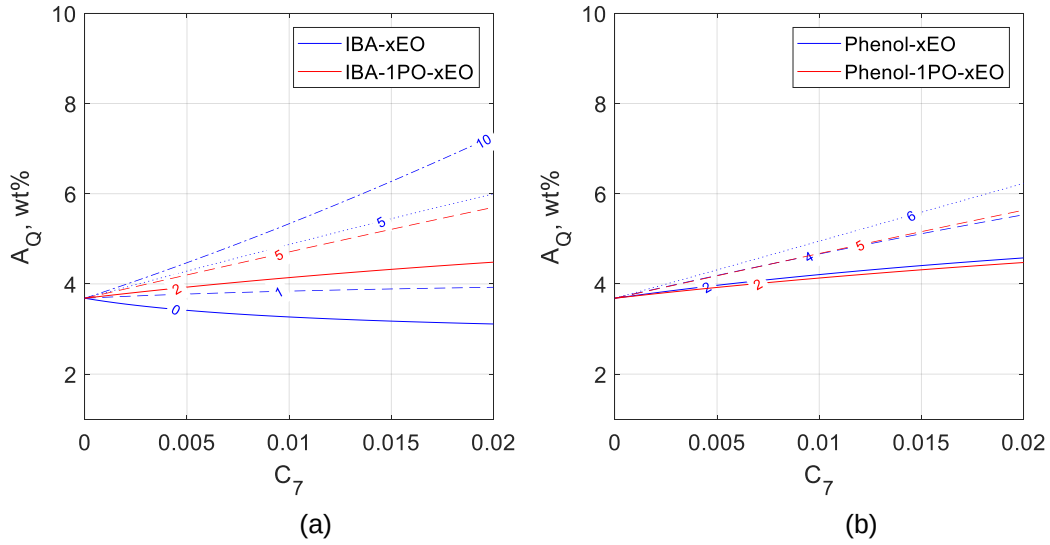

Figure 6.15: Prediction of the effect of co-solvent concentration (C_7) on the aqueous stability limit for a formulation of 0.5% C13-13PO-SO4, 0.5% C20-24 IOS, and co-solvent at 25 °C.

Figure 6.16 shows the effect of the concentration of divalent cations (C_6) on A_Q for a formulation containing 1wt% of 10 mol% C28-40PO-ethoxy-COO, 90 mol% C19-23 IOS, and 0.2% polymer at 100 °C. $\ln A_Q$ is shown to decrease more steeply for lower NEO. $\ln A_Q$ decreases linearly with respect to f_6^S.

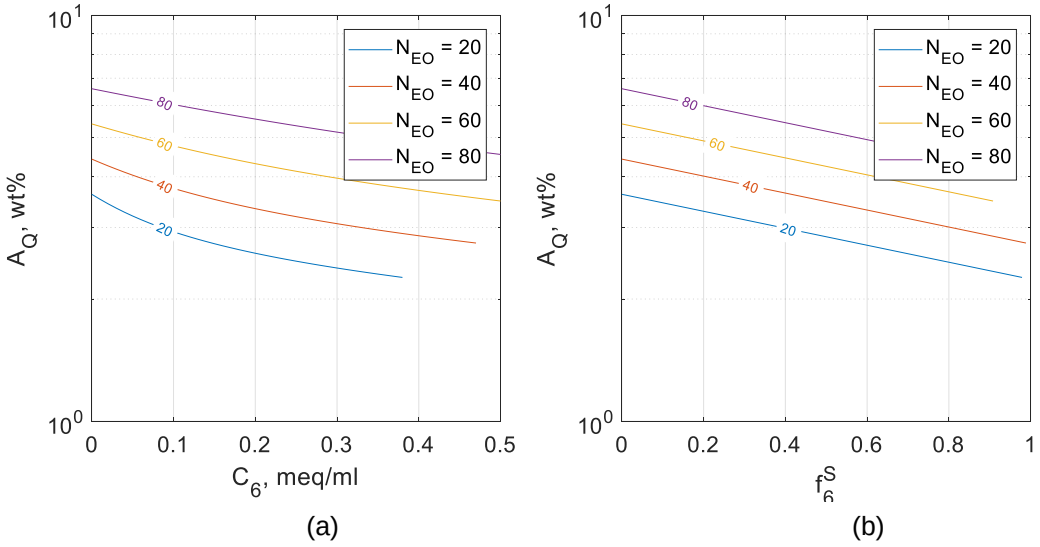

Figure 6.16: Prediction of the effect of (a) divalent cation concentration (C_6)and (b) fraction of surfactant with associated divalent cation (f_6^S) on the aqueous stability limit for a formulation of 1% of 10 mol% C_{28} (L type)-40PO-xEO-COO and 90 mol% C19-23 IOS with 0.2% polymer at 100 °C.

Figure 6.17 shows the effect of (a) temperature and (b) polymer concentration on A_Q for a formulation containing 10 mol% C28-40PO-ethoxy-COO, 90 mol% C20-24 IOS, and 0.2% polymer at 55 °C. $\ln A_Q$ is predicted to decrease linearly with increasing temperature and polymer concentration. The effect of polymer concentration is small as observed experimentally.

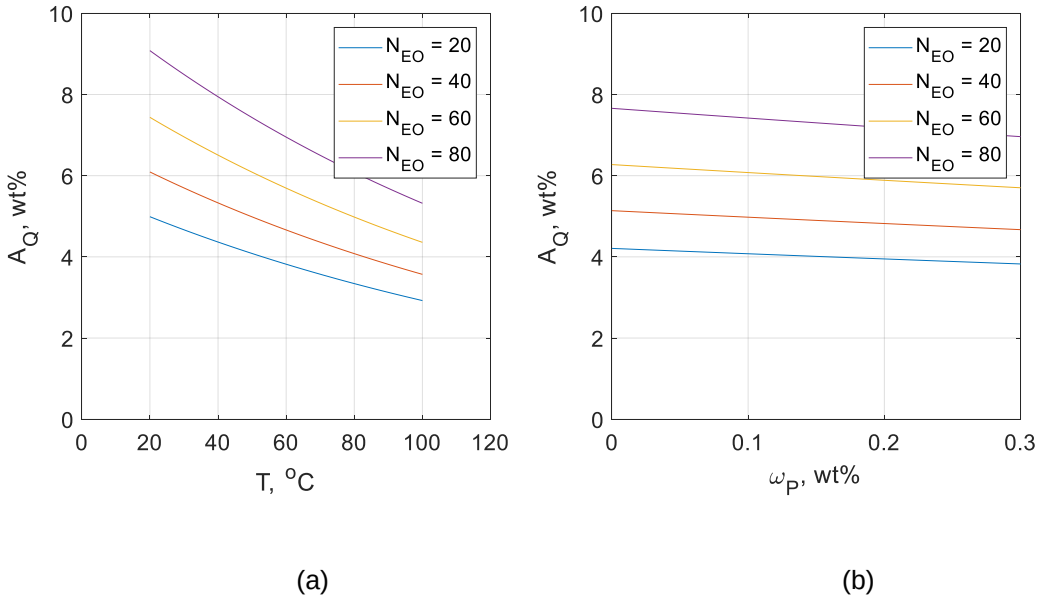

(a) (b)

Figure 6.17: (a) Prediction of the effect of temperature on the aqueous stability limit for formulations containing 10 mol% C_{28} (L type)-40PO-xEO-COO and 90 mol% C20-24 IOS with 0.2% polymer. (b) Prediction of the effect of polymer concentration (ω_P) on the aqueous stability limit for formulations containing 10 mol% C_{28} (L type)-40PO-xEO-COO and 90 mol% C20-24 IOS at 55 °C.

6.3.3 Cross Validation

The dataset was randomly split into 10 subsamples. Nine of the subsamples were used as the training set to develop the model, and the tenth subsample was used as the test set to assess the accuracy of the predictions of the model. The process was repeated 10 times with each subsample being used once as the test set. This is known as 10-fold cross validation. The results are shown in **Table 6.7**. The A_Q can be predicted with an average standard deviation of 1.30 wt% and average relative deviation of 39%.

Table 6.7: 10-Fold Cross Validation of Aqueous Stability Model

Fold	Training Set				Test Set			
	N	σ_{lnAQ}	σ_{AQ}	$\sigma_{dAQ/AQ}$	N	σ_{lnAQ}	σ_{AQ}	$\sigma_{dAQ/AQ}$
1	758	0.29	1.26	0.34	100	0.27	1.12	0.30
2	771	0.28	1.22	0.32	87	0.33	1.52	0.45
3	785	0.29	1.25	0.34	73	0.32	1.14	0.34
4	765	0.29	1.25	0.34	93	0.28	1.22	0.34
5	780	0.28	1.23	0.33	78	0.31	1.45	0.38
6	776	0.29	1.25	0.34	82	0.28	1.10	0.33
7	761	0.28	1.23	0.33	97	0.31	1.51	0.34
8	769	0.29	1.26	0.34	89	0.28	1.23	0.32
9	776	0.28	1.23	0.33	82	0.36	1.47	0.69
10	781	0.28	1.25	0.33	77	0.31	1.23	0.37

6.3.4 Predictions of S^*, σ^* and A_Q

Figure 6.18(a) shows the measured optimum solubilization ratio versus the measured optimum salinity, and (b) the measured aqueous stability limit versus the measured optimum salinity. **Figure 6.18**(a) shows the 687 experiments from the dataset in Chapter 5. **Figure 6.18**(b) shows the 306 experiments that overlapped between the dataset used in Chapter 5 and 6.

The desired properties for chemical EOR formulations are (1) ultra-low IFT, which corresponds to $\sigma^* > 10$ cc/cc and (2) aqueous stability at the optimum salinity, which corresponds to $A_Q \geq S^*$. The models can be used to find formulations that give $\sigma^* > 10+5$

(5 being the experimental uncertainty of σ^*) and $AQ \geq S^* + 0.5$ (0.5 being the experimental uncertainties of S^* and A_Q), which correspond to the regions above the dashed orange lines in **Figure 6.18**.

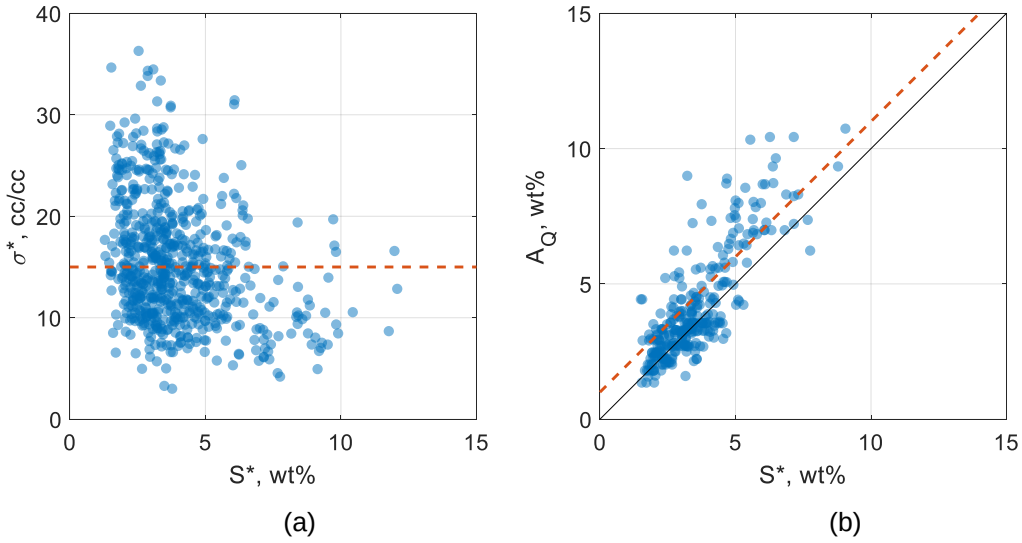

Figure 6.18: (a) Measured optimum solubilization ratio versus measured optimum salinity, and (b) measured aqueous stability limit versus measured optimum salinity.

Figure 6.19 shows the effect of N_{PO} and N_{CL} on (a) σ^* versus S^* and (b) A_Q vs S^* for a formulation of 10 mol% C_{16} to C_{32}(L)-propoxy-10EO-COO and 90 mol% C_{12} ABS with oil of EACN=10 at 100 °C. Increasing N_{PO} is predicted to decrease S^* and increase σ^*, but have little effect on A_Q. Increasing N_{PO} from 10 to 30 increases A_Q slightly but beyond 30 increasing N_{PO} decreases A_Q. Increasing N_{CL} shifts S* and σ* in a similar manner to increasing N_{PO} but to a lesser extent and decreases AQ. In order to increase the solubilization ratio (lower the IFT), increasing N_{PO} rather than N_{CL} is more effective and can increase the excess aqueous stability. In this example, more than 40 PO groups are recommended to achieve ultra-low IFT and aqueous stability at the optimum salinity (i.e. to be in the regions above the dashed orange lines).

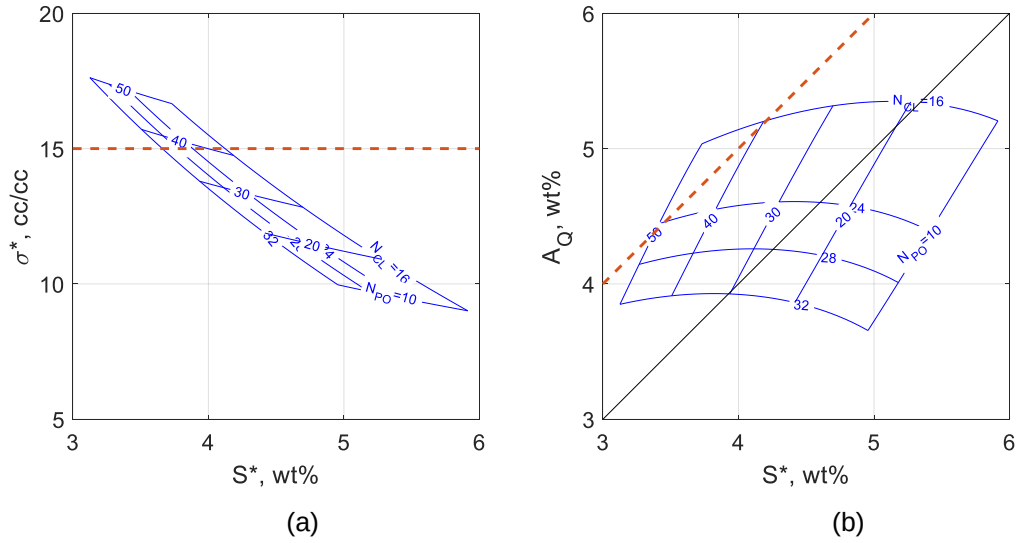

Figure 6.19: Effects of the number of PO groups and hydrophobe carbon number on (a) the optimum solubilization ratio versus optimum salinity, and (b) the aqueous stability limit versus optimum salinity for a formulation of 10 mol% C_{16}(L) to C_{32}(L)-propoxy-10EO-COO and 90 mol% C_{12} ABS with oil of EACN=10 at 100 °C.

Figure 6.20 shows the effect of N_{PO} and N_{EO} on (a) σ^* versus S^* and (b) A_Q vs S^* for a formulation of 10 mol% C_{24}(L)-propoxy-ethoxy-COO and 90 mol% C_{12} ABS with oil of EACN=10 at 100 °C. Increasing N_{EO} is predicted to increase S^*, slightly increase σ^*, and increase A_Q. For this formulation, increasing NEO increases the excess aqueous stability because both the S^* and A_Q increase, with A_Q predicted to increase slightly more so. In this example, N_{PO}>40 is recommended to achieve ultra-low IFT and aqueous stability at the optimum salinity, and the N_{EO} can be varied from 20 to 80 to achieve S^* from approximately 4 to 8 wt%.

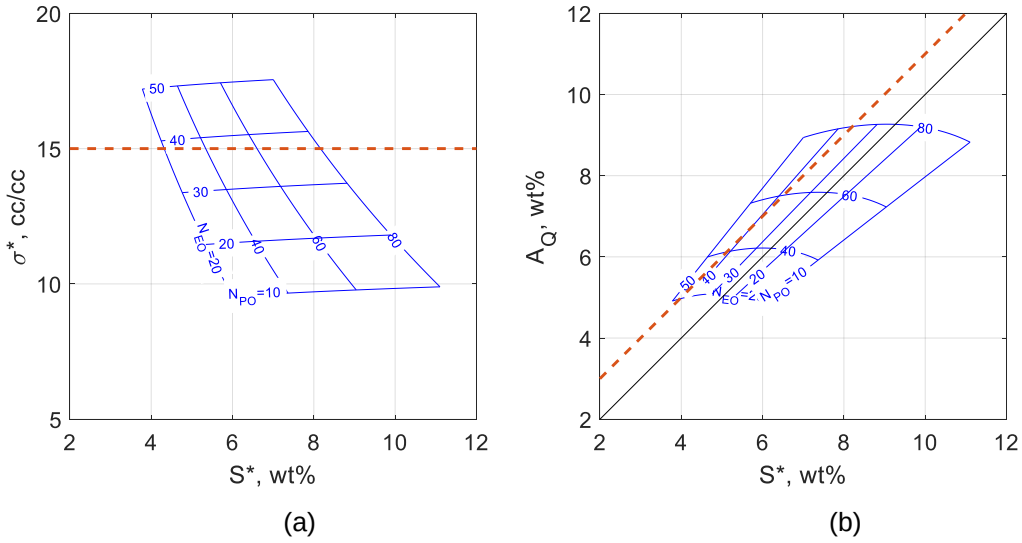

Figure 6.20: Effects of the numbers of PO and EO groups on (a) the optimum solubilization ratio versus optimum salinity, and (b) the aqueous stability limit versus optimum salinity for a formulation of 10 mol% C_{24}(L)-propoxy-ethoxy-COO and 90 mol% C_{12} ABS with oil of EACN=10 at 100 °C.

Figure 6.21 shows the effect the divalent cation concentration (C_6), N_{PO}, and N_{EO} on (a) σ^* versus S^* and (b) A_Q vs S^* for a formulation of 0.6% C_{24}(L)-propoxy-ethoxy-COO and 0.4% C_{12} ABS with oil of EACN=10 at 100 °C. C_6=0.1 meq/ml corresponds to 2000 ppm calcium equivalent. σ* is predicted to be independent of C_6. Increasing C6 is predicted to decrease S^* and A_Q, but S^* more so. Therefore, increasing C_6 can increase the excess aqueous stability, which has been observed experimentally.

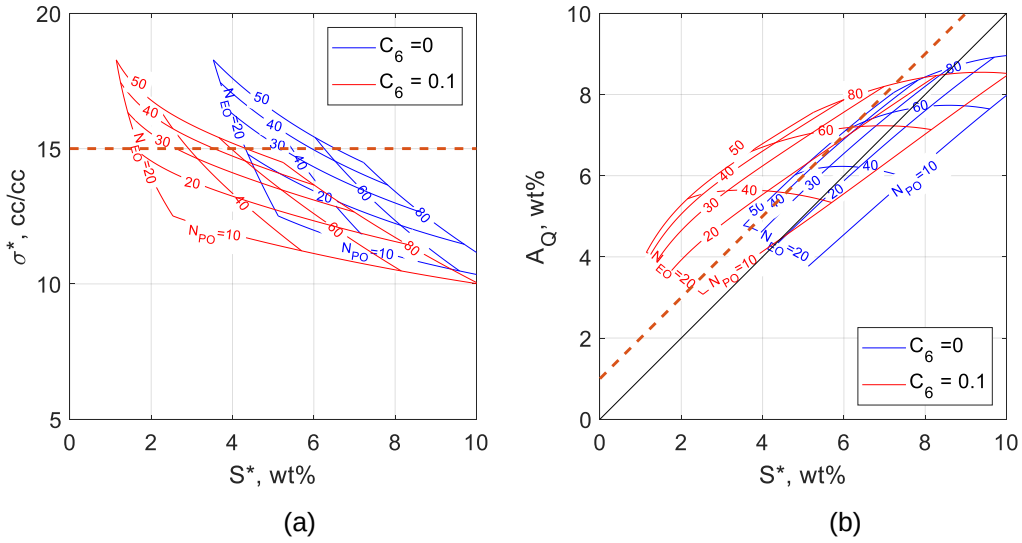

Figure 6.21: Effects of the concentration of divalent cations (C_6) and the numbers of PO and EO groups on (a) the optimum solubilization ratio versus optimum salinity, and (b) the aqueous stability limit versus optimum salinity for a formulation of 0.6% C_{24}(L)-propoxy-ethoxy-COO and 0.4% C_{12} ABS with oil of EACN=10 at 100 °C.

Figure 6.22 shows the effect the oil EACN and co-surfactant type on (a) σ^* versus S^* and (b) A_Q vs S^* for a formulation of 10 mol% C_{24}(L)-45PO-10EO-COO and 90 mol% co-surfactant with variable oil EACN at 100 °C. Four co-surfactants are C_{12} ABS, $C_{15\text{-}17}$ ABS, $C_{15\text{-}18}$ IOS, and $C_{19\text{-}28}$ IOS. Lines of variable oil EACN, ranging from 8 to 16 with increments of 2, are shown. Increasing EACN increases S^* and decreases σ^*, hence negative slopes in **Figure 6.22**(a), and has no effect on AQ, hence zero slopes in **Figure 6.22**(b). Decreasing N_{CABS} and N_{CIOS} increases the S^*, decreases σ^*, and increases A_Q, with A_Q predicted to increase slightly more than S^*.

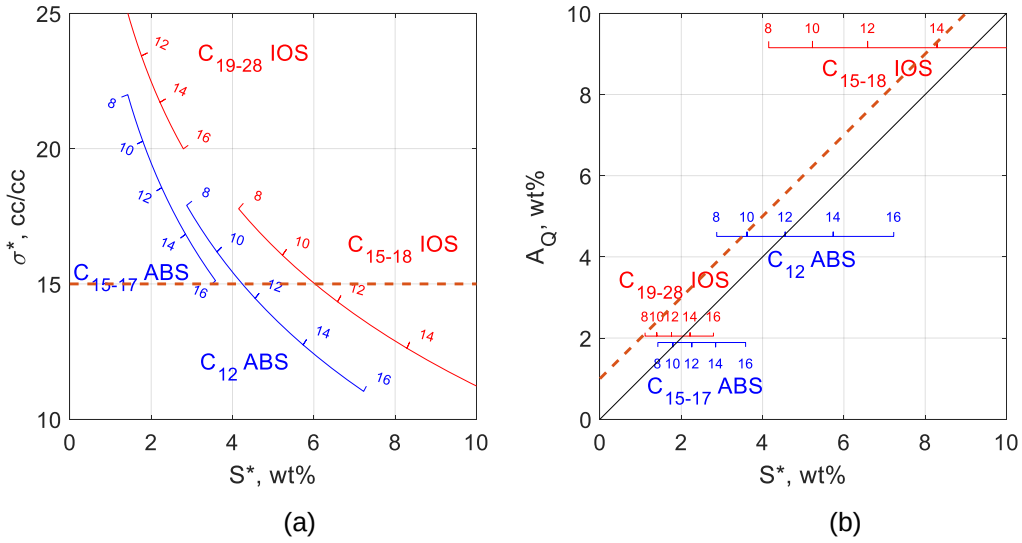

Figure 6.22: Effects of oil EACN and co-surfactant on (a) the optimum solubilization ratio versus optimum salinity, and (b) the aqueous stability limit versus optimum salinity for a formulation of 10 mol% C_{24}(L)-45PO-10EO-COO and 90 mol% co-surfactant with oil EACN ranging from 8 to 16 at 100 °C. Four co-surfactants are C_{12} ABS, $C_{15\text{-}17}$ ABS, $C_{15\text{-}18}$ IOS, and $C_{19\text{-}28}$ IOS.

6.4 Discussion

Without co-solvent, the aqueous stability limit is predicted to be independent of the total surfactant concentration. The structure-concentration effect of co-solvent is a function of the total surfactant concentration, but it has a second order effect. Experimental observations suggest that the total surfactant concentration has a more significant effect on A_Q than predicted by the model. The compositions of mixed micelles can change as the total concentration decreases and approaches the CMC. Impurities or unreacted oil-soluble components in the surfactants could affect the aqueous stability. The models do not capture the CMC of the effects of impurities.

The effect of polymer on the aqueous stability limit is a function of concentration and structure. Regressing upon the concentrations of each polymer type gives values of c_P

for each polymer type. The c_P value was -1.68 (28% relative error) for AN-125, -0.55 (30% relative error) for FP3330S, and -0.45 (30% relative error) for FP3630S. The HPAM co-polymers (FP3630S and FP3330S) have a smaller effect on the aqueous stability than the HPAM-ATBS tertiary polymer, AN-125. However, there may be bias in the data as AN-125 was only used in high salinity and high temperature conditions where HPAM polymers are susceptible to precipitation and thermal degradation. Furthermore, the majority of the aqueous stability experiments used alkali, which causes the acrylamide moieties to hydrolyze to acrylate. Instead of separating based on polymer type, the acrylamide, acrylate, and ATBS contents could be used and may be more useful.

With increasing temperature, the solubility of alkyl anionic (AA) surfactants increases whereas the solubility of alcohol alkoxy anionic (AAA) surfactants decreases. The temperature coefficient was determined to be -0.004, which more closely reflects the behavior of the latter. This is because nearly all of the formulations in the dataset contained AAA surfactants. Similar to the temperature model described for the optimum salinity, the AAA surfactants tend to dominate the interfacial interaction.

Nomenclature

A_Q	=	Aqueous stability limit, wt%
c_i	=	regression coefficient
C_i	=	Concentration of component I (meq/ml)
c_P	=	coefficient for polymer concentration
c_T	=	Slope of lnS* and temperature
E_{ij}	=	Cohesive energy between i and j (L = surfactant lipophile, C = surfactant, W = brine, H = hydrophile)
f_6^S	=	fraction of surfactant with associated divalent cation
$K_{PW,k}$	=	Interface-water partition coefficient of component i

M_i = Molecular weight of component i (g/mol)

N = Sample size

N_{ABS} = Number of benzenesulfonate head groups

$N_{C,A}$ = Carbon number of the A-type hydrophobe

$N_{C,ABS}$ = Carbon number of the ABS hydrophobe

$N_{C,B}$ = Carbon number of the B-type hydrophobe

$N_{C,CS}$ = Carbon number of the co-solvent hydrophobe

$N_{C,IOS}$ = Carbon number of the IOS hydrophobe

$N_{C,L}$ = Carbon number of the L-type hydrophobe

$N_{C,S}$ = Carbon number of the S-type hydrophobe

N_{COO} = Number of carboxylate head groups

N_{EO} = Number of ethylene oxide groups

$N_{EO,CS}$ = Number of ethylene oxide groups in the co-solvent

n_i = Concentration of component I (moles/ml)

N_{IOS} = Number of sulfonate head groups

$N_{j,i}$ = j-type lipophile structure number of component i

N_{OH} = Number of hydroxyl groups

N_{PO} = Number of propylene oxide groups

$N_{PO,CS}$ = Number of propylene oxide groups in the co-solvent

N_{SO4} = Number of sulfate groups

R = Winsor R ratio

ΔT = Temperature difference from 25 °C

V_i = Volume fraction of component i

V_i^S = Volume fraction of interfacial component I

x_i = mole fraction of component i

β_S = Ion exchange constant for the surfactant

δ_i = Structure characteristic of interfacial component i

κ_{jk} = Binary interaction constants between lipophiles of type j and k

ρ_i = Density of component I (g/ml)

σ_{ci} = Standard error of coefficient c_i

ω_P = Mass fraction of polymer

Superscripts

S = Surfactant

Subscripts

1 = Brine

3 = Surfactant

5 = Pseudo-anion

6 = Pseudo-divalent cation

7 = Co-solvent

11 = Pseudo-monovalent cation

CHAPTER 7: SUMMARY, CONCLUSIONS, AND RECOMMENDATIONS

New structure-property models developed to predict the optimum salinity, optimum solubilization ratio, and the aqueous stability limit from the molecular structures of surfactants and co-solvents are in good agreement with an extensive set of experimental data. The models are sufficiently accurate to provide a useful guide to experimental testing programs for the development of chemical formulations for enhanced oil recovery and other similar applications requiring low interfacial tension. Although less comprehensive, previous models have been developed for the optimum salinity, but this is the first time a structure-property model has been developed to predict the optimum solubilization ratio and aqueous stability limit. The solubilization ratio can be used in the Huh equation to predict the interfacial tension, which is the most important property in enhanced oil recovery applications. Structure-property models for the optimum salinity, optimum solubilization ratio, and aqueous stability limit enable the prediction of formulations with ultra-low IFT and aqueous stability needed for chemical EOR to be identified. The structure property models are significantly more complete and accurate because they include the effects of (1) surfactant structure, (2) co-solvent structure and partitioning, (3) soap, and (4) divalent cations.

The molecular structures of internal olefin sulfonate, alkylbenzene sulfonate, alcohol alkoxy sulfate, and alcohol alkoxy carboxylate surfactants were captured using twelve parameters. The structure of hydrophobe (carbon number, degree of branching, polydispersity, and aromaticity), number of propylene oxide groups, number of ethylene oxide groups, and the type of head group (sulfonate, benzene sulfonate, sulfate, carboxylate, hydroxyl) were modeled.

The effect of co-solvent on microemulsion phase behavior is a combination of how the structure influences partitioning to the interface (structure-concentration effect) and how the structures at the interface influences the phase behavior (structure-property effect). Previously the effect of co-solvent structure was modeled as a convolution of both effects because it was difficult to do otherwise, but those models were not predictive. In this dissertation, the two effects were modeled separately. Correlations were developed for the oil-water partition coefficient (K_{OW}) and the interface-water partition coefficient (K_{PW}) of co-solvents and used with pseudophase theory to more accurately model the structure-concentration effect. New measurements of K_{OW} and K_{PW} were made. These new data were combined with the models by Solheim (1990), Dwarakanath & Pope (1998), and Chang et al. (2016) to develop a more complete and accurate K_{OW} model and a rough correlation for K_{PW}. The model includes the effect of co-solvent structure, aromaticity and molecular weight of the crude oil, brine salinity, and temperature. The co-solvent partitioning model was essential to accurately model the effects of co-solvent in the microemulsion phase behavior model.

Soaps were modeled as carboxylate surfactants with unknown hydrophobe structures. Alkali surfactant polymer (ASP) and alkali co-solvent polymer (ACP) formulations were modeled.

Divalent cations have a larger effect on the phase behavior of anionic surfactants than monovalent cations. An ion model was developed that reduces the complexity of real brines by using pseudo-ions. The pseudo-ions were used to calculate the adsorption of divalent cations to surfactant.

New models were developed to account for the effect of temperature and pressure on the optimum salinity and optimum solubilization ratio.

The crude oils were modeled using equivalent alkane carbon numbers (EACN). The EACN values of the crude oils, toluene, cyclohexane, decalin, and light hydrocarbons and carbon dioxide in solution gases were determined. Due to the significant limitations of using EACN, methods to predict and replace the EACN were explored. A new correlation to predict the EACN of crude oils from the oil molar volume and mass fraction of aromatics was developed. This correlation could be used as a starting point for predicting the phase behavior of chemical formulations without the need to first measure the EACN of the crude oil.

The structure-property models for the optimum salinity and optimum solubilization ratio were cross-validated using an independent dataset. The optimum salinities were predicted within a standard error of 1.5 wt% and the optimum solubilization ratios were predicted within a standard error 7.5 cc/cc. The standard errors of the models are approximately equal to the experimental uncertainties in the data.

The structure-property models for the optimum salinity and optimum solubilization ratio were coupled with the HLD-NAC model to accurately predict the entire solubilization ratio curves of new formulations.

A structure-property model was developed to predict the aqueous stability limit (i.e. the salinity at which the aqueous surfactant phase separates). The model includes the effects of surfactant structure, co-solvent partitioning and structure, and divalent cations, similar to that of the optimum salinity. The model also includes the effect of polymer concentration and the interactions between surfactant hydrophobes and the PO groups.

The structure-property models for optimum salinity, optimum solubilization ratio, and aqueous stability limit can be used to predict formulations for a given oil, brine and temperature that are likely to achieve ultra-low IFT with aqueous stability at optimum salinity, i.e. $\sigma^* > 10+5$ cc/cc (5 being the experimental uncertainty of σ^*) and $AQ \geq S^* + 1$

(sum of the experimental uncertainties of A_Q and S^*) and thus greatly accelerate the process of finding the best formulations to test for chemical EOR. A reasonable approach for a new oil would be to (1) use the oil properties to estimate the EACN, (2) use the models to predict a formulation with $\sigma^* > 10+5$ cc/cc and $AQ \geq S^* + 1$, (3) use the experimental data to refine the model parameters and (4) iterate as needed to optimize the formulation. This approach could be used to develop formulations more quickly and with less effort and cost. As an example, suppose the model predicts an optimum solubilization ratio of 20 cc/cc. The chances are good that the measured value will exceed the minimum of 10 cc/cc needed for ultra-low IFT since the uncertainty in the prediction is about 5 cc/cc. Furthermore, as illustrated with several examples in Chapters 4 and 5, the model can be used to predict the changes in chemical structures that are likely to result in the desired optimum salinity and aqueous stability limit while still exceeding the minimum solubilization ratio of 10 needed for ultra-low IFT. The model could even be used to lower chemical costs by exploring alternatives.

The UTCEOR Database used to develop the model is a collection of highest-quality experimental data conducted at The University of Texas at Austin from 2005 to 2018. The database contains over 2000 microemulsion phase behavior experiments and over 1000 aqueous stability tests. These experiments used 36 unique crude oils, 294 unique surfactants, and 70 unique co-solvents. The structures of the surfactants and co-solvents are characterized and include variations in the type of hydrophobe (carbon number, degree of branching, polydispersity, and aromaticity), number of alkoxylate groups (butylene oxide, propylene oxide, and ethylene oxide), and the type of head group (anionic, nonionic, and cationic). The data was pooled from the thousands of experiments involved in the research, development, and optimization of formulations for chemical EOR under a wide variety of reservoir conditions. The model does not attempt to cover all chemical structures

but instead focuses on blends of anionic surfactants and nonionic co-solvents that are not only well studied and have been tested, but also are commercially available and cost-effective.

7.1 Recommendations for Future Work

It is recommended that further research be undertaken in the following areas:

Add new experimental data to supplement the existing database. New data can be efficiently added to the existing database using several tools that were made to assist with (1) transferring data in the current MS Excel file formats into the database, (2) checking and manipulating the data in the database, (3) visualizing and fitting the data.

Extend the model to other surfactant and co-solvent structures. A fraction of the available experiments was used to develop the models because the datasets were restricted to formulations using very specific types of molecules. The database contains numerous experiments using several other types of surfactant and co-solvent structures that were not modeled. For some of these structures, the numbers of experiments are near critical mass, so a minimal number of experimental measurements would be required in order to incorporate the experiments into the dataset and justify adding new parameters to the model. These structures include (1) gemini surfactants, (2) alcohol alkoxylate nonionic surfactants, (3) alkyl polyglucoside surfactants, (4) cationic surfactants, (5) zwitterionic surfactants, and (6) amine-based cationic co-solvents.

Develop a better way to model crude oils as an alternative to EACN. The EACN concept has significant limitations as discussed in section 5.3.4. The oil molecular weight, density, and molar volume do not uniquely characterize the composition of crude oils. The SARA (saturates, aromatics, resins, asphaltenes) analysis only captures the composition of the topped fraction of the crude oil and is a poor predictor variable. Ultimately all

characteristics of crude oils are attributed to composition. The crude oil composition with sufficient detail to model PVT properties, such as that measured using gas chromatography, could be used to correlate or replace EACN.

Add the structure-property models for the optimum salinity and optimum solubilization ratio to the UTCHEM reservoir simulator. The effects of surfactant and co-solvent structure could be added to the UTCHEM reservoir simulator. The functionalities for soap, co-solvent, and divalent cations are already included in the UTCHEM model.

Investigate the effects of surfactant dispersity and heterogeneity on microemulsion and aqueous phase behavior. Nearly all surfactants and co-solvents are distributions of molecules. IOS and ABS surfactants are distributions of carbon numbers, isomers, numbers and types of head groups, degrees of ramifications, etc. The numbers of PO and EO groups in surfactant and co-solvent molecules inherently follow distributions related to reactor conditions and reaction kinetics. Crude oils are complex mixtures of hydrocarbons that follow distributions. The premises are that (1) a targeted and dispersed distribution of surfactants may interact more favorably with a distribution of hydrocarbons and (2) increasing the dispersity of surfactant distributions may decrease surfactant-surfactant interactions which would favor higher interfacial fluidity (i.e. lower microemulsion viscosity). This concept can be tested by artificially increasing the dispersity without shifting the average by mixing different distributions of molecules and observing the shift. The structure-property models currently use the averages of the molecular distributions. The distributions of molecular structure can be measured or estimated in order to model the structure-property effects.

Improve the model for the interface-water partition coefficient (K_{PW}). A rough correlation was used for K_{PW} (for microemulsions) due to scarcity of data. The partition

coefficients can be measured for samples prepared in large volumes such as those used for microemulsion rheology measurements which also typically contain co-solvents. An alternative approach is to apply molecular modeling techniques to predict the composition of the interface as shown in Buijse et al. (2012). K_{PW} (for aqueous stability) was assumed to be 10, but K_{PW} may be quantifiable from coacervated samples.

Improve the model for soap. The concentration of the soap generated by an active crude oil in the presence of alkali was assumed to be only a function of TAN. As observed by Ding et al. (2016) and Mohammadi et al. (2009), the effective amount of soap is a complex function of TAN, pH, salinity, surfactant, co-solvent, and partition coefficients. The average molecular weight of soap was assumed to be 400 g/mol but it is highly uncertain. The analytical methods described in Zhang et al., (2004) may be used to better quantify the properties of soaps.

Model microemulsion rheology. The structure-property models demonstrate that it is possible to empirically correlate the structures of the surfactants and co-solvents with the microemulsion phase behavior. The UTCEOR Database contains over 100 microemulsion viscosity measurements. The model by Tagavifar et al. (2016) uses a single parameter (v) related to the structure of the co-solvent to model the effect of co-solvent on the microemulsion rheology. It may be possible to model microemulsion rheology, which has implications related to coalescence rate and surfactant retention.

APPENDIX A: STRUCTURE COEFFICIENTS FOR STRUCTURE PROPERTY MODELS

Table A.1, **Table A.2**, **Table A.3**, and **Table A.4** show the surfactant characteristics for internal olefin sulfonate (IOS), alkylbenzene sulfonate (ABS), alcohol alkoxy sulfate (SO4) and alcohol alkoxy carboxylate (COO) surfactants, respectively. **Table A.5** shows the structure characteristics for the co-solvents. N is the number of times the surfactant was used. The molecular weights (MW) in g/mol were calculated assuming the surfactants were anionic surfactant-sodium salts. C and D are the surfactant characteristics for the optimum salinity and the optimum solubilization ratio models, respectively.

Table A.1. Characteristics of Internal Olefin Sulfonate Surfactants

	N	MW	$N_{C,IOS}$	N_{IOS}	C	D
C_{15-18} IOS	151	333	16.5	1	1.69	10.7
C_{19-23} IOS	174	396	21	1	0.75	17.2
C_{20-24} IOS	160	410	22	1	0.54	18.6
C_{19-28} IOS	175	431	23.5	1	0.23	20.8
C_{24-28} IOS	1	466	26	1	-0.30	24.4

Table A.2. Characteristics of Alkylbenzene Sulfonate Surfactants

	N	MW	$N_{C,ABS}$	N_{ABS}	C	D
C_{12} ABS	49	348	12	1	1.28	10.8
C_{14} ABS	3	376	14	1	0.89	13.1
C_{14-15} ABS	2	383	14.5	1	0.80	13.7
C_{14-18} ABS	1	404	16	1	0.50	15.4
C_{15-17} ABS	78	404	16	1	0.50	15.4
C_{15-18} ABS	4	411	16.5	1	0.41	16.0
C_{14-30} ABS	4	488	22	1	-0.67	22.2

Table A.3. Characteristics of Alcohol Alkoxy Sulfate Surfactants

	N	MW	$N_{C,L}$	$N_{C,S}$	$N_{C,B}$	$N_{C,A}$	N_{PO}	N_{EO}	N_{SO4}	C	D
C_{16}-7PO-SO_4-	1	750	16				7		1	0.20	24.9
C_{16}-7PO-2EO-SO_4-	1	838	16				7	2	1	0.40	25.0
C_{16}-7PO-6EO-SO_4-	2	1014	16				7	6	1	0.82	25.2
C_{16}-7PO-10EO-SO_4-	3	1190	16				7	10	1	1.23	25.4
C_{24}-25PO-10EO-SO_4-	2	2346	24				25	10	1	-1.73	64.7
C_{24}-25PO-15EO-SO_4-	1	2566	24				25	15	1	-1.22	65.0
C_{24}-25PO-26EO-SO_4-	21	3050	24				25	26	1	-0.08	65.6
C_{24}-35PO-20EO-SO_4-	9	3366	24				35	20	1	-1.86	84.4
C_{28}-25PO-10EO-SO_4-	2	2402	28				25	10	1	-2.18	67.1
C_{28}-25PO-15EO-SO_4-	1	2622	28				25	15	1	-1.66	67.4
C_{28}-25PO-25EO-SO_4-	1	3062	28				25	25	1	-0.63	67.9
C_{28}-35PO-10EO-SO_4-	27	2982	28				35	10	1	-3.33	86.3
C_{28}(O)-35PO-20EO-SO_4-	1	3438	28				35	20	1	-2.30	86.8
C_{28}-35PO-20EO-SO_4-	7	3422	28				35	20	1	-2.30	86.8
C_{28}(O)-35PO-30EO-SO_4-	5	3878	28				35	30	1	-1.27	87.4
C_{28}-35PO-50EO-SO_4-	3	4742	28				35	50	1	0.80	88.5
C_{28}-45PO-10EO-SO_4-	24	3562	28				45	10	1	-4.48	105.4
C_{28}-45PO-20EO-SO_4-	2	4002	28				45	20	1	-3.45	106.0
C_{28}-45PO-45EO-SO_4-	2	5102	28				45	45	1	-0.87	107.3
C_{32}-7PO-18EO-SO_4-	4	1766	32				7	18	1	0.28	35.5
C_{32}-15PO-10EO-SO_4-	2	1878	32				15	10	1	-1.47	50.4
C_{32}-25PO-10EO-SO_4-	3	2458	32				25	10	1	-2.62	69.5
C_{32}-25PO-22EO-SO_4-	3	2986	32				25	22	1	-1.38	70.2
C_{32}-35PO-10EO-SO_4-	2	3038	32				35	10	1	-3.77	88.7
C_8-4PO-SO_4-	2	464		8			4		1	1.41	19.4
C_8-7PO-SO_4-	46	638		8			7		1	1.06	25.1
$C_{12\text{-}13}$-7PO-SO_4-	10	701		12.5			7		1	0.55	30.7
$C_{12\text{-}13}$-8PO-SO_4-	2	759		12.5			8		1	0.43	32.6
$C_{12\text{-}13}$-13PO-SO_4-	100	1049		12.5			13		1	-0.14	42.2
C_{13}-7PO-SO_4-	4	708		13			7		1	0.49	31.3
C_{13}-9PO-SO_4-	4	824		13			9		1	0.26	35.1
C_{13}-13PO-SO_4-	135	1056		13			13		1	-0.20	42.8
C_{13}-15PO-SO_4-	1	1172		13			15		1	-0.43	46.6
C_{13}-35PO-10EO-SO_4-	4	2772		13			35	10	1	-1.71	85.5
C_{13}-45PO-10EO-SO_4-	55	3352		13			45	10	1	-2.86	104.6
C_{13}-45PO-20EO-SO_4-	11	3792		13			45	20	1	-1.83	105.1
C_{16}-17-7PO-SO_4-	26	757		16.5			7		1	0.10	35.6
C_{17}-7PO-SO_4-	1	764		17			7		1	0.04	36.2
C_{17}-14PO-SO_4-	2	1170		17			14		1	-0.77	49.6
C_{18}-25PO-15EO-SO_4-	1	2480			18		25	15	1	0.13	38.1
C_{18}-35PO-10EO-SO_4-	4	2840			18		35	10	1	-1.54	57.0
C_{18}-35PO-30EO-SO_4-	1	3720			18		35	30	1	0.53	58.0
C_{18}-45PO-10EO-SO_4-	5	3420			18		45	10	1	-2.69	76.1
C_{18}-45PO-20EO-SO_4-	15	3860			18		45	20	1	-1.66	76.6
C_{18}-45PO-60EO-SO_4-	1	5620			18		45	60	1	2.47	78.8
C_{30}(TSP)-7PO-12EO-SO_4-	5	1442				30	7	12	1	2.47	4.3
C_{30}(TSP)-35PO-20EO-SO_4-	21	3418				30	35	20	1	0.07	58.3
C_{30}(TSP)-45PO-10EO-SO_4-	5	3558				30	45	10	1	-2.12	76.9
C_{30}(TSP)-45PO-20EO-SO_4-	4	3998				30	45	20	1	-1.09	77.5

Table A.4. Characteristics of Alcohol Alkoxy Carboxylate Surfactants

	N	MW	$N_{C,L}$	$N_{C,S}$	$N_{C,B}$	$N_{C,A}$	N_{PO}	N_{EO}	N_{COO}	C	D
C_{20}-45PO-30EO-COO-	2	4308	20				45	30	1	-1.91	101.5
C_{24}-25PO-18EO-COO-	5	2676	24				25	18	1	-1.28	65.0
C_{28}-25PO-15EO-COO-	4	2600	28				25	15	1	-2.04	67.2
C_{28}(O)-25PO-25EO-COO-	3	3056	28				25	25	1	-1.00	67.7
C_{28}-25PO-25EO-COO-	5	3040	28				25	25	1	-1.00	67.7
C_{28}(O)-25PO-45EO-COO-	1	3936	28				25	45	1	1.06	68.8
C_{28}-25PO-45EO-COO-	21	3920	28				25	45	1	1.06	68.8
C_{28}-25PO-55EO-COO-	3	4360	28				25	55	1	2.09	69.4
C_{28}(O)-35PO-10EO-COO-	45	2976	28				35	10	1	-3.71	86.1
C_{28}-35PO-10EO-COO-	30	2960	28				35	10	1	-3.71	86.1
C_{28}(O)-35PO-20EO-COO-	19	3416	28				35	20	1	-2.67	86.6
C_{28}-35PO-20EO-COO-	5	3400	28				35	20	1	-2.67	86.6
C_{28}-35PO-30EO-COO-	1	3840	28				35	30	1	-1.64	87.2
C_{28}-35PO-50EO-COO-	6	4720	28				35	50	1	0.42	88.3
C_{28}(O)-35PO-60EO-COO-	1	5176	28				35	60	1	1.45	88.8
C_{28}-45PO-10EO-COO-	8	3540	28				45	10	1	-4.86	105.2
C_{28}(O)-45PO-15EO-COO-	12	3776	28				45	15	1	-4.34	105.5
C_{28}-45PO-30EO-COO-	5	4420	28				45	30	1	-2.80	106.3
C_{28}-45PO-60EO-COO-	2	5740	28				45	60	1	0.30	108.0
C28-45PO-80EO-COO-	1	6620	28				45	80	1	2.36	109.0
C32-7PO-32EO-COO-	2	2360	32				7	32	1	1.35	36.1
C18-35PO-20EO-COO-	3	3258			18		35	20	1	-0.88	57.3
C18-45PO-30EO-COO-	42	4278			18		45	30	1	-1.00	77.0
C30(TSP)-45PO-COO-	7	3096				30	45	0	1	-3.52	76.2

Table A.5. Characteristics of Co-solvents

	N	MW	N_{OH}	$N_{C,CS}$	$N_{PO,CS}$	$N_{EO,CS}$	C	D
IBA	99	74	1	4			0.03	13.3
SBA	0	74	1	4			0.03	13.3
IBA-1EO	1	118	1	4		1	0.50	6.8
DEGBE	20	162	1	4		2	0.98	0.3
Butanol-2.15EO	2	168.6	1	4		2.15	1.05	-0.6
IBA-3EO	22	206	1	4		3	1.45	-6.2
TEGBE	20	206	1	4		3	1.45	-6.2
IBA-4EO	2	250	1	4		4	1.92	-12.7
IBA-5EO	15	294	1	4		5	2.40	-19.2
IBA-1PO-2EO	5	220	1	4	1	2	1.88	8.9
Phenol-2EO	60	182	1	6		2	-0.17	-4.0
Phenol-4EO	14	270	1	6		4	0.78	-17.0
Phenol-5EO	5	314	1	6		5	1.25	-23.5
Phenol-6EO	92	358	1	6		6	1.73	-30.0
Phenol-9.8EO	6	525.2	1	6		9.8	3.53	-54.7
Phenol-1PO-2EO	16	240	1	6	1	2	0.74	4.5
Phenol-1PO-5EO	6	372	1	6	1	5	2.16	-15.0
Phenol-2PO-2EO	1	298	1	6	2	2	1.64	13.0

BIBLIOGRAPHY

Acosta, E. J. (2008). The HLD-NAC equation of state for microemulsions formulated with nonionic alcohol ethoxylate and alkylphenol ethoxylate surfactants. *Colloids and Surfaces A: Physicochemical and Engineering Aspects*, *320*(1–3), 193–204. https://doi.org/10.1016/j.colsurfa.2008.01.049

Acosta, E. J., & Bhakta, A. S. (2009). The HLD-NAC model for mixtures of ionic and nonionic surfactants. *Journal of Surfactants and Detergents*, *12*(1), 7–19. https://doi.org/10.1007/s11743-008-1092-4

Acosta, E., Szekeres, E., Sabatini, D. A., & Harwell, J. H. (2003). Net-average curvature model for solubilization and supersolubilization in surfactant microemulsions. *Langmuir*, *19*(1), 186–195. https://doi.org/10.1021/la026168a

Adkins, S., Liyanage, P. J., Pinnawala Arachchilage, G. W. P., Mudiyanselage, T., Weerasooriya, U., & Pope, G. A. (2010). A New Process for Manufacturing and Stabilizing High-Performance EOR Surfactants at Low Cost for High-Temperature, High-Salinity Oil Reservoirs. In *SPE Improved Oil Recovery Symposium*. Society of Petroleum Engineers. https://doi.org/10.2118/129923-MS

Adkins, S., Pinnawala Arachchilage, G. W. P., Solairaj, S., Lu, J., Weerasooriya, U., & Pope, G. A. (2012). Development of Thermally and Chemically Stable Large-Hydrophobe Alkoxy Carboxylate Surfactants. In *SPE Improved Oil Recovery Symposium*. Society of Petroleum Engineers. https://doi.org/10.2118/154256-MS

Anton, R. E., Graciaa, A., Lachaise, J., & Salager, J. L. (1992). Surfactant-Oil-Water Systems Near the Affinity Inversion, Part VIII : Optimum Formulation and Phase Behavior of Mixed Anionic-Nonionic Systems Versus Temperature. *Journal of Dispersion Science and Technology*, *13*(5), 565–579. https://doi.org/10.1080/01932699208943334

Aoudia, M., Wade, W. H., & Weerasooriya, V. (1995). Optimum Microemulsions Formulated with Propoxylated Guerbet Alcohol and Propoxylated Tridecyl Alcohol Sodium Sulfates. *Journal of Dispersion Science and Technology*, *16*(2), 115–135. https://doi.org/10.1080/01932699508943664

Austad, T., Hodne, H., & Staurland, G. (1990). Effects of pressure, temperature and salinity on the multiphase behavior of the surfactant/methane and n-decane/NaCl brine system. In *Surfactants and Macromolecules: Self-Assembly at Interfaces and in Bulk* (pp. 296–310). Darmstadt: Steinkopff. https://doi.org/10.1007/BFb0118272

Austad, T., & Strand, S. (1996). Chemical flooding of oil reservoirs 4. Effects of temperature and pressure on the middle phase solubilization parameters close to optimum flood conditions. *Colloids and Surfaces A: Physicochemical and Engineering Aspects*, *108*(2–3), 243–252. https://doi.org/10.1016/0927-

7757(95)03406-4

Barnes, J., Groen, K., On, A., Dubey, S., Reznik, C., Buijse, M., & Shepherd, A. (2012). Controlled Hydrophobe Branching To Match Surfactant To Crude Composition For Chemical EOR. In *Presented at the SPE Improved Oil Recovery Symposium*. Tulsa, Ok, 14-18 April. SPE-154084-MS. https://doi.org/10.2118/154084-MS

Barnes, J. R., Smit, J., Smit, J., Shpakoff, G., Raney, K. H., & Puerto, M. (2008). Development of Surfactants for Chemical Flooding at Difficult Reservoir Conditions. In *SPE Symposium on Improved Oil Recovery*. Society of Petroleum Engineers. https://doi.org/10.2118/113313-MS

Basilio, E., Mu, B., Jin, L., & Jamili, A. (2017). A Predictive Equation-of-State for Modeling Microemulsion Phase Behavior with Phase Partitioning of Co-Solvent. *SPE International Conference on Oilfield Chemistry This*.

Bourrel, M., Salager, J. L., Schechter, R. S., & Wade, W. H. (1980). A correlation for phase behavior of nonionic surfactants. *Journal of Colloid And Interface Science*, *75*(2), 451–461. https://doi.org/10.1016/0021-9797(80)90470-1

Bourrel, M., & Schechter, R. S. (1988). *Microemulsions and Related Systems: Formulation, Solvency, and Physical Properties* (Second).

Bourrel, M., Verzaro, F., & Chambu, C. (1987). Effect of Oil Type on Solubilization by Amphiphiles. *SPE Reservoir Engineering*, *2*(1), 41–53. https://doi.org/10.2118/12674-PA

Buijse, M., Exploration, S. I., Tandon, K., & Jain, S. (2012). Surfactant optimization for EOR using advanced chemical computational methods. *Eighteenth SPE Improved Oil Recovery Symposium*, 1–12. https://doi.org/10.2118/154212-MS

Cayias, J. L., Schechter, R. S., & Wade, W. H. (1976). Modeling Crude Oils for Low Interfacial Tension. *Society of Petroleum Engineers Journal*, *16*(6), 351–357. https://doi.org/10.2118/5813-PA

Chang, L., Jang, S. H., Tagavifar, M., & Pope, G. A. (2018). Structure-Property Model for Microemulsion Phase Behavior. In *SPE Improved Oil Recovery Conference*. Society of Petroleum Engineers. https://doi.org/10.2118/190153-MS

Chang, L., Pope, G. A., Jang, S. H., & Tagavifar, M. (2019). Prediction of microemulsion phase behavior from surfactant and co-solvent structures. *Fuel*, *237*, 494–514. https://doi.org/10.1016/J.FUEL.2018.09.151

Chang, L. Y. (2014). *New Correlation for Predicting the Best Surfactant and Co-solvent Structures to Evaluate for Chemical EOR*. University of Texas at Austin.

Chang, L. Y., Lansakara-P, D. S. P., Jang, S. H., Weerasooriya, U. P., & Pope, G. A. (2016). Co-solvent Partitioning and Retention. In *SPE Improved Oil Recovery Conference*. Society of Petroleum Engineers. https://doi.org/10.2118/179676-MS

Closmann, P. J., & Seba, R. D. (1990). A Correlation Of Viscosity And Molecular Weight. *Journal of Canadian Petroleum Technology*, *29*(04). https://doi.org/10.2118/90-04-11

Davies, J. T. (1957). Emulsion Type . I . Physical Chemistry of. *Gas/Liquid and Liquid/Liquid Interfaces*, 426–438.

Dean, R. M. (2011). *By Selection and Evaluation of Surfactants for Field Pilots*. University of Texas at Austin.

Delshad, M., Bhuyan, D., Pope, G. A., & Lake, L. W. (1986). Effect of Capillary Number on the Residual Saturation of a Three-Phase Micellar Solution. In *SPE Enhanced Oil Recovery Symposium*. Society of Petroleum Engineers. https://doi.org/10.2118/14911-MS

Ding, L., Zhang, G., Behling, J., Lopez-Salinas, J. L., Ge, J., Puerto, M. C., … Miller, C. A. (2016). Determination of the Active Soap Number of Crude Oil and Soap Partitioning Behavior. *Energy and Fuels*, *30*(12), 10106–10116. https://doi.org/10.1021/acs.energyfuels.6b01603

Do, L. D., Withayyapayanon, A., Harwell, J. H., & Sabatini, D. A. (2009). Environmentally Friendly Vegetable Oil Microemulsions Using Extended Surfactants and Linkers. *Journal of Surfactants and Detergents*, *12*(2), 91–99. https://doi.org/10.1007/s11743-008-1096-0

Dwarakanath, V., & Pope, G. A. (1998). New approach for estimating alcohol partition coefficients between nonaqueous phase liquids and water. *Environmental Science and Technology*, *32*(11), 1662–1666. https://doi.org/10.1021/es9707441

Flaaten, A. (2007). *Experimental Study of Microemulsion Characterization and Optimization in Enhanced Oil Recovery : A Design Approach for Reservoirs with High Salinity and Hardness*. University of Texas at Austin.

Flaaten, A., Nguyen, Q. P., Pope, G. A., & Zhang, J. (2009). A Systematic Laboratory Approach to Low-Cost, High-Performance Chemical Flooding. *SPE Reservoir Evaluation & Engineering*, *12*(05), 713–723. https://doi.org/10.2118/113469-PA

Fortenberry, R., Kim, D. H., Nizamidin, N., Adkins, S., Arachchilage, G. W. P. P., Koh, H. S., … Pope, G. A. (2015a). Use of Cosolvents To Improve Alkaline/Polymer Flooding. *SPE Journal*, *20*(02), 255–266. https://doi.org/10.2118/166478-PA

Fortenberry, R., Kim, D. H., Nizamidin, N., Adkins, S., Arachchilage, G. W. P. P., Koh, H. S., … Pope, G. A. (2015b). Use of Cosolvents To Improve Alkaline/Polymer Flooding. *SPE Journal*, *20*(02), 255–266. https://doi.org/10.2118/166478-PA

Fortenberry, R. P. (2013). *Experimental Demonstration and Improvement of Chemical EOR Techniques in Heavy Oils*. University of Texas at Austin.

Ghosh, S., & Johns, R. T. (2016a). An Equation-of-State Model To Predict Surfactant/Oil/Brine-Phase Behavior. *SPE Journal*, *21*(04), 1106–1125.

https://doi.org/10.2118/170927-PA

Ghosh, S., & Johns, R. T. (2016b). Dimensionless Equation of State to Predict Microemulsion Phase Behavior. *Langmuir*, *32*(35), 8969–8979. https://doi.org/10.1021/acs.langmuir.6b02666

Graciaa, A., Lachaise, J., Cucuphat, ? C, Bourre1, ? M, & Salagere, J. L. (1993). Improving Solubilization in Microemulsions with Additives. 1. The Lipophilic Linker Role. *Langmuir*, *9*, 669–672. Retrieved from http://pubs.acs.org/doi/pdf/10.1021/la00027a010

Green, D. W., & Willhite, G. P. (1998). *Enhanced oil recovery* (Vol. 6). Henry L. Doherty Memorial Fund of AIME, Society of Petroleum Engineers Richardson, TX.

Griffin, W. C. (1949). Classification of surface-active agents by" HLB". *Journal of the Society of Cosmetic Chemists*, *1*(5), 311–326. Retrieved from http://journal.scconline.org//pdf/cc1949/cc001n05/p00311-p00326.pdf

Hammond, C. E., & Acosta, E. J. (2012). On the characteristic curvature of alkyl-polypropylene oxide sulfate extended surfactants. *Journal of Surfactants and Detergents*, *15*(2), 157–165. https://doi.org/10.1007/s11743-011-1303-2

Healy, R. N., Reed, R. L., & Stenmark, D. G. (1976). Multiphase Microemulsion Systems. *Society of Petroleum Engineers Journal*, *16*(03), 147–160. https://doi.org/10.2118/5565-PA

Hirasaki, G. (1982). Interpretation of the Change in Optimal Salinity With Overall Surfactant Concentration. *Society of Petroleum Engineers Journal*, *22*(6), 971–982. https://doi.org/10.2118/10063-PA

Hirasaki, G., Miller, C. A., & Puerto, M. (2011). Recent advances in surfactant EOR. *SPE Journal*, *16*(04), 889–907. https://doi.org/10.2118/115386-PA

Jang, S. H., Liyanage, P. J., Lu, J., Kim, D. H., Arachchilage, G. W. P. P., Britton, C., … Pope, G. A. (2014). Microemulsion Phase Behavior Measurements Using Live Oils at High Temperature and Pressure. In *SPE Improved Oil Recovery Symposium*. Society of Petroleum Engineers. https://doi.org/10.2118/169169-MS

Jang, S. H., Liyanage, P. J., Tagavifar, M., Chang, L. Y., Upamali, K. A. N., Lansakara-P, D. S., … Pope, G. A. (2016). A Systematic Method for Reducing Surfactant Retention to Extremely Low Levels. In *Presented at the SPE Improved Oil Recovery Conference*. Tulsa, OK, 11–13 April. SPE-179685-MS.

Jin, L., Jamili, A., Li, Z., Lu, J., Luo, H., Ben Shiau, B. J., … Harwell, J. H. (2015). Physics based HLD-NAC phase behavior model for surfactant/crude oil/brine systems. *Journal of Petroleum Science and Engineering*, *136*, 68–77. https://doi.org/10.1016/j.petrol.2015.10.039

Kim, D. H., Lee, S., Ahn, C. H., Huh, C., & Pope, G. A. (2010). Development of a Viscoelastic Property Database for EOR Polymers. In *SPE Improved Oil Recovery*

Symposium. Society of Petroleum Engineers. https://doi.org/10.2118/129971-MS

Kim, M. W., Bock, J., & Huang, J. S. (1985). Pressure-Induced Critical Phenomena of a Microemulsion System. *Physical Review Letters*, *54*(1), 46–48. https://doi.org/10.1103/PhysRevLett.54.46

Kim, M. W., Gallagher, W., & Bock, J. (1988). Pressure dependence on multiphase microemulsions. *The Journal of Physical Chemistry*, *92*(5), 1226–1230. https://doi.org/10.1021/j100316a043

Koh, H. (2015). *Experimental Investigation of the Effect of Polymers on Residual Oil Saturation*. University of Texas at Austin.

Kulawardana, E. U., Koh, H., Kim, D. H., Liyanage, P. J., Upamali, K., Huh, C., … Pope, G. A. (2012). Rheology and Transport of Improved EOR Polymers under Harsh Reservoir Conditions. In *SPE Improved Oil Recovery Symposium*. Society of Petroleum Engineers. https://doi.org/10.2118/154294-MS

Levitt, D., Jackson, A., Heinson, C., Britton, L. N., Malik, T., Dwarakanath, V., & Pope, G. A. (2009). Identification and Evaluation of High-Performance EOR Surfactants. *SPE Reservoir Evaluation & Engineering*, *12*(02), 243–253. https://doi.org/10.2118/100089-PA

Li, Y. (2016). *Experimental Investigation of Imbibition in Oil-Wet Carbonates*. University of Texas at Austin.

Li, Y., Pope, G. A., Lu, J., Churchwell, L., Tagavifar, M., & Weerasooriya, U. P. (2017). Scaling of Low-Interfacial-Tension Imbibition in Oil-Wet Carbonates. *SPE Journal*, *22*(05), 1349–1361. https://doi.org/10.2118/179684-PA

Liyanage, P. J., Lu, J., Arachchilage, G. W. P., Weerasooriya, U. P., & Pope, G. A. (2015). A novel class of large-hydrophobe tristyrylphenol (TSP) alkoxy sulfate surfactants for chemical enhanced oil recovery. *Journal of Petroleum Science and Engineering*, *128*, 73–85. https://doi.org/10.1016/J.PETROL.2015.02.023

Liyanage, P. J., Solairaj, S., Pinnawala Arachchilage, G., Linnemeyer, H. C., Kim, D. H., Weerasooriya, U., & Pope, G. A. (2012). Alkaline Surfactant Polymer Flooding using a Novel Class of Large Hydrophobe Surfactants. In *SPE Improved Oil Recovery Symposium*. Society of Petroleum Engineers. https://doi.org/10.2118/154274-MS

Lu, J. (2014). *Development of Novel Surfactants and Surfactant Methods for Chemical Enhanced Oil Recovery*. University of Texas at Austin.

Lu, J., Britton, C., Solairaj, S., Liyanage, P. J., Kim, D. H., Adkins, S., … Pope, G. A. (2014). Novel Large-Hydrophobe Alkoxy Carboxylate Surfactants for Enhanced Oil Recovery. *SPE Journal*, *19*(06), 1024–1034. https://doi.org/10.2118/154261-PA

Magzymov, D., Qiao, C., Johns, R. T., & Pennsylvania, T. (2016). SPE-181651-MS Impact of Surfactant Mixtures on Microemulsion Phase Behavior, (September), 26–28. https://doi.org/10.2118/181651-MS

Maubert, M., Jith Liyanage, P., Pope, G., Upamali, N., Chang, L., Ren, G., … Morel, D. (2018). ASP Experiments in Indiana Limestone using NaOH to Reduce Surfactant Retention. In *SPE Improved Oil Recovery Conference*. Society of Petroleum Engineers. https://doi.org/10.2118/190187-MS

Mohammadi, H., Delshad, M., & Pope, G. A. (2009). Mechanistic Modeling of Alkaline/Surfactant/Polymer Floods. *SPE Reservoir Evaluation & Engineering*, *12*(04), 518–527. https://doi.org/10.2118/110212-PA

Nelson, R. C., Lawson, J. B., Thigpen, D. R., & Stegemeier, G. L. (1984). Cosurfactant-Enhanced Alkaline Flooding. In *SPE Enhanced Oil Recovery Symposium*. Society of Petroleum Engineers. https://doi.org/10.2118/12672-MS

Pinnawala Arachchilage, G. W. P., Spilker, K. K., Tao, E. B., Alexis, D., & Linnemeyer, H. (2018). Evaluating the Effect of Temperature on Surfactant Phase Behavior and Aqueous Stability to Forecast Optimum Salinity at High Temperature. https://doi.org/10.2118/190249-ms

Pope, G. A., Lake, L. W., & Helfferich, F. G. (1978). Cation Exchange in Chemical Flooding: Part 1--Basic Theory Without Dispersion. *Society of Petroleum Engineers Journal*, *18*(06), 418–434. https://doi.org/10.2118/6771-PA

Prouvost, L. P., Satoh, T., Sepehrnoori, K., & Pope, G. a. (1984). A New Micellar Phase-Behavior Model for Simulating Systems With Up to Three Amphiphilic Species. *Proceedings of SPE Annual Technical Conference and Exhibition*. https://doi.org/10.2523/13031-MS

Prouvost, L., Pope, G., & Rouse, B. (1985). Microemulsion Phase Behavior: A Thermodynamic Modeling of the Phase Partitioning of Amphiphilic Species. *Society of Petroleum Engineers Journal*, *25*(5). https://doi.org/10.2118/12586-PA

Puerto, M. C., & Reed, R. L. (1983). A Three-Parameter Representation of Surfactant/Oil/Brine Interaction. *Society of Petroleum Engineers Journal*, *23*(4), 669–682. https://doi.org/10.2118/10678-PA

Puerto, M., Hirasaki, G. J., Miller, C. A., & Barnes, J. R. (2012). Surfactant Systems for EOR in High-Temperature, High-Salinity Environments. *SPE Journal*, *17*(01), 11–19. https://doi.org/10.2118/129675-PA

Rajapaksha, S., Britton, C., McNeil, R. I., Kim, D. H., Unomah, M., Kulawardana, E., … Pope, G. A. (2014). Restoration of Reservoir Cores to Reservoir Condition before Chemical Flooding Tests. In *SPE Improved Oil Recovery Symposium*. Society of Petroleum Engineers. https://doi.org/10.2118/169887-MS

Reed, R. L., & Healy, R. N. (1977). Some physicochemical aspects of microemulsion flooding: a review. *Improved Oil Recovery by Surfactant and Polymer Flooding*, 383–437.

Rosen, M. J. (2004). *Surfactants and Interfacial Phenomena*. Hoboken, NJ, USA: John

Wiley & Sons, Inc. https://doi.org/10.1002/0471670561

Sahni, V., Dean, R. M., Britton, C., Kim, D. H., Weerasooriya, U., & Pope, G. A. (2010). The role of co-solvents and co-surfactants in making chemical floods robust. *Spe 130007*, (1976). https://doi.org/10.2118/130007-MS

Sahni, V. M. (2009). *Experimental Evaluation of Co-Solvents in Development of High Performance Alkali / Surfactant / Polymer Formulations for Enhanced Oil Recovery APPROVED BY SUPERVISING COMMITTEE :* University of Texas at Austin.

Salager, J.-L., Forgiarini, A. M., & Bullón, J. (2013). How to Attain Ultralow Interfacial Tension and Three-Phase Behavior with Surfactant Formulation for Enhanced Oil Recovery: A Review. Part 1. Optimum Formulation for Simple Surfactant–Oil–Water Ternary Systems. *Journal of Surfactants and Detergents*, *16*(4), 449–472. https://doi.org/10.1007/s11743-013-1470-4

Salager, J. L. (1977). *Physio-Chemical Properties of Surfactant-Water-Oil Mixtures: Phase Behavior, Microemulsion Fomration and Interfacial Tension*. University of Texas at Austin.

Salager, J. L., Bourrel, M., Schechter, R. S., & Wade, W. H. (1979). Mixing Rules for Optimum Phase-Behavior Formulations of Surfactant/Oil/Water Systems. *SPE Journal*, *19*(05), 271–278. https://doi.org/http://dx.doi.org/10.2118/7584-PA

Salager, J. L., Forgiarini, A. M., Márquez, L., Manchego, L., & Bullón, J. (2013). How to attain an ultralow interfacial tension and a three-phase behavior with a surfactant formulation for enhanced oil recovery: A Review. Part 2. performance improvement trends from Winsor's premise to currently proposed inter- and intra-molecular mixtu. *Journal of Surfactants and Detergents*, *16*(5), 631–663. https://doi.org/10.1007/s11743-013-1485-x

Salager, J. L., Morgan, J. C., Schechter, R. S., Wade, W. H., & Vasquez, E. (1979). Optimum Formulation of Surfactant/Water/Oil Systems for Minimum Interfacial Tension or Phase Behavior. *Society of Petroleum Engineers Journal*, *19*(02), 107–115. https://doi.org/10.2118/7054-PA

Sandvik, E. I., Gale, W. W., & Denekas, M. O. (1977). Characterization of Petroleum Sulfonates. *Society of Petroleum Engineers Journal*, *17*(03), 184–192. https://doi.org/10.2118/6120-PA

Scamehorn, J. ., Schechter, R. ., & Wade, W. . (1982a). Adsorption of surfactants on mineral oxide surfaces from aqueous solutions: I: Isomerically pure anionic surfactants. *Journal of Colloid and Interface Science*, *85*(2), 463–478. https://doi.org/10.1016/0021-9797(82)90013-3

Scamehorn, J. ., Schechter, R. ., & Wade, W. . (1982b). Adsorption of surfactants on mineral oxide surfaces from aqueous solutions: III. Binary mixtures of anionic and nonionic surfactants. *Journal of Colloid and Interface Science*, *85*(2), 494–501. https://doi.org/10.1016/0021-9797(82)90015-7

Sharma, H., Lu, J., Weerasooriya, U. P., Pope, G. A., & Mohanty, K. K. (2016). Adsorption in Chemical Floods with Ammonia as the Alkali. In *SPE Improved Oil Recovery Conference*. Society of Petroleum Engineers. https://doi.org/10.2118/179682-MS

Sharma, H., Weerasooriya, U., Pope, G. A., & Mohanty, K. K. (2016). Ammonia-based ASP floods in carbonate cores containing gypsum. *Fuel*, *184*, 362–370. https://doi.org/10.1016/J.FUEL.2016.07.014

Shinoda, K., & Takeda, H. (1970). The effect of added salts in water on the hydrophile-lipophile balance of nonionic surfactants: The effect of added salts on the phase inversion temperature of emulsions. *Journal of Colloid and Interface Science*, *32*(4), 642–646. https://doi.org/10.1016/0021-9797(70)90157-8

Skauge, A., & Fotland, P. (1990). Effect of Pressure and Temperature on the Phase Behavior of Microemulsions. *SPE Reservoir Engineering*, *5*(04), 601–608. https://doi.org/10.2118/14932-PA

Solairaj, S. (2011). *New Method of Predicting Optimum Surfactant Structure for EOR*. University of Texas at Austin.

Solairaj, S., Britton, C., Kim, D. H., Weerasooriya, U., & Pope, G. A. (2012). Measurement and Analysis of Surfactant Retention. In *SPE Improved Oil Recovery Symposium*. Society of Petroleum Engineers. https://doi.org/10.2118/154247-MS

Solairaj, S., Britton, C., Lu, J., Kim, D. H., Weerasooriya, U., & Pope, G. A. (2012). New Correlation to Predict the Optimum Surfactant Structure for EOR. *SPE Improved Oil Recovery Symposium*, *0*(April), 2–11. https://doi.org/10.2118/154262-MS

Solheim, A. (1990). Partition Of Alcohol Between Excess Oil And Aqueous Phases In Surfactant Flooding Processes. Retrieved from https://www.onepetro.org/general/SPE-20803-MS

Tagavifar, M., Herath, S., Weerasooriya, U. P., Sepehrnoori, K., & Pope, G. (2016). Measurement of Microemulsion Viscosity and Its Implications for Chemical EOR. In *SPE Improved Oil Recovery Conference*. Society of Petroleum Engineers. https://doi.org/10.2118/179672-MS

Talley, L. D. (1988). Hydrolytic Stability of Alkylethoxy Sulfates. *SPE Reservoir Engineering*, *3*(01), 235–242. https://doi.org/10.2118/14912-PA

Unomah, M. (2013). *Chemical Enhanced Oil Recovery Utilizing Alternative Alkalis*. University of Texas at Austin.

Upamali, K. A. N., Liyanage, P. J., Lu, J., Cai, J., Jang, S. H., Weerasooriya, U., & Pope, G. A. (2016). New Surfactant and Co-Solvent Increase Oil Recovery and Reduce Cost. In *Presented at the SPE Improved Oil Recovery Conference*. Tulsa, OK, 11–13 April. SPE-179702-MS.

Velásquez, J., Scorzza, C., Vejar, F., Forgiarini, A. M., Antón, R. E., & Salager, J. L. (2010). Effect of temperature and other variables on the optimum formulation of

anionic extended surfactant-alkane-brine systems. *Journal of Surfactants and Detergents*, *13*(1), 69–73. https://doi.org/10.1007/s11743-009-1142-6

Walker, D. (2011). *Experimental Investigation of the Effect of Increasing the Temperature on ASP Flooding*. University of Texas at Austin.

Walker, D., Britton, C., Kim, D. H., Dufour, S., Weerasooriya, U., & Pope, G. A. (2012). The Impact of Microemulsion Viscosity on Oil Recovery. In *SPE Improved Oil Recovery Symposium*. Tulsa, OK: Society of Petroleum Engineers. https://doi.org/10.2118/154275-MS

Wang, D. (2018). *Surfactant Retention in Limestones*. University of Texas at Austin.

Wang, D., Maubert, M., Pope, G. A., Liyanage, P. J., Jang, S. H., Upamali, K. A. N., … Morel, D. (2018). Reduction of Surfactant Retention in Limestones Using Sodium Hydroxide. *SPE Journal*. https://doi.org/10.2118/194009-PA

Wang, P.-T. F. (1979). *The Exchange Reaction for Sodium and Calcium with Chloride and Sulfonate Anions on Montmorillonite*. Austin, Texas: The University of Texas at Austin.

Winsor, P. A. (1954). Solvent Properties of Amphiphilic Compounds. *Butterworths Scientific Publications.*, *58*(12), 1103–1104. https://doi.org/10.1002/lipi.19560581222

Winters, M. H. (2012). *Experimental Development of a Chemical Flood and the Geochemistry of Novel Alkalis*. University of Texas at Austin.

Yang, H. T. (2010). *Development of Improved ASP Formulations for Reactive and Non-reactive Crude Oils*. University of Texas at Austin.

Yang, H. T., Britton, C., Liyanage, P., Solairaj, S., Kim, D. H., Nguyen, Q., … Pope, G. (2010). Low-Cost, High-Performance Chemicals for Enhanced Oil Recovery. In *SPE Improved Oil Recovery Symposium*. Tulsa, OK.

Zhang, G., Yu, J., Du, C., & Lee, R. (2015). Formulation of Surfactants for Very Low/High Salinity Surfactant Flooding without Alkali. Society of Petroleum Engineers. https://doi.org/10.2118/173738-MS

Zhang, L., Luo, L., Zhao, S., Xu, Z. cheng, An, J. yi, & Yu, J. yong. (2004). Effect of different acidic fractions in crude oil on dynamic interfacial tensions in surfactant/alkali/model oil systems. *Journal of Petroleum Science and Engineering*, *41*(1–3), 189–198. https://doi.org/10.1016/S0920-4105(03)00153-0

Zhao, P., Jackson, A., Britton, C., Kim, D. H., Britton, L. N., Levitt, D., & Pope, G. A. (2008). Development of High-Performance Surfactants for Difficult Oils. In *SPE Symposium on Improved Oil Recovery*. Society of Petroleum Engineers. https://doi.org/10.2118/113432-MS